

Renormalization Group Approach to Superfluid Neutron Matter

**Vom Fachbereich Physik
der Technischen Universität Darmstadt**

**zur Erlangung des Grades
eines Doktors der Naturwissenschaften
(Dr. rer. nat.)**

genehmigte Dissertation von

**Dipl.-Phys. Kai Hebler
aus Bad Hersfeld**

Darmstadt 2007

D17

Referent: Prof. Dr. Bengt Friman
Koreferent: Prof. Dr. Jochen Wambach

Tag der Einreichung: 23. Januar 2007
Tag der Prüfung: 12. Februar 2007

Meinen Eltern.

*The most incomprehensible thing about the world
is that it is at all comprehensible.*

Albert Einstein

Contents

List of Figures	V
Introduction and Overview	i
1. Superfluid Nuclear systems	1
1.1. History of Superconductivity	1
1.2. The Cooper Phenomenon	3
1.3. The Superconducting Ground State	6
1.4. From Superconductivity to Superfluidity	11
1.5. Superfluidity in Neutron Matter	13
1.6. Nambu-Gorkov Propagators	15
1.7. Scattering Equation in a Superfluid	21
1.8. Separable Model	29
1.9. Relation between Gap Equation and Scattering Equation	36
1.10. Problems and Limitations of the Inversion Approach	38
2. RG approach to Superfluid many-body systems	41
2.1. Basic Ideas	41
2.2. RG Approach to Many-Fermion Systems	43
2.3. Solving Many-Body Problems by using the RG	46
2.4. Interaction Dependence of the Pairing Gap	51
2.5. RG Evolution from the Normal into the Superfluid Phase	57
2.6. Results for Realistic Interactions	68
3. Beyond the BCS approximation	75
3.1. Overview	75
3.2. RG Approach to the Parquet Equations	80
3.3. Self-Energy Corrections	83
3.4. Generalized Gap Equation	86
3.5. Comparison to the Exact RG Equations	93
3.6. Parquet Equations in a Superfluid	98
3.7. Partial Wave Coupling	104
4. Conclusions and Outlook	107

A. Appendix	111
A.1. Numerical Evaluation of the Flow Equation	111
A.2. Particle-Hole Interaction	113
A.3. Flow Equations in Vacuum	114
Bibliography	117

List of Figures

1.1. Heat capacity of a superconductor.	2
1.2. The three many-body channels.	3
1.3. Analytic structure of the vertex function in the Cooper problem.	5
1.4. Final state phase space in the Cooper problem.	6
1.5. Distribution functions and excitation spectrum in superfluid systems.	9
1.6. Excitation spectrum of liquid ${}^4\text{He}$	12
1.7. ${}^1\text{S}_0$ and ${}^3\text{P}_2 - {}^3\text{F}_2$ pairing gap in neutron matter in the BCS approximation	14
1.8. One-body Nambu-Gorkov propagator in the BCS approximation	16
1.9. Gap function and gap equation in the BCS approximation	17
1.10. Two-body Nambu-Gorkov propagator in the BCS approx.	20
1.11. Illustration of the possible processes in a superfluid system.	22
1.12. Antisymmetrized bare two-particle interaction.	23
1.13. Typical diagrams of the two-particle Nambu-Gorkov propagator in second-order perturbation theory.	25
1.14. The non-superfluid limit of the BCS-channel scattering equation.	26
1.15. The three Bethe-Salpeter equations in a normal system.	27
1.16. Analytic structure of the vertex function in the superconducting ground state.	32
1.17. Pairing gap as a function of density for a separable model.	33
1.18. Dispersion relation of the Goldstone boson.	34
1.19. Imaginary part of the vertex function as a function of energy for a separable model.	34
1.20. Real part of the vertex function as a function of energy for a separable model.	35
2.1. Comparison of the low momentum one-body Hilbert space in vacuum and medium.	43
2.2. Kinematics of interacting low lying excitations in a many-body system.	44
2.3. Marginal interaction processes in a many-body system at tree level.	46
2.4. Spurious poles of the on-shell T-matrix elements.	52
2.5. Neutron-neutron pairing gaps as a function of density for low momentum interactions.	54
2.6. Charge dependence of the pairing gap.	55

2.7. Pairing gaps at fixed densities as a function of the cutoff for different widths.	56
2.8. Pairing gaps at fixed densities as a function of the cutoff for different interactions.	57
2.9. Different cutoff functions.	61
2.10. Formation of the gap as a function of the cutoff.	62
2.11. Snapshots of the vertex function at different cutoff scales.	63
2.12. Results of the RG algorithm for the real part of vertex function as a function of energy.	64
2.13. Results of the RG algorithm for the imaginary part of vertex function as a function of energy.	65
2.14. Illustration of flow into the broken phase.	67
2.15. Real part of the vertex function as a function of momentum at fixed energies for realistic interactions.	68
2.16. Results for the real part of the vertex function on the Fermi surface for realistic interactions.	69
2.17. Results for the imaginary part of the vertex function on the Fermi surface for realistic interactions.	70
2.18. Real part of the vertex function for realistic interactions on the Fermi surface for different CM momenta.	72
2.19. Imaginary part of the vertex function on the Fermi surface for different CM momenta.	73
3.1. Self-energy effects in the gap function in quasiparticle approx.	76
3.2. Defining system for the induced interaction.	78
3.3. Monte-Carlo simulation results for the gap function.	79
3.4. Results for the 1S_0 gap function in different approaches.	80
3.5. The one-loop particle-hole parquet flow equation.	81
3.6. 1S_0 pairing gap in the RG approach to the particle-hole parquet.	82
3.7. Dyson equations for the single-particle Gorkov propagators.	84
3.8. The two-particle irreducible vertex functions.	90
3.9. Representations of the gap function.	90
3.10. The generalized gap equation.	91
3.11. The exact RG equations for the four point vertex.	95
3.12. Two representations of the flow equation for the two-point function.	97
3.13. Bethe-Salpeter equations in a superfluid.	99
3.14. Parquet equations in a superfluid.	100
3.15. Comparison of the explicit and iterative solution.	103
3.16. Illustration of the properties of Γ with partial wave coupling.	106
3.17. Collective excitation spectrum in an attractive partial wave.	106

Introduction and Overview

The pairing phenomenon plays a central role in cold fermionic many-body systems. From the present theoretical understanding pairing should appear in almost every many-fermion system at sufficiently low temperatures. Indeed, during the last century it has been observed in many different systems like metals [1], atomic nuclei [2] and liquid ^3He [3]. The basic underlying microscopic mechanism was discovered in the pioneering work of Bardeen, Schrieffer and Cooper [4] in 1957, today well known as the BCS theory of superconductivity. Based on this theory the occurrence of superconductivity and superfluidity can be understood quite intuitively on the basis of simple phase space arguments.

In general two particular scattering processes play a special role in isotropic many-fermion systems at low energies. The first corresponds to forward scattering processes. These form the basis of Landau's theory of Fermi Liquids and describe the dominant interactions of low energy elementary excitations in *normal* Fermi systems. The second corresponds to two body processes at zero center of mass (CM) momentum. In the case of attractive interparticle interactions these processes lead naturally to an instability of the system towards the formation of two-particle bound states called *Cooper pairs*. The characteristic phenomenology of superfluid and superconducting systems can be *qualitatively* understood solely by the presence of the *condensate*, a macroscopically populated collective state consisting of Cooper pairs. In this sense the occurrence of pairing and superfluidity in Fermi systems is a natural consequence of the exclusion principle and consequently the fundamental properties of superfluid systems can qualitatively be understood from first principles.

However, a *quantitative* understanding of the bulk properties of these systems is much more involved. In general many-body correlations, which are neglected in the original BCS theory, will change the value of the condensate considerably. Especially in strongly correlated systems like nuclear systems, it is a very complex task to treat all interparticle correlations at different length scales in a systematic way. On the other hand many macroscopic properties depend very sensitively on the particular value of the condensate. Thus for a systematic quantitative understanding of these systems the application of controlled *microscopic* techniques is necessary.

In the case of nuclear systems the basic ingredient of such microscopic approaches is the two-body nucleon-nucleon (NN) interaction and possible three-body (3N) interactions, determined from vacuum scattering experiments and the properties of the deuteron. The NN-interaction has been studied in great de-

tail during the last decades. At present there exist different models which all fit the basic observables to very good accuracy. All these models share some basic features.

- Almost all potentials parametrize the interaction only for energies below the pion production threshold. Beyond this scale the potential description of the interaction breaks down and the non-relativistic quantum mechanical description must be replaced by an effective quantum field theory. Due to this principal limitation, only neutron systems up to a maximal density of about twice nuclear density ρ_n can be properly described microscopically starting from these NN interactions.
- The potential includes strong repulsion at small distances and an attractive long range part. These properties lead naturally to the saturation of nuclear systems.
- Scattering experiments show a large negative scattering length in the 1S_0 partial wave channel signalling the presence of an almost bound ("anti-bound") state. In contrast, due to the presence of the tensor force component in the spin-triplet 3S_1 - 3D_1 channel, the neutron-proton interaction can support a bound state, the deuteron, whereas the corresponding neutron-neutron state in the same partial wave channel remains unbound. Due to the large scattering length a , low density approximations, based on an expansion in the small parameter ak_F , already break down at quite small Fermi momenta k_F .

Starting from this "bare" interaction all many-body correlation effects leading to the formation of many-body bound states, collective excitation modes etc. are generated dynamically by solving the many-body problem in a certain approximation.

In nature, the size of the Cooper Pair wave function in typical superfluids covers many other particles. Due to the presence of these particles the bare interaction gets modified substantially by many-body effects. Beside these polarization effects, the presence of the other particles will affect the single-particle properties. Ideally these two effects have to be taken into account at the same time and on equal footing.

A promising approach to this complex problem is the Renormalization Group (RG): instead of trying to solve the equations in one step for all momentum scales, one divides the problem into smaller and easier steps by introducing a cutoff scale Λ . This scale represents the dividing line between the *slow* and the *fast modes* of the system. The slow modes represent the modes of the effective Hilbert space at the current scale, whereas the fast modes have already been integrated out into the effective operators of the Hamiltonian at this scale. The RG flow equation describes how the effective Hamiltonian is modified when the cutoff scale is changed. In this sense the RG can be considered as a powerful tool

for successively integrating out correlations in the system at the different length scales in a systematic way.

This philosophy has been applied successfully in many different contexts (see chapter 2). In the present work we apply this technique to the pairing problem in neutron matter at zero temperature. The fundamental objects of investigation are the two-point self-energy and the four-point vertex function. Much of the interesting information about the system like the bound states, collective modes, self-energies, transport coefficients and thermodynamic quantities can be extracted out of this function.

In the first chapter we discuss, after a brief historic and formal introduction, the basic characteristic properties of the vertex function for a separable interaction in the BCS approximation. For such interactions the one-channel scattering problem can be solved explicitly. It turns out that already at this level, the four-point vertex function Γ has a quite complex and rich analytical structure.

However, the traditional inversion approach to the solution of the two-body scattering equation is quite limited if one tries to generalize the calculations to more realistic interactions and to approximation schemes beyond the BCS level. We will show in the second chapter how instead RG methods can be used as an alternative and more flexible approach to this problem.

In general, low lying modes around the Fermi surface dominate the physics of many-fermion systems at low temperatures. The fast modes are almost blind to the presence of the other particles and can to a good approximation be integrated out in vacuum. This procedure provides an effective low momentum vacuum interaction at a certain scale Λ . As long as the size of the effective many-body Hilbert space is not too small, the final answers can be shown to be independent of the choice of Λ . Furthermore as we will show, the required effort for the many-body calculations can be reduced considerably by a judicious choice of Λ .

The explicit treatment of the remaining modes around the Fermi surface is also done in the RG framework. However, the application of the RG to superfluid systems is complicated by the presence of poles in the vertex during the RG flow. The appearance of such poles usually signals instabilities in the system, which in the present case can be identified as the phase transition from the normal to the superfluid state.

At the beginning of the RG calculation no pairing correlations have been integrated out and consequently the RG flow is initialized in the normal phase. Hence in order to enter the new phase in a controlled way, one has to change the formal parametrization of the system beyond this pole. One possibility consists of bosonization of the fermionic degrees of freedom (cf. chapter 2): in every RG step, the pairing correlations at the current scale are integrated out via a Hubbard-Stratonovich transformation into a bosonic field, which represents the Cooper pairs. By this the original fermionic field theory is during the flow transformed into a theory of interacting Fermions and Bosons.

Here we will use a different approach following a strategy similar to the one

presented by Salmhofer [5]. At the beginning of the flow no fluctuations have been integrated out and the condensate is actually vanishing. Instead of introducing Bose fields we break the symmetry in the original theory *explicitly* by a very small - ideally infinitesimal - amount. In this approach the theory remains purely fermionic at every cutoff scale.

By the initial explicit symmetry breaking, we offer the system the possibility to evolve *dynamically* during the RG flow to the state with broken symmetry. We show in chapter 2 explicitly how the results of chapter 1 can be reproduced to high accuracy in the RG framework for a separable interaction. However, in contrast to the explicit analytic solution, the applicability of the flow equation is *not* restricted to separable interactions. Consequently it is possible to apply this RG scheme to different realistic interaction models and hence study the model dependence of the results on the interactions. Furthermore we can compare thus explicitly the results of the flow equations in medium and vacuum and explicitly justify the vacuum flow used for the fast modes.

Although in the present work only nuclear systems are treated explicitly, it should be emphasized that the fundamental strategy is quite general and related to RG approaches in other fields like condensed matter physics (cf. chapter 2). So far, these approaches are usually aimed at the calculation of thermodynamic quantities. In this case, it is sufficient to evaluate the two and four-point functions for imaginary energies. On the one hand, this simplifies the calculations considerably due to the simpler analytic structure in this region. On the other hand however, the vertex function on the real energy axis contains more interesting information like the properties of the collective modes and bound states in the system. The RG framework presented in this work is set up for the calculation of the non-relativistic in-medium scattering amplitude for real energies.

Apart from the technical conveniences of the RG approach mentioned above, this framework has the other even more important conceptual advantage that it can quite naturally be extended beyond the BCS approximation. There have been quite clear indications that additional many-body effects, which are not included at BCS level, are required for a realistic description of the system (cf. e.g. [6]). Several different strategies have been developed during the recent decades to take these effects into account (cf. chapter 3). In most of the works the vertex corrections and the self-energy effects have been treated separately. In contrast, in the RG approach these two effects can be treated at the same time since the two-point and four point functions are consistent with each other by construction on the one particle propagator level. Since in the present formalism the Cooper instability is treated explicitly, one can in principle treat all many body channels at the same time on an equal footing.

Usually a decoupling of the particle-hole channels and particle-particle channel is assumed. After the particle-hole part has been integrated by using some approximation the effective particle-hole reducible vertex is used as the kernel of the gap equation, which integrates the particle-particle diagrams. However, it

is not a priori clear, to what extent this decoupling assumption is valid. Especially for strongly interacting systems like ${}^3\text{He}$ the inclusion of a finite gap in the calculation of polarisation contributions to the effective pairing interaction can influence substantially the stability of different superfluid phases [7, 8], of course, the full coupled problem is very complicated. Furthermore the evaluation of the flow equation is quite complex and involves numerical subtleties already at the BCS level. Nevertheless, the RG approach opens the possibility to include additional many-body correlations in a systematic framework. Since in general the components of the vertex function are changing smoothly during the flow, one can apply iterative solution techniques for the solution of the flow equation. In contrast to a naive iterative approach that includes the integration of all momentum components at once, the convergence can be dramatically improved by the use of RG methods since usually the vertex functions of the previous RG step provide an excellent initial guess leading to a rapid convergence. We show in chapter 3 by explicit calculation that the combination of iterative and RG techniques provides quite a promising strategy to tackle the coupled channel problem.

Furthermore, this framework does not rely on the assumption of scale separation. In the standard approach it is assumed that the correlations included in the quasiparticle states participating in the pairing processes are energetically well separated from the characteristic energy scales of the Cooper-pairs [9, 10]. However, in the nuclear systems, where the Fermi energy is about 50 MeV for typical densities, the gaps are one the order of MeV. Furthermore, the quasiparticle concept remains valid up to an energy scale typically on the order of 10 MeV. Hence it is not so clear, to what extent the scale separation assumption is valid in these systems. Since in the present approach the different correlations are treated on an equal footing, the present framework offers a possibility to treat such systems.

In the current state of the work we have implemented the one-channel problem in the BCS approximation. We can reproduce the explicit results for separable interactions to high accuracy including all pole structure in the vertex function. Hence in this sense the calculations should be considered as exploratory, showing the feasibility of practical calculations in this approach. Furthermore we show that the same results can also be obtained without using the explicit form of the flow equation, which is only valid in the one-channel case. This offers the possibility to apply the same techniques to the coupled channel problem and shows clearly the flexibility of this approach.

1. Superfluid Nuclear systems

1.1. History of Superconductivity

The phenomenon of superconductivity attracted the attention of physicists for the first time in 1911 when H. Kamerlingh Onnes [1] observed vanishing d-c electrical resistance in mercury below 4 Kelvin. His experiment provided the first indication for fundamental changes of the microscopic and macroscopic properties in certain metals when the temperature is lowered below a critical temperature T_c .

Beside these radical changes of the electrical properties, which is probably still today the most striking manifestation of superconductivity, the superconducting state is also characterized by very different magnetic and thermodynamic properties compared to the normal state:

- In 1932 Keesom *et al.* [11] found a fundamental change of the behaviour in the heat capacity below the critical temperature T_c . Starting above T_c the system at first showed the typical linear behaviour $C \sim \gamma T$ of a normal Fermi fluid. At T_c however a discontinuity appeared followed by an exponential decrease below T_c (cf. Fig. 1.1).
- In 1933 Meissner and Ochsenfeld [12] discovered that a superconductor is a perfect diamagnet, i.e. that external magnetic fields were expelled from the interior of the system. They found a penetration depth of about $\lambda \simeq 10^{-5}$ cm.

However, at the time of these experiments, there was still only a poor understanding of the microscopic mechanisms responsible for these observations. In 1934 F. and H. London [13] presented a phenomenological two fluid model on the basis of the work of Gorter and Casimir [14] that was capable of describing the magnetic properties of superconductors. The central idea consists of dividing the total particle density ρ into a superfluid density ρ_s and a normal density ρ_n with $\rho = \rho_s + \rho_n$. The associated fluid current densities were postulated to satisfy

$$\frac{d\mathbf{j}_s}{dt} = \frac{\rho_s e^2}{m} \mathbf{E}, \quad \mathbf{j}_n = \sigma_n \mathbf{E}, \quad \nabla \times \mathbf{j}_s = -\frac{\rho_s e^2}{m} \mathbf{B}.$$

The first equation simply express that the superfluid part moves without energy dissipation through the system, whereas the second equation describes a normal

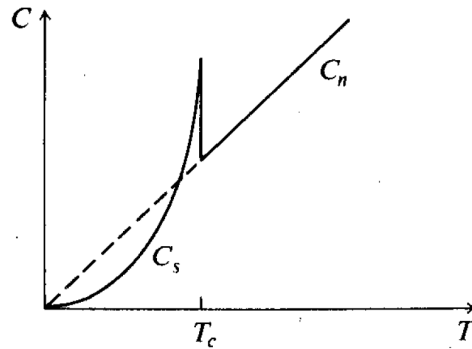


Figure 1.1.: Heat capacity of a superconductor as a function of temperature. Figure taken from [15].

fluid, which produces a finite conductivity σ_n . Finally, the last equation immediately leads to the Meissner-Ochsenfeld effect by using the Maxwell equations.

In the following years some extensions of the London theory were developed like Pippard's nonlocal generalization in 1953 [16], which took into account the effect of impurities and the Ginsburg-Landau theory in 1950 [17], where the space dependent effective wave function $|\Psi(\mathbf{r})|^2 = \rho_s(\mathbf{r})/\rho$ was used as the order parameter of the transition at T_c (cf. section 1.3).

Despite the success of all these phenomenological models in describing different properties of superconductors, they were not able to clarify the microscopic mechanisms responsible for superconductivity. The first crucial microscopic progress was made in 1950. In this year H. Fröhlich [18] suggested that the interaction of crystal lattice vibrations and the electrons could be the basic phenomenon leading to superconductivity. The independent experimental discovery of the *isotope effect* in the same year by C.A. Reynolds *et al.* [19] and E. Maxwell [20, 21] gave strong support to this idea. They found that the critical temperature depends on the isotope mass M in the following way:

$$T_c \sim \frac{1}{M^\alpha} \quad \text{with } \alpha \simeq 0.5. \quad (1.1)$$

However, Fröhlich tried to treat the interaction in a perturbative way and ran into mathematical problems similarly to J. Bardeen [22] in 1951. The principal significance of these difficulties was first pointed out by Schafroth [23], who showed that the Meissner effect cannot be obtained in a perturbative treatment. Later Migdal [24] proved that at any finite order of perturbation theory the characteristic single particle energy excitation spectrum of a superconductor cannot be obtained in perturbation theory. These works already gave indications of the non-perturbative character of the phenomenon of superconductivity.

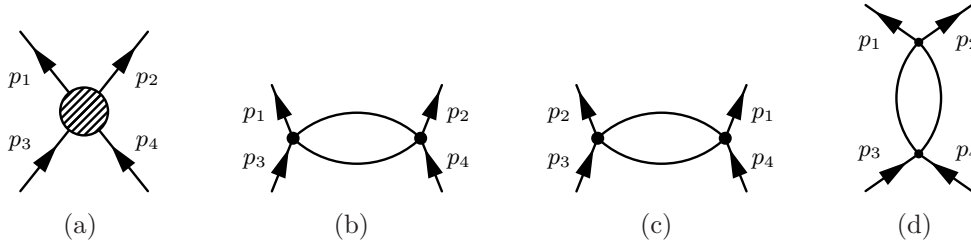


Figure 1.2.: The three many-body channels: a) $\Gamma(p_1, p_2, p_3, p_4)$, b) ZS channel, c) ZS' channel, d) BCS-channel

1.2. The Cooper Phenomenon

The next crucial step towards the final microscopic BCS-theory was the work of Cooper [25] in 1956, where it was shown that in the case of an attractive effective electron-electron interaction between states in the vicinity of the Fermi surface, the interacting pair forms a bound state. His arguments are quite general and independent of the strength of the interaction as long as it is attractive.

Of course, in nature the sign of the effective interaction between electrons depends on the ratio of the attractive electron-phonon interaction and the repulsive coulomb interaction. Usually it is very complicated to assess the relative strength of these two forces due to the complicated anisotropic crystal structures of the metals. Hence for simplicity for the following instructive discussion, the effective interaction is assumed to be weak, isotropic, spin independent and constant in the vicinity of the Fermi surface, whereas away from the Fermi surface the particles are assumed to be non-interacting (compare also [26]):

$$\hat{H}_I = \frac{g}{2} \sum_{\mathbf{p}_1 + \mathbf{p}_2 = \mathbf{p}_3 + \mathbf{p}_4} \hat{a}_{\mathbf{p}_1}^\dagger \hat{a}_{\mathbf{p}_2}^\dagger \hat{a}_{\mathbf{p}_3} \hat{a}_{\mathbf{p}_4} \Theta_{\mathbf{p}_1} \Theta_{\mathbf{p}_2} \Theta_{\mathbf{p}_3} \Theta_{\mathbf{p}_4} \quad (1.2)$$

with

$$\Theta_{\mathbf{p}} = \begin{cases} 1 & \text{for } |\varepsilon_{\mathbf{p}} - \mu| < \omega_\Lambda \\ 0 & \text{for } |\varepsilon_{\mathbf{p}} - \mu| > \omega_\Lambda \end{cases}, \quad |g| \ll 1$$

Bound states and collective modes appear as singularities of the four point vertex function $\Gamma(p_1, p_2, p_3, p_4)$ [15] (cf. Fig. 1.2). In general the calculation of the full two body vertex is a very complicated coupled problem. However, the diagrams of the particle-hole channels in Fig. 1.2 (b) and (c) only lead to singularities of the *zero sound* type [26] at small momentum transfers $q = p_1 - p_2 \rightarrow 0$, whereas the diagrams in the BCS channel Fig. 1.2 d) become singular for small values of the total four momentum $P = (P_0, \mathbf{P}) = p_1 + p_2$. The latter ones correspond precisely to the bound states found by Cooper in his work. The scattering equation for two interacting particles in a background of noninteracting fermions in the BCS

channel reads

$$\begin{aligned} \Gamma(p_1, p_2, p_3, p_4) &= \Gamma_0(p_1, p_2, p_3, p_4) + \\ &\frac{i}{2} \int \frac{d^4q}{(2\pi)^4} \Gamma_0(p_1, p_2, q, P - q) G_0(q) G_0(P - q) \Gamma(q, P - q, p_3, p_4), \end{aligned} \quad (1.3)$$

where Γ_0 is the irreducible part of Γ in the BCS channel. G_0 denotes the non-relativistic free propagator:

$$G_0(p) = \frac{\Theta(\varepsilon_{\mathbf{p}} - \mu)}{p_0 - \varepsilon_{\mathbf{p}} + i\eta} + \frac{\Theta(\mu - \varepsilon_{\mathbf{p}})}{p_0 - \varepsilon_{\mathbf{p}} - i\eta}, \quad (1.4)$$

where the first term describes the propagation of particles and the second the hole propagation.

The kernel Γ_0 contains by construction no singular terms for small P . For the present weak interaction model it can be shown [26] that Γ_0 can be replaced by the first order vertex g . The singular behaviour of the vertex Γ results from the particular properties of the particle-particle/hole-hole correlation function, whose momentum integral is restricted to the phase space, where the interaction is nonvanishing according to the interaction (1.2):

$$\begin{aligned} \frac{i}{2\pi} \int d^4q \Theta_{\mathbf{P}-\mathbf{q}} \Theta_{\mathbf{q}} G_0(q) G_0(P - q) &= \int d^3\mathbf{q} \Theta(\omega_{\Lambda} - |\xi_{\mathbf{q}}|) \Theta(\omega_{\Lambda} - |\xi_{\mathbf{P}-\mathbf{q}}|) \cdot \\ &\cdot \left[\frac{\Theta(\xi_{\mathbf{q}}) \Theta(\xi_{\mathbf{P}-\mathbf{q}})}{P_0 - \xi_{\mathbf{q}} - \xi_{\mathbf{P}-\mathbf{q}} + i\eta} - \frac{\Theta(-\xi_{\mathbf{q}}) \Theta(-\xi_{\mathbf{P}-\mathbf{q}})}{P_0 - \xi_{\mathbf{q}} - \xi_{\mathbf{P}-\mathbf{q}} - i\eta} \right], \end{aligned} \quad (1.5)$$

with $\xi_{\mathbf{p}} = \varepsilon_{\mathbf{p}} - \mu$. In the back-to-back case $\mathbf{P} = 0$ one finds for $|P_0| \ll \omega_{\Lambda}$:

$$\Gamma(p_1, p_2, p_3, p_4) = \Gamma(P_0) = \Gamma(\omega) = g \left[1 + g\nu(0) \left(\ln \left| \frac{2\omega_{\Lambda}}{\omega} \right| + \frac{i\pi}{2} \right) \right]^{-1}, \quad (1.6)$$

where $\nu(0) = \frac{mk_{\text{F}}}{2\pi^2}$ is the density of states at the Fermi surface, m the mass of the particles and k_{F} the Fermi momentum. Thus in the case of an attractive interaction ($g < 0$), we find two poles on the imaginary axis positioned symmetrically around the origin of the complex energy plane at the positions (cf. Fig. 1.3)

$$\omega^{\pm} = \pm 2i\omega_{\Lambda} \exp \left[-\frac{1}{|g|\nu(0)} \right]. \quad (1.7)$$

The distance $|\omega^{\pm}|$ from these two poles to the real axis is the binding energy 2Δ of the Cooper bound state. However, the fact that these bound states appear on non-physical Riemann sheets on the imaginary energy axis already indicates that the assumed ground state in the present problem cannot be realized in this form

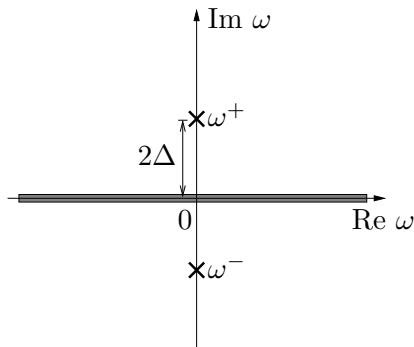


Figure 1.3.: Analytic structure of the vertex function $\Gamma(\omega)$ in the Cooper problem at zero CM momentum. The two poles ω^\pm are located on the imaginary axis symmetrically around the real axis. The cut of the logarithm in eq. (1.6), denoted by the grey area, extends over the entire real axis.

in nature, since one of the solutions in (1.7) necessarily leads to an instability in the time evolution of the system. Note also that the coupling constant g enters in a non-analytical way in the final result. This fact is just a formal expression of the non-perturbative nature of this problem as already mentioned above.

For finite and small \mathbf{P} the binding energy of the bound state is decreased [26]:

$$|\omega^\pm(\mathbf{P})| = 2\Delta - \frac{v_f |\mathbf{P}|}{2}. \quad (1.8)$$

The appearance of these bound states can be understood quite intuitively by considering the phase space integral (1.5) in more detail. The presence of the Fermi sea restricts the integrals to a small area around the Fermi surface. In this region the energy of the fermions is a *linear* function in momentum $\varepsilon_{\mathbf{q}} - \mu \sim \frac{k_F}{m}(|\mathbf{q}| - k_F)$. Hence for the radial phase space we can rewrite:

$$\mathbf{q}^2 d|\mathbf{q}| \sim d\varepsilon_{\mathbf{q}} m k_F \quad (1.9)$$

leading finally to logarithmic singularities in the vertex. In contrast, in the absence of a Fermi sea the single particle kinetic energies behave *quadratically* at the lower bound ($|\mathbf{q}| = 0$) of the phase space integral and we have an additional small factor

$$\mathbf{q}^2 d|\mathbf{q}| \sim d\varepsilon_{\mathbf{q}} m |\mathbf{q}|, \quad (1.10)$$

which cures the logarithmic singularities encountered above. Thus the Cooper bound states can be considered as an immediate consequence of the exclusion principle and are in this sense a general property of quantum mechanical many-body systems with attractive effective two body interactions. This situation is quite different compared to vacuum bound states. Here the presence of bound

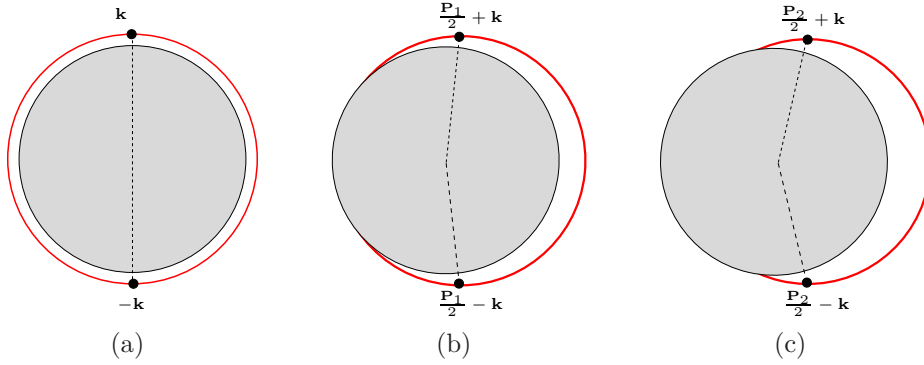


Figure 1.4.: Scattering of two particles in back-to-back kinematic (a) and at finite CM momentum (b) and (c) with $|\mathbf{P}_1| < |\mathbf{P}_2|$. The circle denotes the final state phase space. Analogous arguments apply to hole states around the Fermi surface.

states depends crucially on the strength of the particle interaction, i.e. there always exists a lower bound g_{\min} below which the interaction is no longer able to support a bound state. In contrast, in the present case the primary mechanism for the formation of the Cooper pairs is *not* based on the strength of the interaction, but only on the presence of the Fermi sea.

Also the fact that the bound state energy is a decreasing function with increasing central mass momentum of the interacting pair, can be easily understood by using phase space arguments. If two particle/holes are interacting in back-to-back kinematics both momenta of the final pair are located automatically outside/inside of the Fermi surface and consequently, there are no angular phase space restrictions. In contrast, for finite \mathbf{P} the final state phase space gets suppressed leading to a smaller binding energy of the pair. The situation is illustrated for two particles in Fig. 1.4.

1.3. The Superconducting Ground State

It should be emphasized again that the single pair problem discussed in the previous section has a *continuous* single particle energy spectrum without an energy gap around the Fermi surface since we can create arbitrarily low lying particle-hole excitations out of the Fermi sea. In nature however, all particles in the vicinity of the Fermi sea are subject to the Cooper phenomenon and no pair can be singled out as in Cooper's work. Hence, at first sight the physical situation has changed dramatically: instead of being an *independent-pair* problem, pairing in strongly correlated many-body systems is rather a problem of many *strongly interacting pairs*. Indeed, the smallest length scale in the pairing problem is inversely proportional to the value of the condensate Δ (cf. below): $\xi \sim v_f \Delta^{-1}$ [15].

Typical values for the correlation length ξ range from several times the interparticle distance up to thousands of times the interparticle distance, depending on the strength of the interaction. Thus the question arises, to what extent these strong overlaps of the wave functions destroy the concept of Cooper pairs.

This question can be addressed in the framework of Landau's Fermi Liquid theory [27, 28, 29]. The basic idea consists of introducing new effective degrees of freedom for low energy excitations around the Fermi surface, called *quasiparticles*. Due to phase space restrictions these quasiparticle states are well defined long lived excitations, as opposed to bare particles. Typically in superconducting/fluid systems the characteristic temperature T_L up to which the quasiparticle picture remains valid is much larger than the critical temperature T_c of the phase transition (e.g. in ^3He we have $T_L \sim 100\text{mK}$ and $T_c \sim 3\text{mK}$). Hence usually we have a *separation of energy scales*, the correlations, which determine the single-quasiparticle properties are energetically well separated from the typical energy scales of the Cooper problem [9].

Thus from the viewpoint of Fermi Liquid theory, Cooper's two-*particle* problem is actually a two-*quasiparticle* problem. Most of the correlations that could lead to the breakdown of the Cooper pair concept are included in the single quasiparticle effective degrees of freedom. The only remaining relevant quasiparticle interactions are:

- Forward scattering processes of two quasiparticles at the Fermi surface. These interactions are parametrized by the Landau-Parameters (cf. section 2.2).
- The residual quasiparticle pairing interaction, which is not included in the normal Fermi-Liquid theory, is responsible for the formation of quasiparticle Cooper pairs. Such a system is called a *superfluid Fermi liquid* [10, 30, 31].

Hence as a starting point for the construction of the superconducting ground state, it is quite reasonable to neglect at first all forward scattering processes, i.e. set all Landau-Parameters to zero. This approximation is usually called *pairing approximation* or *BCS-approximation*.

Each Cooper pair, being a bound state of two fermionic quasiarticles, can be described by an effective bosonic field. The system of all these bound states consequently forms a *Bose fluid*. By lowering the temperature, the thermal wavelength of the bosons increases until at a certain transition temperature, the strong overlap of the individual boson wave functions leads finally to the phenomenon of Bose-Einstein *condensation* [32, 33]. This state is characterized by the fact that a finite fraction of all particles in the system occupy a common quantum state, the *condensate*. The onset of this condensation process is accompanied by the spontaneous breakdown of the $U(1)$ symmetry of the system (cf. below). Generally, several such condensates could be present in bosonic many-body systems. In reality however, it turns out that only the condensate state with the lowest energy

(which is usually non-degenerate) survives (cf. also section 1.4), whereas all other instabilities are stabilized by this one condensate. Hence in the case of a superconductor, only the Cooper pairs with $\mathbf{P} = 0$ form a macroscopically populated condensate [34]. In technical terms that means that effectively only back-to-back interactions contribute to the pairing correlations, i.e. the system is described in this approximation in the case of spin-singlet pairing by the Hamiltonian

$$\hat{H}_{BCS} = \sum_{\mathbf{k}, \sigma} \varepsilon_{\mathbf{k}} \hat{a}_{\mathbf{k}\sigma}^\dagger \hat{a}_{\mathbf{k}\sigma} + \sum_{\mathbf{k}, \mathbf{k}'} \langle \mathbf{k}' - \mathbf{k}' | V | \mathbf{k} - \mathbf{k} \rangle \hat{a}_{\mathbf{k}'\uparrow}^\dagger \hat{a}_{-\mathbf{k}'\downarrow}^\dagger \hat{a}_{\mathbf{k}\uparrow} \hat{a}_{-\mathbf{k}\downarrow}, \quad (1.11)$$

with the quasiparticle field operators $\hat{a}_{\mathbf{k}\sigma}$ and the interaction matrix elements $\langle \mathbf{k}'_1 \mathbf{k}'_2 | V | \mathbf{k}_1 \mathbf{k}_2 \rangle$, where \mathbf{k}_i and \mathbf{k}'_i denote the initial and final momenta respectively. As the subscript suggests, this Hamiltonian forms the basis of the BCS-theory of superconductivity presented by Bardeen, Cooper and Schrieffer in 1957 [35]. The ground state and the ground state energy of this Hamiltonian can be determined in the mean field approximation most easily using the variational principle. Bardeen *et. al.* used the following Ansatz for the ground state:

$$|\psi_{BCS}^0\rangle = \prod_{\mathbf{k}} \left[u_{\mathbf{k}} + v_{\mathbf{k}} e^{i\phi} \hat{a}_{\mathbf{k}\uparrow}^\dagger \hat{a}_{-\mathbf{k}\downarrow}^\dagger \right] |0\rangle, \quad (1.12)$$

where $|0\rangle$ is the vacuum state and ϕ an arbitrary phase. This Ansatz is quite natural, since the state (1.12) is the most general uncorrelated many-body state that has non-vanishing amplitudes for even numbers of particles, where each pair occupies the states with the quantum numbers $(\mathbf{k} \uparrow, -\mathbf{k} \downarrow)$ in a singlet spin state. However, it should be emphasized that the number of particles of this state is not fixed. The coefficients $u_{\mathbf{k}}$ and $v_{\mathbf{k}}$ have to be chosen appropriately so that the *mean* number of particles has the required value N . By minimizing the free energy F , i.e.

$$\begin{aligned} \delta F &= \delta \langle \psi_{BCS}^0 | \hat{H}_{BCS} - \mu \sum_{\mathbf{k}, \sigma} \hat{a}_{\mathbf{k}\sigma}^\dagger \hat{a}_{\mathbf{k}\sigma} | \psi_{BCS}^0 \rangle \\ &= \delta \left[\sum_{\mathbf{k}} 2(\varepsilon_{\mathbf{k}} - \mu) v_{\mathbf{k}}^2 + \sum_{\mathbf{k}, \mathbf{k}'} \langle \mathbf{k}' - \mathbf{k}' | V | \mathbf{k} - \mathbf{k} \rangle u_{\mathbf{k}} v_{\mathbf{k}} u_{\mathbf{k}'} v_{\mathbf{k}'} \right] = 0, \end{aligned} \quad (1.13)$$

one finds

$$u_{\mathbf{k}}^2 = \frac{1}{2} \left[1 + \frac{\xi_{\mathbf{k}}}{\sqrt{\xi_{\mathbf{k}}^2 + \Delta_{\mathbf{k}}^2}} \right], \quad v_{\mathbf{k}}^2 = \frac{1}{2} \left[1 - \frac{\xi_{\mathbf{k}}}{\sqrt{\xi_{\mathbf{k}}^2 + \Delta_{\mathbf{k}}^2}} \right], \quad u_{\mathbf{k}}^2 + v_{\mathbf{k}}^2 = 1 \quad (1.14)$$

with $\xi_{\mathbf{k}} = \varepsilon_{\mathbf{k}} - \mu$ and the *gap-function* implicitly given by

$$\Delta_{\mathbf{k}} = - \sum_{\mathbf{k}'} \langle \mathbf{k}' - \mathbf{k}' | V | \mathbf{k} - \mathbf{k} \rangle u_{\mathbf{k}'} v_{\mathbf{k}'}. \quad (1.15)$$

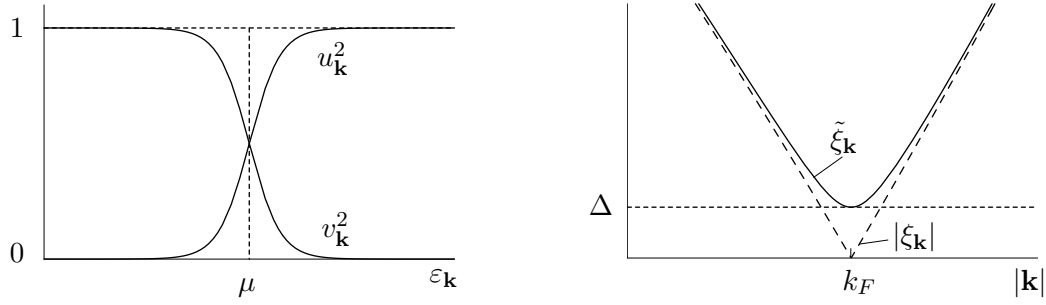


Figure 1.5.: Distribution function (left) and the one-particle energies (right) in a superfluid.

In the case of a repulsive interaction around the Fermi surface, eq. (1.15) has only the trivial solution $\Delta_{\mathbf{k}} = 0$ and the functions $u_{\mathbf{k}}$ and $v_{\mathbf{k}}$ reduce to the normal distribution functions $\Theta(-\xi_{\mathbf{k}})$ and $\Theta(\xi_{\mathbf{k}})$. For certain attractive interactions however, the gap equation also possesses nontrivial solutions $\Delta_{\mathbf{k}}$. In this case the superconducting ground state is usually energetically favoured and thus realized in nature. This state is characterized by a smeared out Fermi surface due to the formation of Cooper pairs and the amount of energy needed to break up one bound state appears as an energy gap $\Delta_{\mathbf{k}}$ in the single particle excitation spectrum (see Fig. 1.5).

For the understanding of the nature of the elementary excitations, it is crucial to note that the BCS-ground state $|\psi_{BCS}^0\rangle$ is *not* a many-body state with a definite number of particles. That implies that the action of particle operators and hole operators on this state can yield the same state. In fact, the states $\hat{a}_{\mathbf{k}\uparrow}^\dagger |\psi_{BCS}^0\rangle$ and $\hat{a}_{-\mathbf{k}\downarrow} |\psi_{BCS}^0\rangle$ are *identical* up to numerical factors:

$$\hat{a}_{\mathbf{k}\uparrow}^\dagger |\psi_{BCS}^0\rangle = u_{\mathbf{k}} |\psi_{\mathbf{k}\uparrow}\rangle, \quad \hat{a}_{-\mathbf{k}\downarrow} |\psi_{BCS}^0\rangle = -v_{\mathbf{k}} |\psi_{\mathbf{k}\uparrow}\rangle, \quad (1.16)$$

with $|\psi_{\mathbf{k}\uparrow}\rangle = \hat{a}_{\mathbf{k}\uparrow} \prod_{\mathbf{p} \neq \mathbf{k}} [u_{\mathbf{p}} + v_{\mathbf{p}} \hat{a}_{\mathbf{p}\uparrow}^\dagger \hat{a}_{-\mathbf{p}\downarrow}] |0\rangle$.

Thus it is quite natural to combine these two operators into one new operator that creates the normalized state $|\psi_{\mathbf{k}\uparrow}\rangle$. These were first introduced independently by Bogoliubov [36] and Valatin [37]:

$$\begin{aligned} \hat{\gamma}_{\mathbf{k}\uparrow}^\dagger &= u_{\mathbf{k}} \hat{a}_{\mathbf{k}\uparrow}^\dagger - v_{\mathbf{k}} \hat{a}_{-\mathbf{k}\downarrow}, & \hat{\gamma}_{\mathbf{k}\downarrow}^\dagger &= u_{\mathbf{k}} \hat{a}_{\mathbf{k}\downarrow}^\dagger + v_{\mathbf{k}} \hat{a}_{-\mathbf{k}\uparrow} \\ \hat{a}_{\mathbf{k}\uparrow}^\dagger &= u_{\mathbf{k}} \hat{\gamma}_{\mathbf{k}\uparrow}^\dagger + v_{\mathbf{k}} \hat{\gamma}_{-\mathbf{k}\downarrow}, & \hat{a}_{\mathbf{k}\downarrow}^\dagger &= u_{\mathbf{k}} \hat{\gamma}_{\mathbf{k}\downarrow}^\dagger - v_{\mathbf{k}} \hat{\gamma}_{-\mathbf{k}\uparrow}. \end{aligned} \quad (1.17)$$

The states created by these operators are usually called *Bogoliubov quasiparticles*. In order to avoid confusion with the quasiparticles of Landau's Fermi Liquid theory, we will in the following denote the Fermi-Liquid quasiparticle states, created by the operators \hat{a}^\dagger , as *particles*, whereas the states $|\psi_{\mathbf{k}\uparrow}\rangle$ and $|\psi_{-\mathbf{k}\downarrow}\rangle$ that are created by $\hat{\gamma}^\dagger$ as *quasiparticles*.

Since the transformation (1.17) is canonical the new operators still obey the usual Fermi-anticommutator relations. In this basis the BCS-Hamiltonian (1.11) reads (cf. also [15])

$$\hat{H}_{BCS} = \sum_{\mathbf{k}} 2\xi_{\mathbf{k}} v_{\mathbf{k}}^2 + \sum_{\mathbf{k}, \mathbf{k}'} \langle \mathbf{k}' - \mathbf{k}' | V | \mathbf{k} - \mathbf{k} \rangle u_{\mathbf{k}} v_{\mathbf{k}} u_{\mathbf{k}'} v_{\mathbf{k}'} + \sum_{\mathbf{k}, \sigma} \tilde{\xi}_{\mathbf{k}} \hat{\gamma}_{\mathbf{k}\sigma}^{\dagger} \hat{\gamma}_{\mathbf{k}\sigma} + \hat{V}_{QP}, \quad (1.18)$$

with

$$\tilde{\xi}_{\mathbf{k}} = \sqrt{\xi_{\mathbf{k}}^2 + \Delta_{\mathbf{k}}^2}. \quad (1.19)$$

The term \hat{V}_{QP} represents terms with four quasiparticle operators and clearly describes the interaction between the quasiparticles. Since the BCS-ground state is the quasiparticle vacuum state, i.e.

$$\hat{\gamma}_{\mathbf{k}\uparrow} |\psi_{BCS}^0\rangle = \hat{\gamma}_{\mathbf{k}\downarrow} |\psi_{BCS}^0\rangle = 0, \quad (1.20)$$

in eq. (1.18) one can directly read off the ground state energy and the excitation spectrum. However, the relations (1.17) can be quite misleading for the quantum mechanical interpretation of the quasiparticle excitation, because they suggest at first sight that a quasiparticle is a *superposition* of a particle and a hole. However, this is *not true*. In fact, in a many-body system with a fixed number N of particles, the quasiparticle excitation created by $\hat{\gamma}_{\mathbf{k}\uparrow}^{\dagger}$ consists of a particle occupying state $(\mathbf{k} \uparrow)$, whereas its mate state $(-\mathbf{k} \downarrow)$ is empty. Only the fact that the *BCS*-ground state is an ensemble of states with different particle numbers leads to the situation that one state can be created by different operators (cf. eq. (1.16)) and consequently the quasiparticle creation operators are a sum of a particle and a hole operators.

The breakdown of the global $U(1)$ symmetry

$$\hat{a}_{\mathbf{k}\sigma}^{\dagger} \rightarrow \hat{a}_{\mathbf{k}\sigma}^{\dagger} e^{i\lambda} \quad (1.21)$$

in a superfluid or superconductor is formally expressed by the finite expectation value of the order parameter

$$\Psi(\mathbf{r}) = \langle \psi_{BCS}^0 | \hat{\psi}_{\uparrow}^{\dagger}(\mathbf{r}) \hat{\psi}_{\downarrow}^{\dagger}(\mathbf{r}) | \psi_{BCS}^0 \rangle, \quad \hat{\psi}_{\sigma}^{\dagger}(\mathbf{r}) = \frac{1}{\sqrt{V}} \sum_{\mathbf{k}} e^{-i\mathbf{k}\mathbf{r}} \hat{a}_{\mathbf{k}\sigma}^{\dagger}. \quad (1.22)$$

The transformation (1.21) connects all possible energetically degenerated BCS states (1.12), each labeled by the phase ϕ . The spontaneous breakdown of the symmetry leads to important differences in charged and neutral systems. Since the charged particles in a superconductor couple to the gauge field, the Goldstone boson of the broken symmetry loses its physical significance ("is eaten up by the gauge boson") and can be removed completely from the theory by a gauge transformation. In contrast, in a electrically neutral system the Goldstone excitations

appear as massless excitations in the system (cf. next section). Physically these excitations correspond to slow variations of ϕ in space, in complete analogy to the spin-wave excitations in ferromagnets.

1.4. From Superconductivity to Superfluidity

From a modern point of view the phenomenon of superconductivity is nothing else but a special form of superfluidity occurring in a system consisting of charged particles. Thus essentially all microscopical mechanisms described in the previous sections also apply to superfluid systems. In general, one can divide superfluid systems into different classes:

- Neutral Bose systems (^4He , ^{23}Na , ^{87}Rb)
- Neutral BCS-paired Fermi systems (^3He , ^6Li , ^{40}K , neutrons in nuclear matter)
- Charged BCS-paired Fermi systems, i.e. superconducting systems (electrons in metals, protons in nuclear matter, color-superconductivity in quark matter)
- Bosonic superconductors (charged pion condensates)

Apart from the last class, all types of superfluids have been observed in nature. The original observation of superfluidity was made in the Bose liquid ^4He by Kapitza [38] in 1937, who observed for the first time the λ -transition from the normal to a new state, characterized by a very small viscosity at $T_c = 2.17\text{ K}$. In the same year he introduced the name *superfluid* for the new state. Only a few months later J.F. Allen and A.D. Misener [39] measured the flow rate of ^4He through a capillary with varying radii and fluid velocities. They found that "the observed type of flow cannot be treated as laminar nor turbulent" and concluded that the hydrodynamics of helium below T_c cannot be explained classically. Only another two month later F. London [40] proposed Bose-Einstein-Condensation (BEC) to be the underlying microscopic mechanism leading to superfluidity. However, at that time BEC, predicted theoretically by Einstein [32, 33] only a few years before for a gas of noninteracting bosons, was still believed to be a pathological effect that disappears in the presence of particle interactions. On the basis of Einstein's calculation London obtained a transition temperature of 3.3 K by treating the helium system as a noninteracting gas.

Inspired by the model of London, Gorter and Casimir [13, 14] for superconductors, in the same year, Tisza [41] presented a phenomenological two-fluid model for superfluids. The superfluid part shows zero entropy and viscosity, whereas the normal part behaves like a common liquid. This model was able to explain the observed fountain effect observed by Allen and Jones [42] and predicted thermal wave excitations, called second sound, where these two fluids oscillate out of

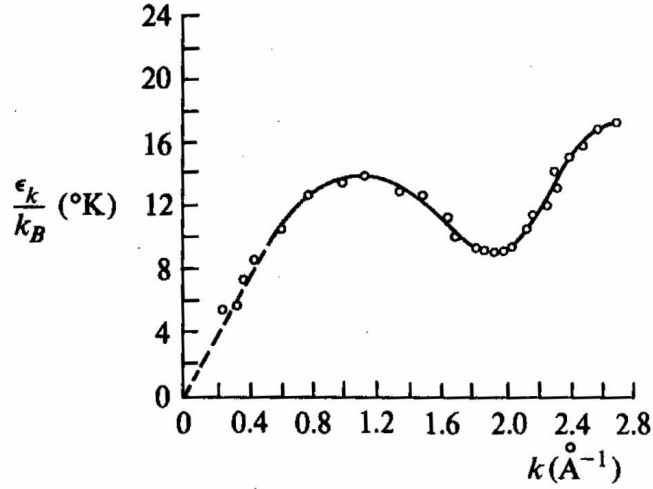


Figure 1.6.: Excitation spectrum of ${}^4\text{He}$ (figure taken from [15], data points of [46]), solid line: fit of measured points. The linear part at small momenta shows the phonon branch $\varepsilon_k = c_p k$ whereas the roton branch behaves like $\varepsilon_k = \Delta + c_r (k - k_0)^2$ with $k_0 \sim 2 \text{ \AA}^{-1}$.

phase. Later, in 1941 Landau [43] refined this model and predicted the existence of *roton* excitations, a new branch in the excitation spectrum of the liquid (cf. Fig. 1.6). Furthermore he predicted the existence of a critical fluid velocity v_c , below which the viscosity of the fluid vanishes, only by assuming the typical linear dispersion law for the low momentum phonon excitation branch, representing the Goldstone excitations in the system (cf. previous section).

The complete disregard of London's BEC idea however, led to many controversies between London and Landau in the following years. The first step toward the unification of their two approaches was made by the work of Bogoliubov [44] in 1947. He showed that if one *assumes* that a weakly coupled Bose system with a repulsive interaction undergoes BEC, the postulated phonon excitation spectrum of Landau's model is an immediate consequence of Bose statistics. Despite this nice insight, in nature the ${}^4\text{He}$ -liquid is far from being a weakly coupled system and the question arises, to what extent this result can be taken seriously for the He system. This question was answered in 1956 by Feynman and Cohen [45], who could verify the results of Bogoliubov by using a variational approach and could furthermore show explicitly that the transition from the phonon branch to the roton branch is continuous (cf. Fig. 1.6). The latter result could also be verified later experimentally in neutron scattering experiments [46].

In the light of these works it turned out that all the postulates of Landau on the ground state can be understood as a natural consequence of BEC and in essence the two approaches are not contradicting but rather supplementing each other. From the present viewpoint, the basic assumption for the understanding

of superfluidity is the presence of *one and only one* single-particle state that is populated by a finite fraction of all particles, called *condensate*. Apart from noninteracting bosonic systems, this basic assumption usually cannot be justified rigorously for more realistic systems. However, after taking this fact for granted, one can understand the basic properties of liquid ${}^4\text{He}$ from first principles [47, 48].

Thus the microscopic mechanisms in superconductors and ${}^4\text{He}$ are closely related. In Fermi systems, the formation of Cooper pairs and the condensation of these states are not two distinct processes, but occur simultaneously. The role of the BEC condensate wave function in ${}^4\text{He}$ is the analog to the center of mass wave function of the Cooper pairs in Fermi systems. Indeed, in 1972 Osheroff, Richardson and Lee [3, 49] found that ${}^3\text{He}$ also becomes superfluid below 3 mK , i.e. at a transition temperature which is three orders of magnitude smaller than in ${}^4\text{He}$. This large difference can be quite easily understood by noting that the Cooper pairs in ${}^3\text{He}$ are only very loosely bound states compared to the nuclear bound ${}^4\text{He}$ particles.

1.5. Superfluidity in Neutron Matter

Strictly speaking, the statement above that Osheroff *et al.* were the first to observe superfluidity in fermionic systems is actually not quite correct. Many years before, measurements of different nuclei showed significant signals of systematic mass differences between even-even, even-odd and odd-odd nuclei and typical energy gaps of 1 MeV for the first excited states in even-even nuclei [2]. (Of course, atomic nuclei are actually not electrically neutral. However since the nuclear force is charge independent to first approximation, atomic nuclei can be considered as a neutral Fermi system in this context) These observations lead Bohr, Mottelson and Pines [51] in 1958, i.e. right after the publication of the BCS-theory, to the suggestion that similar mechanisms could be active in nuclei as in BCS superconductors.

The first detailed microscopic description of this effect was published one year later by Migdal [52, 53], who explicitly suggested neutron matter as a natural candidate for a superfluid. He presented the first microscopic calculations based on the BCS-theory for nuclear systems and pointed out the importance of pairing for the properties of stellar objects like neutron stars. However due to the particular properties of the NN-interaction (cf. Introduction) and the fact that nuclear matter is a *strongly interacting* Fermi system, the following questions are raised:

- Does an interaction with a hard core like the nucleon-nucleon interaction allow in principle the presence of superfluidity?
- If superfluidity is possible, to what extent are the results of the BCS-approximation quantitatively valid and how can one improve, if necessary, the approximation to achieve reliable answers?

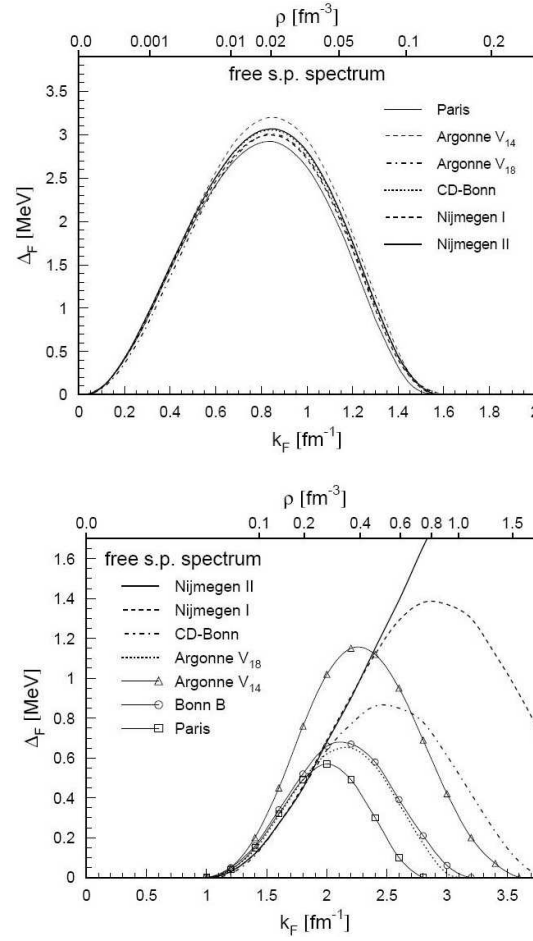


Figure 1.7.: Pairing gaps in neutron matter as a function of density in the 1S_0 channel (upper plot) and in the triplet channel $^3P_2 - ^3F_2$ (lower plot). Plots taken from [50]

This first question was investigated by Cooper, Mills and Sessler [54] in 1959 and refined one year later by Emery and Sessler [55], who showed, based on a variational approach that the BCS formalism can indeed be successfully applied to nuclear matter and superfluidity is possible for this kind of interaction. Indeed, in the following decades some experimental indications were also found for the presence of superfluid phases in neutron stars were found:

- *Pulsar glitches*: The spin down rate after glitches, the sudden increase of the rotation speed in neutron stars, can only be understood in the presence of superfluid phases [56, 57, 58]. The observed relaxation times are orders of magnitude too large for normal systems.
- *Cooling rates*: Superfluidity plays a central role for neutrino emission mechanisms, the basic cooling process in neutron stars. Although the theoretical

calculations of cooling rates involve many uncertainties, the models seem to favour the presence of superfluidity [59, 60, 61, 62].

The second question however is much more difficult to answer and is still unsettled today. However, the simplicity and crudeness of the BCS approximation suggests that for the typical densities in neutron stars the standard BCS scheme does not give reliable quantitative results. Due to the strong interparticle correlations, the nucleons participating in the pairing coupling screen the pairing correlations at the same time. Since the size of the gap depends exponentially on the strength of the interaction, the inclusion of these many-body effects is absolutely crucial in realistic calculations.

However, despite these complicated problems, it can be quite instructive to treat superfluid nuclear matter using some simple approximations. Some quite common approximations are:

- Use the free single particle energies $\xi_{\mathbf{k}} = \xi_{\mathbf{k}}^0 = \mathbf{k}^2/(2m) - k_{\text{F}}^2/(2m)$ where m is the nucleon free mass or an effective mass. All further self-energy corrections are neglected.
- Replace the pairing interaction by a free vacuum interaction. All many-body vertex corrections are neglected.

After expanding the gap equation in partial waves, the solution of the equation (1.15) is in principle straightforward. Nonvanishing gaps can be found for the different potential models in the singlet channel $^1\text{S}_0$ [63, 64, 65, 66, 67] and the coupled triplet channel $^3\text{P}_2 - ^3\text{F}_2$ [50, 68, 69, 70]. The corresponding results for the gaps are shown in Fig. 1.7 for different potentials as a function of density. It is quite remarkable that in this approximation scheme all interaction models provide almost the same gaps as a function of density in the $^1\text{S}_0$ channel. We will investigate this property in more detail in chapter 2.4.

In the $^3\text{P}_2 - ^3\text{F}_2$ channel one finds in this approximation nonvanishing gaps at higher densities. At these momentum scales the NN-interaction, which is only fitted up to energies of 350 MeV (or $k \sim 2.1 \text{ fm}^{-1}$) in the CM frame, is not well constrained anymore and leads consequently to a much larger model dependence in the gap function.

1.6. Nambu-Gorkov Propagators

Due to the presence of a condensate in a many-body system, the propagation of particles (i.e. Landau-quasiparticles) through the system becomes more complex compared to normal systems. If we assume that at time $t = 0$ a particle is present with momentum \mathbf{k} , there are two contributions to the propagator (if we neglect finite lifetime effects of the particles at this point):

$$\mathbf{G}^{(BCS)} = \begin{pmatrix} G^{(BCS)} & F^{(BCS)} \\ F^{\dagger(BCS)} & G^{- (BCS)} \end{pmatrix} = \begin{pmatrix} \uparrow & \downarrow \\ \downarrow & \uparrow \end{pmatrix}$$

Figure 1.8.: Diagrammatical representation of the one-body Nambu-Gorkov propagators (1.27).

- a) The particle propagates as in a normal Fermi-liquid, i.e. we still find a particle with momentum \mathbf{k} at time $t' > t$.
- b) The particle interacts with the condensate and is thus transformed into a hole at $t' > t$, i.e. the number of particles in the system is reduced by two. The presence of these processes is an immediate consequence of the finite expectation value of the order parameter (cf. section 1.3):

$$\langle \psi_{BCS}^0 | \hat{a}_{\mathbf{k}\uparrow}^\dagger \hat{a}_{-\mathbf{k}\downarrow}^\dagger | \psi_{BCS}^0 \rangle = u_{\mathbf{k}} v_{\mathbf{k}} = \frac{\Delta_{\mathbf{k}}}{2\tilde{\xi}_{\mathbf{k}}} \quad (1.23)$$

and leads to the characteristic smearing of the Fermi surface (cf. Fig. 1.5).

Due to this particle-hole mixing, the one-body propagator acquires additional *anomalous* elements. In contrast to normal systems where particle states form a complete basis of the one-body propagator, the basis in superfluids contains two states. For example one could choose the states $\hat{a}_{\mathbf{k}\uparrow}^\dagger | \psi_{BCS}^0 \rangle$ and $\hat{a}_{-\mathbf{k}\downarrow} | \psi_{BCS}^0 \rangle$. These states span a complete basis for the one-body propagator:

$$i\mathbf{G}^{(BCS)}(\mathbf{k}, t) = \begin{pmatrix} \langle \psi_{BCS}^0 | T \hat{a}_{\mathbf{k}\uparrow}(t) \hat{a}_{\mathbf{k}\uparrow}^\dagger | \psi_{BCS}^0 \rangle & \langle \psi_{BCS}^0 | T \hat{a}_{\mathbf{k}\uparrow}(t) \hat{a}_{-\mathbf{k}\downarrow} | \psi_{BCS}^0 \rangle \\ \langle \psi_{BCS}^0 | T \hat{a}_{-\mathbf{k}\downarrow}^\dagger(t) \hat{a}_{\mathbf{k}\uparrow}^\dagger | \psi_{BCS}^0 \rangle & \langle \psi_{BCS}^0 | T \hat{a}_{-\mathbf{k}\downarrow}^\dagger(t) \hat{a}_{-\mathbf{k}\downarrow} | \psi_{BCS}^0 \rangle \end{pmatrix} \quad (1.24)$$

The elements can be most easily calculated by first evaluating the corresponding quasiparticle propagator

$$i\mathcal{G}^{(BCS)}(\mathbf{k}, t) = \begin{pmatrix} \langle \psi_{BCS}^0 | T \hat{\gamma}_{\mathbf{k}\uparrow}(t) \hat{\gamma}_{\mathbf{k}\uparrow}^\dagger | \psi_{BCS}^0 \rangle & \langle \psi_{BCS}^0 | T \hat{\gamma}_{\mathbf{k}\uparrow}(t) \hat{\gamma}_{-\mathbf{k}\downarrow} | \psi_{BCS}^0 \rangle \\ \langle \psi_{BCS}^0 | T \hat{\gamma}_{-\mathbf{k}\downarrow}^\dagger(t) \hat{\gamma}_{\mathbf{k}\uparrow}^\dagger | \psi_{BCS}^0 \rangle & \langle \psi_{BCS}^0 | T \hat{\gamma}_{-\mathbf{k}\downarrow}^\dagger(t) \hat{\gamma}_{-\mathbf{k}\downarrow} | \psi_{BCS}^0 \rangle \end{pmatrix} \quad (1.25)$$

which takes a very simple diagonal form:

$$\mathcal{G}^{(BCS)}(\mathbf{k}, \omega) = \begin{pmatrix} \frac{1}{\omega - \tilde{\xi}_{\mathbf{k}} + i\delta} & 0 \\ 0 & \frac{1}{\omega + \tilde{\xi}_{\mathbf{k}} - i\delta} \end{pmatrix}. \quad (1.26)$$

Note that the quasiparticle propagator is independent of the spin.

By transforming this matrix into the normal basis by using the transformation

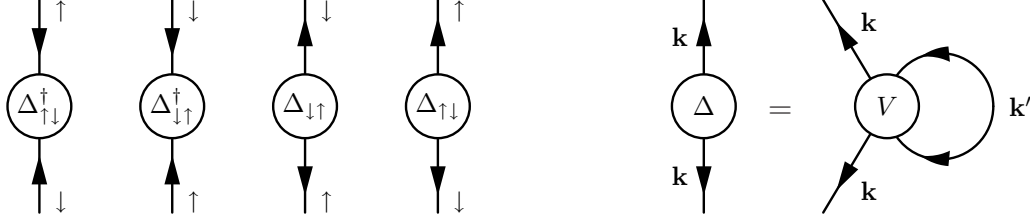


Figure 1.9.: Diagrammatic representation of the gap functions and the BCS gap equation (1.15), where V is the bare back-to-back interparticle interaction.

(1.17), one easily obtains (cf. Fig. 1.8):

$$\begin{aligned}
\mathbf{G}^{(BCS)}(\mathbf{k}, \omega) &\equiv \begin{pmatrix} G^{(BCS)}(\mathbf{k}, \omega) & F^{(BCS)}(\mathbf{k}, \omega) \\ F^{\dagger(BCS)}(\mathbf{k}, \omega) & G^{- (BCS)}(\mathbf{k}, \omega) \end{pmatrix} \\
&= \begin{pmatrix} G_{\uparrow\uparrow}^{(BCS)}(\mathbf{k}, \omega) & F_{\uparrow\downarrow}^{(BCS)}(\mathbf{k}, \omega) \\ F_{\downarrow\uparrow}^{\dagger(BCS)}(\mathbf{k}, \omega) & G_{\downarrow\downarrow}^{- (BCS)}(\mathbf{k}, \omega) \end{pmatrix} \\
&= \frac{1}{\omega - \tilde{\xi}_{\mathbf{k}} + i\delta} \begin{pmatrix} u_{\mathbf{k}}^2 & -u_{\mathbf{k}}v_{\mathbf{k}} \\ -u_{\mathbf{k}}v_{\mathbf{k}} & v_{\mathbf{k}}^2 \end{pmatrix} \\
&\quad + \frac{1}{\omega + \tilde{\xi}_{\mathbf{k}} - i\delta} \begin{pmatrix} v_{\mathbf{k}}^2 & u_{\mathbf{k}}v_{\mathbf{k}} \\ u_{\mathbf{k}}v_{\mathbf{k}} & u_{\mathbf{k}}^2 \end{pmatrix} \quad (1.27)
\end{aligned}$$

with $G^{- (BCS)}(\mathbf{k}, \omega) = -G^{(BCS)}(\mathbf{k}, -\omega)$. In the case of real gaps, we have also $F^{\dagger(BCS)}(\mathbf{k}, \omega) = F^{(BCS)}(\mathbf{k}, \omega)$.

Note that due to the spin dependence of the transformation (1.17), this propagator depends on the spin, in contrast to the quasiparticle propagator above:

$$\begin{aligned}
G^{(BCS)}(\mathbf{k}, \omega) &= G_{\uparrow\uparrow}^{(BCS)}(\mathbf{k}, \omega) = G_{\downarrow\downarrow}^{(BCS)}(\mathbf{k}, \omega), \\
F^{\dagger(BCS)}(\mathbf{k}, \omega) &= F_{\downarrow\uparrow}^{\dagger(BCS)}(\mathbf{k}, \omega) = -F_{\uparrow\downarrow}^{\dagger(BCS)}(\mathbf{k}, \omega), \\
F^{(BCS)}(\mathbf{k}, \omega) &= F_{\uparrow\downarrow}^{(BCS)}(\mathbf{k}, \omega) = -F_{\downarrow\uparrow}^{(BCS)}(\mathbf{k}, \omega), \quad (1.28)
\end{aligned}$$

whereas all remaining one-particle propagators are vanishing. The analogous spin dependence appears in the gap function:

$$\begin{aligned}
\Delta_{\mathbf{k}\uparrow\downarrow}^{\dagger} &= 2\tilde{\xi}_{\mathbf{k}} \langle \psi_{BCS}^0 | \hat{a}_{\mathbf{k}\uparrow}^{\dagger} \hat{a}_{-\mathbf{k}\downarrow}^{\dagger} | \psi_{BCS}^0 \rangle = -\Delta_{\mathbf{k}\downarrow\uparrow}^{\dagger} \\
\Delta_{\mathbf{k}\uparrow\downarrow} &= 2\tilde{\xi}_{\mathbf{k}} \langle \psi_{BCS}^0 | \hat{a}_{\mathbf{k}\uparrow} \hat{a}_{-\mathbf{k}\downarrow} | \psi_{BCS}^0 \rangle = -\Delta_{\mathbf{k}\downarrow\uparrow}, \quad (1.29)
\end{aligned}$$

whereas the gap functions are related by

$$\Delta_{\mathbf{k}} \equiv \Delta_{\mathbf{k}\uparrow\downarrow}^{\dagger} = \Delta_{\mathbf{k}\downarrow\uparrow} = -\Delta_{\mathbf{k}\downarrow\uparrow}^{\dagger} = -\Delta_{\mathbf{k}\uparrow\downarrow}. \quad (1.30)$$

The corresponding two-particle propagator can be separated into a disconnected free part, describing the free propagation of two particles and a interaction part, parametrizing the scattering of the two particles, i.e. schematically (we use a similar notation as that used in ref. [71])

$$\mathbf{K}(1, 2, 3, 4) = \mathbf{G}\mathbf{G}(1, 2, 3, 4) + \delta\mathbf{K}(1, 2, 3, 4). \quad (1.31)$$

At this point we are only interested in the free part $\mathbf{G}\mathbf{G}$. This part is needed for the determination of the interaction part $\delta\mathbf{K}$ as discussed in the next section. For the calculation of $\mathbf{G}\mathbf{G}$, we consider the propagation of a pair of states with total momentum $\mathbf{k}_1 + \mathbf{k}_2 = \mathbf{P}$. Due to the presence of the condensate, this state can be a particle-particle (pp), particle-hole (ph), hole-particle (hp) or a hole-hole (hh) state. A quasiparticle spin singlet and triplet state can be represented in terms of the field operators as follows:

$$\begin{aligned} |\mathbf{k}_1, \mathbf{k}_2; S = 0, M_s = 0\rangle_{QP} &= \frac{1}{\sqrt{2}} \left[\hat{\gamma}_{\mathbf{k}_1\uparrow}^\dagger \hat{\gamma}_{\mathbf{k}_2\downarrow}^\dagger - \hat{\gamma}_{\mathbf{k}_1\downarrow}^\dagger \hat{\gamma}_{\mathbf{k}_2\uparrow}^\dagger \right] |\psi_{BCS}^0\rangle \\ |\mathbf{k}_1, \mathbf{k}_2; S = 1, M_s = 1\rangle_{QP} &= \hat{\gamma}_{\mathbf{k}_1\uparrow}^\dagger \hat{\gamma}_{\mathbf{k}_2\uparrow}^\dagger |\psi_{BCS}^0\rangle \\ |\mathbf{k}_1, \mathbf{k}_2; S = 1, M_s = 0\rangle_{QP} &= \frac{1}{\sqrt{2}} \left[\hat{\gamma}_{\mathbf{k}_1\uparrow}^\dagger \hat{\gamma}_{\mathbf{k}_2\downarrow}^\dagger + \hat{\gamma}_{\mathbf{k}_1\downarrow}^\dagger \hat{\gamma}_{\mathbf{k}_2\uparrow}^\dagger \right] |\psi_{BCS}^0\rangle \\ |\mathbf{k}_1, \mathbf{k}_2; S = 1, M_s = -1\rangle_{QP} &= \hat{\gamma}_{\mathbf{k}_1\downarrow}^\dagger \hat{\gamma}_{\mathbf{k}_2\downarrow}^\dagger |\psi_{BCS}^0\rangle \end{aligned} \quad (1.32)$$

In order to see more explicitly the different contributions included in these two-quasiparticle states, let us consider the $M_s = 0$ states in more detail:

$$\begin{aligned} &\frac{1}{\sqrt{2}} \left[\hat{\gamma}_{\mathbf{k}_1\uparrow}^\dagger \hat{\gamma}_{\mathbf{k}_2\downarrow}^\dagger \mp \hat{\gamma}_{\mathbf{k}_1\downarrow}^\dagger \hat{\gamma}_{\mathbf{k}_2\uparrow}^\dagger \right] |\psi_{BCS}^0\rangle \\ &= \frac{u_{\mathbf{k}_1} u_{\mathbf{k}_2}}{\sqrt{2}} \left[\hat{a}_{\mathbf{k}_1\uparrow}^\dagger \hat{a}_{\mathbf{k}_2\downarrow}^\dagger \mp \hat{a}_{\mathbf{k}_1\downarrow}^\dagger \hat{a}_{\mathbf{k}_2\uparrow}^\dagger \right] |\psi_{BCS}^0\rangle \\ &\quad + \frac{u_{\mathbf{k}_1} v_{\mathbf{k}_2}}{\sqrt{2}} \left[\hat{a}_{\mathbf{k}_1\uparrow}^\dagger \hat{a}_{-\mathbf{k}_2\uparrow} \pm \hat{a}_{\mathbf{k}_1\downarrow}^\dagger \hat{a}_{-\mathbf{k}_2\downarrow} \right] |\psi_{BCS}^0\rangle \\ &\quad - \frac{v_{\mathbf{k}_1} u_{\mathbf{k}_2}}{\sqrt{2}} \left[\hat{a}_{-\mathbf{k}_1\downarrow} \hat{a}_{\mathbf{k}_2\downarrow}^\dagger \pm \hat{a}_{-\mathbf{k}_1\uparrow} \hat{a}_{\mathbf{k}_2\uparrow}^\dagger \right] |\psi_{BCS}^0\rangle \\ &\quad - \frac{v_{\mathbf{k}_1} v_{\mathbf{k}_2}}{\sqrt{2}} \left[\hat{a}_{-\mathbf{k}_1\downarrow} \hat{a}_{-\mathbf{k}_2\uparrow} \mp \hat{a}_{-\mathbf{k}_1\uparrow} \hat{a}_{-\mathbf{k}_2\downarrow} \right] |\psi_{BCS}^0\rangle \\ &= u_{\mathbf{k}_1} u_{\mathbf{k}_2} |\psi_{\mathbf{k}_1\mathbf{k}_2}^{pp}\rangle + u_{\mathbf{k}_1} v_{\mathbf{k}_2} |\psi_{\mathbf{k}_1\mathbf{k}_2}^{ph}\rangle - v_{\mathbf{k}_1} u_{\mathbf{k}_2} |\psi_{\mathbf{k}_1\mathbf{k}_2}^{hp}\rangle - v_{\mathbf{k}_1} v_{\mathbf{k}_2} |\psi_{\mathbf{k}_1\mathbf{k}_2}^{hh}\rangle. \end{aligned} \quad (1.33)$$

Hence the quasiparticle spin singlet (triplet) state is clearly a mixture of pp , ph , hp and hh singlet (triplet) states, whereas the different distribution functions give the relative weights of the contributions. This implies that the pp , ph , hp and hh singlet/triplet states form a complete basis of states for the propagation of these

states in superfluids, i.e. a singlet (triplet) state remains a singlet (triplet) state under interaction with the condensate.

For the explicit evaluation of the propagators, it is convenient to calculate first the quasiparticle propagator \mathcal{GG} . For this, we choose the following set of complete quasiparticle operators for the $M_s = 0$ propagator (the $M_s = \pm 1$ case is done in complete analogy) describing the propagation of a singlet/triplet state with the momentum $\mathbf{P} = \mathbf{k}_1 + \mathbf{k}_2$:

$$\hat{\mathcal{A}}_1^\dagger = \hat{\gamma}_{\mathbf{k}_1\uparrow}^\dagger \hat{\gamma}_{\mathbf{k}_2\downarrow}^\dagger, \quad \hat{\mathcal{A}}_2^\dagger = \hat{\gamma}_{\mathbf{k}_1\uparrow}^\dagger \hat{\gamma}_{-\mathbf{k}_2\uparrow}^\dagger, \quad \hat{\mathcal{A}}_3^\dagger = \hat{\gamma}_{-\mathbf{k}_1\downarrow}^\dagger \hat{\gamma}_{\mathbf{k}_2\downarrow}^\dagger, \quad \hat{\mathcal{A}}_4^\dagger = \hat{\gamma}_{-\mathbf{k}_1\downarrow}^\dagger \hat{\gamma}_{-\mathbf{k}_2\uparrow}^\dagger \quad (1.34)$$

$$\hat{\mathcal{B}}_1^\dagger = \hat{\gamma}_{\mathbf{k}_1\downarrow}^\dagger \hat{\gamma}_{\mathbf{k}_2\uparrow}^\dagger, \quad \hat{\mathcal{B}}_2^\dagger = \hat{\gamma}_{\mathbf{k}_1\downarrow}^\dagger \hat{\gamma}_{-\mathbf{k}_2\downarrow}^\dagger, \quad \hat{\mathcal{B}}_3^\dagger = \hat{\gamma}_{-\mathbf{k}_1\uparrow}^\dagger \hat{\gamma}_{\mathbf{k}_2\uparrow}^\dagger, \quad \hat{\mathcal{B}}_4^\dagger = \hat{\gamma}_{-\mathbf{k}_1\uparrow}^\dagger \hat{\gamma}_{-\mathbf{k}_2\downarrow}^\dagger \quad (1.35)$$

The corresponding two-body quasiparticle propagators for $M_s = 0$ are:

$$\begin{aligned} \mathcal{GG}_{ij}^{S=0}(\mathbf{k}_1, \mathbf{k}_2, t_1, t_2) &= \frac{1}{2} \langle \psi_{BCS}^0 | T \left\{ [\hat{\mathcal{A}}_i(t_2) - \hat{\mathcal{B}}_i(t_2)] [\hat{\mathcal{A}}_j^\dagger(t_1) - \hat{\mathcal{B}}_j^\dagger(t_1)] \right\} | \psi_{BCS}^0 \rangle \\ \mathcal{GG}_{ij}^{S=1}(\mathbf{k}_1, \mathbf{k}_2, t_1, t_2) &= \frac{1}{2} \langle \psi_{BCS}^0 | T \left\{ [\hat{\mathcal{A}}_i(t_2) + \hat{\mathcal{B}}_i(t_2)] [\hat{\mathcal{A}}_j^\dagger(t_1) + \hat{\mathcal{B}}_j^\dagger(t_1)] \right\} | \psi_{BCS}^0 \rangle. \end{aligned} \quad (1.36)$$

Both are diagonal and coincide. For the sake of simple notation the index (*BCS*) is omitted and implicitly understood in the following. After Fourier transformation one obtains

$$\mathcal{GG}_{11}^{S=0}(\mathbf{k}_1, \mathbf{k}_2, \omega) = \mathcal{GG}_{11}^{S=1}(\mathbf{k}_1, \mathbf{k}_2, \omega) = \frac{1}{\omega - \tilde{\xi}_{\mathbf{k}_1} - \tilde{\xi}_{\mathbf{k}_2} + i\delta} \quad (1.37)$$

$$\mathcal{GG}_{44}^{S=0}(\mathbf{k}_1, \mathbf{k}_2, \omega) = \mathcal{GG}_{44}^{S=1}(\mathbf{k}_1, \mathbf{k}_2, \omega) = -\frac{1}{\omega + \tilde{\xi}_{\mathbf{k}_1} + \tilde{\xi}_{\mathbf{k}_2} - i\delta}, \quad (1.38)$$

where all remaining elements including the couplings between spin singlet and triplet states vanish. This facts also hold with respect to the $M_s = \pm 1$ states, which just shows that S and M_s are good quantum numbers in this "free" propagation.

This propagator can be transformed into the normal basis by virtue of the relation (1.17), i.e. explicitly:

$$\hat{\mathcal{A}}_1^\dagger = \hat{a}_{\mathbf{k}_1\uparrow}^\dagger \hat{a}_{\mathbf{k}_2\downarrow}^\dagger, \quad \hat{\mathcal{A}}_2^\dagger = \hat{a}_{\mathbf{k}_1\uparrow}^\dagger \hat{a}_{-\mathbf{k}_2\uparrow}^\dagger, \quad \hat{\mathcal{A}}_3^\dagger = \hat{a}_{-\mathbf{k}_1\downarrow}^\dagger \hat{a}_{\mathbf{k}_2\downarrow}^\dagger, \quad \hat{\mathcal{A}}_4^\dagger = \hat{a}_{-\mathbf{k}_1\downarrow}^\dagger \hat{a}_{-\mathbf{k}_2\uparrow}^\dagger \quad (1.39)$$

whereas these normal operators are connected to the quasiparticle operators by the unitary transformation

$$\hat{\mathcal{A}}_i^\dagger = U_{ij} \hat{\mathcal{A}}_j^\dagger, \quad \mathbf{U} = \begin{pmatrix} u_{\mathbf{k}_1} u_{\mathbf{k}_2} & -u_{\mathbf{k}_1} v_{\mathbf{k}_2} & v_{\mathbf{k}_1} u_{\mathbf{k}_2} & -v_{\mathbf{k}_1} v_{\mathbf{k}_2} \\ u_{\mathbf{k}_1} v_{\mathbf{k}_2} & u_{\mathbf{k}_1} u_{\mathbf{k}_2} & v_{\mathbf{k}_1} v_{\mathbf{k}_2} & v_{\mathbf{k}_1} u_{\mathbf{k}_2} \\ -v_{\mathbf{k}_1} u_{\mathbf{k}_2} & v_{\mathbf{k}_1} v_{\mathbf{k}_2} & u_{\mathbf{k}_1} u_{\mathbf{k}_2} & -u_{\mathbf{k}_1} v_{\mathbf{k}_2} \\ -v_{\mathbf{k}_1} v_{\mathbf{k}_2} & -v_{\mathbf{k}_1} u_{\mathbf{k}_2} & u_{\mathbf{k}_1} v_{\mathbf{k}_2} & u_{\mathbf{k}_1} u_{\mathbf{k}_2} \end{pmatrix}. \quad (1.40)$$

$$\mathbf{GG} = \begin{pmatrix} \uparrow\uparrow & \uparrow\downarrow & \uparrow\uparrow & \uparrow\downarrow & \uparrow\uparrow & \uparrow\downarrow \\ \uparrow\downarrow & \uparrow\downarrow & \uparrow\downarrow & \uparrow\downarrow & \uparrow\downarrow & \uparrow\downarrow \\ \downarrow\uparrow & \downarrow\uparrow & \downarrow\uparrow & \downarrow\uparrow & \downarrow\uparrow & \downarrow\uparrow \\ \downarrow\downarrow & \downarrow\downarrow & \downarrow\downarrow & \downarrow\downarrow & \downarrow\downarrow & \downarrow\downarrow \end{pmatrix} \quad \mathbf{gg} = \begin{pmatrix} \uparrow\uparrow & \uparrow\downarrow & \uparrow\uparrow \\ \downarrow\downarrow & \downarrow\uparrow & \downarrow\downarrow \end{pmatrix}$$

Figure 1.10.: Representation of the free two-particle Nambu-Gorkov propagators in the BCS approximation .

Consequently in the normal basis we obtain

$$\begin{aligned} GG_{ij}(\mathbf{k}_1, \mathbf{k}_2, t_1, t_2) &= \langle \psi_{BCS}^0 | T \{ \hat{A}_i(t_2) \hat{A}_j^\dagger(t_1) \} | \psi_{BCS}^0 \rangle \\ GG_{ij}(\mathbf{k}_1, \mathbf{k}_2, \omega) &= U_{ik} \mathcal{G} \mathcal{G}_{km}(\mathbf{k}_1, \mathbf{k}_2, \omega) U_{mj}^\dagger, \end{aligned} \quad (1.41)$$

i.e. in more explicit form (cf. Fig. 1.10):

$$\begin{aligned} \mathbf{GG}(\mathbf{k}_1, \mathbf{k}_2, \omega) &= \begin{pmatrix} GG & GF^\dagger & F^\dagger G & F^\dagger F^\dagger \\ GF & GG^- & F^\dagger F & F^\dagger G^- \\ FG & FF^\dagger & G^- G & G^- F^\dagger \\ FF & FG^- & G^- F & G^- G^- \end{pmatrix} \\ &= \frac{1}{\omega - (\tilde{\xi}_{\mathbf{k}_1} + \tilde{\xi}_{\mathbf{k}_2}) + i\delta} \begin{pmatrix} u_1^2 u_2^2 & u_1^2 u_2 v_2 & -u_1 v_1 u_2^2 & -u_1 u_2 v_1 v_2 \\ u_1^2 u_2 v_2 & u_1^2 v_2^2 & -u_1 v_1 u_2 v_2 & -u_1 v_1 v_2^2 \\ -u_1 u_2^2 v_1 & -u_1 u_2 v_1 v_2 & v_1^2 u_2^2 & v_1^2 u_2 v_2 \\ -u_1 u_2 v_1 v_2 & -u_1 v_1 v_2^2 & v_1^2 u_2 v_2 & v_1^2 v_2^2 \end{pmatrix} \\ &\quad - \frac{1}{\omega + (\tilde{\xi}_{\mathbf{k}_1} + \tilde{\xi}_{\mathbf{k}_2}) - i\delta} \begin{pmatrix} v_1^2 v_2^2 & -v_1^2 u_2 v_2 & u_1 v_1 v_2^2 & -u_1 v_1 u_2 v_2 \\ -v_1^2 u_2 v_2 & v_1^2 u_2^2 & -u_1 u_2 v_1 v_2 & u_1 u_2^2 v_1 \\ u_1 v_1 v_2^2 & -u_1 u_2 v_1 v_2 & u_1^2 v_2^2 & -u_1^2 u_2 v_2 \\ -u_1 u_2 v_1 v_2 & u_1 v_1 u_2^2 & -u_1^2 u_2 v_2 & u_1^2 u_2^2 \end{pmatrix}. \end{aligned} \quad (1.42)$$

with $u_1 = u_{k_1} = u_{\mathbf{k}_1} = u_{-\mathbf{k}_1}$.

It is quite instructive to take the limit $\Delta_{\mathbf{k}} \rightarrow 0$. In this case we have

$$\tilde{\xi}_{\mathbf{k}} = |\xi_{\mathbf{k}}| = |\varepsilon_{\mathbf{k}} - \mu|, \quad v_{\mathbf{k}} = n_{\mathbf{k}} = \Theta(\mu - \varepsilon_{\mathbf{k}}), \quad u_{\mathbf{k}} = 1 - n_{\mathbf{k}}. \quad (1.43)$$

The particle-hole and particle-particle decouple, i.e. all nondiagonal elements are vanishing and we recover the ordinary particle-particle, particle-hole and hole-

hole correlation functions:

$$\begin{aligned}
GG_{\Delta=0}(\mathbf{k}_1, \mathbf{k}_2, \omega) &= \frac{(1 - n_{\mathbf{k}_1})(1 - n_{\mathbf{k}_2})}{\omega + 2\mu - (\varepsilon_{\mathbf{k}_1} + \varepsilon_{\mathbf{k}_2}) + i\delta} - \frac{n_{\mathbf{k}_1}n_{\mathbf{k}_2}}{\omega + 2\mu - (\varepsilon_{\mathbf{k}_1} + \varepsilon_{\mathbf{k}_2}) - i\delta} \\
GG_{\Delta=0}^-(\mathbf{k}_1, \mathbf{k}_2, \omega) &= \frac{(1 - n_{\mathbf{k}_1})n_{\mathbf{k}_2}}{\omega - (\varepsilon_{\mathbf{k}_1} - \varepsilon_{\mathbf{k}_2}) + i\delta} - \frac{n_{\mathbf{k}_1}(1 - n_{\mathbf{k}_2})}{\omega - (\varepsilon_{\mathbf{k}_1} - \varepsilon_{\mathbf{k}_2}) - i\delta} \\
G^-G_{\Delta=0}(\mathbf{k}_1, \mathbf{k}_2, \omega) &= \frac{n_{\mathbf{k}_1}(1 - n_{\mathbf{k}_2})}{\omega - (\varepsilon_{\mathbf{k}_2} - \varepsilon_{\mathbf{k}_1}) + i\delta} - \frac{(1 - n_{\mathbf{k}_1})n_{\mathbf{k}_2}}{\omega - (\varepsilon_{\mathbf{k}_2} - \varepsilon_{\mathbf{k}_1}) - i\delta} \\
G^-G_{\Delta=0}^-(\mathbf{k}_1, \mathbf{k}_2, \omega) &= \frac{n_{\mathbf{k}_1}n_{\mathbf{k}_2}}{\omega - 2\mu + \varepsilon_{\mathbf{k}_1} + \varepsilon_{\mathbf{k}_2} + i\delta} - \frac{(1 - n_{\mathbf{k}_1})(1 - n_{\mathbf{k}_2})}{\omega - 2\mu + \varepsilon_{\mathbf{k}_1} + \varepsilon_{\mathbf{k}_2} - i\delta}
\end{aligned} \tag{1.44}$$

As will be shown in section 1.9, the particular symmetry properties of the two-particle propagator $\mathbf{G}\mathbf{G}$ in back-to-back kinematics leads to a decoupling of certain elements in the scattering problem. For later purposes we also introduce a "reduced" propagator $\mathbf{g}\mathbf{g}$, which contains only elements with two normal or anomalous propagators, i.e. explicitly (cf. Fig. 1.10):

$$\mathbf{g}\mathbf{g}(\mathbf{k}_1, \mathbf{k}_2, t) = \begin{pmatrix} GG & F^\dagger F^\dagger \\ FF & G^-G^- \end{pmatrix}. \tag{1.45}$$

This propagator has the advantage that the complexity of the scattering problem discussed in the next section is reduced substantially, whereas most of the essential features are already included in this reduced problem.

1.7. Scattering Equation in a Superfluid

We consider now the one-channel scattering problem $\mathbf{P} = \mathbf{k}_1 + \mathbf{k}_2 \rightarrow \mathbf{k}'_1 + \mathbf{k}'_2$ in a superfluid system whereas, as pointed out in the previous section, the initial and final state includes in general pp , ph , hp and hh components. Consequently the particle-hole and particle-particle scattering processes are all coupled with one another (cf. Fig. 1.11) by virtue of the off-diagonal elements of the free two-particle propagator $\mathbf{G}\mathbf{G}$.

Formally the operator equation for the scattering problem takes the form[72] (cf. App. A.3)

$$\hat{\Gamma} = \hat{\Gamma}_0 + \hat{\Gamma}_0 \widehat{\mathbf{G}\mathbf{G}} \hat{\Gamma}. \tag{1.46}$$

Here $\hat{\Gamma}_0$ is the irreducible driving term and $\hat{\Gamma}$ the full vertex operator. The definition of irreducibility in superfluid systems involves some subtleties and will be discussed in detail below. The vertex operators are by definition related by

$$\hat{\Gamma}_0 |\chi_{\mathbf{k}_1\mathbf{k}_2}\rangle = \hat{\Gamma} |\phi_{\mathbf{k}_1\mathbf{k}_2}\rangle = \hat{\Gamma} |\mathbf{k}_1\mathbf{k}_2\rangle, \tag{1.47}$$

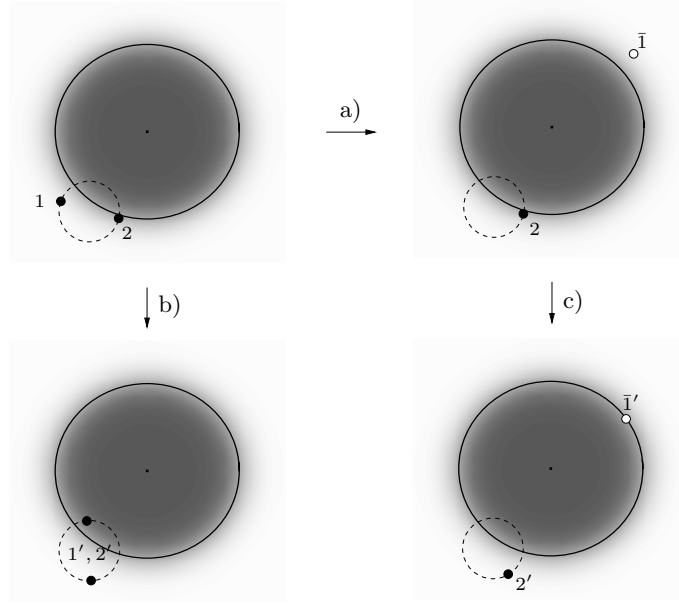


Figure 1.11.: Illustration of the possible processes for two particles in the initial states with momenta 1 and 2. In a) one particle interacts with the condensate and is transformed into a hole; b) shows pp -scattering to the final states 1' and 2', whereas c) shows ph -scattering.

where the state vectors $|\phi\rangle$ denote the plane-wave states and $|\chi\rangle$ the scattering states. Each of these states contains pp , ph , hp and hh components (see below).

In general, $\mathbf{\Gamma}$ and $\mathbf{\Gamma}_0$ are 4x4 matrices in Gorkov space as is the propagator $\mathbf{G}\mathbf{G}$. Since the two body propagator $\mathbf{G}\mathbf{G}$ and the two-body interaction kernel $\mathbf{\Gamma}_0$ are spin conserving, the different spin channels decouple completely. Hence by choosing the initial and final states as $S = 0$ or $S = 1$, the corresponding singlet and triplet components of the vertex function

$$\hat{\mathbf{\Gamma}} = \hat{\mathbf{\Gamma}}^{S=0} + \hat{\mathbf{\Gamma}}^{S=1} \quad (1.48)$$

are projected out. Alternatively, one can choose a simpler form, where the spin multiplet is not fixed from the beginning. By introducing the short hand notation for the quantum numbers of the particles $1 = \{\mathbf{k}_1\sigma_1\}$, $1' = \{\mathbf{k}'_1\sigma'_1\}$ etc, we can write the basis states as

$$|\Psi_{12}\rangle \equiv |\mathbf{k}_1\mathbf{k}_2\rangle = \begin{pmatrix} \hat{a}_{\mathbf{k}_1\uparrow}^\dagger \hat{a}_{\mathbf{k}_2\downarrow}^\dagger |\psi_{BCS}^0\rangle \\ \hat{a}_{\mathbf{k}_1\uparrow}^\dagger \hat{a}_{-\mathbf{k}_2\uparrow} |\psi_{BCS}^0\rangle \\ \hat{a}_{-\mathbf{k}_1\downarrow} \hat{a}_{\mathbf{k}_2\downarrow}^\dagger |\psi_{BCS}^0\rangle \\ \hat{a}_{-\mathbf{k}_1\downarrow} \hat{a}_{-\mathbf{k}_2\uparrow} |\psi_{BCS}^0\rangle \end{pmatrix} \quad (1.49)$$

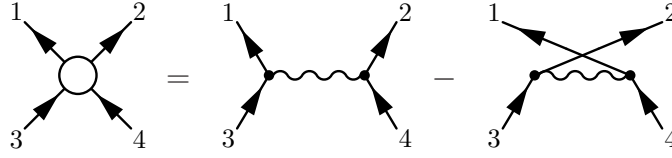


Figure 1.12.: The antisymmetrized bare two-particle interaction $\tilde{V}(\mathbf{k}_1\sigma_1, \mathbf{k}_2\sigma_2, \mathbf{k}_3\sigma_3, \mathbf{k}_4\sigma_4) = \tilde{V}(1, 2, 3, 4)$ in pp -basis.

The spin multiplets in eq. (1.48) can be projected out by *explicitly* taking only the spin singlet or triplet part of the irreducible kernel $\mathbf{\Gamma}_0$. This way one obtains a general scattering equation for singlet and triplet scattering.

Since the state vector $|\Psi_{12}\rangle$ was used for the construction of the two-particle propagator $\mathbf{G}\mathbf{G}$, we can represent the vertex matrix in complete analogy in diagrammatical form as:

$$\langle \Psi_{1'2'} | \hat{\mathbf{\Gamma}} | \Psi_{12} \rangle = \begin{array}{c} \begin{array}{c} 1' \quad 2' \\ \diagdown \quad \diagup \\ \text{---} \text{---} \\ \diagup \quad \diagdown \\ 1 \quad 2 \end{array} \\ \text{---} \text{---} \end{array} = \begin{pmatrix} \begin{array}{cccc} \text{---} \text{---} & \text{---} \text{---} & \text{---} \text{---} & \text{---} \text{---} \\ \text{---} \text{---} & \text{---} \text{---} & \text{---} \text{---} & \text{---} \text{---} \\ \text{---} \text{---} & \text{---} \text{---} & \text{---} \text{---} & \text{---} \text{---} \\ \text{---} \text{---} & \text{---} \text{---} & \text{---} \text{---} & \text{---} \text{---} \end{array} \\ \vdots \\ \begin{array}{cccc} \text{---} \text{---} & \text{---} \text{---} & \text{---} \text{---} & \text{---} \text{---} \\ \text{---} \text{---} & \text{---} \text{---} & \text{---} \text{---} & \text{---} \text{---} \\ \text{---} \text{---} & \text{---} \text{---} & \text{---} \text{---} & \text{---} \text{---} \\ \text{---} \text{---} & \text{---} \text{---} & \text{---} \text{---} & \text{---} \text{---} \end{array} \end{pmatrix}.$$

The irreducible driving term $\mathbf{\Gamma}_0$ is taken, for the present one-channel problem, to be approximated by the totally irreducible antisymmetrized vacuum interaction (cf. Fig. 1.12).

The elements of this matrix can be determined by calculating the two-particle propagator elements in lowest order perturbation theory for the two-body interaction of the form:

$$\hat{V}(t') = \frac{1}{4} \sum_{\mathbf{k}_i, \sigma_i} \tilde{V}(\mathbf{k}_1\sigma_1, \mathbf{k}_2\sigma_2, \mathbf{k}_3\sigma_3, \mathbf{k}_4\sigma_4) a_{\mathbf{k}_1\sigma_1}^\dagger(t') a_{\mathbf{k}_2\sigma_2}^\dagger(t') a_{\mathbf{k}_4\sigma_4}(t') a_{\mathbf{k}_3\sigma_3}(t') \quad (1.50)$$

with the antisymmetrized interaction matrix \tilde{V} :

$$\begin{aligned} \tilde{V}(\mathbf{k}_1\sigma_1, \mathbf{k}_2\sigma_2, \mathbf{k}_3\sigma_3, \mathbf{k}_4\sigma_4) &= -\tilde{V}(\mathbf{k}_1\sigma_1, \mathbf{k}_2\sigma_2, \mathbf{k}_4\sigma_4, \mathbf{k}_3\sigma_3) \\ &= -\tilde{V}(\mathbf{k}_2\sigma_2, \mathbf{k}_1\sigma_1, \mathbf{k}_3\sigma_3, \mathbf{k}_4\sigma_4) \end{aligned} \quad (1.51)$$

whereas $\mathbf{k}_1\sigma_1$ denotes the left outgoing line, $\mathbf{k}_2\sigma_2$ the right outgoing line, $\mathbf{k}_3\sigma_3$ the left incoming line and $\mathbf{k}_4\sigma_4$ the right incoming line (cf. Fig. 1.12). For the

first element of the propagator one obtains:

$$\begin{aligned}
GG^{(1)}(\mathbf{k}_1, \mathbf{k}_2, t_0; \mathbf{k}'_1, \mathbf{k}'_2, t) &= \int dt' \left\langle T \hat{a}_{\mathbf{k}'_2 \downarrow}(t) \hat{a}_{\mathbf{k}'_1 \uparrow}(t) \hat{V}(t') \hat{a}_{\mathbf{k}_1 \uparrow}^\dagger(t_0) \hat{a}_{\mathbf{k}_2 \downarrow}^\dagger(t_0) \right\rangle \\
&= GG(\mathbf{k}'_1, \mathbf{k}'_2, t) V_{11} GG(\mathbf{k}_1, \mathbf{k}_2, t_0) \\
&+ GF(\mathbf{k}'_1, \mathbf{k}'_2, t) V_{22} GF^\dagger(\mathbf{k}_1, \mathbf{k}_2, t_0) \\
&+ FG(\mathbf{k}'_1, \mathbf{k}'_2, t) V_{23} GF^\dagger(\mathbf{k}_1, \mathbf{k}_2, t_0) \\
&+ GF(\mathbf{k}'_1, \mathbf{k}'_2, t) V_{32} F^\dagger G(\mathbf{k}_1, \mathbf{k}_2, t_0) \\
&+ FG(\mathbf{k}'_1, \mathbf{k}'_2, t) V_{33} F^\dagger G(\mathbf{k}_1, \mathbf{k}_2, t_0) \\
&+ FF(\mathbf{k}'_1, \mathbf{k}'_2, t) V_{44} F^\dagger F^\dagger(\mathbf{k}_1, \mathbf{k}_2, t_0)
\end{aligned} \tag{1.52}$$

with

$$\begin{aligned}
V_{11} &= \tilde{V}(\mathbf{k}'_1 \uparrow, \mathbf{k}'_2 \downarrow, \mathbf{k}_1 \uparrow, \mathbf{k}_2 \downarrow) \\
V_{22} &= \tilde{V}(\mathbf{k}'_1 \uparrow, -\mathbf{k}_2 \uparrow, \mathbf{k}_1 \uparrow, -\mathbf{k}'_2 \uparrow) \\
V_{23} &= \tilde{V}(\mathbf{k}'_2 \downarrow, -\mathbf{k}_2 \uparrow, \mathbf{k}_1 \uparrow, -\mathbf{k}'_1 \downarrow) \\
V_{32} &= \tilde{V}(\mathbf{k}'_1 \uparrow, -\mathbf{k}_1 \downarrow, \mathbf{k}_2 \downarrow, -\mathbf{k}'_2 \uparrow) \\
V_{33} &= \tilde{V}(-\mathbf{k}_1 \downarrow, \mathbf{k}'_2 \downarrow, -\mathbf{k}'_1 \downarrow, \mathbf{k}_2 \downarrow) \\
V_{44} &= \tilde{V}(-\mathbf{k}_1 \downarrow, -\mathbf{k}_2 \uparrow, -\mathbf{k}'_1 \downarrow, -\mathbf{k}'_2 \uparrow).
\end{aligned} \tag{1.53}$$

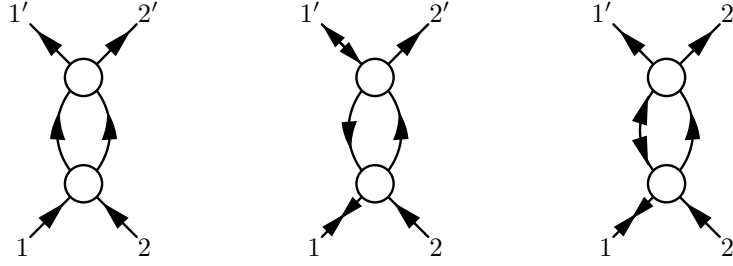
The other elements of $\mathbf{GG}^{(1)}$ can be evaluated in an analogous fashion. The result can be compactly written in the matrix form

$$\mathbf{GG}^{(1)}(\mathbf{k}_1, \mathbf{k}_2, t_0; \mathbf{k}'_1, \mathbf{k}'_2, t) = \mathbf{GG}(\mathbf{k}'_1, \mathbf{k}'_2, t) \langle \Psi_{1'2'} | \mathbf{V} | \Psi_{12} \rangle \mathbf{GG}(\mathbf{k}_1, \mathbf{k}_2, t_0) \tag{1.54}$$

where the irreducible interaction matrix takes the form

$$\langle \Psi_{1'2'} | \mathbf{V} | \Psi_{12} \rangle = \begin{pmatrix} \text{Diagram 1} & & & & \\ & \text{Diagram 2} & \text{Diagram 3} & & \\ & \text{Diagram 4} & \text{Diagram 5} & & \\ & & & & \text{Diagram 6} \end{pmatrix} = \begin{pmatrix} V_{11} & 0 & 0 & 0 \\ 0 & V_{22} & V_{23} & 0 \\ 0 & V_{32} & V_{33} & 0 \\ 0 & 0 & 0 & V_{44} \end{pmatrix}. \tag{1.55}$$

It should be emphasized that in general the matrix $\langle \Psi_{1'2'} | \mathbf{\Gamma}_0 | \Psi_{12} \rangle$ is fully populated as is the reducible vertex $\mathbf{\Gamma}$. Only due to the fact that the kernel is approximated at this point by the vacuum interaction does it show the characteristic structure (1.55). Not all interaction elements (1.53) are independent. By using the time reversal symmetry and hermiticity of the interaction one can see that only three terms are independent, which can readily be identified as the

Figure 1.13.: Typical diagrams contributing to $GG^{(2)}$.

particle-particle interaction V_{pp} , the particle-hole interaction V_{ph} and the particle hole interaction in the exchange channel $V_{\overline{ph}}$:

$$V_{pp} = V_{11} = V_{44}, \quad V_{ph} = V_{22} = V_{33}, \quad V_{\overline{ph}} = V_{23} = V_{32}. \quad (1.56)$$

This first order evaluation determines the structure of the interaction matrix. For the calculation of the symmetry factors, one has to proceed to the second order. This procedure involves some subtleties. Hence we discuss one element in more detail. We will consider the element

$$GG^{(2)}(\mathbf{k}_1, \mathbf{k}_2, t_0, \mathbf{k}'_1, \mathbf{k}'_2, t) = \int dt' dt'' \langle T \hat{a}_{\mathbf{k}'_2 \downarrow}(t) \hat{a}_{\mathbf{k}'_1 \uparrow}(t) \hat{V}(t') \hat{V}(t'') \hat{a}_{\mathbf{k}_1 \uparrow}^\dagger(t_0) \hat{a}_{\mathbf{k}_2 \downarrow}^\dagger(t_0) \rangle \quad (1.57)$$

Here, only the direction of the ends of the external lines is fixed. Already in second order the number of contributing diagrams to $GG^{(2)}$ is quite large (some examples are shown in Fig. 1.13). Hence instead of a complete discussion we will restrict ourselves to a qualitative discussion with emphasis on the symmetry factors.

For the first diagram in Fig. 1.13, one has two possibilities to contract the field operators at time t_0 with the destruction operators at time t'' . The same holds for the contraction of the final state field operators with the creation operators of $\hat{V}(t')$. The remaining internal contractions provide an additional symmetry factor 2, which in total, combined with the factor $1/16$ of the interaction Hamiltonian \hat{V} , leads to an effective factor of $1/2$ together with the remaining internal spin sum. Additional contributions from the possible interchange $\hat{V}(t') \leftrightarrow \hat{V}(t'')$ are taken care of by the overall factor $1/2$ in second order perturbation theory.

In diagrams including internal particle-hole propagators like the second one in Fig. 1.13, there are four possible contractions of the final state and the initial state operator, each providing in total a factor of 16. For the remaining internal propagators, there is only one possible contraction left together with one internal spin sum. Hence we find a relative factor of 2 compared to the particle-particle diagram, which is connected to the fact that for antisymmetrized vertices the diagrams with internal GG^- and G^-G is not distinguishable and therefore provide the same contributions. This symmetry factor that appears here naturally by the

matrix structure in Gorkov space has to be included by hand in normal systems, taking into account that both internal lines are identical in the BCS channel [71]. Hence the scattering equation in total takes the form

$$\langle \Psi_{1'2'} | \Gamma(\omega) | \Psi_{12} \rangle = \langle \Psi_{1'2'} | \mathbf{V} | \Psi_{12} \rangle + \frac{1}{2} \sum_{3,4,\sigma} \langle \Psi_{1'2'} | \mathbf{V} | \Psi_{34} \rangle \mathbf{G} \mathbf{G}(3,4) \langle \Psi_{34} | \Gamma(\omega) | \Psi_{12} \rangle \quad (1.58)$$

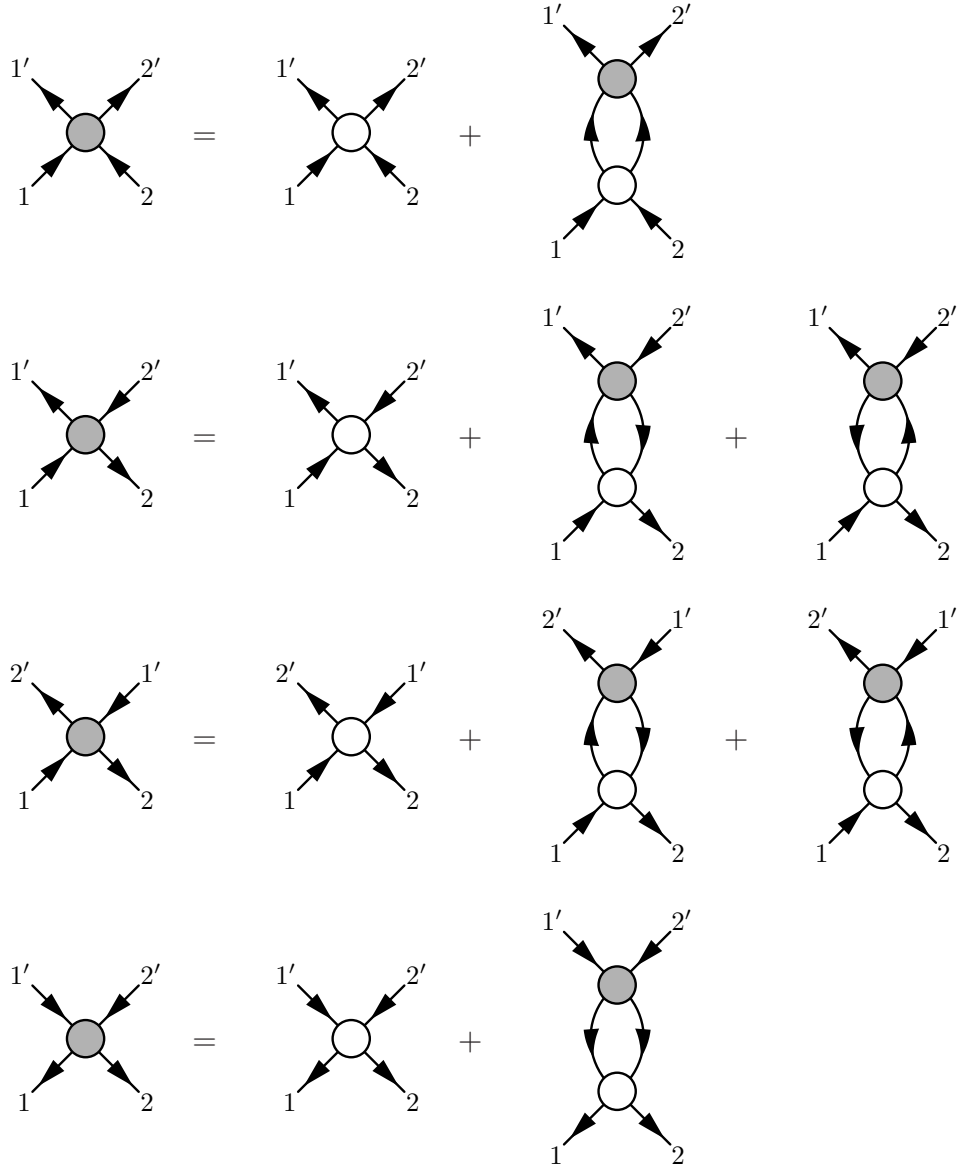


Figure 1.14.: The four independent equations in the limit $\Delta \rightarrow 0$ resulting from eq. (1.58). The two integrals on the right hand side of the second and third equation give the same contribution.

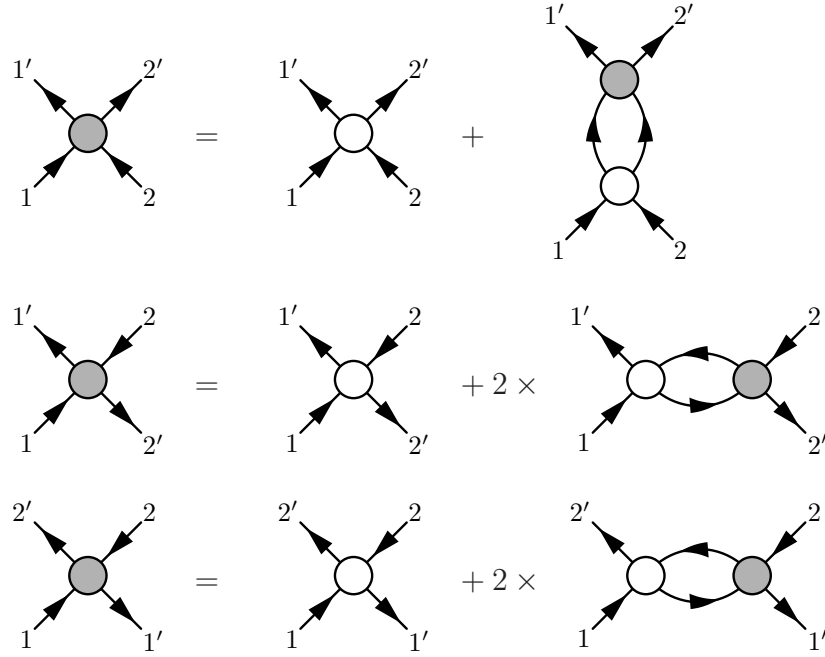


Figure 1.15.: The three possible decompositions of the full reducible vertex in the pp (BCS), ph (ZS) and the \overline{ph} (ZS') channel in a normal Fermi system. The unshaded circles denote the irreducible vertices in the corresponding channels. The relative factor $1/2$ in the BCS channel stems from the fact that the internal lines are identical (cf. ref. [71]).

It is quite instructive to consider the limit $\Delta \rightarrow 0$ of eq. (1.58). In this case, the two-particle propagator becomes diagonal (cf. eq. (1.44)) and the non-particle conserving elements in Γ clearly vanish. Hence the original 4x4 matrix equation (1.58) reduces to a system of 6 equations, whose number immediately reduces further to four due to the symmetry relations (1.44) and (1.56). The resulting diagrams are shown in Fig. 1.14. Furthermore, the two integrals on the right hand side of the two equations for the particle-hole vertices give the same contributions. This can be understood as follows: the internal particle-hole propagators are just related by a relabeling of the internal momenta, i.e. switching the roles of the two internal lines whereas the vertices also switch the roles of the two internal lines. In total the effects cancel and one obtains as a result an effective factor of 2.

Due to this decoupling of the equations at $\Delta \rightarrow 0$, the external lines in the four equations can be chosen independently, providing equations identical to the Bethe-Salpeter equations for the particle-particle, particle-hole and hole-hole vertices in normal systems in the BCS , ZS and ZS' channels (see Fig. 1.15).

By this one could be tempted to think that the 4x4 matrix equation (1.58) provides in this sense a generalization of this coupled system and hence includes

already all three many body channels. However, this is not true, since in the case of a finite gap all vertices are coupled with each other and consequently the external labels cannot be chosen independently anymore in the different elements of Γ . In this case the equations in the normal system and the reduction of eq. (1.58) are only *structurally* identical but no more completely equivalent.

In order to clarify this important point as explicitly as possible, let us consider in comparison the particle-particle scattering Bethe-Salpeter equation in normal systems for the process $1 + 2 \rightarrow 1' + 2'$ (Fig. 1.15). In contrast to superfluid systems, the nature of the internal and external lines is fixed by the channel. By a transformation to the particle-hole basis a particle of the final state is transformed into a hole state in the initial state and vice versa just by flipping the corresponding external lines in the diagram. That means that the particle in this basis is interacting with the hole state of momentum $1'$ or $2'$. There are no other hole states. In contrast, in superfluid systems, the nature of the initial states is not fixed - it can be a pair of particles, a particle-hole pair or a hole pair. In the case of a particle-hole pair, the particle-hole vertices in Fig. 1.15 describe the scattering of a particle with momentum 1 off a hole with momentum 2, not $1'$ or $2'$. Hence despite the presence of particle-hole diagrams in the matrix equation it is still a *one-channel* equation according to the topology of the diagrams with respect to the external labels. We will return to this problem in section 3.6, where the different channels in superfluid systems are discussed.

We now return to eq. (1.58). The complexity of the equation simplifies considerably by a partial wave decomposition of Γ and Γ_0 with respect to the relative momenta

$$\mathbf{k} = \frac{\mathbf{k}_1 - \mathbf{k}_2}{2} = \mathbf{k}_1 - \frac{\mathbf{P}}{2}, \quad \mathbf{k}' = \frac{\mathbf{k}'_1 - \mathbf{k}'_2}{2} = \mathbf{k}'_1 - \frac{\mathbf{P}}{2}, \quad k, k' = |\mathbf{k}|, |\mathbf{k}'| \quad (1.59)$$

in the standard way¹:

$$\langle \mathbf{k}' | X | \mathbf{k} \rangle = (4\pi)^2 \sum_{l, l', m, m'} i^{l-l'} \langle \mathbf{k}' | l' m' \rangle \langle k' l' m' | X | k l m \rangle \langle l m | \mathbf{k} \rangle. \quad (1.60)$$

The propagator is expanded as follows:

$$\mathbf{G}\mathbf{G}(q, P, \hat{\mathbf{P}} \cdot \hat{\mathbf{q}}, \omega) = \sum_l (2l + 1) \mathbf{G}\mathbf{G}_l(q, P, \omega) P_l(\hat{\mathbf{P}} \cdot \hat{\mathbf{q}}). \quad (1.61)$$

¹Note that this expansion is different from the historical expansion of Fermi-Liquid theory $f(\mathbf{k}, \mathbf{k}') = \sum_l f_l P_l(\cos \theta_{\mathbf{k}\mathbf{k}'})$. Here the expansion (1.60) reduces for diagonal matrices ($l = l'$) independent of m to

$$\langle \mathbf{k}' | X | \mathbf{k} \rangle = 4\pi \sum_l (2l + 1) X_l(k, k') P_l(\cos \theta_{\mathbf{k}\mathbf{k}'}).$$

Thus some care must be taken in the extraction of Landau-Parameters.

After projecting on the partial waves (l, m) and (l', m') we obtain:

$$\begin{aligned} \langle k'l'm' | \Gamma(\omega) | klm \rangle &= \langle k'l' | \mathbf{V} | kl \rangle \delta_{mm'} + \\ &+ \int dq q^2 \sum_{l_1, l_2, l_3} i^{l_1 - l_3} \Omega_{l_1 l_2 l_3}^{m'} \langle k'l' | \mathbf{V} | ql_1 \rangle \mathbf{G} \mathbf{G}_{l_2}(q, P, \omega) \langle ql_3 m' | \Gamma(\omega) | klm \rangle \end{aligned} \quad (1.62)$$

with the angular coupling coefficients

$$\Omega_{l_1 l_2 l_3}^m = 8Y_{l_2}^0(\hat{\mathbf{P}}) (-1)^m \sqrt{\frac{(2l_1 + 1)(2l_2 + 1)(2l_3 + 1)}{4\pi}} \begin{pmatrix} l_1 & l_2 & l_3 \\ 0 & 0 & 0 \end{pmatrix} \begin{pmatrix} l_1 & l_2 & l_3 \\ -m & 0 & m \end{pmatrix} \quad (1.63)$$

and the partial wave coefficients of the propagator

$$\mathbf{G} \mathbf{G}_l(q, P, \omega) = \frac{1}{2} \int dx P_l(x) \mathbf{G} \mathbf{G}(q, P, x, \omega) \quad \text{with} \quad x = \hat{\mathbf{P}} \cdot \hat{\mathbf{q}}. \quad (1.64)$$

By choosing the quantization axis in the direction of the CM momentum \mathbf{P} the propagator is always diagonal in the m quantum numbers. The ph -elements of \mathbf{V} in a given partial wave can be calculated from the corresponding pp -elements as described in Appendix A.2.

In general the different partial waves in eq. (1.62) are coupled to each other by virtue of the propagator $\mathbf{G} \mathbf{G}$ and the interaction \mathbf{V} . However there are some special cases where the problem simplifies:

- In back-to-back kinematics $\mathbf{P} = 0$ the angular dependence of the propagator drops out and consequently becomes diagonal in the l quantum numbers. The two-dimensional integral equation (1.62) reduces to a one-dimensional problem. For small \mathbf{P} the coupling is weak and becomes stronger with increasing CM momentum \mathbf{P} .
- In the spin-singlet channel only central interaction parts of the NN-interaction are present: $\langle k'l' | \mathbf{V} | kl \rangle = \langle k'l' | \mathbf{V} | kl \rangle \delta_{ll'}$.

Hence in the case of a central interaction in back-to-back kinematics all partial waves decouple completely and we obtain:

$$\begin{aligned} \langle k'l' | \Gamma^m(\omega) | kl \rangle &= \langle k'l' | \mathbf{V} | kl \rangle + \\ &+ \frac{2}{\pi} \int q^2 dq \langle k'l' | \mathbf{V} | ql \rangle \mathbf{G} \mathbf{G}_0(q, P = 0, \omega) \langle ql | \Gamma^m(\omega) | kl \rangle \end{aligned} \quad (1.65)$$

1.8. Separable Model

In general, it is not straightforward to solve the scattering equation (1.58) by inversion due to the complicated pole structure of the propagators (cf. section

1.10). In order to get an impression of the basic properties of Γ it is quite instructive to first consider a simple interaction model, where the equation can be solved explicitly. This is possible for a *separable interaction*, i.e.

$$\langle k'l | \mathbf{V} | kl \rangle = \lambda \mathbf{V}_l(k') \mathbf{V}_l(k) \quad (1.66)$$

In this case the k' -dependence factorizes and the vertex Γ takes the form:

$$\langle k'l | \Gamma(\omega, m) | kl \rangle = \mathbf{V}_l(k') \Gamma_{l'l}^m(\omega, k) \quad (1.67)$$

with

$$\Gamma_{l'l}^m(\omega, k) = \lambda \mathbf{V}_l(k) \delta_{ll'} + \int q^2 dq \sum_{l_2, l_3} \Omega_{l', l_2, l_3}^m \lambda \mathbf{V}_{l'}(q) \mathbf{G} \mathbf{G}_{l_2}(q, P, \omega) \mathbf{V}_{l_3}(q) \Gamma_{l_3 l}^m(\omega, k). \quad (1.68)$$

This equation can be inverted explicitly in momentum space. By neglecting the partial wave coupling (which is small for small \mathbf{P}), we obtain

$$\tilde{\Gamma}_{l'l}^m(\omega, k) = \tilde{\Gamma}_l^m(\omega, k) \delta_{ll'} \quad (1.69)$$

and the vertex can be written in the explicit form:

$$\langle k'l | \Gamma^m(\omega) | kl \rangle = \lambda \mathbf{V}_l(k') \left[\mathbf{1} - \frac{2}{\pi} \int q^2 dq \lambda \mathbf{V}_l(q) \mathbf{G} \mathbf{G}_0(q, P, \omega) \mathbf{V}_l(q) \right]^{-1} \mathbf{V}_l(k). \quad (1.70)$$

In order to keep the discussion at this point as simple as possible, we restrict the dimension in Gorkov space in this section to two, which however includes all essential features (cf. section 1.7). The general case is discussed in the next section.

Hence in the present case the interaction matrix \mathbf{V}_l reads (cf. eq. (1.55)):

$$\mathbf{V}_l(k) = \begin{pmatrix} V_l(k) & 0 \\ 0 & V_l(k) \end{pmatrix}. \quad (1.71)$$

Since the bound states in the system appear as poles in the vertex function Γ the defining equation for these bound states reads:

$$\text{Det } \mathbf{A} = 0 \quad \text{with} \quad \mathbf{A} \equiv \left[\mathbf{1} - \frac{1}{\pi} \int dx \int dq q^2 \lambda \mathbf{V}_l(q) \mathbf{g} \mathbf{g}(q, P, x, \omega) \mathbf{V}_l(q) \right]. \quad (1.72)$$

For small CM momenta \mathbf{P} this equation can be studied analytically by expanding the energy denominator

$$\tilde{\xi}_{|\mathbf{q}+\frac{\mathbf{P}}{2}|} + \tilde{\xi}_{|\mathbf{q}-\frac{\mathbf{P}}{2}|} = 2\tilde{\xi}_q + f(q)P^2x^2 + \mathcal{O}(P^4) \quad (1.73)$$

where $f(q)$ is a dimensionless positive function. All terms with odd powers in x are vanishing in the present case due to the symmetry properties of the propagator $\mathbf{g}\mathbf{g}$ (cf. section 1.6). For the following discussion it is sufficient to put $P = 0$ in the numerator of the propagator, since only numerical coefficients at finite P are affected by this simplification. In this case the propagator, to leading orders in ω and P , takes the following form:

$$\mathbf{g}\mathbf{g}_0(q, P \rightarrow 0, \omega \rightarrow 0) = \begin{pmatrix} -\frac{F(q,P)(u_q^4+v_q^4)}{2\tilde{\xi}_q} - \frac{\omega(u_q^4-v_q^4)}{(2\tilde{\xi}_q)^2} - \frac{\omega^2(u_q^4+v_q^4)}{(2\tilde{\xi}_q)^3} & 2u_q^2v_q^2 \left[\frac{F(q,P)}{2\tilde{\xi}_q} + \frac{\omega^2}{(2\tilde{\xi}_q)^3} \right] \\ 2u_q^2v_q^2 \left[\frac{F(q,P)}{2\tilde{\xi}_q} + \frac{\omega^2}{(2\tilde{\xi}_q)^3} \right] & -\frac{F(q,P)(u_q^4+v_q^4)}{2\tilde{\xi}_q} + \frac{\omega(u_q^4-v_q^4)}{(2\tilde{\xi}_q)^2} - \frac{\omega^2(u_q^4+v_q^4)}{(2\tilde{\xi}_q)^3} \end{pmatrix} \quad (1.74)$$

with $F(q, P) = 1 - \frac{f(q)P^2}{2\tilde{\xi}_q}$. Hence in the case $\omega = 0$ we have $A_{11} = A_{22}$; $A_{12} = A_{21}$ and the solution of eq. (1.72) simply reads $A_{11} = \pm A_{21}$, which corresponds in back-to-back kinematics to the following two equations:

$$1 = -\frac{1}{\pi} \int dq q^2 \frac{\lambda V_l(q) V_l(q)}{\sqrt{\xi_q^2 + \Delta_q^2}} \quad (1.75)$$

$$1 = -\frac{1}{\pi} \int dq q^2 \frac{\lambda V_l(q) V_l(q) \xi_q^2}{(\xi_q^2 + \Delta_q^2)^{3/2}}. \quad (1.76)$$

The first equation (corresponding to the "+" solution) is nothing else but the gap equation (1.15) in the partial wave l for a separable interaction. The second equation does not correspond to physical bound states since the free energy is not minimized by this gap function (cf. section 1.3). Thus the bound states defined by eq. (1.75), which appear in the vertex $\mathbf{\Gamma}$ in the form of a *double pole* at $\mathbf{P} = 0$, $\omega = 0$ in the complex energy plane are indeed the Cooper bound states (cf. Fig. 1.16).

At finite CM momentum \mathbf{P} , the linear terms in ω in the determinant cancel and we find

$$\text{Det } \mathbf{A} \sim \omega^2 - v^2 P^2, \quad (1.77)$$

with a constant v . Thus at finite CM momenta \mathbf{P} the Cooper-double pole is transformed into two single poles at the positions $\omega_G = \omega^+ = vP$ and $\omega_G = \omega^- = -vP$ (cf. figs. 1.16 and 1.18). These poles correspond to the low energy Goldstone excitations in the system (cf. section 1.3 and section 1.4). For the inverse we find:

$$\mathbf{A}^{-1}(\omega \rightarrow 0, P \rightarrow 0) \sim \frac{1}{\omega^2 - v^2 P^2} \begin{pmatrix} +1 & -1 \\ -1 & +1 \end{pmatrix} \left[\frac{1}{4\pi} \int dq q^2 \frac{\lambda V(q) V(q)}{(\xi_q^2 + \Delta_q^2)^{3/2}} \right]^{-1}. \quad (1.78)$$

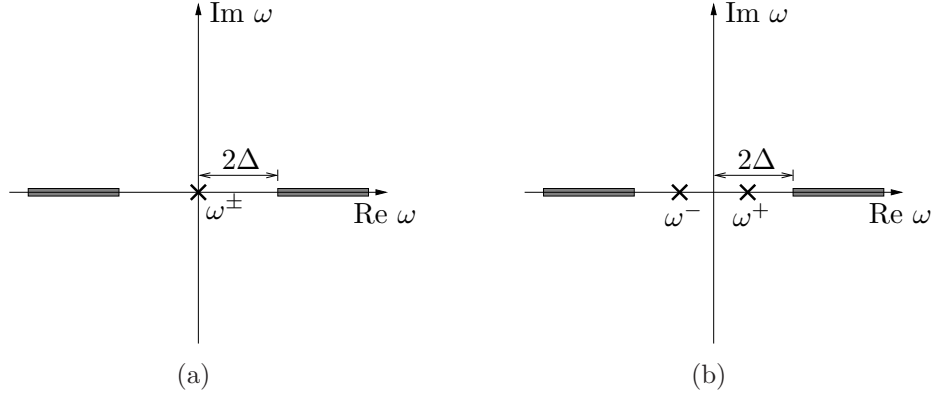


Figure 1.16.: Analytic structure of the vertex function $\Gamma(\omega)$ in back-to-back kinematics (a) and at finite CM momentum (b). The two poles ω^+ and ω^- which are located on the imaginary axis in the normal state (cf. fig. 1.3) are located on the real axis in the superconducting ground state. At $P = 0$ these two poles collapse and form a double pole at $\omega = 0$, representing the Cooper bound states. With increasing CM momentum \mathbf{P} these two poles move in opposite directions on the real axis representing the Goldstone excitations of the Cooper pairs (cf. section 1.3 and 1.4). For small \mathbf{P} the dispersion relation is linear (cf. fig. 1.18). The complex cut is denoted by the grey area.

Since the integrand is strongly peaked around $|\mathbf{q}| = k_F$ it follows that:

$$\mathcal{I}_n = -\frac{1}{\pi} \int dq q^2 \frac{\lambda V(q)V(q)}{(\xi_q^2 + \Delta_q^2)^{n/2}} \Rightarrow \Delta_{k_F}^{n-1} \mathcal{I}_n \sim \mathcal{O}(1). \quad (1.79)$$

Using $\mathcal{I}_1 = 1$ we finally obtain:

$$\begin{aligned} \mathbf{A}^{-1}(\omega \rightarrow 0, P \rightarrow 0) &\sim \frac{\Delta^2}{\omega^2 - v^2 P^2} \begin{pmatrix} +1 & -1 \\ -1 & +1 \end{pmatrix} \\ \Gamma(k, k', \omega \rightarrow 0, P \rightarrow 0) &\sim \frac{\Delta_k \Delta_{k'}}{\omega^2 - v^2 P^2} \begin{pmatrix} +1 & -1 \\ -1 & +1 \end{pmatrix}, \end{aligned} \quad (1.80)$$

which shows that the gap function is just the residue of the vertex function Γ around the Cooper singularity.

The second characteristic point on the real energy axis is the two-particle threshold $\omega = 2\Delta$. Here the quantity $\chi \equiv 2\Delta - \omega$ is a small parameter. When ω is approaching the threshold from below ($\chi \rightarrow 0^+$) the real part of \mathbf{A} is diverging for $\mathbf{P} = 0$:

$$\lim_{\chi \rightarrow 0^+} \text{Re} \mathbf{A} \sim - \int dp \frac{1}{\xi_p^2 + \Delta \chi} \sim \frac{1}{\sqrt{\chi}}, \quad (1.81)$$

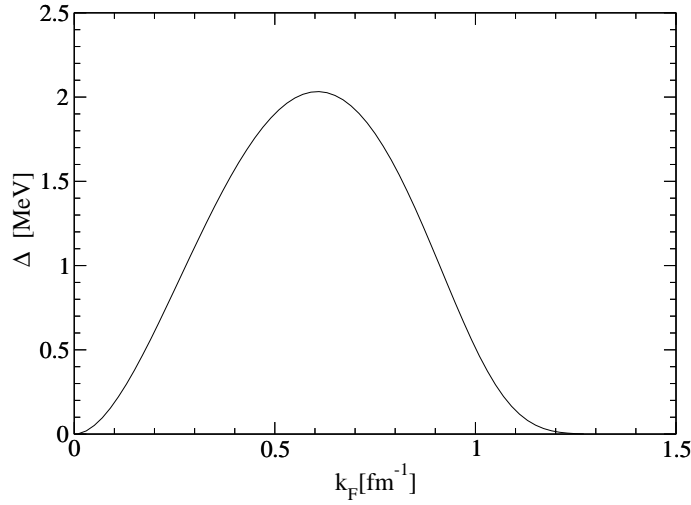


Figure 1.17.: Gap function Δ on the Fermi surface as a function of density for the interaction $\mathbf{V}_0^*(k, k')$

where all numerical factors and regular terms have been omitted. Right above the threshold $\chi \rightarrow 0^-$ the real part is regular. In contrast, the imaginary part is divergent right above the threshold since the radial momentum derivative of the energy denominator is vanishing:

$$\lim_{\chi \rightarrow 0^-} \text{Im} \mathbf{A} \sim \int dp \delta(\omega - 2\tilde{\xi}_p) \sim \sum_n \left[\frac{d}{dp} \sqrt{\xi_p^2 + \Delta(p)^2} \Big|_{p=p_n} \right]^{-1} \sim \frac{1}{\sqrt{-\chi}}, \quad (1.82)$$

where all factors and regular terms have again been suppressed. At finite CM momenta \mathbf{P} , this singular behaviour is removed by the angular integration.

Due to this quite complex analytic structure it may be instructive to calculate some elements of $\mathbf{\Gamma}$ explicitly. A simple example for a separable interaction which allows pairing is a pure S -wave interaction of the following form

$$\mathbf{V}_0^*(k, k') = \lambda^* \mathbf{V}_0^*(k) \mathbf{V}_0^*(k'), \quad \lambda^* = -2.5 \text{ fm}; \quad \mathbf{V}_0^*(k) = \begin{pmatrix} e^{-(ak)^2} & 0 \\ 0 & e^{-(ak)^2} \end{pmatrix}, \quad (1.83)$$

with $a = 1 \text{ fm}$. The solution of the gap equation for this potential as a function of k_F is shown in Fig. 1.17. In Fig. 1.18 the dispersion relation $\omega_G = \omega^+(\mathbf{P})$ for the Goldstone excitation is shown. One finds the typical linear behaviour for small \mathbf{P} , whereas for larger momenta the slope decreases and the Goldstone boson approaches the two-particle threshold in an asymptotic way.

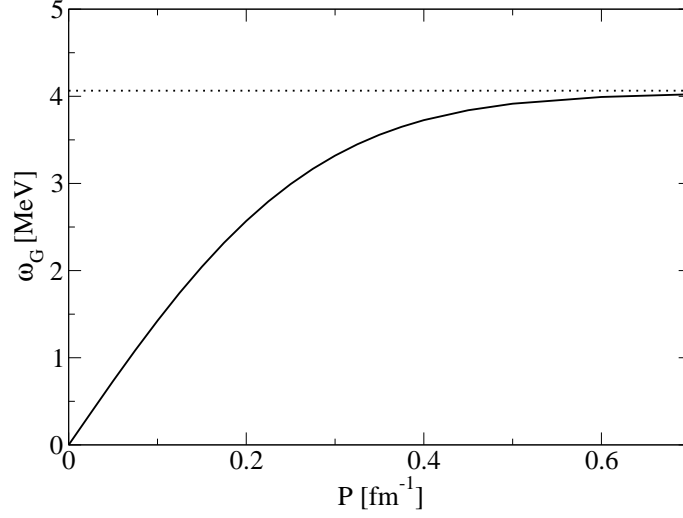


Figure 1.18.: Dispersion relation of the Goldstone boson with energy ω_G for the interaction $\mathbf{V}_0^*(k, k')$ at $k_F = 0.6 \text{ fm}^{-1}$. The dashed line denotes the two-particle threshold 2Δ .

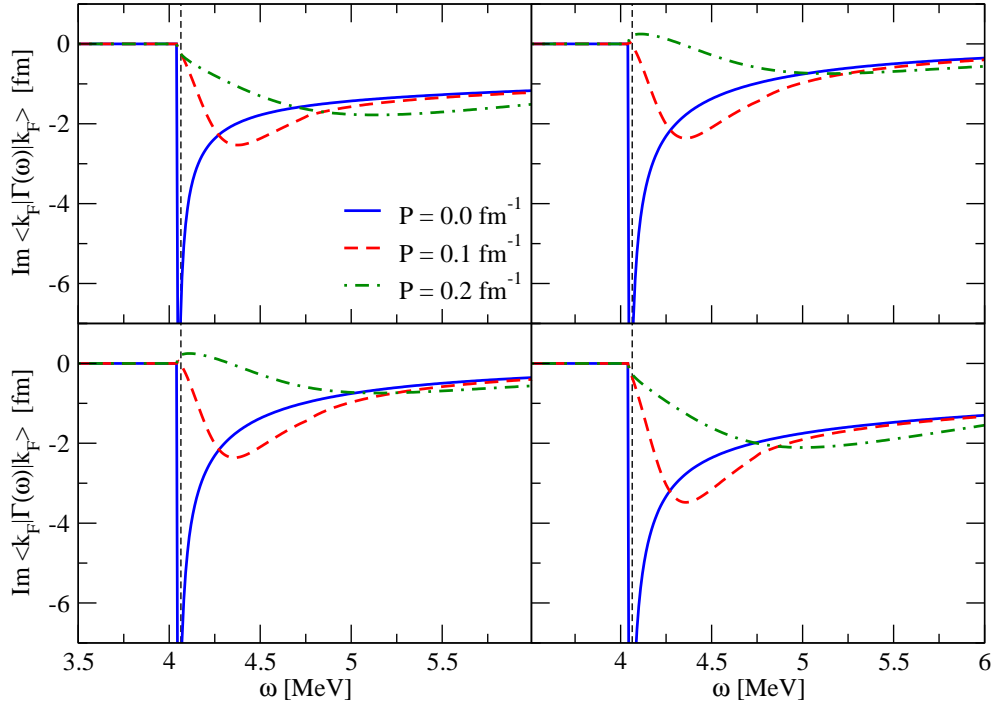


Figure 1.19.: Imaginary part of the vertex function for momenta on the Fermi surface for different CM momenta as a function of energy ω for the interaction $\mathbf{V}_0^*(k, k')$ at $k_F = 0.6 \text{ fm}^{-1}$. The plots show the elements Γ_{11} (upper left), Γ_{14} (upper right), Γ_{41} (lower left) and Γ_{44} (lower right). The vertical dotted line denotes the two-particle threshold.

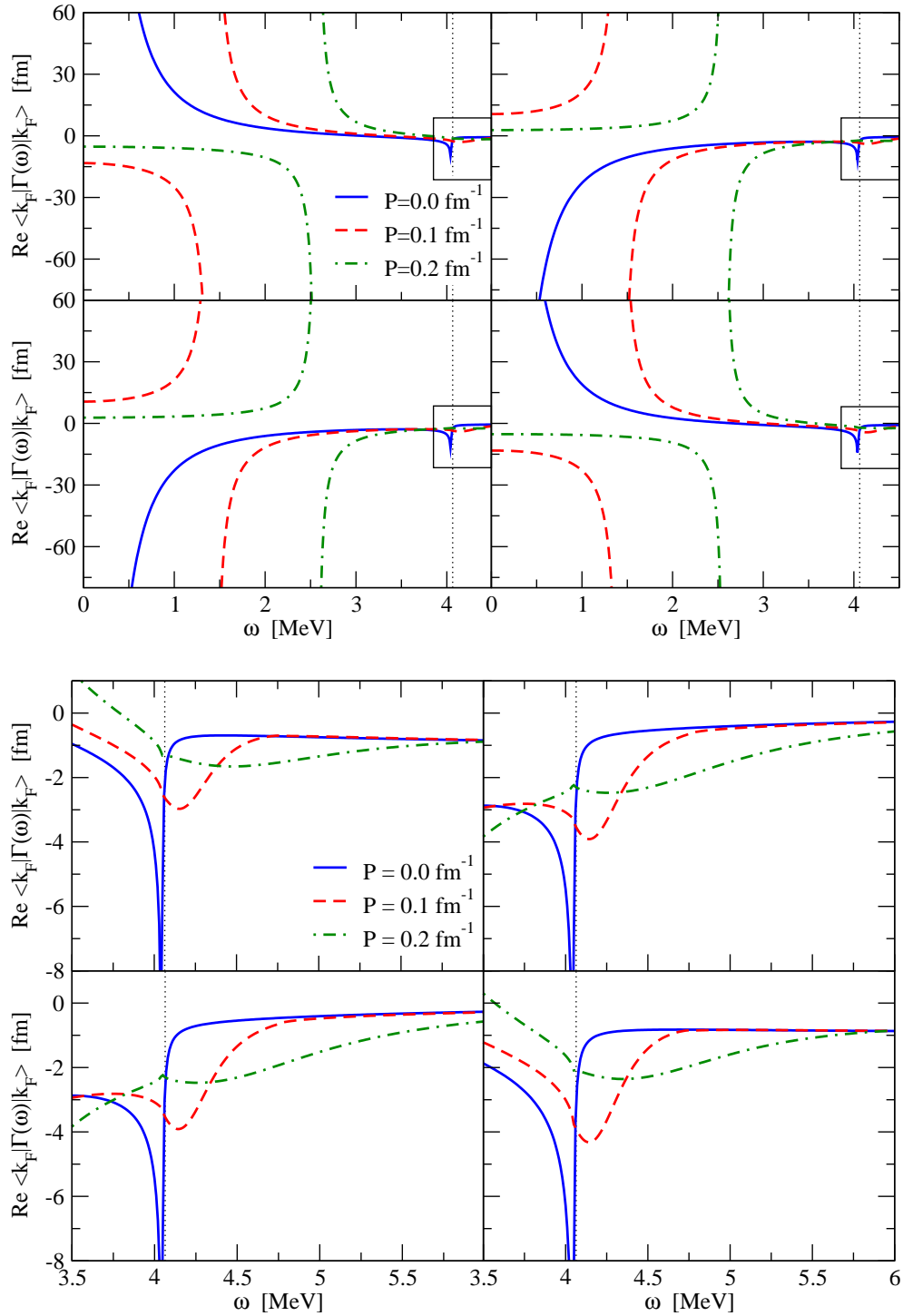


Figure 1.20.: Real part of the four point vertex Γ . The lower panel shows the magnification of the energy region around the two-particle threshold (marked by the boxes in the plots in the upper panel). The same notation and parameters as in Fig. 1.19 have been used.

In Fig. 1.19 and 1.20 are shown the results for the four point vertex on the Fermi surface $\langle k_F | \Gamma | k_F \rangle$ for the interaction \mathbf{V}_0^* as a function of energy ω . The calculations are performed for the 2x2 case in Gorkov space. The graphics arrays in the two figures show the results in the form $\begin{array}{|c|c|} \hline \Gamma_{11} & \Gamma_{14} \\ \hline \Gamma_{41} & \Gamma_{44} \\ \hline \end{array}$. In the case of a linear single-particle dispersion relation $\xi_{\mathbf{p}} \sim v_f(|\mathbf{p}| - k_F)$, the vertex function elements would be perfectly particle-hole symmetric, i.e. $\Gamma_{11} = \Gamma_{44}$. In the present case however, the free single particle spectrum $\xi_{\mathbf{p}} = \frac{\mathbf{p}^2 - k_F^2}{2m}$ has been used. By doing this, the symmetry is broken and consequently the final results for Γ_{11} and Γ_{44} differ slightly. The elements Γ_{14} and Γ_{41} however coincide exactly due to the symmetries of the scattering equation (1.62) (cf. section 1.7). Below the two-body threshold the imaginary part of the vertex elements clearly vanishes, whereas right above the threshold the characteristic singular behaviour appears in the back-to-back case. However, as one can see already at quite small CM momenta \mathbf{P} , these singularities are removed by the angular integrals and the vertex behaves smoothly around the threshold (cf. Fig. 1.19). The real part behaves in a completely analogous way right below the threshold (cf. Fig. 1.20). Additionally the Goldstone pole moves towards the threshold as shown in Fig. 1.18.

1.9. Relation between Gap Equation and Scattering Equation

The appearance of the Cooper pairs as poles in the scattering amplitude, as shown in the last section for a separable interaction, is a general feature of the scattering equation (1.62). We will generalize the discussion of the last section by considering arbitrary non-separable interactions in the 4x4 Gorkov space. By this one can see explicitly, how the particle-hole interactions, i.e. the elements $V_{22}, V_{23}, V_{32}, V_{33}$ in \mathbf{V} (cf. eq. (1.55)) completely decouple in the back-to-back case and consequently only the particle-particle interaction V_{11} enters the gap equation as kernel.

In the vicinity of a pole at ω^* the inhomogeneous part of the scattering equation can be neglected. Furthermore since we are interested in the Cooper bound state it is sufficient to consider only the case $\mathbf{P} = 0$:

$$\langle \mathbf{k}' | \Gamma(\omega \rightarrow \omega^*) | \mathbf{k} \rangle = \sum_{\mathbf{q}} \langle \mathbf{k}' | \mathbf{V} | \mathbf{q} \rangle \mathbf{G} \mathbf{G}(\mathbf{q}, \omega \rightarrow \omega^*) \langle \mathbf{q} | \Gamma(\omega \rightarrow \omega^*) | \mathbf{k} \rangle \quad (1.84)$$

with $\langle \mathbf{k}' | \mathbf{X} | \mathbf{q} \rangle = \langle \mathbf{k}' - \mathbf{k}' | \mathbf{X} | \mathbf{q} - \mathbf{q} \rangle$. The \mathbf{k} -dependence clearly factorizes and we can parametrize the vertex function in the form (the boundary conditions play no role since the energy denominator drops out in the following, hence we leave

them unfixed here):

$$\langle \mathbf{k}' | \Gamma(\omega \rightarrow \omega^*) | \mathbf{k} \rangle = \langle \mathbf{k}' | \Gamma_{\alpha\beta}(\omega \rightarrow \omega^*) | \mathbf{k} \rangle \equiv \frac{u_\alpha(\mathbf{k}') u_\beta(\mathbf{k})}{\omega - \omega^* \pm i\eta} \quad (1.85)$$

with $\alpha, \beta \in \{1, 2, 3, 4\}$. Hence we get

$$u_\alpha(\mathbf{k}') = \sum_{\mathbf{q}} \langle \mathbf{k}' | V_{\alpha\beta} | \mathbf{q} \rangle GG_{\beta\gamma}(\mathbf{q}, \omega \rightarrow \omega^*) u_\gamma(\mathbf{q}). \quad (1.86)$$

The Cooper bound state is located on the Fermi surface at $\omega^* = 0$ (cf. section 1.8). In the back-to-back case the propagator elements depend only on the absolute value of the momenta $GG_{\beta\gamma}(\mathbf{q}, \omega \rightarrow 0) = GG_{\beta\gamma}(q)$ (cf. eq. (1.42))

$$\mathbf{G}\mathbf{G}(q) = -\frac{1}{2\tilde{\xi}_q} \begin{pmatrix} u_q^4 & u_q^3 v_q - u_q v_q^3 & -u_q^3 v_q + u_q v_q^3 & 2u_q^2 v_q^2 \\ u_q^3 v_q - u_q v_q^3 & 2u_q^2 v_q^2 & -2u_q^2 v_q^2 & u_q^3 v_q - u_q v_q^3 \\ u_q v_q^3 - u_q^3 v_q & -2u_q^2 v_q^2 & 2u_q^2 v_q^2 & u_q v_q^3 - u_q^3 v_q \\ -2u_q^2 v_q^2 & u_q^3 v_q - u_q v_q^3 & u_q v_q^3 - u_q^3 v_q & u_q^4 + v_q^4 \end{pmatrix}, \quad (1.87)$$

whereas the interaction matrix obeys, according to eq. (1.53), the following symmetry relations:

$$\begin{aligned} \langle \mathbf{k}' | V_{11} | \mathbf{q} \rangle &= -\langle \mathbf{k}' | V_{11} | -\mathbf{q} \rangle = -\langle -\mathbf{k}' | V_{11} | \mathbf{q} \rangle = \langle -\mathbf{k}' | V_{11} | -\mathbf{q} \rangle \\ \langle \mathbf{k}' | V_{22} | \mathbf{q} \rangle &= \langle \mathbf{k}' | V_{23} | -\mathbf{q} \rangle = \langle -\mathbf{k}' | V_{23} | \mathbf{q} \rangle = \langle -\mathbf{k}' | V_{22} | -\mathbf{q} \rangle \\ \langle \mathbf{k}' | V_{33} | \mathbf{q} \rangle &= \langle \mathbf{k}' | V_{32} | -\mathbf{q} \rangle = \langle -\mathbf{k}' | V_{32} | \mathbf{q} \rangle = \langle -\mathbf{k}' | V_{33} | -\mathbf{q} \rangle \\ \langle \mathbf{k}' | V_{44} | \mathbf{q} \rangle &= -\langle \mathbf{k}' | V_{44} | -\mathbf{q} \rangle = -\langle -\mathbf{k}' | V_{44} | \mathbf{q} \rangle = \langle -\mathbf{k}' | V_{44} | -\mathbf{q} \rangle. \end{aligned} \quad (1.88)$$

The change of sign in the momenta implicitly involves a spin-flip. Due to these special symmetry relations of the vertex and propagator, one can show that the functions $u_2(\mathbf{k}')$ and $u_3(\mathbf{k}')$ decouple in the system (1.86). In order to see this explicitly, let us introduce the symmetrized function $\tilde{u}_\alpha(\mathbf{p}) \equiv \frac{1}{2}[u_\alpha(\mathbf{p}) + u_\alpha(-\mathbf{p})]$. In terms of this function the system (1.86) can be rewritten as:

$$\tilde{u}_1(\mathbf{k}') = \sum_{\mathbf{q}} \langle \mathbf{k}' | V_{11} | \mathbf{q} \rangle GG_{1\alpha}(q) \tilde{u}_\alpha(\mathbf{q}) \quad (1.89)$$

$$\tilde{u}_2(\mathbf{k}') = \frac{1}{2} \sum_{\mathbf{q}} [\langle \mathbf{k}' | V_{2\alpha} | \mathbf{q} \rangle + \langle \mathbf{k}' | V_{3\alpha} | \mathbf{q} \rangle] GG_{\alpha\beta}(q) \tilde{u}_\beta(\mathbf{q}) \quad (1.90)$$

$$\tilde{u}_3(\mathbf{k}') = \frac{1}{2} \sum_{\mathbf{q}} [\langle \mathbf{k}' | V_{2\alpha} | \mathbf{q} \rangle + \langle \mathbf{k}' | V_{3\alpha} | \mathbf{q} \rangle] GG_{\alpha\beta}(q) \tilde{u}_\beta(\mathbf{q}) \quad (1.91)$$

$$\tilde{u}_4(\mathbf{k}') = \sum_{\mathbf{q}} \langle \mathbf{k}' | V_{44} | \mathbf{q} \rangle GG_{4\alpha}(q) \tilde{u}_\alpha(\mathbf{q}). \quad (1.92)$$

The particle hole elements of the two-particle propagator obey in back-to-back

kinematics the relations $GG_{2\alpha}(q) = -GG_{3\alpha}(q)$ and consequently the second and third equation involves the product of a symmetric matrix with an asymmetric one in the index α (note $\langle \mathbf{k}' | V_{22} | \mathbf{q} \rangle = \langle \mathbf{k}' | V_{33} | \mathbf{q} \rangle$ and $\langle \mathbf{k}' | V_{23} | \mathbf{q} \rangle = \langle \mathbf{k}' | V_{32} | \mathbf{q} \rangle$). This implies:

$$\tilde{u}_2(\mathbf{k}') = \tilde{u}_3(\mathbf{k}') = 0. \quad (1.93)$$

By using the explicit expression (1.87) for the propagator elements, it follows that the system

$$\begin{aligned} \tilde{u}_1(\mathbf{k}') &= \sum_{\mathbf{q}} [\langle \mathbf{k}' | V_{pp} | \mathbf{q} \rangle GG_{11}(q) \tilde{u}_1(\mathbf{q}) + \langle \mathbf{k}' | V_{pp} | \mathbf{q} \rangle GG_{14}(q) \tilde{u}_4(\mathbf{q})] \\ \tilde{u}_4(\mathbf{k}') &= \sum_{\mathbf{q}} [\langle \mathbf{k}' | V_{pp} | \mathbf{q} \rangle GG_{41}(q) \tilde{u}_1(\mathbf{q}) + \langle \mathbf{k}' | V_{pp} | \mathbf{q} \rangle GG_{44}(q) \tilde{u}_4(\mathbf{q})] \end{aligned}$$

has the general solution

$$\tilde{u}_1(\mathbf{k}') = \pm \tilde{u}_4(\mathbf{k}'). \quad (1.94)$$

This ambiguity can be resolved by using the arguments of the previous section. Hence by choosing the second solution we obtain:

$$\tilde{u}(\mathbf{k}') = - \sum_{\mathbf{q}} \langle \mathbf{k}' | V_{pp} | \mathbf{q} \rangle \frac{\tilde{u}(\mathbf{q})}{2\tilde{\xi}_q}. \quad (1.95)$$

The single particle energies $\tilde{\xi}_q$ are defined via the gap equation (1.15). Hence consistency requires that we identify

$$\tilde{u}(\mathbf{k}') = \Delta_{\mathbf{k}'}. \quad (1.96)$$

This shows that the bound states at $\omega^* = 0$ are indeed the Cooper pairs.

The chain of arguments above can also be reversed. By starting from the gap equation (1.15), one can show explicitly just by following the steps above backwards that the gap function is indeed the solution of a homogeneous scattering equation. By reasoning in this way the ambiguities encountered above disappear completely.

1.10. Problems and Limitations of the Inversion Approach

Apart from simple separable interactions like \mathbf{V}_0^* where the scattering equation can be solved explicitly, the solution of eq. (3.66) by inversion is quite inconvenient due to several problems:

- The number of poles in the propagator can vary from zero below threshold, over one far above threshold, to two right above threshold. These poles

have to be regularized properly before the equation can be inverted in a similar way to the Lippmann-Schwinger equation in vacuum (see e.g. [73]). However, in contrast to the vacuum case where only one pole is present, the inversion of equations like (1.58), which include two poles is numerically much more demanding.

- At finite CM momentum \mathbf{P} the angular integral contains, even after successful regularization of the radial integral, integrable singular regions (cf. Appendix A), which makes further subtraction procedures necessary.

These problems, connected with the complex analytic structure, are of course also present in the RG flow equations. However in contrast to the inversion approach, in the flow equations the Cauchy principal value integrals only have to be performed over *known functions*. Hence only a proper regularization of the integrals is necessary in order to evaluate the flow equation (cf. Appendix A.1). This simplifies the technical treatment considerably.

Beside these technical problems the inversion approach is also quite limited conceptually:

- It is not so clear how to include systematically effects of additional many-body correlations in a non-perturbative way, since the irreducible kernels are not known a priori, but have to be determined by solving a system of coupled integral equations (cf. chapter 3). Hence, some kind of iterative solution techniques must be applied in order to obtain a consistent solution. However, a naive iterative approach is complicated by the very complex analytical structure of the vertex function Γ (cf. section 1.8), so that a stable convergence is quite unlikely.
- The many-body effects also influence the dispersion properties of the single particle states. The vertices appearing in the self-energies should ideally be self-consistently related to the four-point functions. Vice versa, the single-particle propagators appearing in a diagram of a four-points function is implicitly given by the these self-energies. Hence in general there exist, additional to the channel coupling mentioned above, a self-consistency problem between two and four-point functions, which complicates the problem furthermore.

A promising approach to these problems is the Renormalization Group (RG). In the next chapter we will review very briefly the basic ideas behind renormalization and show how these methods can be applied to the present problem and how the technical difficulties mentioned above can be treated in this scheme. Furthermore it turns out that the RG framework is much more general and flexible from the conceptual point of view for a more realistic treatment of strongly interacting systems than the approach used in section 1.8.

2. RG approach to Superfluid many-body systems

2.1. Basic Ideas

The ideas behind renormalization are very general and can be applied to many different kinds of quantum mechanical systems. Apart from the well known applications in relativistic quantum field theories and critical phenomena (cf. below) in the last century, RG methods have been successfully applied in various areas like atomic systems [74], nonlinear dynamics [75], genetic algorithms [76] and the study of bound states [77]. Although the techniques differ in detail, they were all developed for one common purpose: to treat fluctuations in these systems at certain *scales* in a controlled way.

The original motivation for the development of the concept of renormalization was the discovery of ultraviolet divergences in Quantum Electrodynamics (QED) in the 1920s and 1930s. Various strategies had been developed during this time to deal with these divergences (see ref. [78] for an overview). However, the subtraction of the infinities in these calculations was done in a more or less ad hoc way by introducing cutoffs at reasonable scales. Hence despite the remarkable agreement of the theoretical results for the Lamb shift in 1947 [79, 80] and the anomalous magnetic moment of the electron in 1948 [81], the renormalization procedure was still widely considered as a mysterious procedure that created miraculously finite answers out of infinities. Even after the works of R. Feynman, J. Schwinger, S. Tomonaga and F. Dyson (see [82] and references therein), who showed that perturbatively all the infinities can be absorbed by a mass and charge renormalization, there was a general unease about this procedure. Even several years later in 1975 Dirac expressed it with the words: "Sensible mathematics involves neglecting a quantity when it is small - not neglecting it just because it is infinitely great and you do not want it!" , [83] Feynman himself and also suggested it was "mathematically not legitimate" [84].

The point of view regarding the procedure of renormalization changed substantially with the works of Kadanoff [85] and Wilson [86, 87, 88], who applied RG methods for the first time to critical phenomena in condensed matter systems (for a recent introductory review with historical remarks see [89]). Here the particles are living on a lattice and consequently the inverse lattice spacing provides a natural ultraviolet cutoff, which renders all sums over intermediate momenta finite. Hence from the particle physicist's point of view at that time, there would

have been no need for renormalization at all in these systems.

However, Kadanoff and Wilson gave a different and very intuitive interpretation of renormalization: rather than being a mathematical procedure for removing unpleasant infinities it is a powerful tool for systematically *integrating out* degrees of freedom at a certain scale. This can be seen in a beautiful way in Kadanoff's block spin picture. The basic idea consists of coarse graining degrees of freedom. Kadanoff considered a spin system on a lattice with a spacing a described by the Hamiltonian $H(g)$ with the nearest neighbour coupling g . Instead of trying to solve this system in one step, Kadanoff divided this problem into many, much easier steps. He replaced the spins within a block of side la with $l > 1$ by a single *block spin*, whose magnetization is given by the average over the spins of its constituents (see [90] for details). If the length scales in this block spin system are rescaled in such a way that in the new units the block spins are separated by the original distance of the spins, the new system looks like the original system described now by the new Hamiltonian $H'(g'_i)$, where g'_i describes the interaction between the block spins. Hence the coupling constants have been *renormalized*. The physics of the system is by construction invariant under this transformation. Only the parametrization in the form of the new Hamiltonian has been changed.

However, the fact that the original Hamiltonian $H(g)$ included only a nearest neighbour interaction does *not* automatically imply that only adjacent block spins are interacting. In general many new couplings are generated by this block-spin transformation¹. After one block-spin transformation, the spin fluctuations within one block spin have been integrated out and consequently the number of degrees of freedom has been reduced. The initial cutoff $\Lambda_0 \sim \frac{1}{a}$ is, after rescaling, located at $\Lambda \sim \frac{1}{la} < \Lambda_0$. The transformations of this kind form a group and define the RG.

By iterating this procedure many times towards the infrared $\Lambda \rightarrow 0$ the flow ends at a *fixed point* (if there is one), characterized by the Hamiltonian $H^*(g_i^*)$, which remains invariant under the RG transformation. Depending on the flow behaviour of the different coupling constants around this point, they can be classified as relevant if they are always growing, irrelevant if they are renormalized to zero and marginal in any other case. As the name indicates the macroscopic properties of the system are dominated by the relevant and marginal couplings, whereas the irrelevant are strongly suppressed. However that does not mean that irrelevant operators play no role in the dynamics of the system since they in general affect the flow of the other parameters before they get suppressed around the fixed point.

Due to this suppression of the irrelevant couplings, the physics of the system can be understood much more easily easier by looking at the effective Hamiltonian $H^*(g^*)$ instead of at the original $H(g)$. For example, the phenomenon of universality can be understood quite easily in this formalism. Two systems are

¹Historically this possibility was also excluded in Kadanoff's original work.

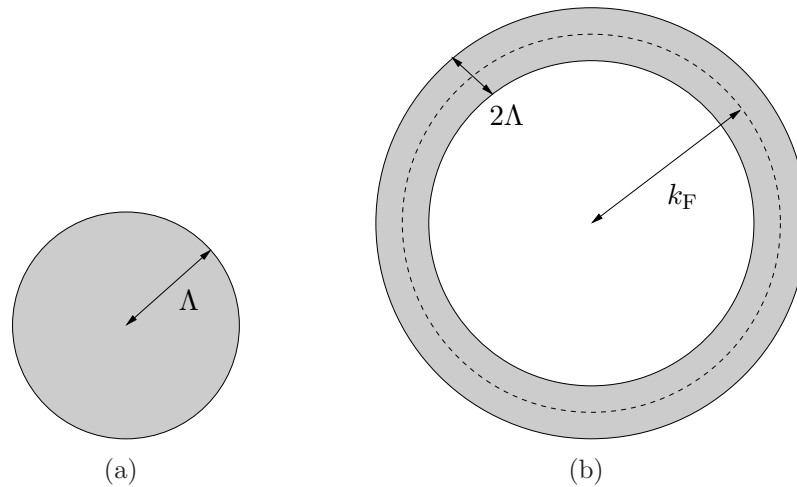


Figure 2.1.: Low momentum one-body Hilbert-space in a) vacuum and b) in many-body systems with a Fermi surface

in the same universality class, if they end up in the same fixed point Hamiltonian H' . Since the scaling behaviour is dominated by the very slow modes ($\xi \rightarrow \infty$), only the relevant couplings are crucial. However, other non-universal observables in general differ.

In this picture the renormalization of QED can be understood quite intuitively. Instead of trying to send the cutoff in QED to infinity, the natural cutoff for a continuum theory, QED should be considered as (and very likely is) an effective theory of a more fundamental theory. In this case a natural cutoff must be introduced, which marks the border line up to where QED is valid and renders all integrals finite. The effects of the modes beyond this line are parametrized by additional local operators (counterterms), whose values have to be fixed by experiment (for details see [91, 92]). From this point of view, renormalization is no more a mysterious procedure but more a natural tool applicable to any effective field theory and has a priori nothing to do with the occurrence of infinities (see also [78]).

2.2. RG Approach to Many-Fermion Systems

In the spirit of Kadanoff and Wilson the floating cutoff Λ represents just the dividing line between the *fast modes* $k > \Lambda$, which have already been integrated out and incorporated into the effective operators of the theory and the *slow modes*, which define the Hilbert space of the effective Hamiltonian. The RG trajectory connects all the effective theories at different scales, which all describe the same physical observables in the infrared.

In the case of vacuum QED and critical systems the infrared momentum region

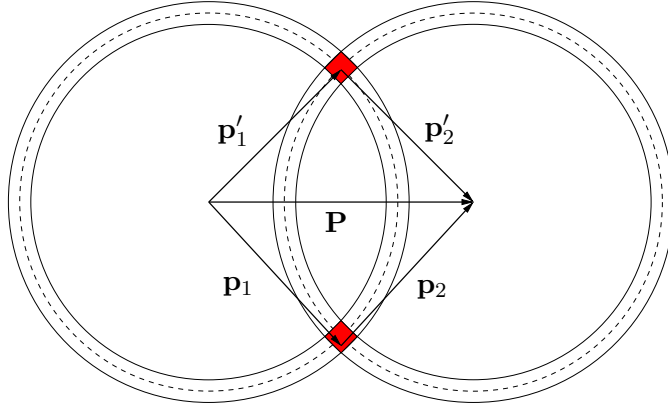


Figure 2.2.: Two dimensional projection of the allowed kinematics for two interacting low lying states for the process $\mathbf{P} = \mathbf{p}_1 + \mathbf{p}_2 \rightarrow \mathbf{p}'_1 + \mathbf{p}'_2$. Due to momentum conservation the final states \mathbf{p}'_1 and \mathbf{p}'_2 are also constrained to the shaded areas. This leads to the two special kinematical cases shown in Fig. 2.3.

can be illustrated by a sphere with radius Λ . From the topology of a sphere it follows immediately that the allowed momentum *transfers* between two momentum states located within this sphere are also limited by 2Λ and consequently vanish in the limit $\Lambda \rightarrow 0$.

The situation changes completely in fermionic many-body systems. The low lying excitations are not located at $k = 0$ but around the Fermi surface $k = k_F$. Hence it is natural and necessary to introduce the momentum cutoff with respect to the Fermi surface (see Fig. 2.1). Since the RG transformations only reduce the Hilbert space perpendicular to the Fermi surface, whereas the tangential direction is unaffected, the low momentum Hilbert space has a completely different topology. Even in the limit $\frac{\Lambda}{k_F} \rightarrow 0$ the momentum transfers in interactions between two states located in the annulus of width 2Λ can still be on the order of k_F . Thus the kinematics of the interactions between the low energy effective degrees of freedom are much more complex than in the vacuum.

Shankar used exactly this insight as the starting point for his RG analysis of the Fermi systems [93]. He initially assumed some small bare two-particle interaction, performed a mode elimination procedure analogous to Kadanoff's and analyzed the flow behaviour of the different interactions under the RG transformations up to one loop order.

The flow behaviour at tree level can be quite easily understood if one considers the kinematics of the possible interactions in the limit $\frac{\Lambda}{k_F} \rightarrow 0$ (see Fig. 2.2). One can verify quite easily that only those couplings in which

$$|\hat{\mathbf{p}}_1 + \hat{\mathbf{p}}_2 - \hat{\mathbf{p}}'_1| = 1 \quad (\hat{\mathbf{p}} = \mathbf{p}/|\mathbf{p}|), \quad (2.1)$$

is satisfied survive the RG flow, whereas $\hat{\mathbf{p}}'_2$ is given by momentum conservation. This equation has the following solutions:

- BCS case: $\mathbf{p}_1 = -\mathbf{p}_2, \mathbf{p}'_1 = -\mathbf{p}'_2$. This interaction is responsible for the Cooper pairing:

$$V(\mathbf{p}_1, \mathbf{p}_2, \mathbf{p}'_1, \mathbf{p}'_2) = V_{BCS}(\mathbf{p}_1 \cdot \mathbf{p}'_1) \quad (2.2)$$

- Landau case: $\hat{\mathbf{p}}_1 \cdot \hat{\mathbf{p}}_2 = \hat{\mathbf{p}}'_1 \cdot \hat{\mathbf{p}}'_2$. This interaction includes the quasiparticle interaction of Landau's Fermi Liquid theory:

$$V(\mathbf{p}_1, \mathbf{p}_2, \mathbf{p}'_1, \mathbf{p}'_2) = V_{Landau}(\mathbf{p}_1 \cdot \mathbf{p}_2). \quad (2.3)$$

The forward scattering case ($\hat{\mathbf{p}}_1 = \hat{\mathbf{p}}'_1, \hat{\mathbf{p}}_2 = \hat{\mathbf{p}}'_2$) corresponds to the quasiparticle interaction parametrized by the Landau Parameters:

$$V_{Landau}(\mathbf{p}_1 \cdot \mathbf{p}_2, \hat{\mathbf{p}}_1 = \hat{\mathbf{p}}'_1, \hat{\mathbf{p}}_2 = \hat{\mathbf{p}}'_2) = F(\cos \theta_{\mathbf{p}_1 \mathbf{p}_2}). \quad (2.4)$$

These forward scattering processes dominate the low-energy physics of a normal Fermi liquid (see discussion below).

Hence by this kinematical analysis, it can be shown that two couplings V_{Landau} and V_{BCS} remain marginal at tree level under the RG flow, whereas all others are renormalized to zero around the fixed point $\frac{\Lambda}{k_F} \rightarrow 0$. To one loop order the analogous analysis has to be done for the internal momenta in the diagrams shown in Fig. 1.2, in the case of the Landau-interaction V_{Landau} the forward scattering processes plays a special role. Here the initial pair of states lies in the same plane as the final pair and hence no restrictions on the angular loop integral appear. In contrast, in the non-forward scattering amplitudes the loop momenta is restricted to a size of Λ/k_F , by which the contribution of these processes is strongly suppressed compared to the forward processes around the fixed point. Since both loop momenta are required to be part of the low momentum Hilbert space, the loop integral is on the order of $d\Lambda^2$, where $d\Lambda$ denotes the thickness of the shell to be eliminated. However, as pointed out by Dupuis [94], this RG scheme generates also a marginal three-body interaction, which has to be taken into account in order to avoid unphysical discontinuities in the Landau interaction in the forward direction. In total, the flow of V_{Landau} around the fixed point vanishes and the quasiparticle interaction F remains marginal to one loop order [93].

Also in the interaction V_{BCS} , interesting things happen at one-loop order. In back-to-back kinematics the angular loop integral can run freely over all angles leading in total to a contribution of order $d\Lambda$. By this the interaction becomes *relevant* in the attractive case and *irrelevant* in the repulsive case [93, 95, 96]. The presence of a relevant coupling leads to singularities in the flow and signals, in the case of Fermi liquids, the transition from the normal to the superfluid state.

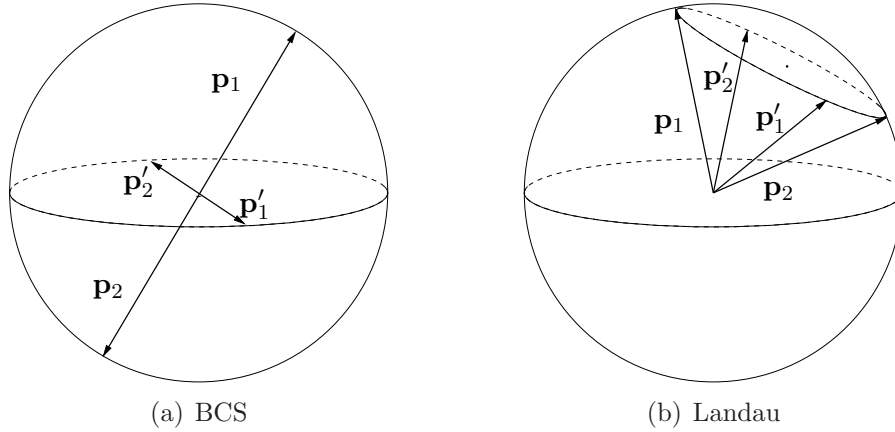


Figure 2.3.: Marginal interactions at tree level in a many-fermion system. At one loop order the BCS coupling becomes relevant in the attractive case and irrelevant in the repulsive case. In the repulsive case the system remains non-superfluid and the Landau interaction (right) is the only marginal coupling in the system.

Hence from this modern point of view, Landau's Fermi-Liquid theory can be identified as a line of fixed point Hamiltonians, which all share the same symmetries but differ in their Landau parameters [97]. These parameters describe the marginal operators of the fixed point Hamiltonians. In this sense, a normal Fermi liquid can be defined in this scheme as a system with no relevant interactions. In the presence of relevant operators the symmetries of the system change fundamentally, signalling the transition to the superfluid phase.

Of course, these results by themselves were by no means new insights at that time. As mentioned in chapter 1 the Cooper phenomenon was known since 1959 and the microscopic foundations of Fermi Liquid theory have been established first by Landau himself in 1956 [27, 28, 29] and later refined in the 1960s [26]. However these calculations involved quite technical manipulations of integral equations. In contrast, the great advantage of the RG approach is its intuitive character, which leads undoubtedly to a better *understanding* of the fundamental mechanisms in these systems.

2.3. Solving Many-Body Problems by using the RG

In the RG formulation of Wilson, Kadanoff and Shankar the mode elimination of one shell always includes a rescaling of the momenta and the field variables. In this case, the RG trajectory consists of a mapping of the original many-body Hamiltonian to a continuum of new effective Hamiltonians, each labelled by the scale Λ , which can all be compared to each other due to the rescaling procedure.

In particular the size of the Hilbert space in terms of the momenta and fields at the different scales does *not* change. Only due to this rescaling does it make sense to define a "flow" of the coupling constants of the effective Hamiltonian at the different scales. The crucial simplification of the problem shows up near the fixed points where the irrelevant couplings are strongly suppressed and the physics of the Hamiltonian becomes much more transparent since the physics is dominated by the few marginal and relevant couplings. These systems can usually be solved in a more controlled way than the original one (see also [98]).

However, RG methods can also be used as a tool to solve many-body problems directly. In this case a RG step consists only of the elimination of the modes at the current scale, whereas the scale of the fields and momenta remain unchanged. This implies that the size of the low energy Hilbert space is changing with every RG step and consequently the effective Hamiltonians cannot be compared immediately at the different scales.

However, in this approach the RG can be considered as a powerful tool for summing diagrams, which has been used by several authors in condensed matter problems [99, 100, 101, 102, 103, 104, 105, 106, 107, 108, 109].

In order to see how this works in detail in the present context, we consider as an example a one-channel two-particle scattering equation in a many-body system

$$\Gamma = \Gamma_0 + \Gamma_0 GG\Gamma. \quad (2.5)$$

Here we have introduced, for the sake of clarity, a compact notation. The product of two terms implicitly includes summations over all internal and external degrees of freedom like momentum, energy and spin-projection. GG is a two body propagator, Γ_0 the two-particle irreducible vertex in the considered channel and Γ the full reducible vertex function.

By introducing a cutoff Λ , we separate the fast modes from the slow modes and rewrite the integral equation (2.5) in the form

$$\Gamma = \Gamma^\Lambda + \Gamma^\Lambda GG^<\Gamma \quad (2.6)$$

$$\Gamma^\Lambda = \Gamma_0 + \Gamma_0 GG^>\Gamma^\Lambda \quad (2.7)$$

where $GG^>$ includes only the fast modes and $GG^<$ only the slow modes, i.e. $GG = GG^< + GG^>$.

Here the function Γ^Λ is the effective vertex function at scale Λ , which includes all contributions of the fast modes beyond this scale. The full vertex is obtained from this effective vertex by integrating only over the low momentum Hilbert space below this scale. Hence the RG trajectory connects the bare vertex Γ_0 for $\Lambda \rightarrow \infty$ with the full vertex Γ at $\Lambda \rightarrow -\infty$, i.e. when all modes have been integrated out.

Although the equations (2.6,2.7) are completely equivalent to the original problem (2.5), the reformulation of the problem in the form of equations (2.6, 2.7) has the advantage that the problem can be divided into many small steps. Instead

of solving the problem (2.5) directly, which usually involves technical problems even in this one-channel problem (cf. Sec 1.10), one can apply RG techniques to the system (2.6, 2.7) and integrate the modes systematically shell by shell.

In general one can set up such RG calculations in two ways:

- a) Keep the scattering amplitude Γ constant and renormalize the effective interaction Γ^Λ by using eq. (2.6). Here the function Γ , which defines the physics of the system, must be known. Under the requirement of the *invariance of the physics*, i.e.

$$\frac{d\Gamma}{d\Lambda} \stackrel{!}{=} 0 \quad (2.8)$$

one can derive the corresponding flow equation for the effective vertex Γ^Λ with the constraint $\lim_{\Lambda \rightarrow \infty} \Gamma^\Lambda = \Gamma_0$. This strategy corresponds to Wilson's idea of using the RG for the construction of different "bare" theories starting from a renormalized theory defined at a certain scale.

- b) Keep the interaction Γ_0 constant and renormalize the scattering amplitude Γ^Λ in eq. (2.7). Here the bare interaction Γ_0 is the experimental input. By imposing

$$\frac{d\Gamma_0}{d\Lambda} \stackrel{!}{=} 0, \quad (2.9)$$

RG methods can be used to calculate the effective vertex Γ^Λ at the different scales Λ , whereas the flow is also initialized by $\lim_{\Lambda \rightarrow \infty} \Gamma^\Lambda = \Gamma_0$. This strategy transforms different renormalized theories into one which corresponds to one bare theory (cf. also [110, 111]).

In principle these two strategies are equivalent and the choice is a matter of convenience. In order to illustrate how these two strategies work in detail in the present context we will consider two examples, which also play a crucial role in the following:

- a) *Effective low momentum interactions:*

The nucleon-nucleon (NN) interaction $\Gamma_0 = V_{bare}^{NN}$ has been determined by measuring phase shifts and the deuteron properties. These correspond to on-shell matrix elements of the *full* vertex function Γ in a certain partial wave²

$$\langle k' | \Gamma(\omega) | k \rangle = \langle k' | T(\omega) | k \rangle, \quad \tan \delta = -k \langle k | T(k^2) | k \rangle, \quad (2.10)$$

where the irreducible vertex is given by the vacuum interaction

$$\langle k' | \Gamma_0 | k \rangle = \langle k' | V_{bare} | k \rangle. \quad (2.11)$$

²For the sake of compact notation we suppress the partial wave index

In the present case the schematic eq. (2.5) is just the partial wave Lippmann-Schwinger-equation

$$\langle k' | T(\omega) | k \rangle = \langle k' | V_{bare} | k \rangle + \frac{2}{\pi} \mathcal{P} \int dq q^2 \langle k' | V_{bare} | q \rangle \frac{1}{\omega - q^2} \langle q | T(\omega) | k \rangle. \quad (2.12)$$

The determination of the matrix elements of V_{bare} from the on-shell elements (2.10) by virtue of eq. (2.12) is not unique due to the fact that potential scattering data can only be measured as a matter of principle up to the pion production threshold. As a consequence, many different interaction models exist [112, 113, 114, 115] that all fit the scattering data to high accuracy although the matrix elements $\langle k' | V_{bare} | k \rangle$ differ substantially. This ambiguity is based on different parametrizations of the experimentally unconstrained high momentum matrix elements.

By performing a RG decimation of the Hilbert space starting from the intrinsic cutoff Λ_0 of the interaction (which can be several GeV) one can construct effective interactions $\langle k' | V^\Lambda | k \rangle$, whose Hilbert space contains only momentum states below Λ but lead to the same observables as the bare interaction.

The flow equation can be derived by introducing a cutoff function $f(q, \Lambda)$ in the integral on the right hand side of eq. (2.12) and imposing the invariance on the experimentally constrained full-on-shell T -Matrix elements

$$\frac{d}{d\Lambda} \langle q | T(q^2) | q \rangle = 0 \quad (2.13)$$

The derivation involves some subtleties due to the on-shell character of the energy $\omega = q^2$. The result reads (the derivation is given in A.3, cf. also [116]):

$$\begin{aligned} \frac{d}{d\Lambda} \langle k' | V^\Lambda | k \rangle &= \frac{1}{\pi} \mathcal{P} \int dq q^2 \left(\frac{d}{d\Lambda} f(q, \Lambda) \right) \times \\ &\times \left[\frac{\langle k' | V^\Lambda | q \rangle \langle q | T(q^2) | k \rangle}{q^2 - k^2} + \frac{\langle k' | T(q^2) | q \rangle \langle q | V^\Lambda | k \rangle}{q^2 - k'^2} \right] \end{aligned} \quad (2.14)$$

This equation is equivalent to a generalization of the Lee-Suzuki transformation [117, 118] and a subsequent Okubo hermitization [119] for smooth cutoffs [116, 120].

Indeed, by evolving the scale Λ down to the pion production scale $\Lambda' \sim 2.1 \text{ fm}^{-1}$ all different models essentially collapse to a unique effective low momentum interaction $\langle k' | V^{\Lambda \sim 2.1} | k \rangle \equiv \langle k' | V_{lowk} | k \rangle$.

It should be noted that these effective interactions could in principle also be obtained by eq. (2.7). In this case one would take a "bare" interac-

tion $\Gamma_0 = V_{bare}$ as input. However in this case the condition (2.13) could not be imposed immediately to the equation since the full vertex does not appear in eq. (2.7). This condition could only be implemented implicitly on the invariance of the bare interaction matrix elements. However this is quite unsatisfactory since these matrix elements are highly model dependent. Thus it is clearly much more advantageous and natural to start from eq. (2.6).

b) *In-medium scattering amplitude:*

Compared to vacuum potential scattering, the analogous processes in nuclear matter are much more difficult - experimentally and theoretically. From the experimental side no simple direct measurements of in-matter scattering amplitudes are possible, whereas the theoretical description is complicated by the fact that the scattering process is now a coupled channel problem instead of a single channel problem.

The microscopic approach to this problem consists of using the vacuum NN-interaction V_{bare} as the input to the scattering equation and incorporating all many-body effects systematically by calculating the corresponding diagrams. Hence in contrast to the vacuum case where the function Γ is the observable, here Γ_0 is the experimental input and the full in-medium vertex function Γ is the function to be determined. This function depends in general on the CM momentum of the interacting pair, the initial and final relative momenta and the off-shell energy of the pair (cf. section 1.7).

The one-channel problem (2.5) could in principle be solved by inversion:

$$\Gamma = (1 - \Gamma_0 G G)^{-1} \Gamma_0. \quad (2.15)$$

However in practice, this approach involves several problems and limitations (cf. 1.10) due to the fact that, on the one hand the inversion routine is very impractical and the more important problem that the kernel Γ_0 is a priori not known in the coupled channel problem.

However, let us first consider the one-channel problem of section 1.7 and reformulate this problem by using RG methods. For this we assume that Γ_0 is known and impose the condition (2.9) on this irreducible kernel. By this one obtains:

$$\frac{d\Gamma^\Lambda}{d\Lambda} = \Gamma_0 \frac{dGG^\Lambda}{d\Lambda} \Gamma^\Lambda + \Gamma_0 GG^\Lambda \frac{d\Gamma^\Lambda}{d\Lambda}. \quad (2.16)$$

This equation can be inverted *explicitly*:

$$\frac{d\Gamma^\Lambda}{d\Lambda} = (1 - \Gamma_0 GG^\Lambda)^{-1} \Gamma_0 \frac{dGG^\Lambda}{d\Lambda} \Gamma^\Lambda = \Gamma^\Lambda \frac{dGG^\Lambda}{d\Lambda} \Gamma^\Lambda, \quad (2.17)$$

where we have used eq. (2.7) in the last step. Clearly, this flow equation

contains no inverse matrices, which turns out to be very convenient in practice especially for multi-dimensional integral equations (see section 1.10).

In the multi-channel problem however, this explicit inversion is not possible anymore. We will return to this problem in chapter 3.

In the following we will apply these two RG approaches to neutron matter. Furthermore it will be shown that in particular a combination of these two approaches provides a quite promising approach to many-body systems.

2.4. Interaction dependence of the pairing gap ³

As mentioned above, for relative momenta $k \lesssim 2 \text{ fm}^{-1}$ NN interactions are well constrained by the existing scattering data [122]. The model dependence for larger momenta shows up prominently, for instance, in the $^3\text{P}_2$ superfluid pairing gaps for Fermi momenta $k_{\text{F}} > 2 \text{ fm}^{-1}$ (cf. Fig. 1.7). However, some uncertainty remains concerning a possible dependence of the $^1\text{S}_0$ pairing gap on the input NN interaction in low-density neutron matter ($k_{\text{F}} < 1.6 \text{ fm}^{-1}$).

In addition to chiral effective-field theory (EFT) and conventional NN interactions, we use the RG to evolve nuclear interactions to a lower resolution scale. The resulting class of low-momentum interactions $V_{\text{low } k}$ [122, 123, 116], which is defined by a regulator with a variable cutoff Λ , reproduces the NN scattering phase shifts for momenta below Λ .

Contact or separable pairing interactions can be implemented directly e.g. in current density-functional calculations of finite nuclei. For low-momentum interactions, the weak-coupling approximation with a density-dependent contact interaction is reliable (see ref. [124]), and a separable approximation is efficient [125]. Therefore, low-momentum interactions offer the possibility for a consistent treatment of the particle-hole and pairing channels in density-functional theory. Moreover, it is straightforward to adapt the RG to microscopically derive the renormalized pairing interaction introduced in the optimal regularization scheme of Bulgac [126].

For conventional large-cutoff and chiral EFT potentials, $\langle k' | V | k \rangle$ includes regulating functions that render the integral convergent. These are of exponential form $\exp[-(k^2/\Lambda^2)^3]$ with $\Lambda = 450 - 600 \text{ MeV}$ in the current chiral EFT interactions at N³LO [112, 127], and phenomenological functions that correspond to large (on the order of a few GeV) cutoffs in conventional NN potential models.

In the following, we will use the projection operator formalism to construct low-momentum interactions with a sharp cutoff $f(k) = \theta(\Lambda - k)$ and solve the RG equation (2.14) for our results obtained with smooth regulators $f(k) = \exp[-(k^2/\Lambda^2)^n]$, where n is a parameter that controls the smoothness. We note that the RG equation cannot be solved directly in the neutron-neutron $^1\text{S}_0$ channel for most of the conventional NN interactions (except for the Nijmegen II

³This section is based upon ref. [121]

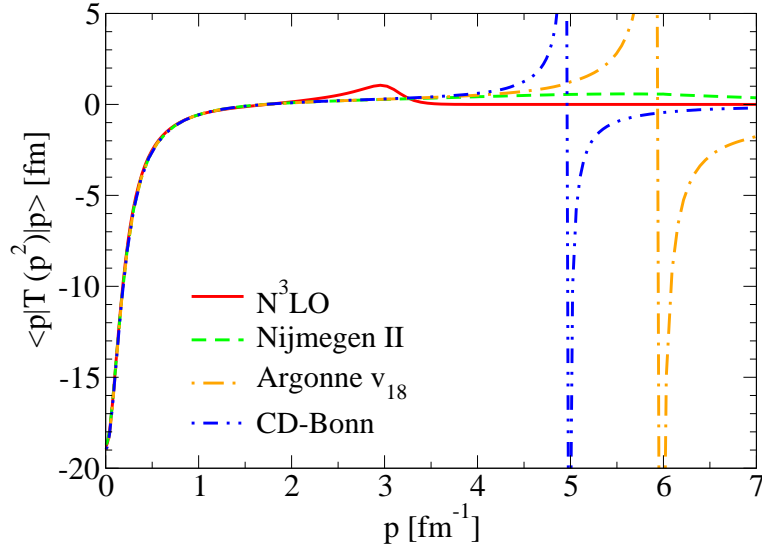


Figure 2.4.: Spurious poles in the on-shell T-Matrix elements for the CD-Bonn and the Argonne v_{18} NN-interaction.

potential), due to spurious resonances at high ($\sim \text{GeV}$) momenta (cf. Fig 2.4). Furthermore it is not possible to solve the RG equation (2.14) using sharp cutoff functions since the flow equation is mathematically ill defined. In the case of a sharp cutoff the upper limit of the principal value integral in eq. (2.14) coincide with the position of the pole:

$$\frac{d}{d\Lambda} \langle k' | V^\Lambda | k \rangle = \frac{1}{\pi} \left[\frac{\langle k' | V^\Lambda | \Lambda \rangle \langle \Lambda | T(\Lambda^2) | k \rangle}{\Lambda^2 - k^2} + \frac{\langle k' | T(\Lambda^2) | \Lambda \rangle \langle \Lambda | V^\Lambda | k \rangle}{\Lambda^2 - k'^2} \right]. \quad (2.18)$$

Unless the matrix elements on the right hand side are non-vanishing at the upper limit Λ of the Hilbert space one inevitably runs into singularities, which cannot be treated numerically in a proper way. In the Lee-Suzuki formalism, which is mathematically equivalent to solving the RG equation (2.18), the Hilbert space reduction is performed in one step and consequently the numerical problems cannot accumulate during the mode elimination procedure. For momenta away from the border Λ this method provides high precision low momentum interactions. In contrast, for the explicit iteration of the flow equation the use of smooth cutoffs is necessary. Nevertheless the accuracy of the final results are comparable.

The freedom in the choice of the regulator $f(k)$ implies a scheme dependence of the gap $\Delta_k \sim f(k)$ at large momenta $k \gg k_F$. We will restrict our results to the gap on the Fermi surface $\Delta \equiv \Delta_{k_F}$, where the momenta are on-shell. In the leading-order pionless EFT with sharp-cutoff regularization, one has $\langle k' | V | k \rangle = \theta(\Lambda - k) \theta(\Lambda - k') / [1/a_s - 2\Lambda/\pi]$ (with scattering length a_s). The resulting gap is cutoff independent for $\Delta \ll \mu$ and large cutoffs, which follows from the gap

equation with $\Delta_k = \theta(\Lambda - k) \Delta$,

$$\frac{1}{a_s} - \frac{2}{\pi} \Lambda = -\frac{1}{\pi} \int_0^\Lambda dq \frac{q^2}{\sqrt{\xi_q^2 + \Delta^2}}. \quad (2.19)$$

For $\Delta \ll \mu$ and large Λ , the integral is given by $2[-2k_F + \Lambda + k_F \ln(8\mu/\Delta)]$. The UV divergence cancels against the cutoff dependence of the interaction in eq. (2.19). This leads to the standard result $\Delta = 8\mu/e^2 \exp[\pi/(2k_F a_s)]$ [128].

For the solution of the gap equation

$$\Delta_k = -\frac{1}{\pi} \int dq q^2 \frac{\langle k|V|q\rangle \Delta_q}{\sqrt{\xi_q^2 + \Delta_q^2}}, \quad (2.20)$$

we follow the method of Khodel *et al.* [67]. We first decompose the interaction into a separable and a non-separable part

$$\langle k'|V|k\rangle = \langle k_F|V|k_F\rangle \phi(k) \phi(k') + W(k, k'), \quad (2.21)$$

where $\phi(k) \equiv \langle k_F|V|k\rangle / \langle k_F|V|k_F\rangle$ and $W(k, k')$ vanishes when at least one argument is on the Fermi surface ($k = k_F$). Then the gap equation (2.20) can be replaced by an equivalent system of two equations,

$$\phi(k) = \chi(k) + \frac{1}{\pi} \int dq q^2 \frac{W(k, q) \chi(q)}{\sqrt{\xi_q^2 + \Delta_q^2}}, \quad (2.22)$$

$$0 = 1 + \langle k_F|V|k_F\rangle \frac{1}{\pi} \int dq q^2 \frac{\phi(q) \chi(q)}{\sqrt{\xi_q^2 + \Delta_q^2}}, \quad (2.23)$$

where $\Delta_k \equiv \Delta \chi(k)$ with $\chi(k_F) = 1$. This system has the advantage that the integrand in eq. (2.22) vanishes on the Fermi surface, and consequently the function $\chi(k)$ is only weakly sensitive to changes of Δ_q in the denominator. Therefore, to a good approximation, eq. (2.22) can be linearized. In the first iteration, we solve eq. (2.22) by inversion using a sufficiently small constant Ansatz for Δ_q in the denominator. Next, we solve eq. (2.23) for Δ using Newton's method with the solution for $\chi(k)$ of the previous step. The iteration of this procedure (where Δ_q in the denominator of eq. (2.22) is updated at each step) leads to a rapidly converging solution for the BCS gaps.

Our results for the density dependence of the neutron-neutron 1S_0 superfluid gap Δ are shown in Fig. 2.5. The low-momentum interactions $V_{\text{low } k}$ are derived from various charge-dependent NN potentials [112, 113, 114, 115] using a sharp cutoff $\Lambda = 2.1 \text{ fm}^{-1}$. We find that the BCS gap is almost independent of the NN interaction. Consequently, we conclude that the 1S_0 gap is strongly constrained by the NN scattering phase shifts. This has been noted previously (see for example

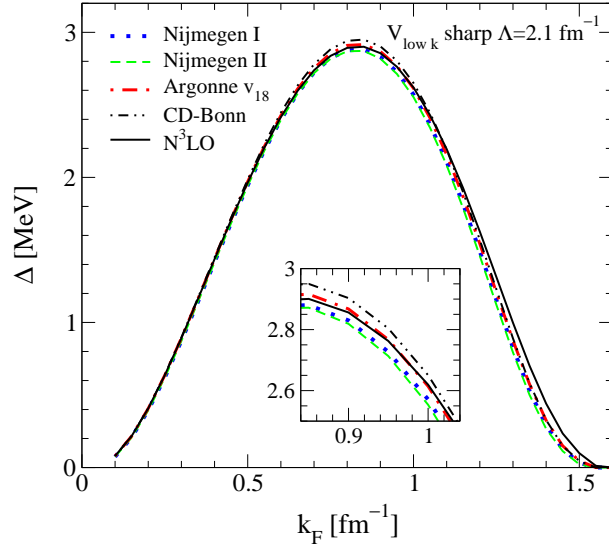


Figure 2.5.: The neutron-neutron 1S_0 superfluid pairing gap on the Fermi surface $\Delta \equiv \Delta_{k_F}$ versus Fermi momentum k_F for low-momentum interactions $V_{\text{low } k}$ with a sharp cutoff $\Lambda = 2.1 \text{ fm}^{-1}$. $V_{\text{low } k}$ is derived from various charge-dependent NN interactions [112, 113, 114, 115]. We have verified that the results are cutoff independent from $\Lambda = 1.6 \text{ fm}^{-1}$ to $\Lambda = 2.5 \text{ fm}^{-1}$. The inset magnifies the small dependence on nuclear interactions near the maximum.

ref. [129]), but without considering the charge dependence. Moreover, these are the first results for chiral interactions at N³LO. We use the N³LO chiral potential of ref. [112], since it is the chiral interaction that most accurately reproduces the phase shifts. The maximal gap at the BCS level is $\Delta \approx 2.9 - 3.0 \text{ MeV}$ for $k_F \approx 0.8 - 0.9 \text{ fm}^{-1}$. The small deviation of the N³LO gap from the band at higher densities in Fig. 2.5 is consistent with the slightly more attractive 1S_0 phase shifts at the corresponding energies (compare, for example, the phase shifts of the CD-Bonn [115] and N³LO potential [112]). We find that the gaps are cutoff independent over the range considered here, $\Lambda = 1.6 \text{ fm}^{-1}$ to $\Lambda = 2.5 \text{ fm}^{-1}$. This result is consistent with the findings of Kaiser *et al.* that the cutoff dependence is substantially reduced for chiral EFT interactions when going from NLO to N²LO [130], since the latter leads to a better description of the NN scattering phase shifts. In addition, the BCS gaps for the "bare" interactions are within 2% of the $V_{\text{low } k}$ results shown in Fig. 2.5 for $k_F \lesssim 1.0 \text{ fm}^{-1}$, and the difference is compatible with the spread in the $V_{\text{low } k}$ result over all densities. (This also holds for Fig. 2.6.) For completeness, we mention that Sedrakian *et al.* [131] have solved the BCS gap equation for one low-momentum interaction ($V_{\text{low } k}$ derived from Nijmegen 93 [113] with $\Lambda = 2.5 \text{ fm}^{-1}$), however they did not explore the

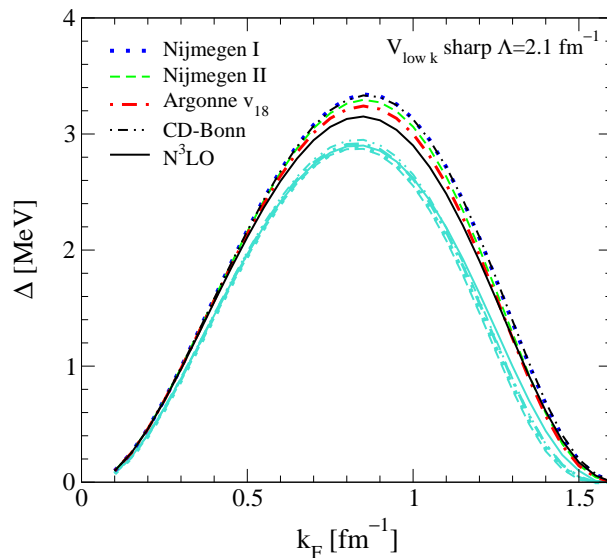


Figure 2.6.: The charge dependence of the 1S_0 superfluid pairing gap Δ versus k_F . The lines indicated in the legend are the neutron-proton gaps, whereas the grey lines show the neutron-neutron gaps from Fig. 2.5. For further details, see the caption of Fig. 2.5. We have also verified that the neutron-proton gaps are cutoff independent over the same sharp-cutoff range.

cutoff dependence.

Isospin symmetry breaking leads to small charge dependencies in nuclear interactions. As a result, the 1S_0 neutron-proton scattering length $a_{np} = -23.768 \pm 0.006$ fm is more attractive than the neutron-neutron scattering length $a_{nn} = -18.5 \pm 0.3$ fm [132] in the same channel. This effect is dominantly due to the charge dependence of the one pion-exchange interaction V_π . The central part of V_π in the neutron-proton charge-exchange channel is of the form $-m_{\pi^\pm}^2/(q'^2 + m_{\pi^\pm}^2)$, where q' is the (exchange) momentum transfer. Since the charged pion is heavier than the neutral one, $m_{\pi^\pm} = 139.57$ MeV and $m_{\pi^0} = 134.98$ MeV, the resulting neutron-proton interaction is more attractive. In Fig. 2.6, we show the charge dependence of the 1S_0 superfluid pairing gap versus Fermi momentum. The neutron-proton gaps are ≈ 0.3 MeV larger at maximum with a slight shift to higher densities. The 10% effect on the pairing gaps clearly reflects the charge dependence of nuclear interactions.

Next, we study the dependence of the neutron-neutron 1S_0 superfluid pairing gap as a function of the cutoff starting from the N^3LO chiral interaction. Our results for three representative densities and different smooth exponential regulators $f(k) = \exp[-(k^2/\Lambda^2)^n]$, as well as for a sharp cutoff, are shown in Fig. 2.7. As long as the cutoff is large compared to the dominant momentum components

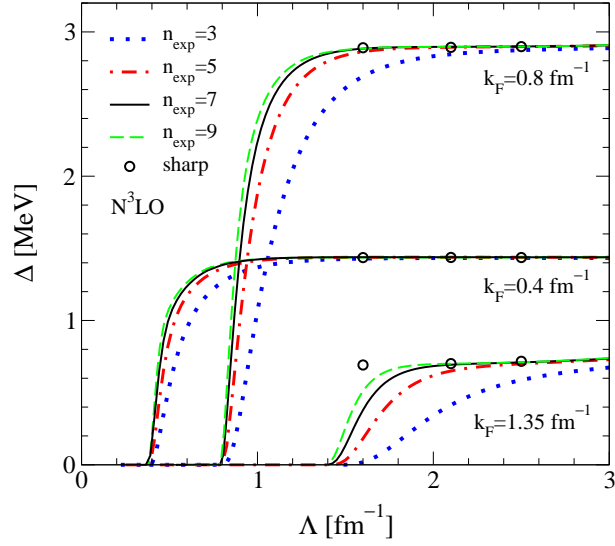


Figure 2.7.: The neutron-neutron $^1\text{S}_0$ superfluid pairing gap Δ as a function of the cutoff Λ for three densities and different smooth exponential regulators, as well as for a sharp cutoff. The low-momentum interactions are derived from the $N^3\text{LO}$ chiral potential of ref. [112].

in the Cooper bound state, the gap depends very weakly on the cutoff. Below this scale, which depends on the density and the smoothness of the regulator, the strength of the bound state decreases, since some of the momentum modes that build up the Cooper pairs are integrated out. From Fig. 2.7, we observe that the cutoff dependence is very weak for sharp or sufficiently narrow smooth regulators with $\Lambda > 1.6 \text{ fm}^{-1}$. It can be seen that $n = 3$ is too smooth, but that $n > 5$ is sufficient. For lower densities, even lower cutoffs with $\Lambda > 1.2k_F$ are possible.

The $N^3\text{LO}$ chiral interaction has a cutoff $\Lambda = 2.5 \text{ fm}^{-1}$ (500 MeV) [112] and one may suspect that the cutoff dependence could be larger for conventional NN potentials. In Fig. 2.8, we show that this is not the case by comparing the gaps from Fig. 2.7 to results obtained with the Nijmegen II potential [113], which has a large ($\sim \text{GeV}$) cutoff. The cutoff dependence is similar and in particular very weak for sharp or sufficiently narrow smooth regulators with $\Lambda > 1.6 \text{ fm}^{-1}$. This shows that the $^1\text{S}_0$ superfluid pairing gap probes low-momentum physics. Low-momentum interactions, via weak-coupling or separable approximations, can be implemented directly in current density-functional calculations. Furthermore, it is straightforward to adapt the RG used here to a microscopic derivation of the optimal pairing interaction of ref. [126].

Thus we find that the BCS gap is well constrained by the NN phase shifts. Therefore, any uncertainties are due to polarization (induced interaction), dispersion and three-nucleon interaction effects.

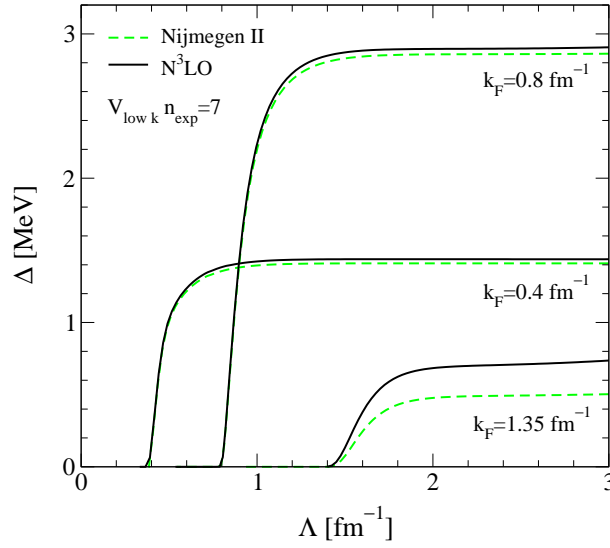


Figure 2.8.: The neutron-neutron 1S_0 superfluid pairing gap Δ as a function of the cutoff Λ for three densities. The low-momentum interactions are derived from the $N^3\text{LO}$ [112] and the Nijmegen II [113] potential with exponential regulator $n = 7$.

2.5. RG Evolution from the Normal into the Superfluid Phase

The integration of many-body correlations in superfluid systems in the RG framework involves a principal problem: at the initialization scale of the RG flow the effective vertex function Γ^Λ coincides with the irreducible kernel Γ_0 since no modes have been integrated out. In particular, no pairing correlations are included in Γ^Λ and consequently this function describes a system in the unbroken phase. However, during the flow these correlations are successively integrated out until the order parameter $|\Psi(\mathbf{r})|$ (cf. section 1.3) develops a finite value, signalling the transition to the superfluid phase. This passage has to be treated carefully in order to ensure that one obtains the correct ground state at the end of the RG flow.

One common approach is based on the exact RG equation of the effective action [133, 134, 135] (cf. also section 3.5). In each RG step a bosonic field representing the condensate is successively introduced by performing a Hubbard-Stratonovich transformation [136, 137]. By using this transformation, the fermionic degrees of freedom at the current scale are fully or partially integrated out and transformed into collective bosonic fields, which include all contributions of the symmetry breaking correlations above the current renormalization scale. By this the original purely fermionic theory is successively transformed (“partially bosonized”) into

an interacting fermion-boson theory (cf. e.g. refs. [77, 101, 138, 139, 140]).

However, as shown by Salmhofer *et al.* [5] for superfluid systems, it is also possible to obtain a smooth flow into the broken symmetry phase in a purely fermionic picture. By violating the symmetry *explicitly* at the beginning of the flow by an infinitesimal amount, one offers the system the freedom to evolve *dynamically* into a state with broken symmetry. In this section we show how this strategy can be used to treat the scattering problem in a superfluid, as discussed in section 1.7, in the RG framework.

The basic task is the solution of

$$\langle k' | \mathbf{\Gamma}(\omega) | k \rangle = \langle k' | \mathbf{V} | k \rangle + \frac{1}{\pi} \int dq dx q^2 \langle k' | \mathbf{V} | q \rangle \mathbf{G}\mathbf{G}(q, x, P, \omega, \Delta) \langle q | \mathbf{\Gamma}(\omega) | k \rangle \quad (2.24)$$

for the vertex $\mathbf{\Gamma}$, where the bare vacuum interaction $\langle k' | \mathbf{V} | k \rangle$ is the experimentally determined totally irreducible kernel. According to section 2.3 the strategy for the RG treatment is as follows:

- 1.) Introduce a cutoff function $f(q, x, P, \Lambda, k_F) \equiv f(q, x, \Lambda)$ which cuts out the low lying momentum states around the Fermi surface. By this procedure, the vertex function $\mathbf{\Gamma}$, the off-diagonal self-energy Δ and the two-body propagator $\mathbf{G}\mathbf{G}$ become cutoff-dependent functions:

$$\langle k' | \mathbf{\Gamma}^\Lambda(\omega) | k \rangle = \langle k' | \mathbf{V} | k \rangle + \frac{1}{\pi} \int dq dx q^2 \langle k' | \mathbf{V} | q \rangle \mathbf{G}\mathbf{G}^\Lambda(q, x) \langle q | \mathbf{\Gamma}^\Lambda(\omega) | k \rangle \quad (2.25)$$

with

$$\mathbf{G}\mathbf{G}^\Lambda(q, x) \equiv f(q, x, \Lambda) \mathbf{G}\mathbf{G}(q, x, P, \omega, \Delta^\Lambda) \quad (2.26)$$

- 2.) In the case $\Lambda \rightarrow \infty$ the integral vanishes and the equation becomes trivial. Consequently we can initialize the flow by

$$\langle k' | \mathbf{\Gamma}^{\Lambda \rightarrow \infty}(\omega) | k \rangle = \langle k' | \mathbf{V} | k \rangle. \quad (2.27)$$

According to section 1.9 the gap equation can be extracted from the homogeneous part of the scattering equation around the pole. At $\Lambda \rightarrow \infty$ there are no poles and we have

$$\Delta_{\mathbf{k}}^{\Lambda \rightarrow \infty} = 0. \quad (2.28)$$

- 3.) According to the discussion in section 2.3, the flow equation takes the form

$$\begin{aligned} & \frac{d}{d\Lambda} \langle k' | \mathbf{\Gamma}^\Lambda(\omega) | k \rangle \\ &= \frac{1}{\pi} \frac{d}{d\Lambda'} \left[\int dq dx q^2 \langle k' | \mathbf{\Gamma}^\Lambda(\omega) | q \rangle \mathbf{G}\mathbf{G}^{\Lambda'}(q, x) \langle q | \mathbf{\Gamma}^\Lambda(\omega) | k \rangle \right]_{\Lambda'=\Lambda} \end{aligned} \quad (2.29)$$

The derivative involves explicit derivatives of the cutoff function $f(q, x, \Lambda)$ and implicit derivatives of the gap function $\frac{d\Delta_k^\Lambda}{d\Lambda}$. In principle this derivative could be extracted from the derivative of the vertex function based on the discussion of section 1.9. However, in practice it is much more convenient to iterate the gap function parallel to the vertex function. The derivation of the corresponding flow equation is straightforward by starting from the gap equation

$$\Delta_k^\Lambda = -\frac{1}{\pi} \int dq q^2 f(q, \Lambda, k_F) \langle k|V|q\rangle F^{(BCS)}(q, \omega = 0, \Delta^\Lambda). \quad (2.30)$$

The corresponding flow equation can be obtained by simply taking the derivative with respect to Λ on both sides. By this one obtains an implicit equation for the derivative of the gap function:

$$\frac{d}{d\Lambda} \Delta_k^\Lambda = -\frac{1}{\pi} \int dq q^2 \langle k|V|q\rangle \frac{d}{d\Lambda} [f(q, \Lambda, k_F) F^{(BCS)}(q, \omega = 0, \Delta^\Lambda)], \quad (2.31)$$

where we have used the fact that the kernel V is cutoff independent in the BCS approximation. Since the cutoff is changing smoothly, this equation can be easily solved by iteration. In every RG step one already obtains excellent convergence after one or two iteration steps.

However, the flow equation (2.31) is always fulfilled by the trivial solution $\Delta_k^\Lambda = 0$ for all Λ . Hence due to the initial condition (2.28), the solution will stay at $\Delta_k^\Lambda = 0$ for all Λ . In order to allow the system to develop a finite gap during the RG flow we have to break the symmetry explicitly by a small amount, i.e. we set

$$\Delta_{\mathbf{k}}^{\Lambda \rightarrow \infty} = \eta, \quad (2.32)$$

where η is an arbitrary but very small value. It can be checked explicitly at the end that the final value of the gap is independent of the value of η . In every iteration step the derivative of the gap first has to be determined, so that this function can be used for the calculation of the derivatives of the vertex according to eq. (2.29). In the present case this can be done consecutively since the vertex Γ does not couple into the gap equation. This situation changes if (normal) self-energy corrections beyond the BCS approximation are taken into account (cf. chapter 3).

The numerical implementation of this scheme involves some subtleties. The following issues require particular attention:

- *Numerical evaluation of the flow equation:*

For energies above the two-particle threshold, the flow equations (2.29) involve the evaluation of principal value integrals. In this case, the derivative and the integrals in eq. (2.29) do *not* commute. Consequently subtractions

in the angular and radial integral are necessary before the derivative can be applied to the integrand. For details see Appendix A.1.

- *Floating energy grid below threshold:*

For energies just above the threshold, the angular integral involves integrable singularities (see Appendix A.1). Since the location of the threshold is scale dependent (typically growing), the position of this numerically critical region is also changing. Thus, in the case of a fixed energy mesh system all grid points which are located below the threshold at the end of the flow have to cross this critical area during the flow. This leads in general to poor numerical results. Instead it is much more convenient to use a scale dependent energy variable below the threshold

$$\omega^\Lambda = 2x\Delta^\Lambda \quad \text{for } x < 1 \quad (2.33)$$

By construction, these points never crosses the threshold and the quality of the results is improved considerably compared to a fixed mesh system.

- *Treatment of the Goldstone boson:*

The treatment of singular points like the Goldstone excitation below the threshold (cf. section 1.8) in a differential equation requires special care. In the present case these singularities appear due to a vanishing determinant of the vertex function in the Gorkov space (cf. section 1.8), i.e. the elements of the *inverse* vertex $\tilde{\Gamma}$ in Gorkov space

$$\langle k' | \Gamma(\omega) | k \rangle \langle k' | \tilde{\Gamma}(\omega) | k \rangle = \mathbf{1} \quad (2.34)$$

remain well behaved in this pole region. Clearly it is advantageous to evolve the elements of $\langle k' | \tilde{\Gamma}(\omega) | k \rangle$. The corresponding flow equation is readily obtained by using

$$\frac{d}{d\Lambda} \langle k' | \tilde{\Gamma}^\Lambda(\omega) | k \rangle = - \langle k' | \tilde{\Gamma}^\Lambda(\omega) | k \rangle \left[\frac{d}{d\Lambda} \langle k' | \Gamma^\Lambda(\omega) | k \rangle \right] \langle k' | \tilde{\Gamma}^\Lambda(\omega) | k \rangle. \quad (2.35)$$

It should also be noted that this procedure could lead to numerical problems in the large momentum region where all elements of Γ^Λ are very small. Consequently a mixed scheme, where the inverse matrix is iterated a few times around the singular point, and otherwise the flow eq. (2.29) for Γ is used, yields optimal numerical results.

- *Choice for the cutoff function:*

By a proper choice of the cutoff function the quality of the final results can be improved considerably. In principle, the cutoff function $f(q, x, P, \Lambda)$

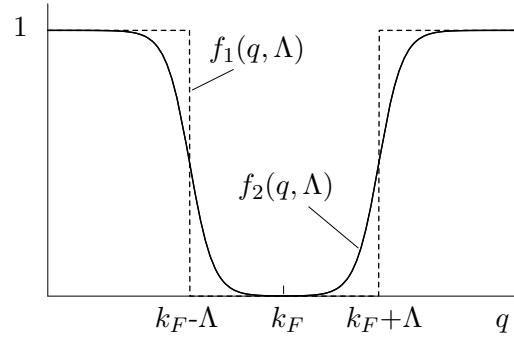


Figure 2.9.: Sharp and smooth cutoff functions for the RG in medium.

(with $x = \hat{\mathbf{P}} \cdot \hat{\mathbf{q}}$) is constrained by the conditions

$$f(q, x, P, \Lambda \rightarrow \infty) = 0, \quad f(q, x, P, \Lambda \rightarrow -\infty) = 1. \quad (2.36)$$

One possible choice is a *sharp* cutoff function which cuts out the intermediate single-particle states symmetrically around the Fermi surface (cf. Fig. 2.9):

$$f_1(q, \Lambda) = \Theta(|q - k_F| - \Lambda). \quad (2.37)$$

while a possible smooth cutoff function reads (cf. Fig. 2.9)

$$f_2(q, \Lambda) = 2 - [n(k_F - q - \Lambda, c) + n(q - k_F - \Lambda, c)] \quad (2.38)$$

with

$$n(x, c) = [\exp(x/c) + 1]^{-1}. \quad (2.39)$$

However, in practice sharp cutoff functions are quite inconvenient, unless the flow equations can be evaluated analytically. The numerical treatment is simplified considerably, if the contributions of the low lying modes are introduced *smoothly* by choosing a finite width c in f_2 .

Furthermore one has an additional freedom in the way how the cutoff is applied to the intermediate momenta q_1 and q_2 . One could restrict both or only a single momentum. In the present single-channel problem the final result is invariant under these different choices. In the following we will use

$$f(q, x, P, \Lambda) = f_2(q_+, \Lambda)f_2(q_-, \Lambda) \quad \text{with} \quad q_{\pm} = \sqrt{q^2 + P^2/4} \pm Pqx \quad (2.40)$$

Starting from the initial energy independent interaction \mathbf{V} , the gap Δ and the four point vertex $\mathbf{\Gamma}$ are iterated simultaneously in every RG step. For large cutoffs the vertex function $\mathbf{\Gamma}^\Lambda$ remains almost energy dependent. At the scale

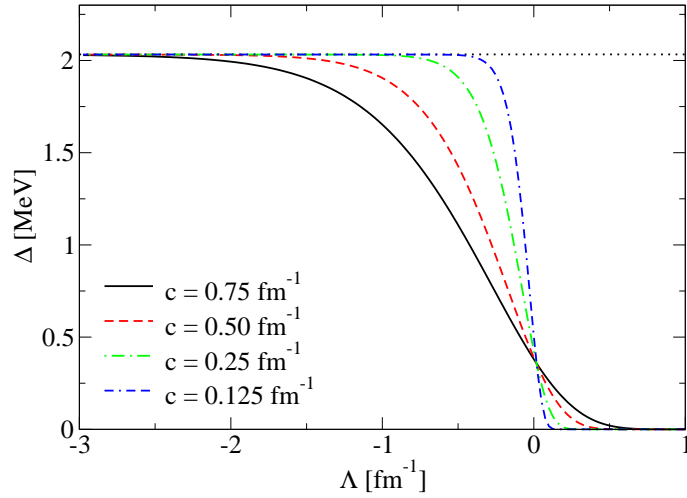


Figure 2.10.: Formation of gap during the flow at $k_F = 0.6 \text{ fm}^{-1}$ for different widths c in the cutoff function $f(q, x, P, \Lambda)$. The horizontal line denotes the solution of the gap equation using the inversion procedure of section 2.4.

of the onset of the phase transition (in Fig. 2.11 at around $\Lambda = 0.5 \text{ fm}^{-1}$) the gap starts to develop a finite value (see Fig. 2.10). From this scale on the vertex function shows the characteristic energy dependence discussed in sec. 1.8. The final results of the RG algorithm for $\Lambda \rightarrow -\infty$ are in remarkably good agreement with the explicit solution for the separable interaction \mathbf{V}^* (cf. Figs. 2.12 and 2.13)). Only small deviations can be found in the vertex right above the threshold due to the numerical problems discussed in Appendix A.1.

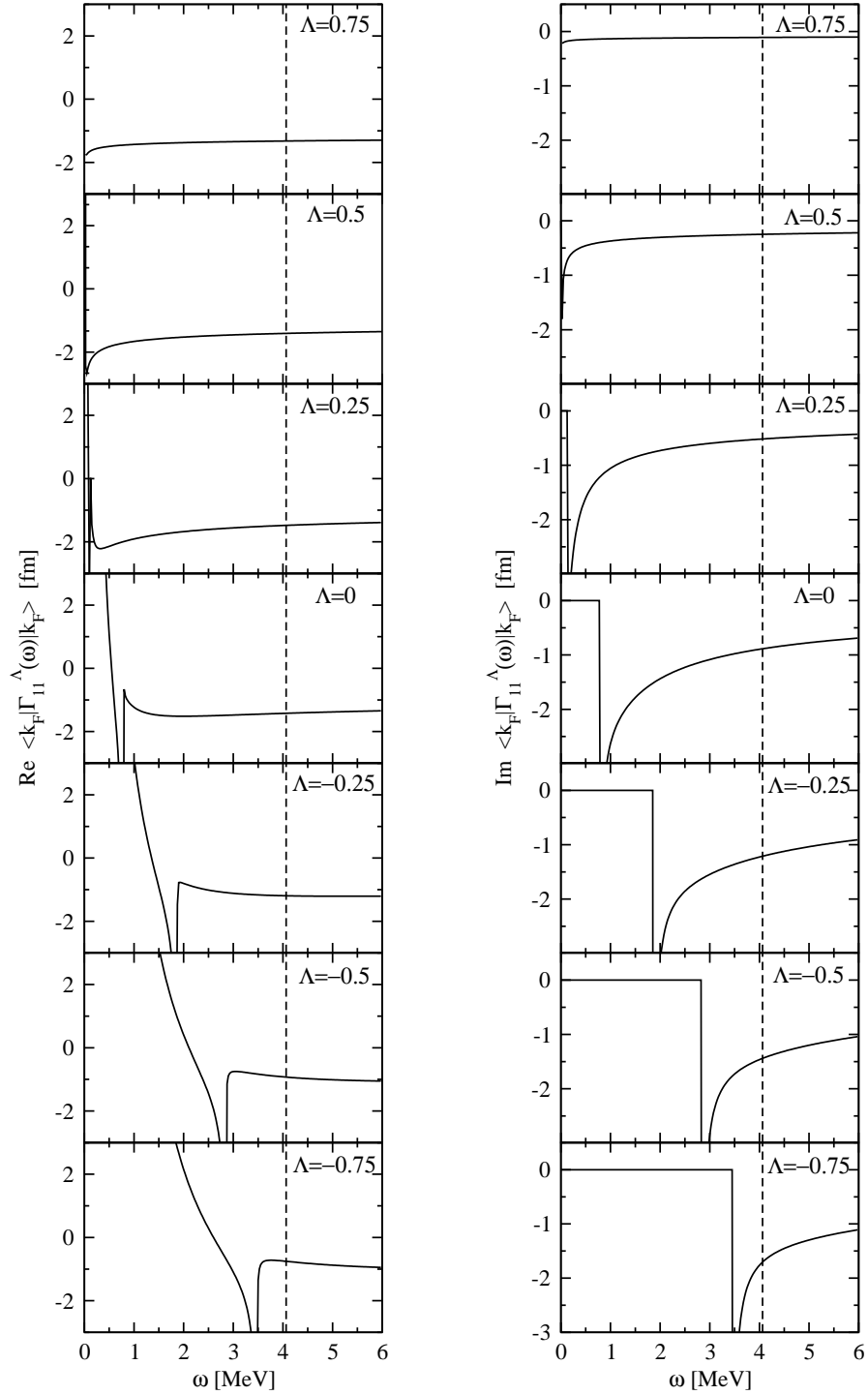


Figure 2.11.: Snapshots of $\langle k_F | \Gamma_{11}^\Lambda(\omega) | k_F \rangle$ (left: real part, right: imaginary part) during the flow at intermediate scales Λ (in fm^{-1}) in the back-to-back case $P = 0$ and the cutoff width $c = 0.5 \text{ fm}^{-1}$ for the separable interaction \mathbf{V}^* . The dashed line denotes the position of the threshold at $\Lambda \rightarrow -\infty$.

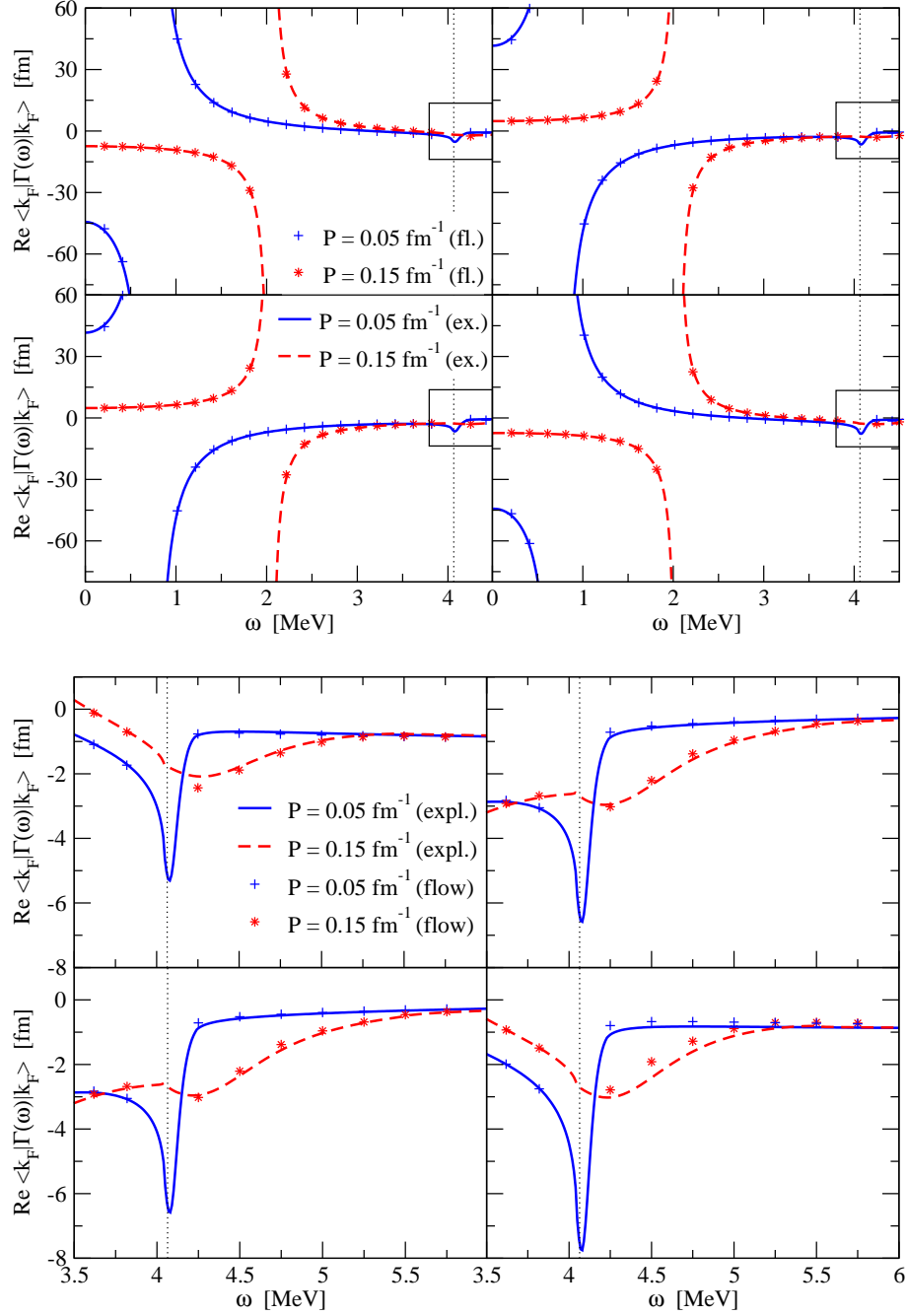


Figure 2.12.: Comparison of the elements of the real part of Γ between the explicit solution obtained (see section 1.8) denoted by the solid and dashed lines and the solutions of the flow equation (2.29) denoted by the single data points for two different CM momenta at $k_F = 0.6 \text{ fm}^{-1}$. The dotted line denotes the two-particle threshold. Upper panel: energy region below threshold; lower panel: Energy region around the two-particle threshold (indicated in the upper plots by the boxes). Compare also Fig. 1.20.

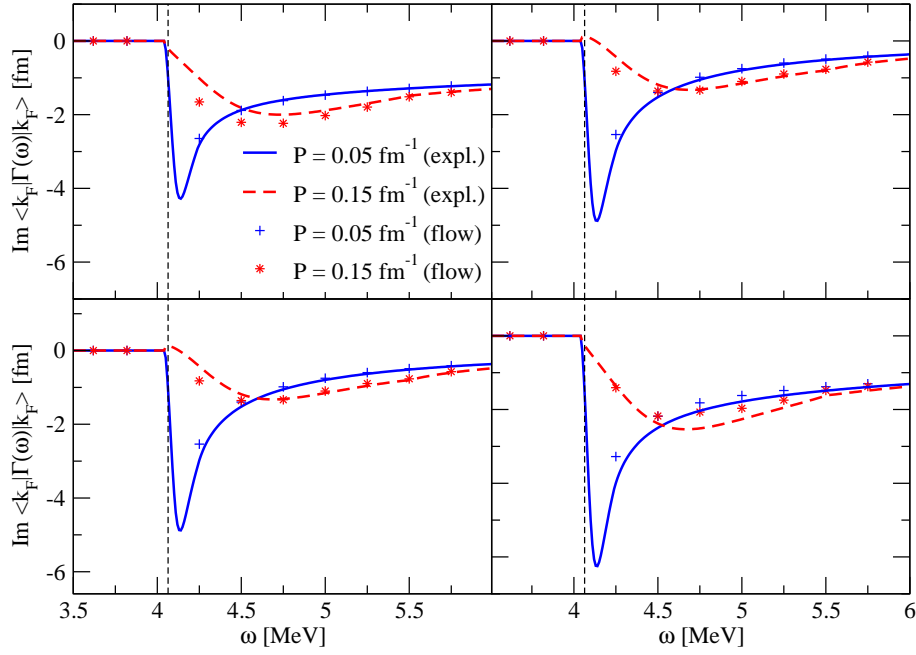


Figure 2.13.: Comparison of the imaginary part of Γ between the explicit and RG solution. The same notation and parameters as in Fig. 2.12 have been used.

We also emphasize that at no point has the separability of the interaction been used explicitly and consequently this algorithm can also be applied to general interactions. This will be done in the next section. However, before turning to these results, it is quite instructive to investigate in more detail the role of the infinitesimal gap in eq. (2.32) as a starting point of the flow. The solution $\Delta_k^\Lambda = 0$ corresponds to the normal system where all anomalous components vanish and the *normal* particle-particle vertex function $\langle k' | \Gamma_{\text{norm}}^\Lambda(\omega) | k \rangle$ is satisfied the two-particle scattering equation

$$\begin{aligned} \langle k' | \Gamma_{\text{norm}}^\Lambda(\omega) | k \rangle &= \langle k' | V | k \rangle + \frac{1}{\pi} \int dq dx q^2 \langle k' | V | q \rangle G G_{\text{norm}}^\Lambda(q, x, \omega) \langle q | \Gamma_{\text{norm}}^\Lambda(\omega) | k \rangle \end{aligned} \quad (2.41)$$

with

$$G G_{\text{norm}}^\Lambda(q, x, \omega) = f(q, \Lambda) \left[\frac{\Theta(q_1 - k_F) \Theta(q_2 - k_F)}{\omega - \xi_{\mathbf{q}_1} - \xi_{\mathbf{q}_2} + i\delta} - \frac{\Theta(k_F - q_1) \Theta(k_F - q_2)}{\omega - \xi_{\mathbf{q}_1} - \xi_{\mathbf{q}_2} - i\delta} \right]. \quad (2.42)$$

The corresponding flow equation can also be obtained easily in complete analogy

to eq. (2.29):

$$\begin{aligned} & \frac{d}{d\Lambda} \langle k' | \Gamma_{\text{norm}}^\Lambda(\omega) | k \rangle \\ &= \frac{1}{\pi} \frac{d}{d\Lambda'} \left[\int d q d x q^2 \langle k' | \Gamma_{\text{norm}}^\Lambda(\omega) | q \rangle G G_{\text{norm}}^{\Lambda'}(q, x, \omega) \langle q | \Gamma_{\text{norm}}^\Lambda(\omega) | k \rangle \right]_{\Lambda'=\Lambda}. \end{aligned} \quad (2.43)$$

According to the discussion of section 2.2, the BCS instability should show up in the form of a singularity when the cutoff approaches the Fermi surface. We now investigate this pole in detail by comparing the flow of the particle-particle vertices Γ_{11}^Λ and $\Gamma_{\text{norm}}^\Lambda$ for the separable interaction \mathbf{V}^* .

Clearly, as long as the gap remains at the initial value η , the two functions Γ_{11}^Λ and $\Gamma_{\text{norm}}^\Lambda$ coincide. However, beyond the scale of the "gap opening" ($\Lambda \sim 0.25 \text{ fm}^{-1}$) the two vertices begin to differ. Due to the Cooper instability the vertex function $\Gamma_{\text{norm}}^\Lambda$ no longer describes the ground state. Instead of a minimum, the normal state is now represented by a local maximum in the effective potential (cf. Fig. 2.14). The singularity in the flow of $\Gamma_{\text{norm}}^\Lambda$ is just the formal manifestation of the metastability of this maximum against small perturbations. In contrast, the matrix $\mathbf{\Gamma}^\Lambda$ includes all necessary degrees of freedom to allow the system to remain in the true ground state. As a result, the singularity disappears and the flow remains well-behaved down to $\Lambda \rightarrow -\infty$ (see. Fig. 2.14).

As indicated in Fig. 2.11, the Cooper singularity first appears at the energy $\omega = 0$. In the function $\mathbf{\Gamma}^\Lambda$ a decrease of Λ leads to the "gap opening", i.e. for this the threshold border moves to finite ω , whilst below, the Goldstone pole remains at $\omega = 0$. This cannot happen in the function $\Gamma_{\text{norm}}^\Lambda$ since the system remains in the normal ground state and the singularity remains at $\omega = 0$ for all Λ . It follows that for finite ω the vertex function $\Gamma_{\text{norm}}^\Lambda$ does not show the presence of the Cooper instability.

In exact back-to-back kinematics at $\omega = 0$, both $\mathbf{\Gamma}^\Lambda$ and $\Gamma_{\text{norm}}^\Lambda$ show singular behaviour for $\Lambda \rightarrow -\infty$. However, the double pole in $\mathbf{\Gamma}^\Lambda$ at $\omega = 0$ corresponds to the Goldstone boson and does not signal an instability of the system (cf. sec. 1.8). In order to avoid the singularities in this special case, we will perform the explicit calculations at finite \mathbf{P} and compare the flow behaviour of these two functions. The results for the separable potential \mathbf{V}^* are shown in Fig. 2.14. The fact that the singularity in $\Gamma_{\text{norm}}^\Lambda$ appears just at the scale where the gap becomes finite clearly indicates the close connection between the gap formation and the occurrence of poles.

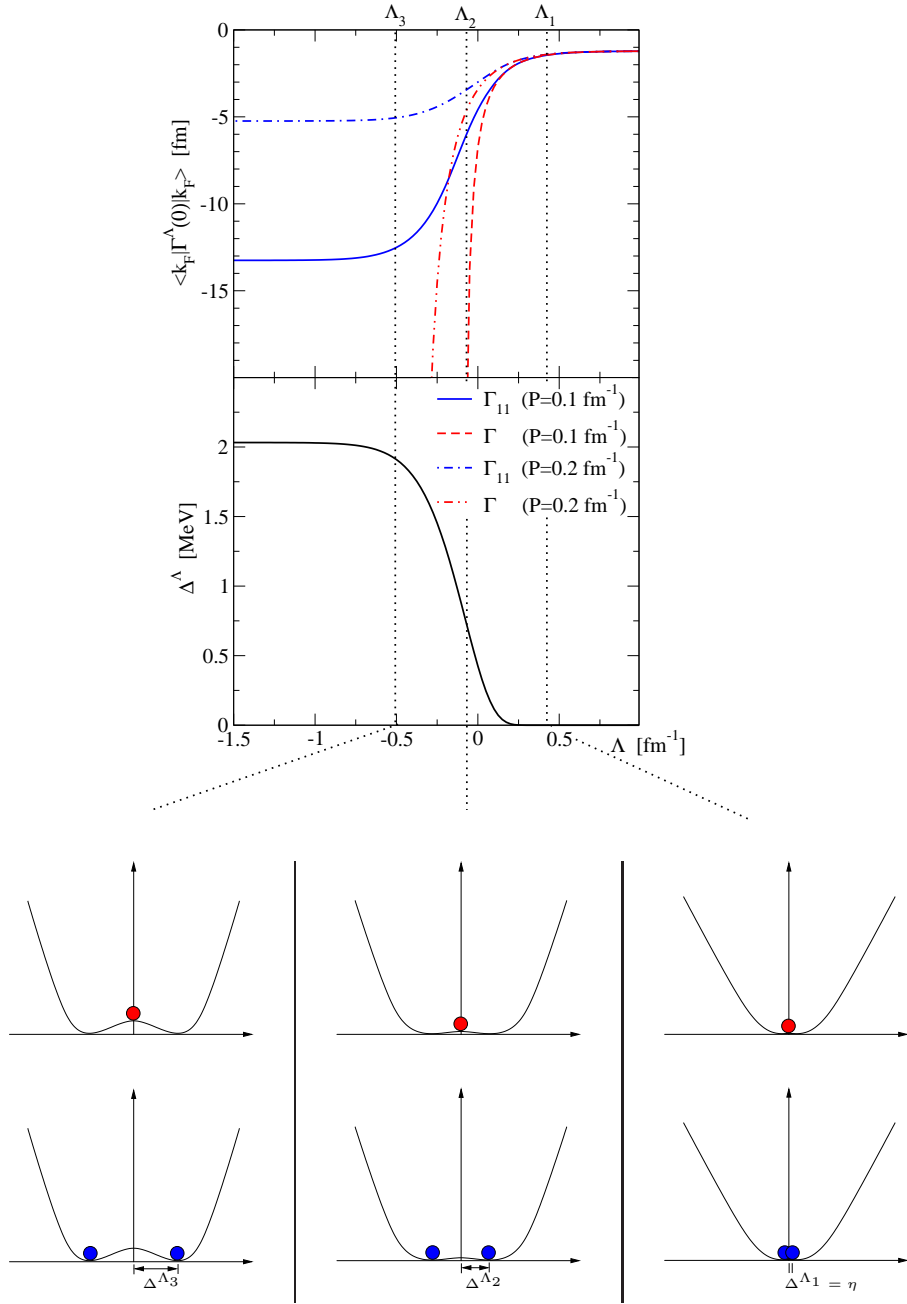


Figure 2.14.: Comparison of $\langle k_F | \Gamma_{11}^\Lambda(0) | k_F \rangle$ and $\langle k_F | \Gamma_{\text{norm}}^\Lambda(0) | k_F \rangle$ at $k_F = 0.6 \text{ fm}^{-1}$ and the width $c = 0.25 \text{ fm}^{-1}$. The lower pictures show the effective potential of the system at the current scale. Here the circle represents the corresponding ground state assumed in the calculation of $\Gamma_{\text{norm}}^\Lambda$ (upper row) and Γ_{11}^Λ (lower row) at $\Lambda = \Lambda_3$ (left column), $\Lambda = \Lambda_2$ (middle column) and $\Lambda = \Lambda_1$ (right column).

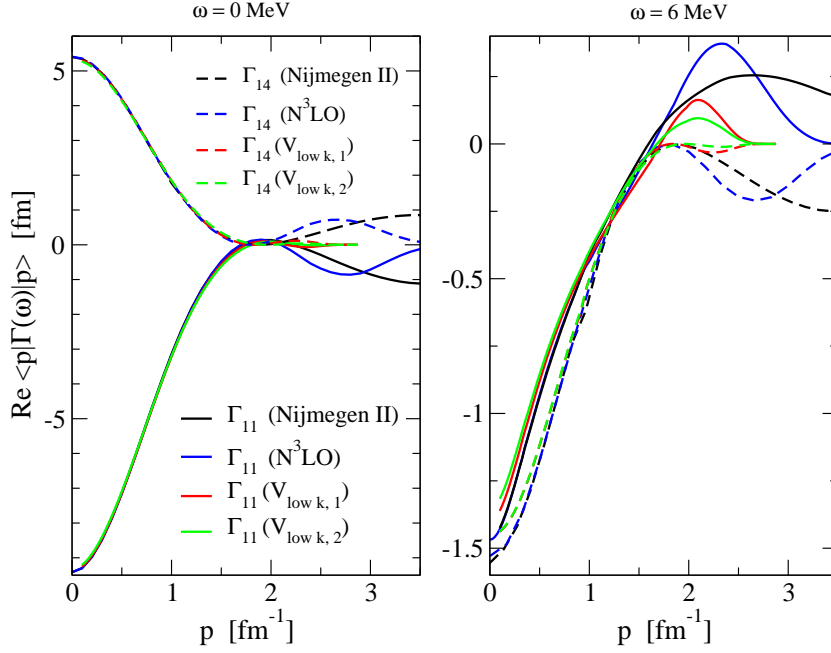


Figure 2.15.: Real part of the diagonal matrix elements in momentum space $\langle p | \Gamma(\omega) | p \rangle$ at $k_F = 0.6 \text{ fm}^{-1}$ and $P = 0.2 \text{ fm}^{-1}$ for two energies: left below threshold, right above. For the calculation of $V_{lowk,i}$ based on the bare interactions for $N^3\text{LO}$ for $i = 1$ and Nijmegen II for $i = 2$ a smooth cutoff of $\Lambda = 2.5 \text{ fm}^{-1}$ with $n = 7$ (cf. section 2.4).

2.6. Results for Realistic Interactions

The application of the algorithm discussed in the previous section to realistic NN interaction models is in principle straightforward since at no point has the separability of the interaction been used. However, for some particular interaction models like the CD-Bonn and the Argonne v_{18} , technical difficulties arise due to the appearance of spurious poles in the T-Matrix elements (cf. Fig. 2.4). Furthermore the bare interactions are usually defined at very large cutoffs, i.e. the interaction matrix elements are non-vanishing up to momenta of around 15 fm^{-1} for the Nijmegen and Argonne potentials and even higher for the CD-Bonn potential.

Besides the technical difficulties, connected with the required huge momentum mesh system, it is also from the theoretical side quite unnatural to include fluctuations in many-body calculations that are located far outside of the low energy Hilbert space around the Fermi surface. Instead, it is much more convenient and natural to use low momentum interactions, whose effective Hilbert space only consists of modes which are well constrained by experiment.

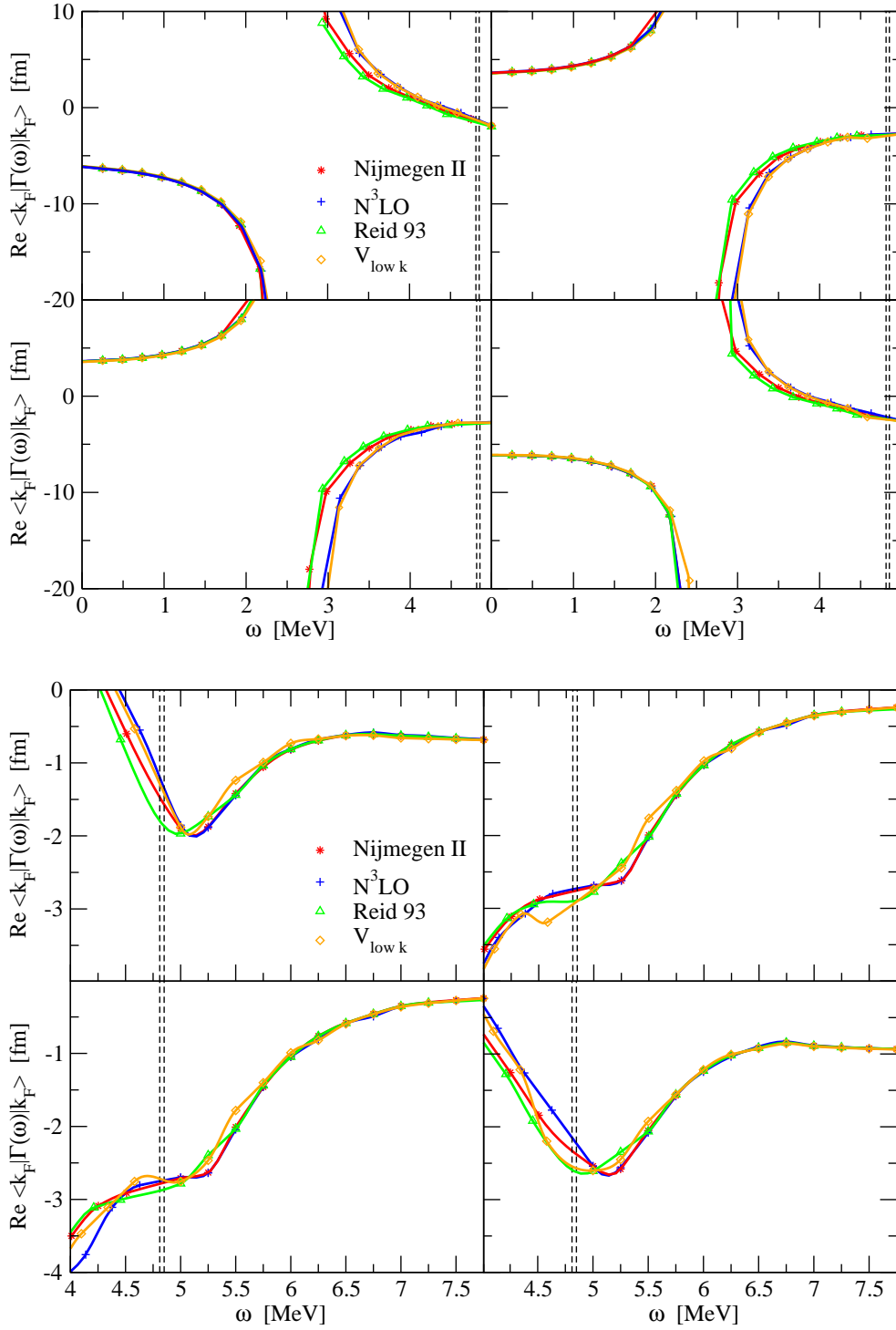


Figure 2.16.: Comparison of the elements of the real part of Γ between different realistic interaction models. Upper plots: below the threshold, lower plots: around the threshold. CM momentum $P = 0.2 \text{ fm}^{-1}$ and $k_F = 0.6 \text{ fm}^{-1}$. The dotted line denotes the two-particle threshold. The V_{lowk} interaction is determined from $N^3\text{LO}$ at $\Lambda = 2.5 \text{ fm}^{-1}$.

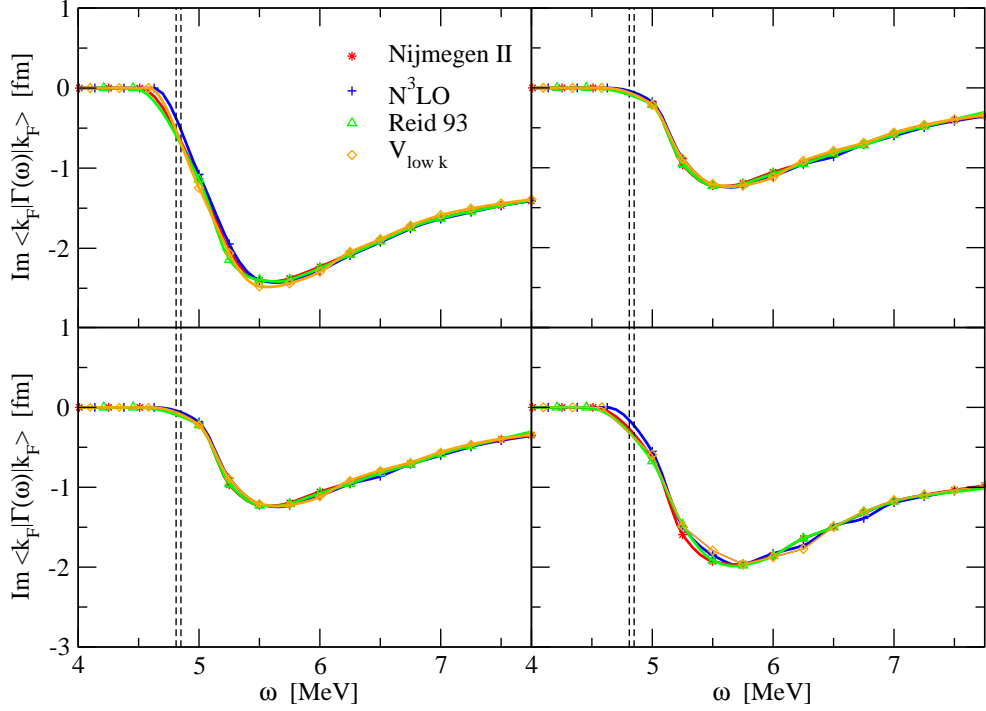


Figure 2.17.: Comparison of the imaginary part for different realistic interactions. The same parameters as in Fig. 2.18 have been used.

Indeed we will show that the final results are independent of the interaction as long as certain constraints on the cutoff scale are fulfilled. In detail the procedure works as follows:

- Start from a (possibly very large) initial cutoff Λ'_0 , which is given by the intrinsic cutoff of the bare interaction, i.e. $\Lambda'_0 \sim 15 \text{ fm}^{-1}$ for Nijmegen II or $\Lambda'_0 \sim 4 \text{ fm}^{-1}$ for N³LO.
- Evolve these interactions down to a cutoff Λ_0 . This cutoff depends on the density of the many-body system under consideration. As shown in Fig. 2.6 and Fig. 2.8, the 1S_0 gap function remains constant with varying cutoff scale, as long as the size of the Hilbert space is large enough to include all dominant modes of the pair wave function.
- The in-medium flow equation (2.29) is initialized at the cutoff scale Λ_0 . Since the low momentum interaction elements are strongly suppressed beyond this scale, one can restrict the size of the momentum mesh system to approximately this scale.

In the following we will choose $\Lambda_0 = 2.5 \text{ fm}^{-1}$. At this scale all interesting densities can be treated from one low momentum interaction for a given model.

This choice is also justified by explicitly comparing the results obtained from the bare and low momentum interactions (see. Figs. 2.15, 2.16 and 2.17).

Clearly the final results at momenta below the initial cutoff scale Λ_0 are essentially independent of the choice of Λ_0 and the interaction model, which just expresses the fact that for large cutoffs the flow in vacuum and medium are the same. This can be understood quite intuitively since the high momentum modes are very insensitive to the presence of other particles in the system. Also the different treatment of the external energy variable (on-shell in vacuum and off-shell in medium) poses no problem, since the vertex function is almost energy independent at large cutoffs (cf. Fig. 2.11). The agreement is valid over the whole energy range for the real and imaginary parts (cf. Figs. 2.16 and 2.17). Hence in the BCS approximation the (off-shell) in-medium scattering amplitude matrix elements seem to be strongly constrained by vacuum phase shift data.

In Figs. 2.18 and 2.19 are shown the results of the RG algorithm for the low momentum interaction derived from the N³LO interaction at $\Lambda_0 \sim 2.5 \text{ fm}^{-1}$ and $k_F = 0.8 \text{ fm}^{-1}$ for different CM momenta. Due to the approximate particle-hole symmetry of the free single particle spectrum only the results for Γ_{11} and Γ_{14} are shown. As can be seen in Fig. 2.18, the RG approach can nicely resolve the characteristic pole structure below threshold. As discussed in section 1.8 the matrix elements of the real part is discontinuously around the threshold in the back-to-back case. Despite the finite resolution of the energy mesh this feature is clearly resolved. For larger momenta this behaviour is smeared out and we obtain a continuous transition to the region above the threshold. Similarly, the characteristic behaviour of the imaginary part above the threshold is significant (cf. 2.19).

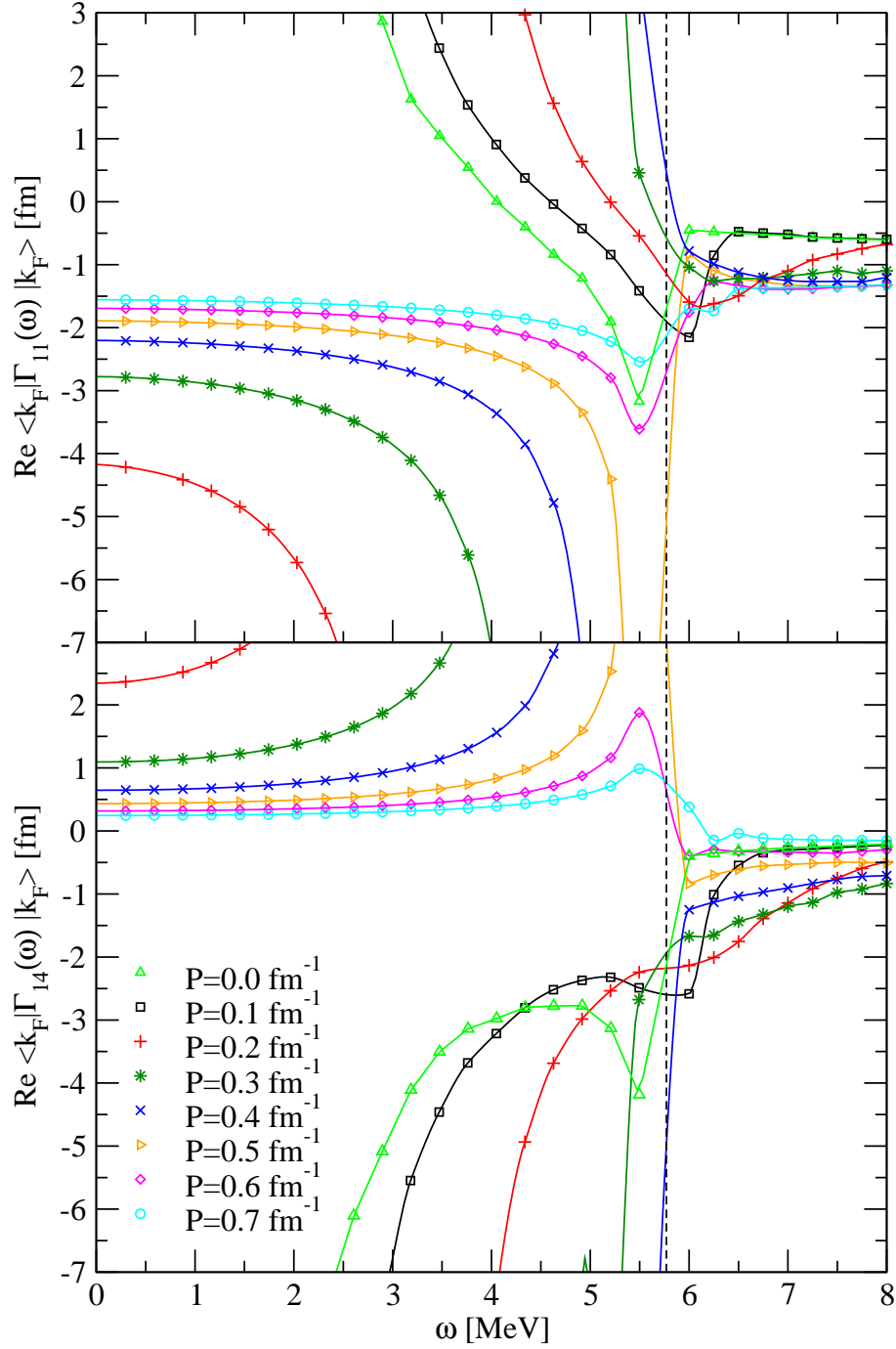


Figure 2.18.: Results for the real part of the vertex function as a function of energy for $k_F = 0.8 \text{ fm}^{-1}$ for different CM momenta. The V_{lowk} interaction derived from the $N^3\text{LO}$ interaction at $\Lambda = 2.5 \text{ fm}^{-1}$ and a cutoff width $c = 0.5 \text{ fm}^{-1}$ has been used as the kernel. The vertical dashed line denotes the two-particle threshold.

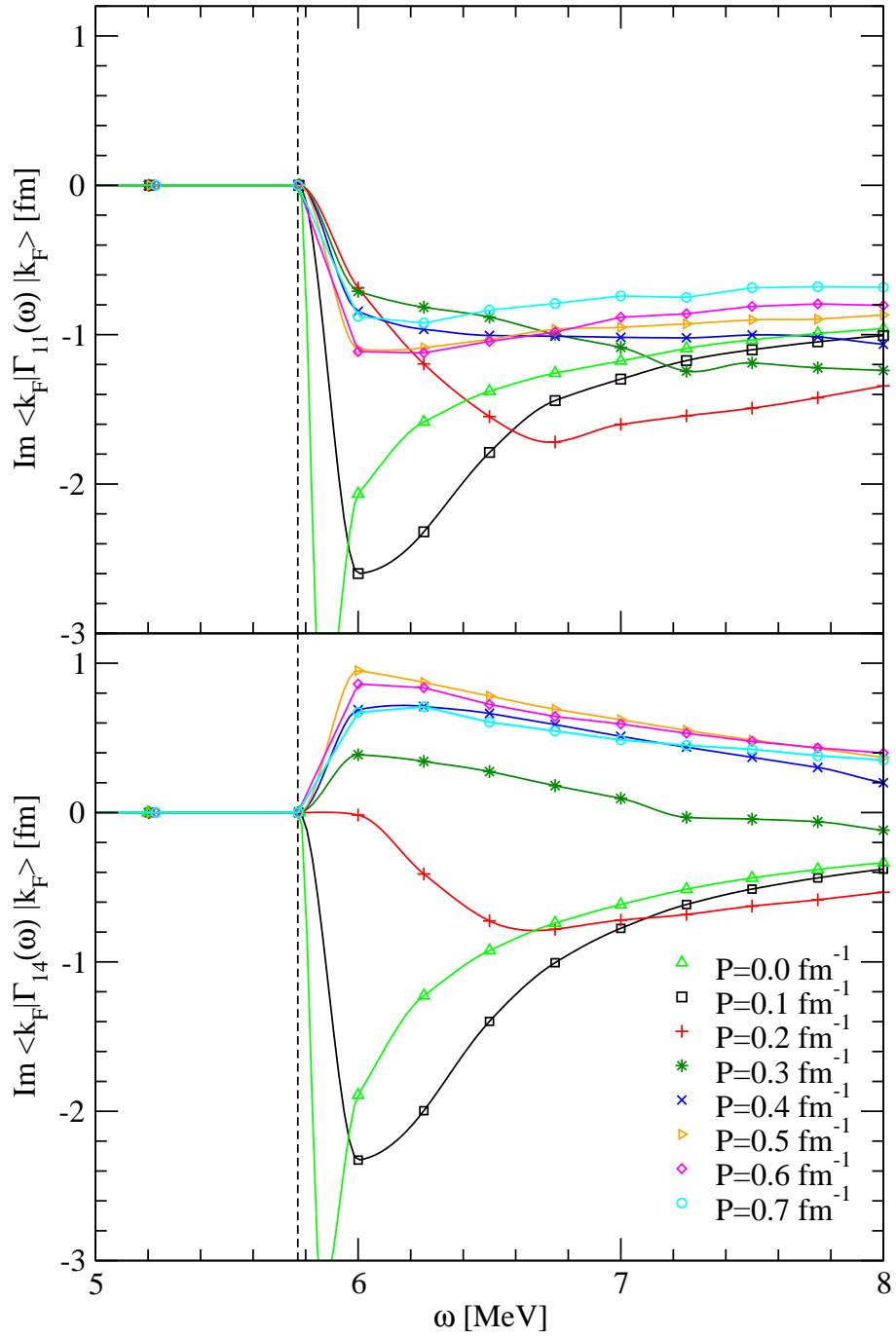


Figure 2.19.: Results for the imaginary part of the vertex function for different CM momenta. The same notation and parameters as in Fig. 2.18 are used.

3. Beyond the BCS approximation

3.1. Overview

In the present work the RG has so far been used as a tool to compute the vertex function in a superfluid using the BCS approximation. By applying RG techniques the initial problem of solving a set of multi-dimensional integral equations was transformed into the problem of solving differential equations and evaluating multi-dimensional integrals. By employing this method subtle inversion routines have been completely avoided. The equivalence of these two formulations was shown explicitly for the separable interaction \mathbf{V}_0^* (cf. section 2.5) in the one-channel case.

However, irrespective of these technical advantages, the real power of the RG method shows up if one wants to include correlations beyond the BCS-approximation. A more realistic treatment of pairing in strongly coupled many-body systems like nuclear matter requires the inclusion of (normal) self-energy effects on the one hand and vertex corrections on the other hand. Ideally these effects should be treated on an equal footing.

Usually the treatment of many-body effects like particle-hole screening in superfluids is done in two separate steps:

- a) The particle-hole correlations are calculated in the normal system, i.e. without a gap.
- b) The particle-particle correlations are taken into account by solving the gap equation using the effective vertex obtained in a) as the kernel.

Hence, effectively one assumes a *decoupling* of the particle-particle and particle-hole contributions, which simplifies the calculations considerably compared to the full coupled problem. However, from the beginning it is quite unclear, to what extent this decoupling assumption is justified since in particular low energy particle-hole excitations can in general be strongly influenced by the presence of a gap.

For a systematic investigation of the screening effects on the effective interaction, it is necessary to take the gap in all internal propagators into account. The first systematic perturbation theory for strongly interacting superfluid systems was presented by Nozieres [71]. Starting from an *unperturbed* theory, this scheme can be used to include many-body effects in a systematic way. In contrast to

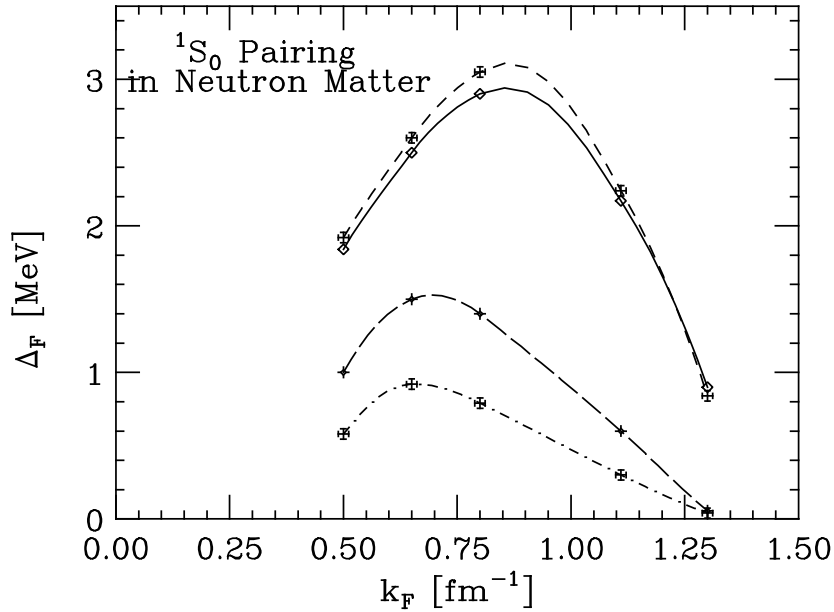


Figure 3.1.: Self-energy effects for the gap function. The upper dashed line represents the BCS approximation with free single particle spectrum. The upper solid line arises from an Brueckner-Hartree-Fock approach. The two lower lines show the results of different approximations of the self-energy in the quasiparticle approximation. For details see [129, 144]. Plot taken from [129].

the usual perturbation theory for normal systems, the unperturbed state cannot be taken as free, where all interparticle interactions are neglected, since this state has the wrong symmetry. At zero temperature, a perturbative expansion around a free Fermi gas can only generate a normal Fermi liquid. Hence instead of perturbing around a free gas, it is necessary to choose a "free" system with the correct symmetries as the starting point for the perturbation theory. This problem is directly related to the necessity for the introduction of the infinitesimal gap at the beginning of the flow in section 2.5.

The first quantitative calculations of medium effects on the 1S_0 gap were done in 1971 by Yang and Clark [141], who used an variational approach based on the so called Jastrow correlated wave functions and found a slight suppression of the gap compared to the BCS result. Later, Pines argued [142] that polarization effects should *enhance* the gap by a factor of $(1 + F_0)^{-1}$, where F_0 is the first Landau-Parameter of the central spin-isospin independent quasiparticle interaction. However, in later calculations [143], there were clear indications that the many-body effects effectively lead to a *suppression* of the gap. This result has been confirmed in all later calculations.

In the simplest generalization of the BCS approximation, the single particle

states are treated as quasiparticles with a spectral strength z_{k_F} and an effective mass M^* on the Fermi surface. In this case the gap equation takes a shape very similar to that in the BCS approximation. Recently Lombardo *et al.* [129, 144] examined the importance of these self-energy effects in the quasiparticle approximation and found a substantial reduction of the 1S_0 gap (see Fig. 3.1). Thus, due to the exponential dependence of the gap function on modifications in the interaction or single-particle properties, even slight changes can lead to quite large effects in the size of the condensate.

Self-energy effects in neutron matter beyond the quasiparticle approximation have been investigated by Bozek *et al.* [145, 146, 147]. By extracting spectral properties from a scattering equation similar to the one discussed in section 1.7 they found a reduction of the 1S_0 gap of about 30% compared to the BCS result. This effect is mainly due to the reduction of the spectral strength around the Fermi surface and thus essentially also a quasiparticle effect.

In all these works the free NN interaction has been used as the interaction kernel. For the inclusion of the vertex corrections several different strategies have been developed (cf. refs. [148, 149, 150]):

- *Low density approximation:*

In very dilute systems the particle-hole diagrams can be treated perturbatively [151]. The BCS gap function takes the weak coupling form [6, 152, 153]

$$\lim_{k_F \rightarrow 0} \Delta^{BCS} = \frac{8}{e^2} \varepsilon_F \exp \left[\frac{2\pi}{k_F a_{nn}} \right], \quad (3.1)$$

where ε_F is the Fermi energy, $e \simeq 2.7182$ is Euler's number and a_{nn} the neutron-neutron scattering length. It can be shown analytically that the inclusion of polarization effects leads to the new gap Δ of the value [6, 154]

$$\lim_{k_F \rightarrow 0} \Delta = (4e)^{-1/3} \Delta^{BCS} \simeq 0.45 \Delta^{BCS}, \quad (3.2)$$

i.e. the gap is to leading order in the expansion parameter $k_F a_{nn}$ suppressed by about a factor of $\simeq 2.2$, independent of the interaction.

This result is quite remarkable, since it expresses again the nonanalytical dependence of the gap function on the interaction. Despite the fact that the ratio between the in-medium and vacuum interaction approaches unity for small k_F , the ratio between the gaps does not.

However, it is quite unclear how these results extend to more physical densities where the perturbative treatment of the polarization effects is no longer justified. In this regime non-perturbative methods are needed.

- *Induced interaction:*

One non-perturbative strategy is based on the *induced* interaction, first developed by Babu and Brown [155]. The basic idea consists of splitting the

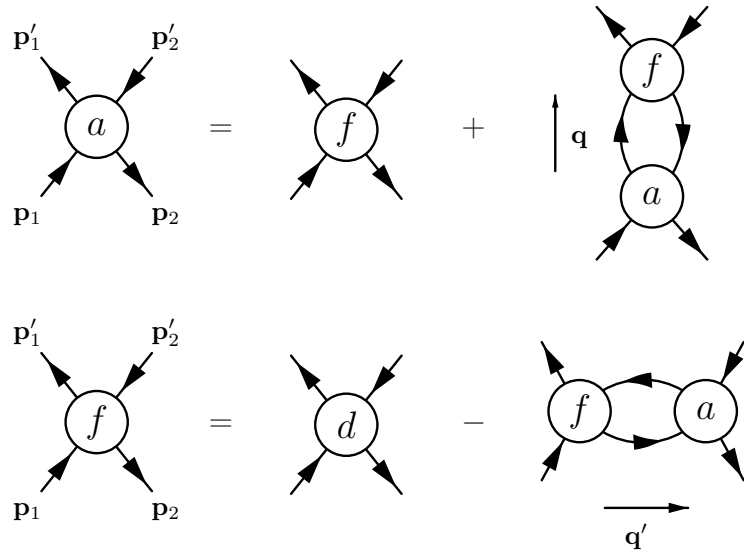


Figure 3.2.: System of integral equations defining the induced interaction f . The particle-hole scattering amplitude is denoted by a and the direct driving term by d (cf. ref. [158]).

particle-hole interaction into a direct part, responsible for the short range correlations and an induced component, which includes the effects of the collective excitation of the medium. This method was developed for the calculation of Landau Parameters in liquid ^3He , but was also applied to nuclear systems [156, 157]. Ainsworth, Wambach and Pines [158, 159] used this approach to estimate the screening effects of the gap by solving the coupled system of equations (Fig. 3.2) for the quasiparticle interaction and the scattering amplitude for all external momenta restricted to the Fermi surface. The particle-hole scattering amplitude a was then used as the kernel of the scattering equation in the weak coupling formula (3.1). The results are included in Fig. 3.4.

A similar strategy was followed by Schulze *et al.* [160]. However, instead of calculating the Landau parameters in the usual way by restricting all momenta to the Fermi surface, they explicitly allowed finite momentum transfers in the direct channel. By retaining the momentum dependence, they could explicitly compare weak coupling results with the full solution of the gap equation. They found large deviations in their model, indicating possible problems with naive applications of the weak coupling approximation.

Shen *et al.* investigated the coupling of self-energy effects with vertex corrections using a phenomenological force to leading order [161] and using the RPA approximation [162]. Similarly to the other works, they also found a strong reduction of about 20 – 30% compared to the BCS approximation.

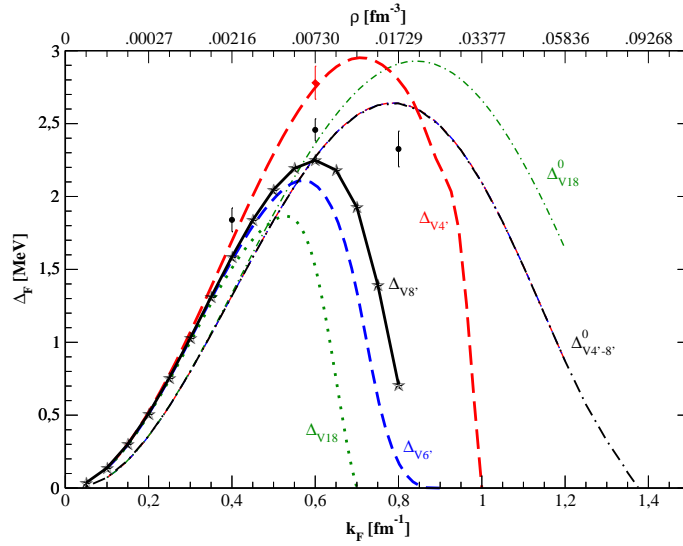


Figure 3.3.: Results of Fabrocini *et al* for the 1S_0 gap in neutron matter using QMC methods and the CBF approach. The $\Delta_{v4'-8'}$ and Δ_{v18} curves show the CBF gaps and the points with error bars show the QMC results. Δ_{v18}^0 and $\Delta_{v4'-8'}^0$ show the BCS results for the different Argonne potentials. For details see [163]. Plot taken from this reference.

- *Correlated basis functions (CBF) and Quantum Monte Carlo (QMC) methods:*

The CBF approach is based on the fact that the interparticle interaction is repulsive at small distances and that consequently the relative wave function of two interacting particles at such distances is small. This fact is incorporated for normal systems by multiplying the ordinary Slater determinant by the Jastrow correlation operator

$$F(r_1, \dots, r_A) = \prod_{i < j}^A f(r_{ij}), \quad (3.3)$$

which suppresses the wave function at small interparticle distances r_{ij} . The application of this correlator to the BCS state leads to the correlated BCS state [164, 165].

Chen *et. al.* [152, 166] calculated the 1S_0 gap in neutron matter to first order in CBF perturbation theory. In this scheme, the single particle energies $\xi_{\mathbf{k}}$ and the interaction matrix elements $\langle \mathbf{k}' - \mathbf{k}' | V | \mathbf{k} - \mathbf{k} \rangle$ get renormalized compared to the uncorrelated BCS scheme via the correlators F . By this, a class of short-range correlations is incorporated into this scheme. As the result, they found a suppression of the gap, compared to BCS theory, similar to that of the other approaches.

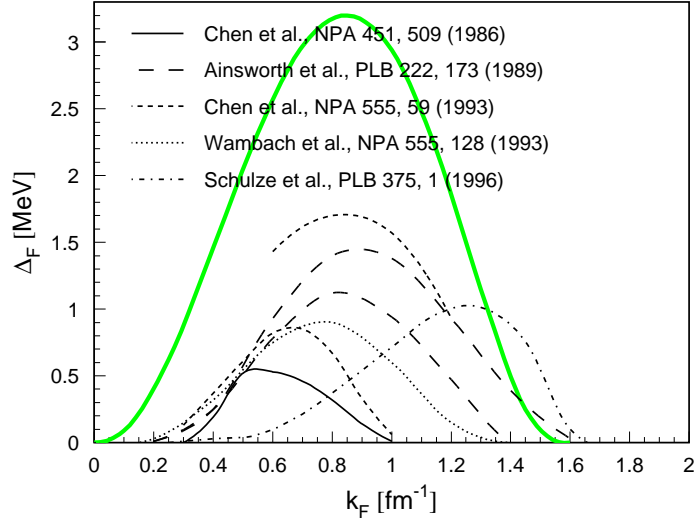


Figure 3.4.: Summary of the results from different approximations for the many body effects. The green curve shows the BCS result. Plot taken from [129].

In contrast to the results above, Fabrocini *et. al.* [163] found only a very slight reduction of the gap compared to the BCS result obtained by using Quantum Monte Carlo methods. However these Monte Carlo calculations may require larger particle numbers to be sensitive to long-range polarization effects. The results are also shown in Fig. 3.3.

- *Parquet equations:*

Another non-perturbative alternative consists of solving the parquet equations [167, 168]. The parquet scheme entails the self-consistent summation of all many-body channels, i.e. all intermediate lines in the diagrams are solutions of the Dyson equation by construction. This ensures self-consistency on the one-body level [169]. This approach will be discussed in more detail in the next section and section 3.6.

3.2. RG Approach to the Parquet Equations

The parquet equations represent a system of coupled Bethe-Salpeter equations, which include correlations of all many-body channels (cf. Fig. 1.15) and section 3.6). Starting from a completely irreducible "bare" driving term, the parquet equations generate all two-body reducible diagrams. By defining formal joining operators, which generate the particle-particle ladders, particle-hole ladders and the particle-hole chains, it can be shown that each diagram is indeed generated exactly once and consequently no double counting occurs [167]. Although a full

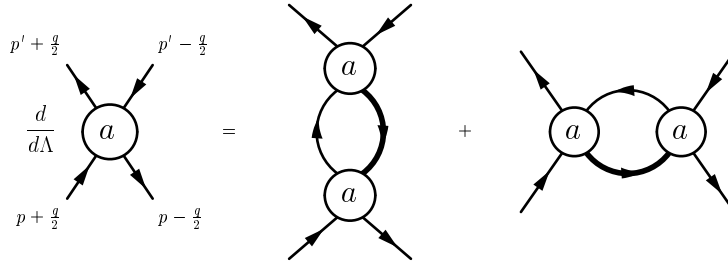


Figure 3.5.: The one-loop flow equation used in [170] for the effective four point vertex $a^\Lambda(\mathbf{p}, \mathbf{p}')$. The thick line represents the line which is integrated out in the corresponding RG step (cf. Fig. 3.2). Diagram taken from [171].

solution of these equations is still out of range of practical calculations, these equations provide a non-perturbative starting point for the application of different approximation schemes.

The Renormalization Group provides a systematic tool for investigating the parquet equations. The efficacy of this method lies in including many-body correlations by successive momentum shells, whereas all effects from the previous shells are included in the effective vertices at the certain cutoff scale Λ .

The complexity of the full parquet equations can be reduced considerably, if the diagrams in the BCS channel are neglected. The resulting system, called the particle-hole parquet, is equivalent to the induced interaction (see Fig. 3.2). Schwenk *et. al.* [124, 170] used the RG approach for the summation of the particle-hole parquet system to one-loop order (cf. below). In this approximation, the flow equations for the effective scattering amplitude $a^\Lambda(\mathbf{p}, \mathbf{p}')$ and the quasiparticle interaction $f^\Lambda(\mathbf{p}, \mathbf{p}')$ take the following explicit form [94, 170] (cf. Fig. 3.5):

$$\frac{df^\Lambda}{d\Lambda} = -a^\Lambda \frac{dGG_{ZS'}^>}{d\Lambda} a^\Lambda. \quad (3.4)$$

$$\frac{da^\Lambda}{d\Lambda} = a^\Lambda \frac{dGG_{ZS}^>}{d\Lambda} a^\Lambda + \frac{df^\Lambda}{d\Lambda} = a^\Lambda \frac{dGG_{ZS}^>}{d\Lambda} a^\Lambda - a^\Lambda \frac{dGG_{ZS'}^>}{d\Lambda} a^\Lambda, \quad (3.5)$$

where the same schematic notation as in section 2.3 has been used.

Starting from a bare vacuum interaction V_{bare} or a low momentum interaction V_{lowk} (as done in [170]) for the driving term d , the flow equation sums contributions to the effective four point vertex $a^\Lambda(\mathbf{p}, \mathbf{p}')$ by successively integrating out the correlation of a momentum shell of width $d\Lambda$. One great advantage of this approach is the fact that the intermediate momenta \mathbf{q} in the direct channel and \mathbf{q}' in the exchange channel (cf. Fig. 3.2) are treated on an equal footing. In this way it is automatically ensured that the scattering amplitude remains antisymmetric and consequently the Pauli principle is obeyed.

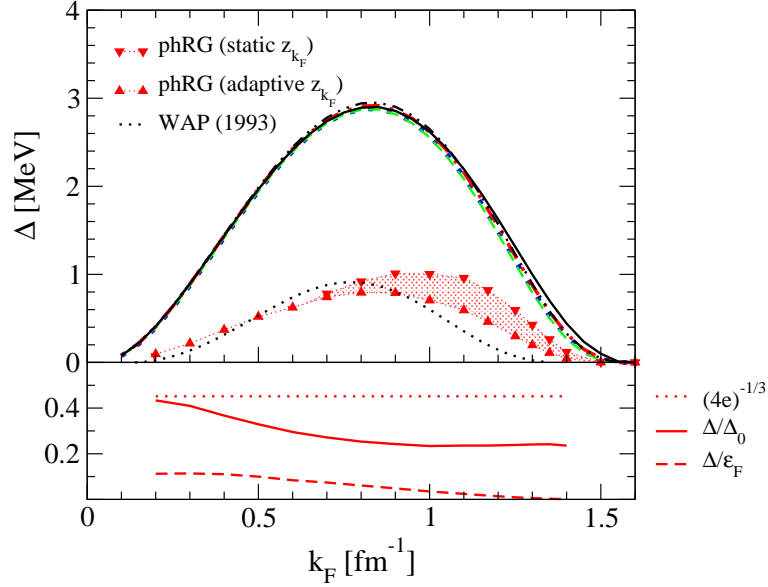


Figure 3.6.: Upper panel: Comparison of the BCS 1S_0 gaps in neutron matter including polarization effects and quasiparticle strength z_{k_F} renormalization (cf. ref. [170]). Lower panel: Comparison to the weak coupling BCS result. Plot taken from [172].

After the RG has been evolved down to the Fermi surface, the effective four point vertex a includes correlations of both ph channels. The pp correlations are accounted for by solving the gap equation in the weak coupling approximation using the effective vertex $a(\mathbf{p}, \mathbf{p}')$ as the interaction kernel. The results (Fig. 3.6) show a reduction of the BCS gap by a factor ~ 3 in qualitative agreement with the results of [158] (cf. Fig. 3.4).

The flow equation (2.29) in the BCS channel problem has a structure similar to the one-loop flow equation (3.5). However, in the one-channel problem the flow equation of this form is *exact*, in the sense that the iteration of the RG equation solves the Bethe-Salpeter equation in the corresponding channel exactly. In the coupled channel problem, the situation is much more involved. Here the one-loop-flow equation (3.5) is only approximate and provides a first order equation in the expansion parameter $\frac{\Lambda}{k_F}$ [173, 174], i.e. the one-loop expansion becomes more and more reliable for smaller cutoffs.

The inclusion of the particle-particle channel into the flow increases the complexity of the problem for two reasons:

- Additional terms appear in the flow equation for the vertex functions due to the presence of additional channels.
- Due to the presence of the BCS singularity, the transition to the superfluid phase has to be treated properly, either by bosonization or using Gorkov

propagators.

In the coupled channel problem the scattering equation in the BCS channel is schematically of the form:

$$\Gamma = \Gamma^{irr} + \Gamma^{irr} GG\Gamma. \quad (3.6)$$

Here Γ^{irr} is the irreducible vertex in this channel, which in contrast to the completely irreducible kernel employed in section 2.5, is *scale dependent* due to the contributions of the other channels. Consequently, the flow equation for this kernel has to be determined from the corresponding Bethe-Salpeter equation (cf. section 3.6). Hence compared to the problem of section 2.5 new contributions appear at this point in the flow equation:

$$\frac{d\Gamma}{d\Lambda} = \frac{d\Gamma^{irr}}{d\Lambda} + \frac{d\Gamma^{irr}}{d\Lambda} GG^> \Gamma + \Gamma^{irr} \frac{dGG^>}{d\Lambda} \Gamma + \Gamma^{irr} GG^> \frac{d\Gamma}{d\Lambda}. \quad (3.7)$$

In contrast to eq. (2.17), this flow equation *cannot* be inverted explicitly and the practical evaluation of this RG equation becomes more complicated. We will return to this technical problem in section 3.6.

The renormalization of the irreducible vertex function Γ^{irr} also generates additional contributions to the flow of the (normal and anomalous) self-energies. Here an important difference to the BCS approximation shows up. At the BCS level the flow of the vertex Γ^Λ is *not* coupled to the flow of the two-point function, since the irreducible vertex Γ_0 - which is the kernel in the gap equation in the BCS approximation - remains unchanged during the flow. On the other hand, the flow of the gap function Δ^Λ affects the flow of the vertex function Γ^Λ (cf. section 2.5), leading to the shift of the location of the two-particle threshold (cf. Fig. 2.11). Hence in this sense, the coupling between the flow equations of the two-point and four-point functions is only unidirectional. Beyond the BCS approximation however, the irreducible driving term Γ^{irr} in the gap equation becomes scale dependent and the coupling of the flow equation of the two and four-point functions is bidirectional. We will return to this problem in more detail in section 3.4.

3.3. Self-Energy Corrections

As pointed out in section 3.1, for a systematic study of many-body correlations in superfluid systems, it is necessary to start with an unperturbed theory, where the symmetry is broken. Hence one could start from the BCS theory and calculate many-body effects on top of the BCS state. To avoid double counting, diagrams included in the BCS approximation are not allowed in the perturbative expansion around the BCS state. Alternatively, one can *explicitly* break the symmetry by decomposing the full Hamiltonian \hat{H} , consisting of a kinetic part \hat{T} and an

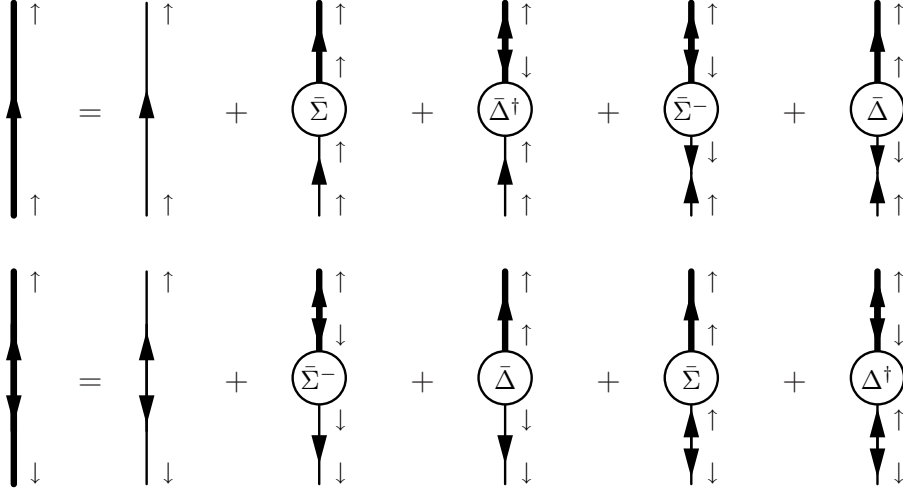


Figure 3.7.: Dyson equations for the single particle Gorkov propagators. The propagators G^- and F^\dagger can be determined by using symmetry relations. See text.

interaction part \hat{V} , in the following way:

$$\hat{H}_0 = \hat{T} - \mu\hat{N} + \hat{U}, \quad \hat{H}_1 = \hat{V} - \hat{U} \quad (3.8)$$

with

$$\hat{T} = \sum_{\mathbf{k},\sigma} \xi_{\mathbf{k}}^0 \hat{a}_{\mathbf{k}\sigma}^\dagger \hat{a}_{\mathbf{k}\sigma}, \quad \hat{U} = \sum_{\mathbf{k},\sigma} \lambda_{\mathbf{k}} \hat{a}_{\mathbf{k}\sigma}^\dagger \hat{a}_{\mathbf{k}\sigma} - \sum_{\mathbf{k}} \alpha_{\mathbf{k}} \left[\hat{a}_{\mathbf{k}\uparrow}^\dagger \hat{a}_{-\mathbf{k}\downarrow}^\dagger + \hat{a}_{-\mathbf{k}\downarrow} \hat{a}_{\mathbf{k}\uparrow} \right]. \quad (3.9)$$

The "free" Hamiltonian \hat{H}_0 can easily be diagonalized by a Bogoliubov transformation (1.17). This leads to the BCS-type bare single particle propagators

$$\mathbf{G}^{(0)}(\mathbf{k}, \omega) = \begin{pmatrix} G_{\uparrow\uparrow}^{(0)}(\mathbf{k}, \omega) & F_{\uparrow\downarrow}^{(0)}(\mathbf{k}, \omega) \\ F_{\downarrow\uparrow}^{(0)\dagger}(\mathbf{k}, \omega) & G_{\downarrow\downarrow}^{(0)-}(\mathbf{k}, \omega) \end{pmatrix} \quad (3.10)$$

where

$$G_{\uparrow\uparrow}^{(0)}(\mathbf{k}, \omega) = \frac{\omega + \xi_{\mathbf{k}}^0 + \lambda_{\mathbf{k}}}{\omega^2 - [\xi_{\mathbf{k}}^0 + \lambda_{\mathbf{k}}]^2 - \alpha_{\mathbf{k}}^2} = -G_{\downarrow\downarrow}^{(0)-}(\mathbf{k}, -\omega) \quad (3.11)$$

$$F_{\uparrow\downarrow}^{(0)}(\mathbf{k}, \omega) = -\frac{\lambda_{\mathbf{k}}}{\omega^2 - [\xi_{\mathbf{k}}^0 + \lambda_{\mathbf{k}}]^2 - \alpha_{\mathbf{k}}^2} = F_{\downarrow\uparrow}^{(0)\dagger}(\mathbf{k}, \omega) \quad (3.12)$$

The values of the parameters $\lambda_{\mathbf{k}}$ and $\alpha_{\mathbf{k}}$ depend on the choice of the unperturbed theory. Apart from convergence problems, these parameters can be chosen rather arbitrarily and the final result is independent of this choice [71].

These parametric self-energy insertions are also included in the self-energy in-

sertions $\bar{\Sigma}$, which appear explicitly as elements in the diagrams in the superfluid perturbation theory. This self-energy has the same symmetries as the free propagators and is denoted by

$$\bar{\Sigma}(\mathbf{k}, \omega) = \begin{pmatrix} \bar{\Sigma}_{\uparrow\uparrow}(\mathbf{k}, \omega) & \bar{\Delta}_{\uparrow\downarrow}(\mathbf{k}, \omega) \\ \bar{\Delta}_{\downarrow\uparrow}^\dagger(\mathbf{k}, \omega) & \bar{\Sigma}_{\downarrow\downarrow}(\mathbf{k}, \omega) \end{pmatrix}. \quad (3.13)$$

For homogeneous systems the corresponding full propagator

$$\mathbf{G}(\mathbf{k}, \omega) = \begin{pmatrix} G_{\uparrow\uparrow}(\mathbf{k}, \omega) & F_{\uparrow\downarrow}(\mathbf{k}, \omega) \\ F_{\downarrow\uparrow}^\dagger(\mathbf{k}, \omega) & G_{\downarrow\downarrow}(\mathbf{k}, \omega) \end{pmatrix} = \mathbf{G}^0(\mathbf{k}, \omega) + \mathbf{G}(\mathbf{k}, \omega) \bar{\Sigma}(\mathbf{k}, \omega) \mathbf{G}^0(\mathbf{k}, \omega) \quad (3.14)$$

obeys $F^\dagger(\mathbf{k}, \omega) = F(\mathbf{k}, \omega)$ and $G^-(\mathbf{k}, \omega) = -G^+(\mathbf{k}, \omega)$ as in the BCS case. Due to these symmetry relations it is sufficient to solve the following system (cf. Fig. 3.3):

$$\begin{aligned} G_{\uparrow\uparrow}(k) &= G_{\uparrow\uparrow}^{(0)}(k) \\ &\quad + G_{\uparrow\uparrow}(k) \bar{\Sigma}_{\uparrow\uparrow}(k) G_{\uparrow\uparrow}^{(0)}(k) + F_{\uparrow\downarrow}(k) \bar{\Delta}_{\downarrow\uparrow}^\dagger(k) G_{\uparrow\uparrow}^{(0)}(k) \\ &\quad + F_{\uparrow\downarrow}(k) \bar{\Sigma}_{\downarrow\downarrow}^-(k) F_{\downarrow\uparrow}^{(0)\dagger}(k) + G_{\uparrow\uparrow}(k) \bar{\Delta}_{\uparrow\downarrow}(k) F_{\downarrow\uparrow}^{(0)\dagger}(k) \\ F_{\uparrow\downarrow}(k) &= F_{\uparrow\downarrow}^{(0)}(k) \\ &\quad + F_{\uparrow\downarrow}(k) \bar{\Sigma}_{\downarrow\downarrow}^-(k) G_{\downarrow\downarrow}^{(0)-}(k) + G_{\uparrow\uparrow}(k) \bar{\Delta}_{\uparrow\downarrow}(k) G_{\downarrow\downarrow}^{(0)-}(k) \\ &\quad + G_{\uparrow\uparrow}(k) \bar{\Sigma}_{\uparrow\uparrow}(k) F_{\uparrow\downarrow}^{(0)}(k) + F_{\uparrow\downarrow}(k) \bar{\Delta}_{\downarrow\uparrow}^\dagger(k) F_{\uparrow\downarrow}^{(0)}(k). \end{aligned} \quad (3.15)$$

By using $F^{(0)\dagger}(p) = F^{(0)}(p)$ and $\bar{\Delta} = -\bar{\Delta}_{\downarrow\uparrow}^\dagger = -\bar{\Delta}_{\uparrow\downarrow}$ one obtains as a solution:

$$\begin{aligned} G &= \frac{1}{\xi} [G^{(0)} + \bar{\Sigma}^- (F^{(0)} F^{(0)} - G^{(0)} G^{(0)-})] \\ F &= \frac{1}{\xi} [F^{(0)} + \bar{\Delta} (F^{(0)} F^{(0)} - G^{(0)} G^{(0)-})] \\ \xi &= 1 - G^{(0)} \bar{\Sigma} - G^{(0)-} \bar{\Sigma}^- + 2F^{(0)} \bar{\Delta} + (\bar{\Delta}^2 - \bar{\Sigma} \bar{\Sigma}^-) (F^{(0)} F^{(0)} - G^{(0)} G^{(0)-}). \end{aligned} \quad (3.16)$$

Inserting the expressions (3.10) this simplifies to (cf. also [71]):

$$G(\mathbf{k}, \omega) = \frac{\omega + \xi_{\mathbf{k}}^0 + \lambda_{\mathbf{k}} - \bar{\Sigma}^-(\mathbf{k}, \omega)}{\zeta(\mathbf{k}, \omega)}, \quad F(\mathbf{k}, \omega) = \frac{[\alpha_{\mathbf{k}} + \bar{\Delta}(\mathbf{k}, \omega)]}{\zeta(\mathbf{k}, \omega)} \quad (3.17)$$

with

$$\zeta(\mathbf{k}, \omega) = [\omega - \xi_{\mathbf{k}}^0 - \lambda_{\mathbf{k}} - \bar{\Sigma}(\mathbf{k}, \omega)] [\omega + \xi_{\mathbf{k}}^0 + \lambda_{\mathbf{k}} - \bar{\Sigma}^-(\mathbf{k}, \omega)] - [\alpha_{\mathbf{k}} + \bar{\Delta}(\mathbf{k}, \omega)]^2 \quad (3.18)$$

The self-energy $\bar{\Sigma}$ includes effects from the interaction \hat{V} and the auxiliary one-

body operator \hat{U} . The one-body operator shifts the self-energies by the parameters $\lambda_{\mathbf{k}}$ and $\alpha_{\mathbf{k}}$ respectively. Hence one can identify the "physical" self-energies by

$$\Sigma(\mathbf{k}, \omega) = \lambda_{\mathbf{k}} + \bar{\Sigma}(\mathbf{k}, \omega), \quad \Delta(\mathbf{k}, \omega) = \alpha_{\mathbf{k}} + \bar{\Delta}(\mathbf{k}, \omega), \quad (3.19)$$

which leads to a quite natural form of the full propagator $\mathbf{G}(\mathbf{k}, \omega)$. The function $\Delta(\mathbf{k}, \omega)$ is usually called the *generalized gap function*.

3.4. Generalized Gap Equation

The generalized gap function can be represented in the form of an integral equation, the *generalized gap equation*. As shown by Nozieres [71], this equation can be derived quite intuitively by analyzing the diagrammatical structure of the self-energy diagrams generated by variations of the Luttinger-Ward functional $\Phi[\mathbf{G}]$, consisting of *skeleton diagrams* including the full single-particle Greens function \mathbf{G} . In terms of this functional, the effective potential $\Gamma[\Psi, \mathbf{G}]$ of a many-fermion system can be written in the form [175, 176, 177, 178]:

$$\Gamma[\Psi, \mathbf{G}] = S_0[\Psi] + \text{Tr} \ln \mathbf{G} - \text{Tr}[\mathbf{G}_0^{-1} \mathbf{G} - 1] + \Phi[\Psi, \mathbf{G}]. \quad (3.20)$$

with $\Psi(p) \in \{\psi(p), \psi^*(p)\}$. At this point, the propagator G and the field ψ and ψ^* are *independent* quantities and the Φ -functional is the generating functional of the self-energy Σ :

$$\frac{\delta \Phi[\Psi, \mathbf{G}]}{\delta \mathbf{G}} \equiv \Sigma[\Psi, \mathbf{G}[\Psi]]. \quad (3.21)$$

The stationary points of the functional with respect to variations of Ψ and \mathbf{G} define the self-consistent equations of motion for Ψ and the exact Greens function $\tilde{\mathbf{G}}$:

$$\left. \frac{\delta \Gamma[\Psi, \mathbf{G}]}{\delta \Psi(p)} \right|_{\Psi=\tilde{\Psi}} = 0, \quad \left. \frac{\delta \Gamma[\Psi, \mathbf{G}]}{\delta \mathbf{G}(p_1, p_2)} \right|_{\mathbf{G}=\tilde{\mathbf{G}}} = \left. \frac{\delta^2 \Gamma[\Psi, \mathbf{G}]}{\delta \Psi(p_1) \delta \Psi(p_2)} \right|_{\mathbf{G}=\tilde{\mathbf{G}}} = 0. \quad (3.22)$$

The latter one leads to the Dyson-Schwinger equations for the Greens function at the mean field Ψ , defining the self-consistent one-body propagator $\tilde{\mathbf{G}}$:

$$\begin{aligned} \tilde{\mathbf{G}}_{p_1, p_2}^{(2)}[\Psi] = \tilde{\mathbf{G}}^{-1}[\Psi](p_1, p_2) &= \mathbf{G}_0^{-1}(p_1, p_2) - \Sigma[\Psi, \tilde{\mathbf{G}}](p_1, p_2) \\ &\equiv \mathbf{G}_0^{-1}(p_1, p_2) - \tilde{\Sigma}[\Psi](p_1, p_2), \end{aligned} \quad (3.23)$$

where we have introduced a compact notation for the N -point functions $\tilde{\mathbf{I}}_{p_1, p_2, \dots, p_N}^{(N)}$. This function is defined by the total number N of external lines, whereas the number of incoming and outgoing lines are arbitrary. The incoming momenta are denoted by p_i and the outgoing by \tilde{p}_i . Hence, for example the 4 elements of

the 2-point function read:

$$\tilde{\Gamma}_{p_1, p_2}^{(2)}[\Psi] = \begin{pmatrix} \frac{\delta^2 \tilde{\Gamma}[\Psi]}{\delta\psi^*(p_1)\delta\psi(p_2)} & \frac{\delta^2 \tilde{\Gamma}[\Psi]}{\delta\psi^*(p_1)\delta\psi^*(p_2)} \\ \frac{\delta^2 \tilde{\Gamma}[\Psi]}{\delta\psi(p_1)\delta\psi(p_2)} & \frac{\delta^2 \tilde{\Gamma}[\Psi]}{\delta\psi(p_1)\delta\psi^*(p_2)} \end{pmatrix} = \begin{pmatrix} \tilde{\Gamma}_{\tilde{p}_1, p_2}^{(2)}[\Psi] & \tilde{\Gamma}_{\tilde{p}_1, \tilde{p}_2}^{(2)}[\Psi] \\ \tilde{\Gamma}_{p_1, p_2}^{(2)}[\Psi] & \tilde{\Gamma}_{p_1, \tilde{p}_2}^{(2)}[\Psi] \end{pmatrix} \quad (3.24)$$

This matrix is antisymmetric under exchange of two momenta due to the Grassmann nature of the fields Ψ .

The 1PI effective action $\tilde{\Gamma}[\Psi]$ is a functional of only the fermion field Ψ , whereas the propagator is always constrained by the Dyson-equation (3.23):

$$\tilde{\Gamma}[\Psi] = \Gamma[\Psi, \tilde{\mathbf{G}}] \quad (3.25)$$

Additional variations provide the Bethe-Salpeter equations for the higher vertex functions describing the fluctuations around the Dyson equations:

$$\begin{aligned} \tilde{\Gamma}_{p_1, p_2, p_3}^{(3)}[\Psi] &= \frac{\delta \tilde{\mathbf{G}}^{-1}[\Psi](p_1, p_2)}{\delta \Psi(p_3)} \\ &= - \left[\frac{\delta \Sigma[\Psi, \mathbf{G}](p_1, p_2)}{\delta \Psi(p_3)} + \text{Tr}_{q, q'} \frac{\delta \Sigma[\Psi, \mathbf{G}](p_1, p_2)}{\delta \mathbf{G}(q, q')} \frac{\delta \tilde{\mathbf{G}}[\Psi](q, q')}{\delta \Psi(p_3)} \right]_{\mathbf{G}=\tilde{\mathbf{G}}} \\ &= -\tilde{\Phi}_{p_1, p_2, p_3}^{(3)} - \tilde{\Phi}_{p_1, p_2, q, q'}^{(4)} \tilde{\mathbf{G}}(q) \tilde{\mathbf{G}}(q') \tilde{\Gamma}_{q, q', p_3}^{(3)} \end{aligned} \quad (3.26)$$

with the *irreducible* kernels

$$\tilde{\Phi}^{(3)}[\Psi] \equiv \left. \frac{\delta \Sigma[\Psi, \mathbf{G}]}{\delta \Psi} \right|_{\mathbf{G}=\tilde{\mathbf{G}}}, \quad \tilde{\Phi}^{(4)}[\Psi] \equiv \left. \frac{\delta \Sigma[\Psi, \mathbf{G}]}{\delta \mathbf{G}} \right|_{\mathbf{G}=\tilde{\mathbf{G}}}. \quad (3.27)$$

It should be noted that the Bethe-Salpeter equation is always defined on top of the Dyson-equation (3.23), i.e. the single particle propagators are always defined self-consistently by the solution of the Dyson-equation. Hence for the derivation of these equations, it is usually easier to start from the 1PI effective action, where the self-consistency on the one-particle propagator level is already incorporated. Products like $\tilde{\Phi}^{(4)} \tilde{\mathbf{G}} \tilde{\mathbf{G}} \tilde{\Gamma}^{(3)}$ implicitly involve all allowed connections of the internal lines. In general, the irreducible vertices are defined by

$$\tilde{\Phi}_{p_1, p_2, \dots, p_{2n-1}, p_{2n}}^{(2n)} = \left. \frac{\delta^n \Phi[\Psi, \mathbf{G}]}{\delta \mathbf{G}(p_1, p_2) \dots \delta \mathbf{G}(p_{2n-1}, p_{2n})} \right|_{\mathbf{G}=\tilde{\mathbf{G}}} \quad (3.28)$$

$$\tilde{\Phi}_{p_1, p_2, \dots, p_{2n}, p_{2n+1}}^{(2n+1)} = \left. \frac{\delta}{\delta \Psi(p_{2n+1})} \left[\frac{\delta^n \Phi[\Psi, \mathbf{G}]}{\delta \mathbf{G}(p_1, p_2) \dots \delta \mathbf{G}(p_{2n-1}, p_{2n})} \right] \right|_{\mathbf{G}=\tilde{\mathbf{G}}}, \quad (3.29)$$

where we have in the exact case $\frac{\delta \Phi[\Psi, \mathbf{G}]}{\delta \mathbf{G}(p_1, p_2)} = \frac{\delta \Phi[\Psi, \mathbf{G}]}{\delta \Psi(p_1) \delta \Psi(p_2)}$. One additional variation yields the Bethe-Salpeter equation for the four-point vertex:

$$\tilde{\Gamma}_{p_1, p_2, p_3, p_4}^{(4)} = \tilde{\Phi}_{p_1, p_2, p_3, p_4}^{(4)} + \text{Tr}_{q, q'} \left[\tilde{\Phi}_{p_1, p_2, q, q'}^{(4)} \tilde{\mathbf{G}}(q) \tilde{\mathbf{G}}(q') \tilde{\Gamma}_{q, q', p_3, p_4}^{(4)} \right], \quad (3.30)$$

where all terms, including vertex functions with an odd number of external lines have been discarded. Since the character of the internal lines in eq. (3.30) is not fixed (it can be a particle or hole), the definition of reducibility in superfluid systems is a little bit more subtle than in normal systems, where the different four point diagrams can be categorized in the following way: If a particle-particle scattering diagram cannot be disconnected into two parts by cutting two internal particle lines (or two hole lines), the diagram is said to be irreducible in the BCS channel. Accordingly, the particle-hole channels ZS and ZS' are defined by the impossibility of dividing the diagram into two pieces by cutting one internal particle-hole pair, whereas the two different particle-hole channels are discriminated by the two topologically different particle-hole diagrams (cf. Fig. 1.15). By contrast, in superfluid systems the nature of the internal and external lines in such scattering diagrams is arbitrary, so that the classification of diagrams into different irreducibility channels must rely only on the topology of the diagrams.

We now discuss how the different channels can be defined in a superfluid. Due to the presence of the condensate, all channels, as defined in the normal system, couple with each other. In this sense the scattering equation for the 4×4 matrix $\tilde{\Gamma}^{(4)}$ already includes the contributions of all three channels BCS , ZS and ZS' in the limit $\Delta \rightarrow 0$ (see. section 1.7). In order to define a scattering equation in superfluid systems, one has to define at first the "incoming" and "outgoing" lines. This definition is necessary for the formal organization of the diagrams and has nothing to do with the direction of the external lines since the "incoming" and "outgoing" lines each contain particle and hole lines. By this formal fixing of the initial and final states, one has to define a proper criterion for the construction of the irreducible vertices. In general four point diagrams in superfluids can be classified by their topological structure upon cutting any two internal lines (2P irreducibility). If one labels the four external lines by 1, 2, 3 and 4, any arbitrary diagram can be either

- a) completely 2P irreducible, if the diagram remains connected under cutting any two internal lines,
- b) 2P reducible in the channel [12,34], if the diagram can be cut into two parts, where the parts containing the external lines (1, 2) and (3, 4) respectively remain connected,
- c) 2P reducible in the channel [13,24],
- d) or in the channel [14,23].

Single diagrams reducible in two or all three channels are topologically impossible.

	0	1	2
$\Phi[\Psi, \mathbf{G}]$			
Σ_{12}			
$\tilde{\Phi}_{1,2,3,4}^{(4)}$			
$\tilde{\Phi}_{1,2,3,4,5,6}^{(6)}$			

Table 3.1.: Diagrams resulting from variations of the 2PI functional Φ in zero, one and two loop order. The directions of the fermionic lines are arbitrary up to particle number conserving constraints at the vertices of the antisymmetrized bare two point interaction (unfilled circles). The internal fermion lines represent the full propagator including all Gorkov components. The resulting 2PI vertices $\tilde{\Phi}^{(4)}$ are all irreducible in the channel [12,34] and reducible in the channel [13,24] or [14,23]. Due to the large number of diagrams in two loop order only two diagrams of the six point vertex are shown.

However, due to the fact that the vertices $\tilde{\Phi}^{(4)}$ are generated by variations of the LW functional, it is not difficult to see that all these diagrams are members of the reducibility classes a), c) or d), i.e. are either completely irreducible or *irreducible* in the channel [12,34]. This can either be seen by explicitly calculating the lowest order diagrams in the loop expansion of Φ (cf. Table 3.1) or by analyzing in general the structure of the self-energy diagrams with the external labels 1 and 2. The core of the self-energy consists in general of an arbitrary number of internal

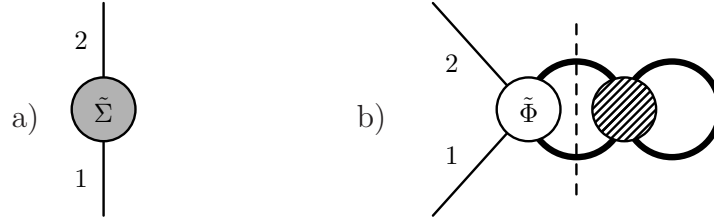


Figure 3.8.: Irreducibility of the vertex function $\tilde{\Phi}^{(4)}$. Due to the skeleton structure the self-energy contains no diagrams of the type b) and is consequently irreducible in this channel.

fermion lines. If we pick out *any* one of these, the self-energy can be represented as shown in Fig. 3.8 a). Due to the skeleton structure of the diagram, this line must not contain any explicit self-energy insertions as shown in Fig. 3.8 b), which just formally express that the the vertex $\tilde{\Phi}^{(4)}$ is irreducible in the channel [12,34] (cf. also [71]).

The skeleton structure of the self-energy can explicitly be used for the derivation of the integral equation for the anomalous self-energy, i.e. the generalized gap function. If a certain diagram for the self-energy in Fig. 3.9 a) contains n internal F propagators, there must be $n-1$ F propagators in the same diagram in order to ensure the overall conservation of particle number. If we select *any* one of the n internal F -propagator lines, the contribution of the corresponding diagram to Δ_p can be represented as shown in Fig. 3.9 b). Summing over all possible choices provides the same diagram n times, once for each selected internal line. Since this sum of diagrams is by definition obtained by all possible variations of the anomalous propagators with subsequent closing of the opened line, the sum can formally be represented by $\text{Tr}_q \left[\frac{\delta \tilde{\Delta}_p}{\delta F(q)} F(q) \right]$, where $\tilde{\Delta}_p$ denotes the diagram under consideration contributing to Δ_p .

If instead, any internal F^\dagger line is singled out, one obtains, in complete analogy to the argument above, the same diagram $n-1$ times. By subtracting the results of the two variation procedures, clearly only the diagram $\tilde{\Delta}_p$ with multiplicity

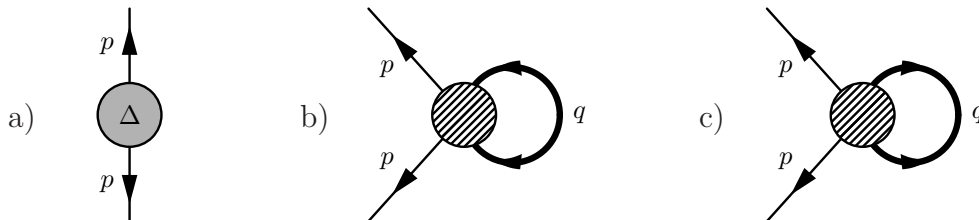


Figure 3.9.: Representations of the gap function after singling out one particular anomalous propagator in a diagram $\tilde{\Delta}_p$ contributing to the generalized gap function Δ_p in Fig a).

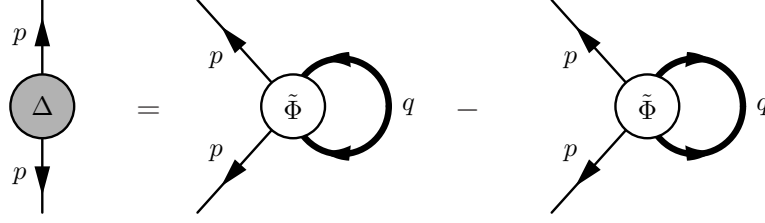


Figure 3.10.: The generalized gap equation (3.31).

one remains. By summing over all diagrams of Δ_p and using the definition (3.29) of the irreducible vertex function $\tilde{\Phi}^{(4)}$ one finally obtains the generalized gap equation (cf. also [71]):

$$\Delta_p \equiv \left. \frac{\delta\Phi[\mathbf{G}]}{\delta F^\dagger(p)} \right|_{\mathbf{G}=\tilde{\mathbf{G}}} = \text{Tr}_q \left[\tilde{\Phi}_{p,q}^{(4)++} F(q) - \tilde{\Phi}_{p,q}^{(4)--} F^\dagger(q) \right]. \quad (3.31)$$

The lower sign indices denote incoming/outgoing lines (+/-) for the first momentum and the upper signs the lines of the second momentum, i.e. explicitly

$$\tilde{\Phi}_{p,p'}^{(4)++} = \left. \frac{\delta\Phi[\mathbf{G}]}{\delta F^\dagger(p)\delta F(p')} \right|_{\mathbf{G}=\tilde{\mathbf{G}}}, \quad \tilde{\Phi}_{p,p'}^{(4)--} = \left. \frac{\delta\Phi[\mathbf{G}]}{\delta F^\dagger(p)\delta F^\dagger(p')} \right|_{\mathbf{G}=\tilde{\mathbf{G}}}. \quad (3.32)$$

By using $F^\dagger(q) = F(q)$, the gap equation (3.31) can be written in a more explicit form (cf. Fig. 3.10)

$$\Delta(\mathbf{p}, \omega) = \int \frac{d\omega'}{2\pi i} \sum_{\mathbf{q}} \left[\tilde{\Phi}_{p,q}^{(4)++} - \tilde{\Phi}_{p,q}^{(4)--} \right] F(\mathbf{q}, \omega'). \quad (3.33)$$

This equation clearly reduces to the gap equation (1.15) in the BCS approximation, when the irreducible vertices $\tilde{\Phi}^{(4)}$ are replaced by the bare interaction elements of \mathbf{V} (cf. eq. (1.55)) and the internal propagator is replaced by the BCS-propagator (cf. eq. (1.27)).

The flow equation for the two point function $\Gamma^{\Lambda(2)}$ can be derived in complete analogy to section 2.5 by introducing a cutoff to the intermediate momenta in eq. (3.23) and taking the derivative:

$$\begin{aligned} \frac{d\tilde{\Gamma}_{p,p}^{\Lambda(2)}}{d\Lambda} &= \frac{d\mathbf{G}_{0\Lambda}^{-1}(p)}{d\Lambda} - \text{Tr}_q \left[\tilde{\Phi}_{p,p,q}^{\Lambda(4)} \frac{d\tilde{\mathbf{G}}_\Lambda(q)}{d\Lambda} \right] \\ &= -\frac{dR_\Lambda}{d\Lambda} \mathbf{1} + \text{Tr}_q \left[\tilde{\Phi}_{p,p,q}^{\Lambda(4)} \tilde{\mathbf{G}}_\Lambda(q) \frac{d\tilde{\Gamma}_{q,q}^{\Lambda(2)}(q)}{d\Lambda} \tilde{\mathbf{G}}_\Lambda(q) \right]. \end{aligned} \quad (3.34)$$

Hence all components of $\tilde{\Gamma}$ and $\tilde{\Phi}^{(4)}$ enter this equation on an equal footing. From this point, it is not a priori obvious that the derivative of the gap equation

(3.31), where two components of the irreducible vertex are singled out, provides an equivalent flow equation. However, it can be shown explicitly that this is indeed the case. A straightforward application of the derivative with respect to Λ of eq. (3.31) provides several terms:

$$\begin{aligned}
\frac{d\Delta_p}{d\Lambda} &= \text{Tr}_{q,q'} \left[\frac{\delta^3\Phi}{\delta F_p^\dagger \delta F_q \delta G_{q'}} F_q \frac{dG_{q'}}{d\Lambda} - \frac{\delta^3\Phi}{\delta F_p^\dagger \delta F_q^\dagger \delta G_{q'}} F_q^\dagger \frac{dG_{q'}}{d\Lambda} \right] \\
&+ \text{Tr}_{q,q'} \left[\frac{\delta^3\Phi}{\delta F_p^\dagger \delta F_q \delta G_{q'}^-} F_q \frac{dG_{q'}^-}{d\Lambda} - \frac{\delta^3\Phi}{\delta F_p^\dagger \delta F_q^\dagger \delta G_{q'}^-} F_q^\dagger \frac{dG_{q'}^-}{d\Lambda} \right] \\
&+ \text{Tr}_{q,q'} \left[\frac{\delta^3\Phi}{\delta F_p^\dagger \delta F_q \delta F_{q'}} F_q \frac{dF_{q'}}{d\Lambda} - \frac{\delta^3\Phi}{\delta F_p^\dagger \delta F_q^\dagger \delta F_{q'}} F_q^\dagger \frac{dF_{q'}}{d\Lambda} + \frac{\delta^2\Phi}{\delta F_p^\dagger \delta F_q} \frac{dF_q}{d\Lambda} \right] \\
&+ \text{Tr}_{q,q'} \left[\frac{\delta^3\Phi}{\delta F_p^\dagger \delta F_q \delta F_{q'}^\dagger} F_q \frac{dF_{q'}^\dagger}{d\Lambda} - \frac{\delta^3\Phi}{\delta F_p^\dagger \delta F_q^\dagger \delta F_{q'}^\dagger} F_q^\dagger \frac{dF_{q'}^\dagger}{d\Lambda} - \frac{\delta^2\Phi}{\delta F_p^\dagger \delta F_q^\dagger} \frac{dF_q^\dagger}{d\Lambda} \right]
\end{aligned} \tag{3.35}$$

This expression simplifies substantially, if one notes that in every diagram of the LW functional Φ , the number of the anomalous propagator lines F and F^\dagger have to coincide in order to ensure particle number conservation. If a particular diagram of Φ includes n of each anomalous propagator the first variation term in (3.35) provides $n \times m$ different diagrams, whereas m is the number of normal G -lines. All diagrams resulting from variations of the n different F -lines provide the same contribution since they are re-closed by the term F_q in (3.35). Similarly, the second term of (3.35) in the first line provides the same $n \times m$ diagrams. However in contrast, here the second variation with respect to F^\dagger provides only a factor $n - 1$. Hence in total in the sum of the first two terms only the natural symmetry factor of the vertex function $n \times m = n \times n \times m - n \times (n - 1) \times m$ remains. The same is true for the second line in (3.35). In the third line one obtains the equation $n \times n = n \times n \times (n - 1) - n \times (n - 1) \times n + n \times n$ and the fourth line one obtains $n \times (n - 1) = n \times n \times (n - 1) - n \times (n - 1) \times (n - 2) - n \times (n - 1)$, which finally leads to

$$\frac{d\Delta_p}{d\Lambda} = \text{Tr}_q \left[\frac{\delta^2\Phi}{\delta F_p^\dagger \delta G_q} \frac{dG_q}{d\Lambda} + \frac{\delta^2\Phi}{\delta F_p^\dagger \delta G_q^-} \frac{dG_q^-}{d\Lambda} + \frac{\delta^2\Phi}{\delta F_p^\dagger \delta F_q} \frac{dF_q}{d\Lambda} + \frac{\delta^2\Phi}{\delta F_p^\dagger \delta F_q^\dagger} \frac{dF_q^\dagger}{d\Lambda} \right]. \tag{3.36}$$

In this form the equation is manifestly equivalent to the anomalous components of equation (3.34).

3.5. Comparison to the Exact RG Equations

In the previous section the flow equations of the two and four-point functions $\tilde{\Gamma}^{\Lambda(2)}$, $\tilde{\Phi}^{\Lambda(4)}$ and $\tilde{\Gamma}^{\Lambda(4)}$ have been derived by performing the following steps:

- Perform variations of the effective action $\tilde{\Gamma}[\Psi]$ to obtain the equations of motion for the N -point functions.
- Introduce a cutoff in the intermediate propagators and take the derivative of the equations of motion, in order to solve the equations by using RG methods.

By reversing the order of these operations, one obtains the "exact RG" equation for the effective action. From this RG equation, all flow equations of the n -point functions can be derived by successive variations with respect to Ψ . In this section we will investigate these flow equations for superfluids and show the equivalence on the exact level for the two-point functions for different schemes. However, at the level of the four-point functions and for approximate calculations, the equivalence is not obvious anymore. Thus for practical calculations, the different formal organizations of the equations can make one scheme preferable compared to the other.

Usually the cutoff in the free theory is introduced in the exact RG scheme in the form

$$\mathbf{G}_{\Lambda 0}^{-1}(p) = \mathbf{1} [p_0 + \mu - \varepsilon_{\mathbf{p}} - R_{\Lambda}(p)], \quad (3.37)$$

where in the present many-body problem the cutoff function R_{Λ} cuts out low lying momentum states around the Fermi surface¹. By this the effective action and the full propagator \mathbf{G} become cutoff dependent functions:

$$\tilde{\Gamma}_{\Lambda}[\Psi] = \Gamma_{\Lambda}[\Psi, \tilde{\mathbf{G}}_{\Lambda}] = S_0^{\Lambda}[\Psi] + \text{Tr} \ln \tilde{\mathbf{G}}_{\Lambda} - \text{Tr}[\mathbf{G}_{\Lambda 0}^{-1} \tilde{\mathbf{G}}_{\Lambda} - 1] + \Phi[\Psi, \tilde{\mathbf{G}}_{\Lambda}] \quad (3.38)$$

Due to the stationarity of $\tilde{\Gamma}_{\Lambda}$ with respect to infinitesimal changes of $\tilde{\mathbf{G}}_{\Lambda}$ (cf. eq. (3.22)), only the explicit variations of $\mathbf{G}_{\Lambda 0}$ contribute to the flow equation of $\tilde{\Gamma}_{\Lambda}$:

$$\frac{d\tilde{\Gamma}_{\Lambda}[\Psi]}{d\Lambda} = \frac{dS_0^{\Lambda}[\Psi]}{d\Lambda} + \text{Tr}_q \left[\frac{\delta \tilde{\Gamma}_{\Lambda}[\mathbf{G}_{\Lambda}, \mathbf{G}_{\Lambda 0}]}{\delta \mathbf{G}_{\Lambda 0}^{-1}(q)} \frac{d\mathbf{G}_{\Lambda 0}^{-1}(q)}{d\Lambda} \right] \quad (3.39)$$

$$= \frac{dS_0^{\Lambda}[\Psi]}{d\Lambda} + \text{Tr}_q \left[\tilde{\mathbf{G}}_{\Lambda}(q) \frac{dR_{\Lambda}(q)}{d\Lambda} \right]. \quad (3.40)$$

¹As a simple example one could choose

$$R_{\Lambda}(p) = p^2 \left[\frac{1}{\Theta_{\epsilon}(p - (k_F + \Lambda)) + \Theta_{\epsilon}((k_F - \Lambda) - p)} - 1 \right] \quad \text{with} \quad \lim_{\epsilon \rightarrow 0} \Theta_{\epsilon}(x) = \Theta(x).$$

This function provides a generalization of the bosonic cutoff function of Morris [179] to fermionic systems.

The flow equation of $\Gamma_{p'_1, p'_2, p_1, p_2}^{\Lambda(4)}$ can be calculated in this scheme by successively taking derivatives with respect to Λ of this flow equation. Note that the kinematical constraints must only be imposed after all variations have been done since additional variations can couple to this propagator and introduce another external momentum in this function. Using

$$\frac{\delta}{\delta\Psi(p)} \text{Tr}_q [\mathbf{G}_\Lambda(q_1, q) \mathbf{G}_\Lambda^{-1}(q, q_2)] = \frac{\delta}{\delta\Psi(p)} \delta(q_1 - q_2) = 0 \quad (3.41)$$

we get

$$\begin{aligned} \frac{\delta}{\delta\Psi(p)} \mathbf{G}_\Lambda(q_1, q_2) &= -\text{Tr}_{q, q'} \left[\mathbf{G}_\Lambda(q_1, q) \left(\frac{\delta}{\delta\Psi(p)} \mathbf{G}_\Lambda^{-1}(q, q') \right) \mathbf{G}_\Lambda(q', q_2) \right] \\ &= -\text{Tr}_{q, q'} \left[\mathbf{G}_\Lambda(q_1, q) \Gamma_{p, q, q'}^{\Lambda(3)} \mathbf{G}_\Lambda(q', q_2) \right] \end{aligned} \quad (3.42)$$

For the one point function one obtains:

$$\frac{d\Gamma_{p_2}^{\Lambda(1)}}{d\Lambda} = \frac{d}{d\Lambda} \frac{\delta S_0^\Lambda[\Psi]}{\delta\Psi(p_2)} - \text{Tr}_{q, q'} \left[\mathbf{G}_\Lambda(q) \Gamma_{p_2, q, q'}^{\Lambda(3)} \mathbf{G}_\Lambda(q') \frac{dR_\Lambda(q')}{d\Lambda} \right]. \quad (3.43)$$

Note that the direction of the external line with momentum p_2 is not fixed. This procedure can be iterated up to the 4-point function:

$$\begin{aligned} \frac{d\Gamma_{p_1, p_2}^{\Lambda(2)}}{d\Lambda} &= \frac{d}{d\Lambda} \frac{\delta^2 S_0^\Lambda[\Psi]}{\delta\Psi(p_1) \delta\Psi(p_2)} - \text{Tr}_{q, q'} \left[\mathbf{G}_\Lambda(q) \Gamma_{p_1, p_2, q, q'}^{\Lambda(4)} \mathbf{G}_\Lambda(q') \frac{dR_\Lambda(q')}{d\Lambda} \right] \\ &\quad + 2 \text{Tr}_{q, q', q''} \left[\mathbf{G}_\Lambda(q) \Gamma_{p_1, q, q'}^{\Lambda(3)} \mathbf{G}_\Lambda(q') \Gamma_{p_2, q', q''}^{\Lambda(3)} \mathbf{G}_\Lambda(q'') \frac{dR_\Lambda(q'')}{d\Lambda} \right] \end{aligned} \quad (3.44)$$

$$\begin{aligned} \frac{d\Gamma_{p'_1, p'_2, p_1, p_2}^{\Lambda(4)}}{d\Lambda} &= +2 \text{Tr}_{q, q', q''} \left[\right. \\ &\quad - \mathbf{G}_\Lambda(q) \Gamma_{p'_1, p_1, q, q'}^{\Lambda(4)} \mathbf{G}_\Lambda(q') \Gamma_{p'_2, p_2, q', q''}^{\Lambda(4)} \mathbf{G}_\Lambda(q'') \frac{dR_\Lambda(q'')}{d\Lambda} \\ &\quad + \mathbf{G}_\Lambda(q) \Gamma_{p'_2, p_1, q, q'}^{\Lambda(4)} \mathbf{G}_\Lambda(q') \Gamma_{p'_1, p_2, q', q''}^{\Lambda(4)} \mathbf{G}_\Lambda(q'') \frac{dR_\Lambda(q'')}{d\Lambda} \\ &\quad \left. + \mathbf{G}_\Lambda(q) \Gamma_{p'_1, p'_2, q, q'}^{\Lambda(4)} \mathbf{G}_\Lambda(q') \Gamma_{p_1, p_2, q', q''}^{\Lambda(4)} \mathbf{G}_\Lambda(q'') \frac{dR_\Lambda(q'')}{d\Lambda} \right] \\ &\quad + \text{Tr}_{q, q'} \left[\mathbf{G}_\Lambda(q) \Gamma_{p'_1, p'_2, p_1, p_2, q, q'}^{\Lambda(6)} \mathbf{G}_\Lambda(q') \frac{dR_\Lambda(q')}{d\Lambda} \right], \end{aligned} \quad (3.45)$$

where all vertices with an odd number of external lines have been neglected. These vertices are vanishing in fermionic systems in the absence of external sources. The contributions of the higher vertex functions can be obtained in

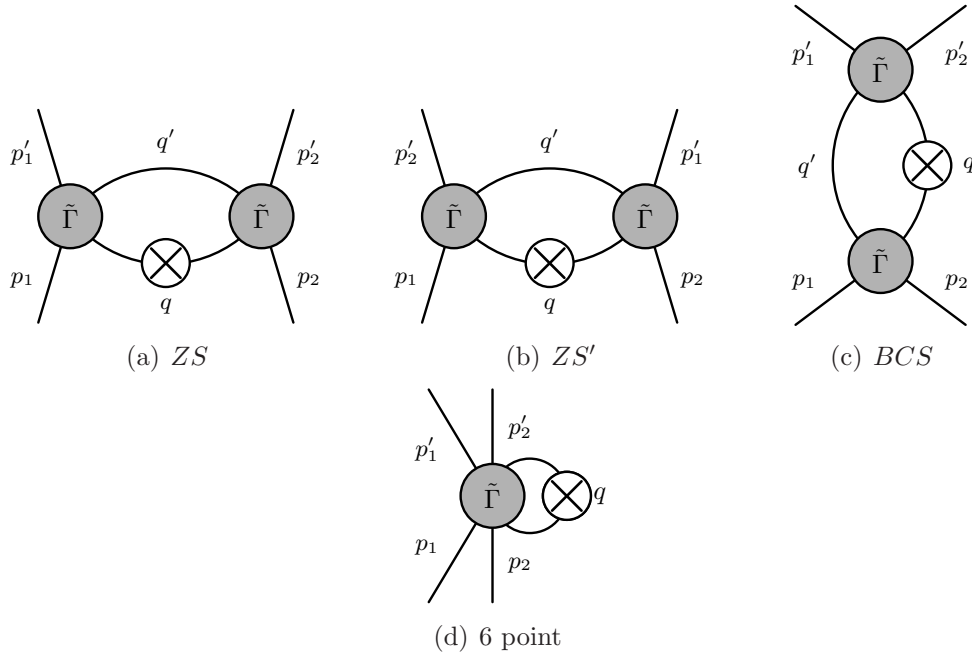


Figure 3.11.: Contributing diagrams to the flow of $\Gamma_{p'_1, p'_2, p_1, p_2}^{\Lambda(4)}$ from the 1PI exact RG equation.

a quite obvious way and the organizational scheme is similar to the Polchinski equation [135].

From eq. (3.45) it follows that the flow equation for the six-point function involves diagrams consisting of three four point functions. Hence even if genuine six-point interactions are neglected, the full reducible six-point vertices acquire quite complicated contributions from the flow of the four point vertices. This couples further back to the eight point function etc. Hence one can see that it is a priori extremely complicated to find a proper truncation scheme for this hierarchy of equations.

The starting point for the flow of the 2PI vertex function $\tilde{\Phi}^{(n)}$ is the equation

$$\frac{d\Phi[\Psi, \mathbf{G}]}{d\Lambda} = 0. \quad (3.46)$$

This equation is trivially fulfilled since Ψ and \mathbf{G} are free variables. Hence the flow of the 2PI vertices $\tilde{\Phi}^{(n)}$ results only from the flow of the propagator $\tilde{\mathbf{G}}_\Lambda$:

$$\begin{aligned} \frac{d}{d\Lambda} \tilde{\Phi}_{p_1, p_2, \dots, p_{2n-1}, p_{2n}}^{\Lambda(2n)} &= \text{Tr}_q \left[\frac{\delta^{n+1} \Phi[\Psi, \mathbf{G}]}{\delta \mathbf{G}(p_1, p_2) \dots \delta \mathbf{G}(p_{2n-1}, p_{2n}) \delta \mathbf{G}(q)} \Big|_{\mathbf{G}=\tilde{\mathbf{G}}_\Lambda} \frac{d\tilde{\mathbf{G}}_\Lambda(q)}{d\Lambda} \right] \\ &= \text{Tr}_q \left[\tilde{\Phi}_{p_1, p_2, \dots, p_{2n-1}, p_{2n}, q, q}^{\Lambda(2n+2)} \frac{d\tilde{\mathbf{G}}_\Lambda(q)}{d\Lambda} \right]. \end{aligned} \quad (3.47)$$

	1PI	2PI
effective action	$\tilde{\Gamma}[\Psi] = \Gamma[\Psi, \tilde{G}]$	$\Gamma[\Psi, G]$
n -point functions	$\tilde{\Gamma}^{(n)} = \frac{\delta^n \tilde{\Gamma}[\Psi]}{\delta \Psi^n}$	$\tilde{\Phi}^{(2n)} = \frac{\delta^n \Phi[\Psi, G]}{\delta G^n} \Big _{G=\tilde{G}}$
functional flow	$\frac{d\tilde{\Gamma}[\Psi]}{d\Lambda} = \frac{dS_0[\Psi]}{d\Lambda} + \text{Tr} \left[\tilde{G} \frac{dR_\Lambda}{d\Lambda} \right]$	$\frac{d\Phi[\Psi, G]}{d\Lambda} = 0$
equations of motion	$\tilde{\Gamma}^{(2)} = \tilde{G}^{-1} = G_0^{-1} - \tilde{\Phi}^{(2)}$ $\tilde{\Gamma}^{(4)} = \tilde{\Phi}^{(4)} + \text{Tr} \left[\tilde{\Phi}^{(4)} \tilde{G} \tilde{G} \tilde{\Gamma}^{(4)} \right]$	
vertex flow equations	$\frac{d\tilde{\Gamma}^{(2)}}{d\Lambda} = -\frac{dR_\Lambda}{d\Lambda} + \text{Tr} \left[\tilde{\Gamma}^{(4)} \tilde{G} \tilde{G} \frac{dR_\Lambda}{d\Lambda} \right]$	$\frac{d\tilde{\Phi}^{(2)}}{d\Lambda} = \text{Tr} \left[\tilde{\Phi}^{(4)} \frac{d\tilde{G}}{d\Lambda} \right]$
	$\frac{d\tilde{\Gamma}^{(4)}}{d\Lambda} = \text{Tr} \left[\tilde{\Gamma}^{(6)} \tilde{G} \tilde{G} \frac{dR_\Lambda}{d\Lambda} \right]$ $+ \text{Tr} \left[\tilde{\Gamma}^{(4)} \tilde{G} \tilde{\Gamma}^{(4)} \tilde{G} \tilde{G} \frac{dR_\Lambda}{d\Lambda} \right]$	$\frac{d\tilde{\Phi}^{(4)}}{d\Lambda} = \text{Tr} \left[\tilde{\Phi}^{(6)} \frac{d\tilde{G}}{d\Lambda} \right]$

Table 3.2.: Comparison of the 1PI and 2PI scheme.

By using eq. (3.34) and eq. (3.44) it follows that the flow of the two-point vertex can be expressed in terms of the 1PI or 2PI four point vertex functions:

$$\frac{d\tilde{\Gamma}_{p,p}^{\Lambda(2)}}{d\Lambda} = -\frac{dR_\Lambda(p)}{d\Lambda} - \text{Tr}_q \left[\tilde{\Gamma}_{p,p,q,q}^{\Lambda(4)} \tilde{\mathbf{G}}_\Lambda(q) \frac{dR_\Lambda(q)}{d\Lambda} \tilde{\mathbf{G}}_\Lambda(q) \right] \quad (3.48)$$

$$= -\frac{dR_\Lambda(p)}{d\Lambda} + \text{Tr}_q \left[\tilde{\Phi}_{p,p,q,q}^{\Lambda(4)} \tilde{\mathbf{G}}_\Lambda(q) \frac{d\tilde{\Gamma}_{q,q}^{\Lambda(2)}}{d\Lambda} \tilde{\mathbf{G}}_\Lambda(q) \right]. \quad (3.49)$$

Obviously, the explicit form of the flow equation for $\tilde{\Gamma}^{\Lambda(2)}$ depends on the used scheme. On the exact level however, one can show the equivalence of these two equations straightforwardly by using the Bethe-Salpeter equation (3.30) in eq. (3.48):

$$\begin{aligned} \frac{d\tilde{\Gamma}_{p,p}^{\Lambda(2)}}{d\Lambda} &= -\frac{dR_\Lambda}{d\Lambda} - \text{Tr}_q \left[\tilde{\Phi}_{p,p,q,q}^{\Lambda(4)} \tilde{\mathbf{G}}_\Lambda(q) \frac{dR_\Lambda(q)}{d\Lambda} \tilde{\mathbf{G}}_\Lambda(q) \right] \\ &\quad - \text{Tr}_{q,q',q''} \left[\tilde{\Phi}_{p,p,q,q'}^{\Lambda(4)} \tilde{\mathbf{G}}_\Lambda(q) \tilde{\mathbf{G}}_\Lambda(q') \tilde{\Gamma}_{q,q',q'',q''}^{\Lambda(4)} \tilde{\mathbf{G}}_\Lambda(q'') \frac{dR_\Lambda(q'')}{d\Lambda} \tilde{\mathbf{G}}_\Lambda(q'') \right] \end{aligned} \quad (3.50)$$

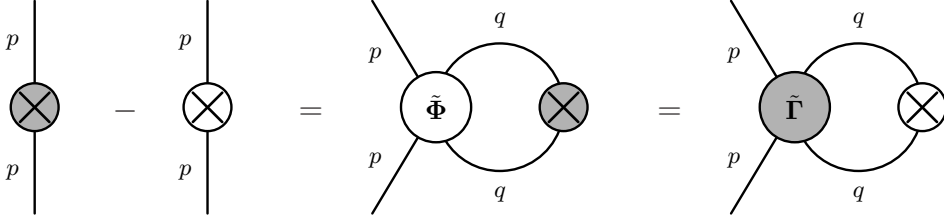


Figure 3.12.: Graphical representation of equations (3.48) and (3.49). The internal lines represent full propagators $\tilde{\mathbf{G}}_\Lambda$. The shaded crossed circles represent the function $\frac{d\tilde{\Gamma}^{(2)}}{d\Lambda}$ and the unfilled $\frac{d\mathbf{G}_{\Lambda 0}^{-1}}{d\Lambda} = -\frac{dR_\Lambda}{d\Lambda}$

By again using eq. (3.48), one can see immediately that the second and the third term can be expressed by the second term in (3.49). This result was also found to leading order by Dupuis [180].

Hence on the exact level all flow equations (3.35,3.48,3.49) for the two-point functions are indeed equivalent. However, for the four-point functions, it is much more difficult to show the equivalence of the two schemes. By taking the derivatives of the Bethe-Salpeter equation (3.30) we obtain:

$$\begin{aligned}
\frac{d\tilde{\Gamma}_{p_1,p_2,p_3,p_4}^{\Lambda(4)}}{d\Lambda} &= \frac{d\tilde{\Phi}_{p_1,p_2,p_3,p_4}^{\Lambda(4)}}{d\Lambda} + \text{Tr}_{q,q'} \left[\frac{d\tilde{\Phi}_{p_1,p_2,q,q'}^{\Lambda(4)}}{d\Lambda} \tilde{\mathbf{G}}_\Lambda(q) \tilde{\mathbf{G}}_\Lambda(q') \tilde{\Gamma}_{q,q',p_3,p_4}^{\Lambda(4)} \right] \\
&\quad - \text{Tr}_{q,q'} \left[\tilde{\Phi}_{p_1,p_2,q,q'}^{\Lambda(4)} \frac{d\tilde{\mathbf{G}}_\Lambda(q)}{d\Lambda} \tilde{\mathbf{G}}_\Lambda(q') \tilde{\Gamma}_{q,q',p_3,p_4}^{\Lambda(4)} \right] \\
&\quad - \text{Tr}_{q,q'} \left[\tilde{\Phi}_{p_1,p_2,q,q'}^{\Lambda(4)} \tilde{\mathbf{G}}_\Lambda(q) \frac{d\tilde{\mathbf{G}}_\Lambda(q')}{d\Lambda} \tilde{\Gamma}_{q,q',p_3,p_4}^{\Lambda(4)} \right] \\
&\quad + \text{Tr}_{q,q'} \left[\tilde{\Phi}_{p_1,p_2,q,q'}^{\Lambda(4)} \tilde{\mathbf{G}}_\Lambda(q) \tilde{\mathbf{G}}_\Lambda(q') \frac{d\tilde{\Gamma}_{q,q',p_3,p_4}^{\Lambda(4)}}{d\Lambda} \right], \tag{3.51}
\end{aligned}$$

whereas the flow of the irreducible vertex is according to (3.47) given by

$$\frac{d\tilde{\Phi}_{p_1,p_2,p_3,p_4}^{\Lambda(4)}}{d\Lambda} = \text{Tr}_q \left[\tilde{\Phi}_{p_1,p_2,p_3,p_4,q,q}^{\Lambda(6)} \frac{d\tilde{\mathbf{G}}_\Lambda(q)}{d\Lambda} \right]. \tag{3.52}$$

Diagrammatically, eq. (3.52) reconnects the lines in the six point function $\tilde{\Phi}^{(6)}$ with the indices (5) and (6) in Tab. 3.1 via the derivative of the propagator and consequently the diagrams are reducible in the channels [13,24] and [14,23] as is $\tilde{\Phi}^{(4)}$. Hence, formally this equation sums the contributions of these two channels in every RG step, where the contribution of the [12,34] channel is included via the flow-equation (3.51). If genuine three-body interactions are neglected,

the coupled system of these flow equations integrate the two-body parquet in a superfluid (cf. section 3.6).

The connection to the flow equation (3.45) however is very complicated due to the extremely complex structure of the six point function $\tilde{\Gamma}^{(6)}$. Apart from contributions of the genuine three-body interaction, this function consists of six-point diagrams like the one shown in Table 3.1, which are dynamically generated by the four point functions in the parquet formulation. Due to this coupling the equivalence of these two flow equations cannot be shown in a straightforward way as it was possible for the two-point functions and will not be attempted here.

3.6. Parquet Equations in a Superfluid

The calculation of the contributions in the channel [13,24] and [14,23] via eq. (3.52) is formally quite inconvenient since the explicit calculation of six point vertices is extremely complicated.

However, if all genuine three body interactions are neglected, these diagrams can be parametrized in terms of four point vertices. These equations are just the Parquet equations and represent the coupled system of Bethe-Salpeter equations for the determination of the full reducible vertex $\tilde{\Gamma}^{(4)}$.

The first equation of this system is just eq. (3.30), which was derived by functional derivative of the Dyson equation. However, it was shown in the previous section that the other two Bethe-Salpeter equations cannot be derived analogously due to the skeleton structure of the Luttinger functional Φ . Hence these equations have to be determined diagrammatically. By using the analogy with normal systems, the equations can be written down in a straightforward way:

$$\tilde{\Gamma}^{(4)} = \tilde{\Phi}_{BCS}^{(4)} + \text{Tr} \left[\tilde{\Phi}_{BCS}^{(4)} \left[\tilde{\mathbf{G}}\tilde{\mathbf{G}} \right]_{BCS} \tilde{\Gamma}^{(4)} \right] \quad (3.53)$$

$$= \tilde{\Phi}_{ZS}^{(4)} + \text{Tr} \left[\tilde{\Phi}_{ZS}^{(4)} \left[\tilde{\mathbf{G}}\tilde{\mathbf{G}} \right]_{ZS} \tilde{\Gamma}^{(4)} \right] \quad (3.54)$$

$$= \tilde{\Phi}_{ZS'}^{(4)} + \text{Tr} \left[\tilde{\Phi}_{ZS'}^{(4)} \left[\tilde{\mathbf{G}}\tilde{\mathbf{G}} \right]_{ZS'} \tilde{\Gamma}^{(4)} \right], \quad (3.55)$$

where the momenta have been suppressed for the sake of simple notation. In order to emphasize the analogy with normal systems we denote in the following the channel [12,34] by BCS , the channel [13,24] by ZS and [14,23] by ZS' . The matrix $[\tilde{\mathbf{G}}\tilde{\mathbf{G}}]_{\alpha}$ denotes the two-particle propagator which connects the momenta of the vertices in the corresponding channels (cf. Fig. 3.13).

The derivation of these equations can be done in complete analogy to normal systems [167], since the topology of the diagrams is exactly the same as in normal systems and the direction of the arrows of the external and internal lines plays no role. By using these arguments, it is ensured that all diagrams are only generated once and no double counting occurs.

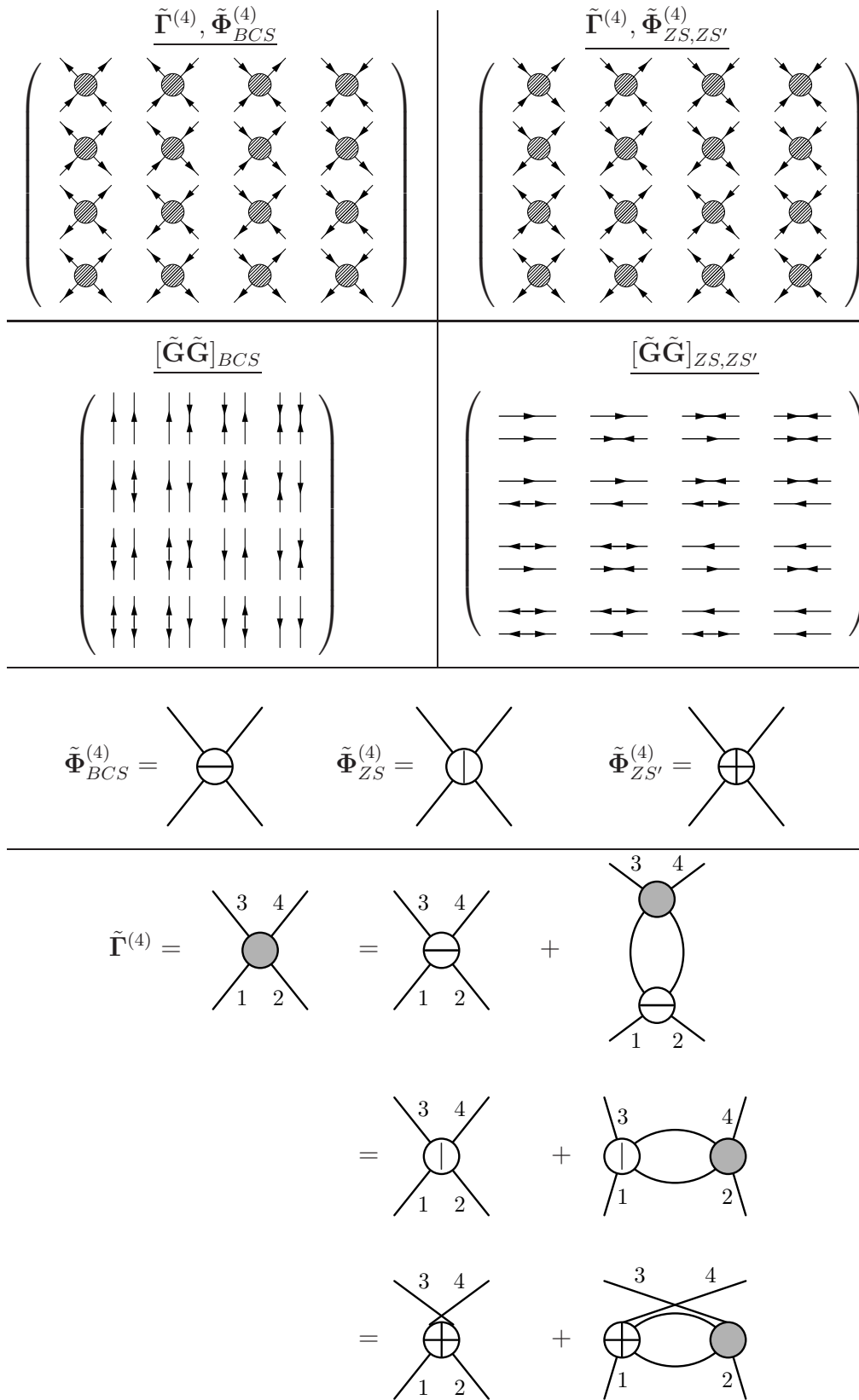


Figure 3.13.: Graphical representation of the Bethe-Salpeter equations (3.53), (3.54) and (3.55) in a superfluid.

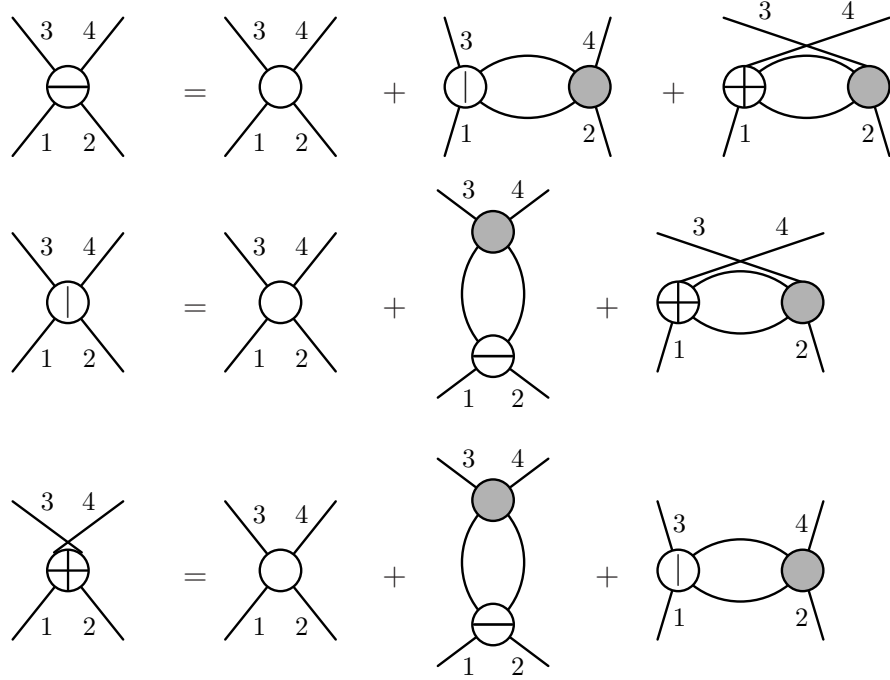


Figure 3.14.: Graphical representation of the Parquet equations (3.58), (3.59) and (3.60). The same notation as in Fig. 3.13 is used. The unfilled circles represent the completely irreducible vertex.

According to the discussion in section 3.4, the full reducible vertex can be decomposed in the following way:

$$\tilde{\Gamma}^{(4)} = \mathbf{I} + \tilde{\Gamma}_{BCS}^{(4)} + \tilde{\Gamma}_{ZS}^{(4)} + \tilde{\Gamma}_{ZS'}^{(4)} \quad (3.56)$$

where \mathbf{I} is the completely irreducible vertex and $\tilde{\Gamma}_{\alpha}^{(4)}$ are the reducible vertices in the channel α , i.e.

$$\tilde{\Gamma}_{\alpha}^{(4)} = \tilde{\Gamma}^{(4)} - \tilde{\Phi}_{\alpha}^{(4)} = \text{Tr} \left[\tilde{\Phi}_{\alpha}^{(4)} \left[\tilde{\mathbf{G}}\tilde{\mathbf{G}} \right]_{\alpha} \tilde{\Gamma}^{(4)} \right]. \quad (3.57)$$

Consequently, the irreducible vertices are given by the following parquet equations

$$\tilde{\Phi}_{BCS}^{(4)} = \mathbf{I} + \text{Tr} \left[\tilde{\Phi}_{ZS}^{(4)} \left[\tilde{\mathbf{G}}\tilde{\mathbf{G}} \right]_{ZS} \tilde{\Gamma}^{(4)} \right] + \text{Tr} \left[\tilde{\Phi}_{ZS'}^{(4)} \left[\tilde{\mathbf{G}}\tilde{\mathbf{G}} \right]_{ZS'} \tilde{\Gamma}^{(4)} \right] \quad (3.58)$$

$$\tilde{\Phi}_{ZS}^{(4)} = \mathbf{I} + \text{Tr} \left[\tilde{\Phi}_{BCS}^{(4)} \left[\tilde{\mathbf{G}}\tilde{\mathbf{G}} \right]_{BCS} \tilde{\Gamma}^{(4)} \right] + \text{Tr} \left[\tilde{\Phi}_{ZS'}^{(4)} \left[\tilde{\mathbf{G}}\tilde{\mathbf{G}} \right]_{ZS'} \tilde{\Gamma}^{(4)} \right] \quad (3.59)$$

$$\tilde{\Phi}_{ZS'}^{(4)} = \mathbf{I} + \text{Tr} \left[\tilde{\Phi}_{BCS}^{(4)} \left[\tilde{\mathbf{G}}\tilde{\mathbf{G}} \right]_{BCS} \tilde{\Gamma}^{(4)} \right] + \text{Tr} \left[\tilde{\Phi}_{ZS}^{(4)} \left[\tilde{\mathbf{G}}\tilde{\mathbf{G}} \right]_{ZS} \tilde{\Gamma}^{(4)} \right]. \quad (3.60)$$

Obviously, the full solution of this system is an extremely difficult task and

still out of range even for lower dimensional systems due to the huge number of external variables and the very rich and complex analytical structure of the full four point function. On the other hand, this complexity contains much of the interesting information about the many-body system like the properties of the collective modes, scattering amplitudes and bound states. In ref. [169] an iterative strategy was used to solve the parquet equations in normal systems for the 2D-Hubbard model in a pseudopotential approximation. However in the present case the analytical structure (cf. section 1.8) is too complex by far to expect a convergence in a straightforward iterative approach to these equations.

Instead RG methods can be used to introduce the fluctuations adiabatically and ensure in this way that all functions are changing only smoothly with variations of the scale Λ . In the following, we will indicate a possible strategy to solve these parquet equations in certain approximations by combining iterative methods with RG methods.

In order to state the problem in a more compact form, we will restrict ourselves first to the two channel problem. In this case the parquet equations read schematically:

$$\begin{aligned}\Gamma^{(4)} &= \tilde{\Phi}_1^{(4)} + \tilde{\Phi}_1^{(4)} [GG]_1 \Gamma^{(4)} = \tilde{\Phi}_2^{(4)} + \tilde{\Phi}_2^{(4)} [GG]_2 \Gamma^{(4)} \\ \tilde{\Phi}_1^{(4)} &= I + \tilde{\Phi}_2^{(4)} [GG]_2 \Gamma^{(4)} \\ \tilde{\Phi}_2^{(4)} &= I + \tilde{\Phi}_1^{(4)} [GG]_1 \Gamma^{(4)},\end{aligned}\tag{3.61}$$

where the same notation as in section 2.3 has been used.

An inversion approach to this coupled system is extremely unpractical (cf. section 1.10). Instead, we will follow the strategy of sec. 2.5 by introducing a cutoff function, which suppresses the states around the Fermi surface in the internal propagators. The resulting flow equations then read:

$$\begin{aligned}\frac{d\Gamma^{\Lambda(4)}}{d\Lambda} &= \frac{d\tilde{\Phi}_{1/2}^{\Lambda(4)}}{d\Lambda} + \frac{d}{d\Lambda} \left[\tilde{\Phi}_{1/2}^{\Lambda(4)} [GG^>]_{1/2} \Gamma^{\Lambda(4)} \right] \\ \frac{d\tilde{\Phi}_1^{\Lambda(4)}}{d\Lambda} &= \frac{d\tilde{\Phi}_2^{\Lambda(4)}}{d\Lambda} [GG^>]_2 \Gamma^{\Lambda(4)} + \tilde{\Phi}_2^{\Lambda(4)} \frac{d[GG^>]_2}{d\Lambda} \Gamma^{\Lambda(4)} + \tilde{\Phi}_2^{\Lambda(4)} [GG^>]_2 \frac{d\Gamma^{\Lambda(4)}}{d\Lambda} \\ \frac{d\tilde{\Phi}_2^{\Lambda(4)}}{d\Lambda} &= \frac{d\tilde{\Phi}_1^{\Lambda(4)}}{d\Lambda} [GG^>]_1 \Gamma^{\Lambda(4)} + \tilde{\Phi}_1^{\Lambda(4)} \frac{d[GG^>]_1}{d\Lambda} \Gamma^{\Lambda(4)} + \tilde{\Phi}_1^{\Lambda(4)} [GG^>]_1 \frac{d\Gamma^{\Lambda(4)}}{d\Lambda}\end{aligned}\tag{3.62}$$

By generalizing the arguments of section 2.5, the strategy is as follows:

- At the initial scale $\Lambda = \Lambda_0 \rightarrow \infty$ the two-particle propagators in *all* channels vanish. Hence one can initialize the flow by:

$$\Gamma^{\Lambda_0(4)} = \tilde{\Phi}_1^{\Lambda_0(4)} = \tilde{\Phi}_2^{\Lambda_0(4)} = I\tag{3.63}$$

where I is the totally irreducible four point vertex. In general this object can by itself be very complex as it contains all "non-planar" diagrams that cannot be generated by the parquet equations. However, in practice this vertex is usually approximated by the bare vacuum interaction, i.e. $I \rightarrow V$.

- In every RG step the coupled system of flow equations (3.62) has to be solved. However, since the scale Λ can be changed in arbitrarily small steps, the vertex functions from the previous iteration step usually provide a very good starting guess for an iterative solution strategy to this system. Hence it is quite natural to combine the RG approach with an iterative techniques in every RG step.
- In most cases, the vertex functions change smoothly with varying cutoff scale Λ . However, at points where the vertex function starts to develop pole structures this is no longer the case for all momentum and energy regions. In these cases, one has to transform the flow equation in such a way that only slowly varying functions have to be iterated. In the BCS channel, this was achieved by iterating the inverse vertex in Gorkov space (cf. section 2.5).
- Ideally, all internal lines in the flow equations are *full* Greens functions at scale Λ . Hence in every RG step one has to iterate simultaneously the four point functions and the two point functions. This in general involves both, the normal and the anomalous parts (cf. section 3.4). Since the flow equations of the self-energies involve integrations over four-point vertices at the current scale, these functions are automatically treated self-consistently, if these contributions are taken into account in the flow equations.

We will illustrate in this section the practical feasibility of the iterative algorithm, first on the basis of a simpler problem, the one-channel problem of section 1.7. By comparing the results of the two equivalent RG equations

$$\frac{d\Gamma^\Lambda}{d\Lambda} = \Gamma^\Lambda \frac{dGG}{d\Lambda} \Gamma^\Lambda \quad (3.64)$$

$$\frac{d\Gamma^\Lambda}{d\Lambda} = \Gamma_0 \frac{dGG}{d\Lambda} \Gamma^\Lambda + \Gamma_0 GG \frac{d\Gamma^\Lambda}{d\Lambda}, \quad (3.65)$$

we can test the accuracy and practical feasibility of the iterative approach. We solve the implicit flow equation (3.65) iteratively by using the results of the previous iteration step as initial guesses in each RG step. The iteration is repeated until sufficient convergence has been achieved. In uncritical regions this is achieved typically after one or two iterations.

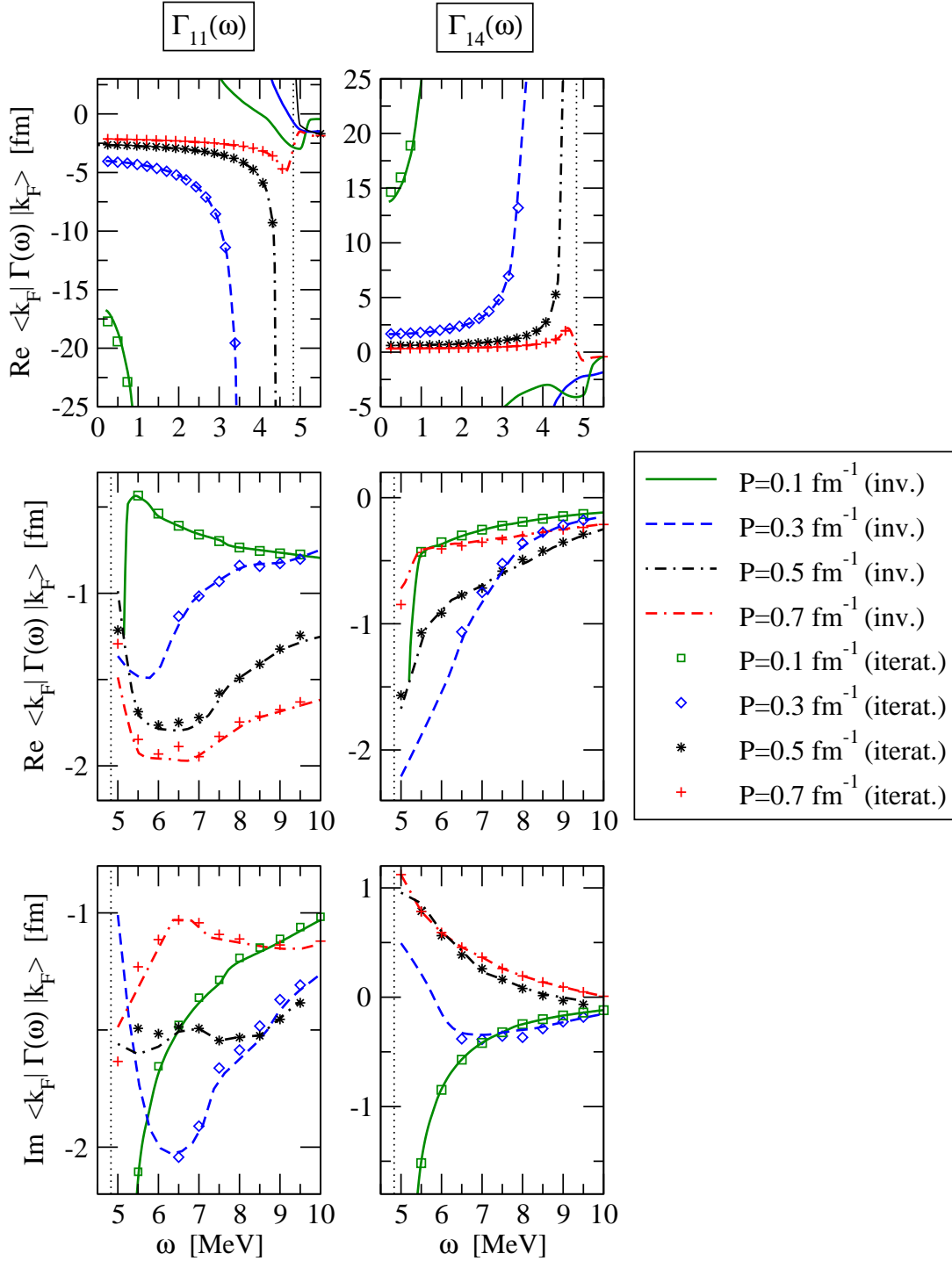


Figure 3.15.: Solutions of the explicit flow equation (3.64) denoted by the lines and eq. (3.65) denoted by the single data points for the V_{lowk} interaction of N^3LO for different CM momenta at $k_F = 0.6 \text{ fm}^{-1}$. The left plots show the particle-particle vertex elements Γ_{11} , the right the matrix elements of the anomalous vertex function $\Gamma_{14} = \Gamma_{41}$. The upper row shows the real part below threshold, the middle row the real part around threshold (ω) and the lower row the imaginary parts. The dotted vertical lines show the two-particle threshold.

The numerical results of this algorithm are shown in Figure 3.15. As can be clearly seen the results coincide to a quite high accuracy over most of the energy regions. Only in the energy region between pole and threshold, the convergence of the iterative approach is not yet fully under control. The results in this critical region are missing in Fig. 3.15. However, the general agreement of the results is quite remarkable and shows that explicit invertibility of the flow equation in the one-channel case (cf. eq. (2.17)) is merely a technical convenience, but not absolutely necessary for the practical iteration of the equation. It should be emphasized that the quality and speed of the iterative algorithm depends crucially on the initial guesses for $\frac{d\Gamma}{d\Lambda}$ at each scale. If the initial value is too bad, the convergence slows down substantially or does not converge at all anymore. Hence the basic feature of the RG framework that all correlations are introduced adiabatically, is very important for the practical feasibility of this iterative approach.

These results show that the present RG framework is quite flexible and is not restricted to the one-channel case. As the next step, the iterative algorithm should be extended to the system (3.62). Although the system is of course more complicated than the implicit equation (3.65), the basic structure is essentially the same. The nice convergence in the present one-channel case indicates that the same strategy could also work for the coupled system. In this case one would obtain a *non-perturbative* method for the systematic inclusion of additional many-body correlations.

3.7. Partial Wave Coupling

So far only the scattering problem in the 1S_0 partial wave has been considered. However, as was pointed out in section 1.7, in the case of finite CM momenta \mathbf{P} , the two-particle propagator $\mathbf{G}\mathbf{G}$ always couples different partial waves. Thus even in the absence of non-diagonal interactions in the l quantum number, the different partial waves are in general coupled to each other.

This coupling can be implemented in a quite straightforward way. The general scattering equation (without many-body channel coupling) in partial wave representation reads according to section 1.7:

$$\begin{aligned} \langle k'l'm' | \Gamma(\omega) | klm \rangle &= \langle k'l' | \mathbf{V} | kl \rangle \delta_{mm'} + \\ &+ \int dq q^2 \sum_{l_1, l_2, l_3} i^{l_1 - l_3} \Omega_{l_1 l_2 l_3}^{m'} \langle k'l' | \mathbf{V} | ql_1 \rangle \mathbf{G}\mathbf{G}_{l_2}(q, P, \omega) \langle ql_3 m' | \Gamma(\omega) | klm \rangle, \end{aligned} \quad (3.66)$$

where the angular coupling coefficients $\Omega_{l_1 l_2 l_3}^m$ obey the following symmetry relation (cf. the definition (1.63)) $\Omega_{l_1 l_2 l_3}^m = \Omega_{l_3 l_2 l_1}^m$. The nonvanishing coefficients for $l \leq 2$ are given in Table 3.3. Partial wave coupling can be taken into account by

$(l_1 l_2 l_3)$	(000)	(101)	(202)	(110)	(220)	(112)	(121)	(222)
$\Omega_{l_1 l_2 l_3}^0$	$\frac{2}{\pi}$	$\frac{2}{\pi}$	$\frac{2}{\pi}$	$\frac{\sqrt{12}}{\pi}$	$\frac{\sqrt{20}}{\pi}$	$\frac{\sqrt{48}}{\sqrt{5}\pi}$	$\frac{4}{\pi}$	$\frac{20}{7\pi}$
$\Omega_{l_1 l_2 l_3}^1$	0	$\frac{2}{\pi}$	$\frac{2}{\pi}$	0	0	$\frac{6}{\sqrt{5}\pi}$	$-\frac{2}{\pi}$	$\frac{10}{7\pi}$
$\Omega_{l_1 l_2 l_3}^2$	0	0	$\frac{2}{\pi}$	0	0	0	0	$-\frac{20}{7\pi}$

Table 3.3.: The lowest order angular coupling coefficients $\Omega_{l_1 l_2 l_3}^m$.

defining the following matrices

$$\begin{aligned}
\langle k' | \bar{\Gamma}^m(\omega) | k \rangle &= \begin{pmatrix} \langle k'0 | \Gamma^m(\omega) | k0 \rangle & \langle k'0 | \Gamma^m(\omega) | k1 \rangle & \langle k'0 | \Gamma^m(\omega) | k2 \rangle \\ \langle k'1 | \Gamma^m(\omega) | k0 \rangle & \langle k'1 | \Gamma^m(\omega) | k1 \rangle & \langle k'1 | \Gamma^m(\omega) | k2 \rangle \\ \langle k'2 | \Gamma^m(\omega) | k0 \rangle & \langle k'2 | \Gamma^m(\omega) | k1 \rangle & \langle k'2 | \Gamma^m(\omega) | k2 \rangle \end{pmatrix} \\
\langle k' | \bar{\mathbf{V}} | k \rangle &= \begin{pmatrix} \langle k'0 | \mathbf{V} | k0 \rangle & \langle k'0 | \mathbf{V} | k1 \rangle & \langle k'0 | \mathbf{V} | k2 \rangle \\ \langle k'1 | \mathbf{V} | k0 \rangle & \langle k'1 | \mathbf{V} | k1 \rangle & \langle k'1 | \mathbf{V} | k2 \rangle \\ \langle k'2 | \mathbf{V} | k0 \rangle & \langle k'2 | \mathbf{V} | k1 \rangle & \langle k'2 | \mathbf{V} | k2 \rangle \end{pmatrix} \\
\overline{\mathbf{G}\mathbf{G}}(q, P, \omega) &= \begin{pmatrix} \Omega_{000}^m \mathbf{G}\mathbf{G}_0 & -i\Omega_{011}^m \mathbf{G}\mathbf{G}_1 & \Omega_{022}^m \mathbf{G}\mathbf{G}_2 \\ +i\Omega_{110}^m \mathbf{G}\mathbf{G}_1 & \Omega_{101}^m \mathbf{G}\mathbf{G}_0 & -i\Omega_{112}^m \mathbf{G}\mathbf{G}_1 \\ \Omega_{220}^m \mathbf{G}\mathbf{G}_2 & +i\Omega_{211}^m \mathbf{G}\mathbf{G}_1 & \Omega_{202}^m \mathbf{G}\mathbf{G}_0 \end{pmatrix} \quad (3.67)
\end{aligned}$$

In terms of these matrices the coupled system (3.66) for $l \leq 2$ can be written in a compact form

$$\langle k' | \bar{\Gamma}^m(\omega) | k \rangle = \langle k' | \bar{\mathbf{V}} | k \rangle + \int q^2 dq \langle k' | \bar{\mathbf{V}} | q \rangle \overline{\mathbf{G}\mathbf{G}}(q, P, \omega) \langle q | \bar{\Gamma}^m(\omega) | k \rangle \quad (3.68)$$

The corresponding flow equation in complete analogy to eq. (2.29) reads:

$$\frac{d}{d\Lambda} \langle k' | \bar{\Gamma}_\Lambda^m(\omega) | k \rangle = \frac{d}{d\Lambda'} \left[\int q^2 dq \langle k' | \bar{\Gamma}_\Lambda^m(\omega) | q \rangle \overline{\mathbf{G}\mathbf{G}}^{\Lambda'}(q, P, \omega) \langle q | \bar{\Gamma}_\Lambda^m(\omega) | k \rangle \right]_{\Lambda'=\Lambda} \quad (3.69)$$

At this point, we will not explicitly iterate this equation, but restrict ourselves to a instructive discussion of the basic properties of the elements of $\bar{\Gamma}$. In order to keep the following discussion as simple as possible, we assume that a non-vanishing gap in the partial wave $l = 0$ is sufficient to stabilize all other channels with attractive interactions. According to the discussion of section 1.8, there should be a Goldstone excitation in the channel with the quantum numbers of the condensate, i.e. in this case $l = 0$.

To see this more explicitly we will take the simple separable interaction \mathbf{V}_0^* as the dominant attractive S -wave interaction, which leads to the formation of the gap Δ_p^0 . In order to avoid technical problems, we take the single particle energies $\tilde{\xi}_p$ as given by Δ_p^0 and consider the case of a weak attractive (left plot in Fig. 3.16) and a repulsive interaction (right plot) in higher partial waves. In both cases, the vertex function shows the typical singular behaviour around the

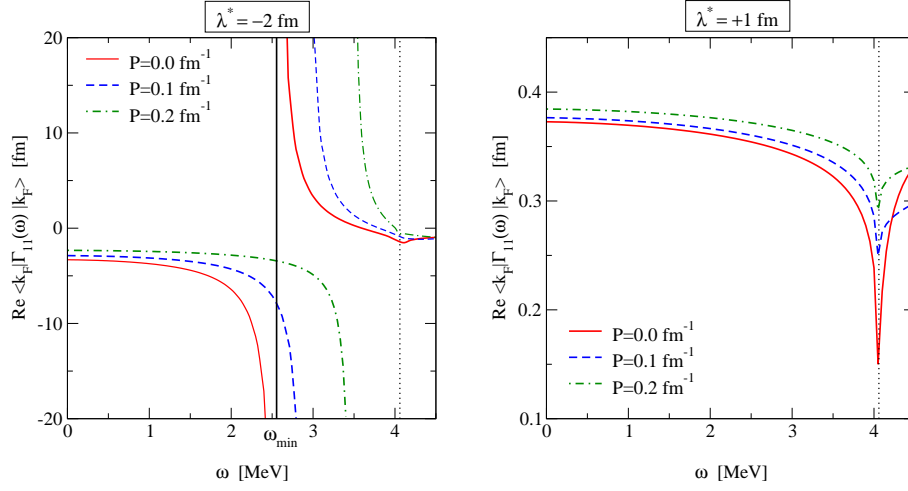


Figure 3.16.: Illustration of the properties of the vertex function for the separable model \mathbf{V}^* (cf. eq. (1.83)) for attractive (left, $\lambda^* = -2$ fm) and repulsive (right, $\lambda^* = +1$ fm) partial waves. The vertical dotted lines show the two-particle threshold $2\Delta^{l=0}$. See main text.

threshold in back-to-back kinematics. This feature is not visible in the left plot in Fig. 3.16 due to the large scaling on the ordinate. Below threshold the vertex function Γ in the attractive channel still contains a pole structure, whereas for a repulsive interaction the vertex function behaves perfectly regular. This pole however corresponds to a *massive* collective excitation with the minimal energy ω_{\min} (cf. Fig. 3.16 and Fig. 3.17).

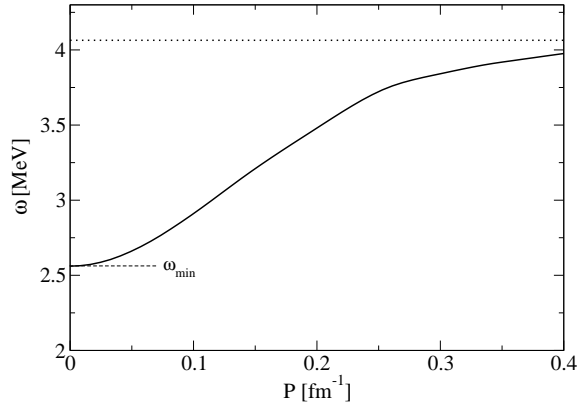


Figure 3.17.: Collective excitation spectrum in an attractive higher partial wave channel ($\lambda^* = -2$ fm). In contrast to the Goldstone excitation (cf. Fig. 1.18), this collective excitation is massive with the energy offset ω_{\min} . See text.

4. Conclusions and Outlook

In the present work we have studied superfluid neutron matter at zero temperature in the framework of the Renormalization Group. We computed the in-medium four point vertex and the self-energy in the BCS approximation by successive mode elimination. By solving the one-channel flow equation, we can to high accuracy reproduce the results for simple interaction models, where the problem can be solved explicitly. Additionally, the RG algorithm was also applied to realistic NN interactions. However in contrast to the explicit results, the RG framework is much more general and can naturally be extended to approximations beyond the BCS level.

The key problem in RG approaches to fermionic superfluids consists of a proper treatment of the pairing correlations. During the RG flow, these correlations are successively integrated out as the cutoff scale Λ approaches the Fermi surface. From a certain scale Λ' on, the gap function starts dynamically to develop a non-zero value and the normal ground state, where the RG flow is initialized, is no more the true ground state of the system. In the present work we obtain a controlled flow into the new phase by explicitly breaking the symmetry at the beginning of the flow by a very small amount. By this, we allow the system to remain in the true ground state, whereas without explicit symmetry breaking, the flow becomes singular when the scale approaches the inverse correlation length of the Cooper-pair wave function $\Lambda \sim \frac{1}{\xi} \sim \frac{\Delta}{v_f}$.

The RG approach has several conceptual and technical advantages:

- In general, the scattering equation for the four-point vertex possesses a complicated pole structure. Thus from the practical point of view, it is convenient, to avoid the computation of inverse matrices as far as possible. In the RG approach, this can be fully achieved in the one-channel problem. In this case, the flow equation takes an explicit form and the problem of solving a multi-dimensional integral equation can be transformed into the problem of solving a differential equation and evaluating multi-dimensional integrals.
- The flow of the two-point functions and the four point functions are in general coupled with to other. By this it is ensured that the self-energy functions are self-consistent at every cutoff scale.
- The RG scheme can be extended to include contributions of additional many-body channels, in order to take polarisation effects into account.

- Since the correlations in the system are successively integrated out, the stability and the accuracy of the numerical algorithm can be checked in every RG step. This will be especially useful in the multi-channel case.
- The complexity of the many-body calculation can be reduced substantially if only the dominant low lying modes around the Fermi surface are treated explicitly. The other modes can be integrated out by performing a RG mode elimination in vacuum.

As long as the matrix elements of the vertex function change smoothly during the flow, the iteration of the flow equation is in principle straightforward. However, the vertex function also possesses a characteristic pole structure which contains much of the physics. It is quite clear that the evolution of such singular matrix elements requires particular care in order to keep the numerics under control. In the present work, we resolve this problem by transforming the flow equation in such a way that only smoothly varying functions have to be iterated. By inverting the transformation after the RG iteration we obtain results, which lie on top of the exact results for the schematic model also close to the singularities. Thus even in the presence of poles, the RG turns out to be a flexible tool for a systematic investigation of many-body physics.

In order to minimize the complexity of the many-body problem for realistic interactions, it is highly convenient to first perform a vacuum mode elimination. By this we can optimize the size of the effective many-body Hilbert space, so that only the dominant modes around the Fermi surface are treated explicitly in the many-body calculation. Apart from the technical convenience, one can also, by using this procedure, study the cutoff dependence of the gap function and importance of three-body forces in a certain partial wave by this procedure.

It turns out that the 1S_0 superfluid pairing gap in the BCS approximation is practically independent of the choice of NN interaction, and therefore well constrained by the NN phase shifts. This includes a very weak cutoff dependence with low-momentum interactions $V_{\text{low } k}$ for sharp or sufficiently narrow smooth regulators with $\Lambda > 1.6 \text{ fm}^{-1}$. For lower densities, it is possible to lower the cutoff further to $\Lambda > 1.2k_F$. Furthermore, the pairing gap clearly reflects the charge dependence of nuclear interactions. Consequently, the uncertainties in 1S_0 superfluidity are due to an approximate treatment of induced interactions and dispersion effects, which go beyond the BCS level, as well as being due to 3N interactions. The weak cutoff dependence indicates that, in the 1S_0 channel, the contribution of 3N interactions is small at the BCS level. Additional insights will come from an investigation of the cutoff dependence of 3S_1 – 3D_1 superfluidity, where the 3N interactions may play an important role.

As the cutoff independence of the 1S_0 pairing gap at BCS level already suggests, the high momentum modes are blind to the presence of a Fermi surface. We also verified this picture by explicit calculation, comparing the final results of the in-medium RG algorithm starting from a bare interaction (with an intrinsic

cutoff of several GeV) with the results of the corresponding low momentum interaction. The final results of the in-medium scattering amplitude are essentially indistinguishable.

So far the numerical calculations in the RG scheme are restricted to the BCS approximation. We solved the flow equations for different realistic interaction models in the 1S_0 channel thereby retaining the full momentum and energy dependence of the scattering amplitude and found remarkable agreement for different interaction models. Hence we conclude that in the BCS approximation the matrix elements of the in-medium scattering amplitude are highly constrained by vacuum scattering phase shifts.

However at the present state of implementation the results should be considered more as a benchmark, showing the practical feasibility of the RG approach to superfluid systems. For more realistic calculations, additional effects have to be taken into account (cf. e.g. [6]), namely:

- *Coupling of partial waves:* This is technically straightforward to implement. The dimension of the objects appearing in the flow equation is higher, which in turn leads to an increase of the required computing time.
- *Self energy effects:* Beside the anomalous self-energy that is already treated in the present scheme, also the flow of the normal self-energy has to be included self-consistently.
- *Many-body channels:* The inclusion of additional many-body channels is technically not straightforward, since the flow equation cannot be inverted explicitly anymore. Instead, one has to solve a coupled system of implicit flow equations. A first step towards a full treatment of this problem has been achieved in the present work by showing that the one-channel flow equation can also be solved iteratively without making use of the particular simplifications of the one-channel problem. Principally the application of this technique to the general case has the potential to treat several channel simultaneously in a non-perturbative way.

Hence a lot of work remains to be done. Nevertheless, the basic approach is a promising starting point for a systematic microscopic investigation of superfluidity in strongly interacting Fermi systems including the effects listed above. Since they are all introduced systematically during the flow, they can all be treated in principle on an equal footing. Moreover, due to the generality of the scheme, the algorithm can in principle also be applied to other strongly correlated system like superconducting quark matter or superfluid ^3He . Although the present RG scheme is set up for the treatment of superfluid systems, also normal Fermi liquids can be treated. In this case, the number of flow equations is reduced substantially due to the absence of the anomalous components. Furthermore, the iteration of the equation simplifies due to the absence of the Goldstone poles.

The importance of polarization contributions to the pairing interaction due to spin-fluctuations was first pointed out by Berk and Schrieffer [7]. Furthermore, Anderson and Brinkman [8] showed that on the one hand in s-waves the spin-wave contribution is repulsive, which may lead to a complete suppression of superfluidity. On the other hand, in p-waves the corresponding contribution is attractive and tends to stabilize the Anderson-Morel phase ("A"-phase) [181] of liquid ^3He . Similar mechanisms can be important in nuclear systems at densities, where spin-singlet and triplet pairing may appear simultaneously. Particularly in the presence of several competing instabilities in a system, a consistent treatment of such effects is absolutely crucial, since the interplay between different correlations effects influences the formation of the different condensates. Since the symmetry breaking occurs dynamically during the flow in the present scheme, the system can "choose" by itself the favoured ground state. By this, the present RG framework is also applicable to systems, where a priori it is not clear, which phase is actually energetically preferred. Moreover we stress that the RG approach outlined in this thesis does not, as discussed in the introduction, depend on the separation of energy scales that forms the basis for the standard theory of superfluid Fermi liquids.

A. Appendix

A.1. Numerical Evaluation of the Flow Equation

The problem of evaluating flow equations like (2.29) can be expressed formally as¹

$$\begin{aligned}
X(\tilde{\omega}) &= \frac{d}{d\Lambda} \int_0^{q_{\max}} dq \int_0^1 dx \frac{f_1(\tilde{\omega}, q, x)}{f_2(\tilde{\omega}, q, x) \pm i\delta} \\
&= \frac{d}{d\Lambda} \int dq dx \left[\mathcal{P} \frac{f_1(\tilde{\omega}, q, x)}{f_2(\tilde{\omega}, q, x)} \mp i\pi f_1(\tilde{\omega}, q, x) \delta(f_2(\tilde{\omega}, q, x)) \right] \\
&\equiv X_{\text{Re}}(\tilde{\omega}) \mp i\pi X_{\text{Im}}(\tilde{\omega}),
\end{aligned} \tag{A.1}$$

where $\tilde{\omega}$ denotes all external parameters ω , P , Λ etc. and f_1 and f_2 are regular functions.

Note that for a Cauchy principal-value integral the derivative and integral operations do in general not commute. However, for a proper evaluation of the flow equation it is of highly practical convenience to apply the derivative directly to the integrand, i.e. commute the integral operation with the derivative. For this, it is necessary to regularize the integrand at the pole positions.

For this we define the root lines at fixed x by q_i^* , i.e.

$$f_2(\tilde{\omega}, q_i^*(\tilde{\omega}, x), x) = 0. \tag{A.2}$$

Typically, this equation has zero, one or two solutions. At the "critical" point $q^*(x^*) = q^*$, where both poles coincide $q^* = q_1^* \rightarrow q_2^*$, the function f_2 and the first derivative are vanishing and we have:

$$f_2(\tilde{\omega}, q \approx q^*, x \approx x^*) \sim a(x - x^*) + b(q - q^*)^2 \tag{A.3}$$

with

$$a = \partial_x f_2(\tilde{\omega}, q^*, x^*), \quad b = \frac{1}{2} \partial_q^2 f_2(\tilde{\omega}, q^*, x^*),$$

Consequently, the radial integral in $X_{\text{Re}}(\tilde{\omega})$ behaves, depending on the sign of

¹We restrict the angular integral to positive x for the sake of simplicity. The integration area $x \in [-1, 0]$ can be done in complete analogy.

$a(x - x^*)/b$, like

$$\lim_{x \rightarrow x^*} \int dq \frac{1}{a(x - x^*) + b(q - q^*)^2} \sim \begin{cases} \frac{1}{\sqrt{a(x - x^*)/b}} & \text{for } a(x - x^*)/b > 0 \\ \text{finite} & \text{for } a(x - x^*)/b < 0 \end{cases} \quad (\text{A.4})$$

Hence in the case of $x^* \in [0, 1]$ we have to split the integration area for the calculation of X_{Re} :

$$\begin{aligned} X_{\text{Re}}^{|x^*| < 1}(\tilde{\omega}) &= \frac{d}{d\Lambda} \left[\mathcal{P} \int_0^{x^*} dx \int dq \frac{f_1(\tilde{\omega}, q, x)}{f_2(\tilde{\omega}, q, x)} + \mathcal{P} \int_{x^*}^1 dx \int dq \frac{f_1(\tilde{\omega}, q, x)}{f_2(\tilde{\omega}, q, x)} \right] \\ &= X_{\text{Re}}^1 + X_{\text{Re}}^2 \end{aligned} \quad (\text{A.5})$$

In the first term the radial integral contains two poles, whereas the angular integrand remains regular. The poles can be regularized by subtraction:

$$\begin{aligned} X_{\text{Re}}^1 &= \frac{d}{d\Lambda} \int_0^{x^*} dx \int dq \left[\frac{f_1(\tilde{\omega}, q, x)}{f_2(\tilde{\omega}, q, x)} - \sum_i \frac{f_1(\tilde{\omega}, q_i^*(\tilde{\omega}, x), x)}{\partial_q f_2(\tilde{\omega}, q_i^*(\tilde{\omega}, x), x)(q - q_i^*(\tilde{\omega}, x))} \right] + \\ &\quad + \frac{d}{d\Lambda} \int_0^{x^*} dx \sum_{i=1}^N \frac{f_1(\tilde{\omega}, q_i^*(\tilde{\omega}, x), x)}{\partial_q f_2(\tilde{\omega}, q_i^*(\tilde{\omega}, x), x)} \log \left| \frac{q_{\text{max}} - q_i^*(\tilde{\omega}, x)}{q_i^*(\tilde{\omega}, x)} \right| \end{aligned} \quad (\text{A.6})$$

Now the integral is regular and the derivative can be applied to the integrand. The radial integral in X_{Re}^2 contains no poles, whereas the angular integrand shows up an integrable square root singularity when x is approaching x^* . This singularity can be treated numerically by a transformation of variables $y = 2\sqrt{x - x^*}$. Thus we have in total

$$\begin{aligned} X_{\text{Re}}^{|x^*| < 1}(\tilde{\omega}) &= \mathcal{P} \int_0^{x^*} dx \frac{d}{d\Lambda} \int dq \frac{f_1(\tilde{\omega}, q, x)}{f_2(\tilde{\omega}, q, x)} \\ &\quad + \frac{1}{2} \int_0^{2\sqrt{1-x^*}} dy \int dq \frac{d}{d\Lambda} \left[y \frac{f_1(\tilde{\omega}, q, y^2/4 + x^*)}{f_2(\tilde{\omega}, q, y^2/4 + x^*)} \right] \\ &\quad + \frac{dx^*}{d\Lambda} \left[\mathcal{P} \int dq \frac{f_1(\tilde{\omega}, q, x^*)}{f_2(\tilde{\omega}, q, x^* - \eta)} - \int dq \frac{f_1(\tilde{\omega}, q, 1)}{f_2(\tilde{\omega}, q, 1)} \right] \end{aligned} \quad (\text{A.7})$$

with $\eta \rightarrow 0$. In the case $x \notin [0, 1]$ the evaluation simplifies since essentially only the term X_{Re}^1 has to be calculated. Below threshold no poles appear and the evaluation poses no problems apart from the region around the Goldstone boson (cf. sect. 2.5).

In contrast, the radial integral in $X_{\text{Im}}(\tilde{\omega})$ behaves like

$$\lim_{x \rightarrow x^*} \int dq \delta(f_2(\tilde{\omega}, q \rightarrow q^*, x \rightarrow x^*)) \sim \begin{cases} \frac{1}{\sqrt{a(x^* - x)/b}} & \text{for } a(x - x^*)/b < 0 \\ 0 & \text{for } a(x - x^*)/b > 0 \end{cases} \quad (\text{A.8})$$

Hence we get for $x^* \notin [0, 1]$:

$$\begin{aligned} X_{\text{Im}}^{|x^*|>1}(\tilde{\omega}) &= \int dx \int dq \frac{d}{d\Lambda} [f_1(q, x, \tilde{\omega}) \delta(f_2(q, x, \tilde{\omega}))] \\ &= \int dx \sum_{i=1}^N \left[\frac{\partial_{\Lambda} f_1(q, x, \tilde{\omega}) - \partial_q \left[f_1(q, x, \tilde{\omega}) \frac{\partial_{\Lambda} f_2(q, x, \tilde{\omega})}{\partial_q f_2(q, x, \tilde{\omega})} \right]}{|\partial_q f_2(q, x, \tilde{\omega})|} \right]_{q=q_i^*(x, \tilde{\omega})} \end{aligned} \quad (\text{A.9})$$

However, for $x^* \in [0, 1]$ the derivative does not commute with the integrals. By introducing a new variable $y = 2\sqrt{x^* - x}$ we have

$$X_{\text{Im}}^{|x^*|<1}(\tilde{\omega}) = \frac{1}{2} \frac{d}{d\Lambda} \int_0^{2\sqrt{x^*}} dy \int dq [f_1(q, x^* - y^2/4, \tilde{\omega}) \delta(f_2(q, x^* - y^2/4, \tilde{\omega}))]. \quad (\text{A.10})$$

This derivative can be evaluated analogously to (A.9), the only difference being that additional derivatives appear due to the Λ -dependence of x^* (cf. eq. A.7).

A.2. Particle-Hole Interaction

The central nucleon-nucleon interaction in neutron matter is of the form

$$V(\mathbf{k} \boldsymbol{\sigma}, \mathbf{k}' \boldsymbol{\sigma}') = f(\mathbf{k}, \mathbf{k}') + g(\mathbf{k}, \mathbf{k}') \boldsymbol{\sigma} \cdot \boldsymbol{\sigma}' \quad (\text{A.11})$$

The particle-hole matrix elements read

$$\begin{aligned} \langle \mathbf{k}' | V_{ph}^{S=0} | \mathbf{k} \rangle &= 2f(\mathbf{k}, \mathbf{k}') \\ \langle \mathbf{k}' | V_{ph}^{S=1} | \mathbf{k} \rangle &= 2g(\mathbf{k}, \mathbf{k}'). \end{aligned} \quad (\text{A.12})$$

For a given nucleon-nucleon interaction $\langle \mathbf{k}_1 S m_s | V_{NN} | \mathbf{k}_2 S m_s \rangle$ non-central terms are also included. The central contributions can be projected out by [182]

$$\begin{aligned} f(\mathbf{k}_1, \mathbf{k}_2) &= \frac{1}{4} \sum_{S, m_s} \langle \mathbf{k}_1 S m_s | V_{NN} | \mathbf{k}_2 S m_s \rangle \\ g(\mathbf{k}_1, \mathbf{k}_2) &= \frac{1}{4} \left[\frac{1}{3} \sum_{m_s} \langle \mathbf{k}_1 1 m_s | V_{NN} | \mathbf{k}_2 1 m_s \rangle - \langle \mathbf{k}_1 00 | V_{NN} | \mathbf{k}_2 00 \rangle \right] \end{aligned} \quad (\text{A.13})$$

By inserting two set of states

$$\begin{aligned} &\langle \mathbf{k}_1 S m_s | V_{NN} | \mathbf{k}_2 S m_s \rangle \\ &= (4\pi)^2 \sum_{l, m, m', J, M} \langle \mathbf{k}_1 | l m' \rangle \langle l m' S m_s | J M \rangle \langle k_1 | V_{lS}^J | k_2 \rangle \langle J M | l m S m_s \rangle \langle l m | \mathbf{k}_2 \rangle \end{aligned}$$

and using the Clebsch-Gordan relations

$$\langle j_1 m_1 j_2 m_2 | j_3 m_3 \rangle = (-1)^{j_2 + m_2} \sqrt{\frac{2j_3 + 1}{2j_1 + 1}} \langle j_2 - m_2 j_3 m_3 | j_1 m_1 \rangle$$

and

$$\sum_{m_1, m_2} \langle JM | j_1 m_1 j_2 m_2 \rangle \langle j_1 m_1 j_2 m_2 | J' M' \rangle = \delta_{JJ'} \delta_{MM'}$$

all sums over the m -quantum numbers can be performed and we find:

$$\begin{aligned} f(\mathbf{k}_1, \mathbf{k}_2) &= \pi \sum_{S, l, J} (2J + 1) P_l(\cos \theta_{\mathbf{k}_1 \mathbf{k}_2}) \langle k_1 | V_{lS}^J | k_2 \rangle \\ g(\mathbf{k}_1, \mathbf{k}_2) &= \pi \sum_{S, l, J} (2J + 1) P_l(\cos \theta_{\mathbf{k}_1 \mathbf{k}_2}) \left[\frac{1}{3} \langle k_1 | V_{l1}^J | k_2 \rangle - \langle k_1 | V_{l0}^J | k_2 \rangle \right]. \end{aligned} \quad (\text{A.14})$$

Consequently, the spin-singlet particle-hole interactions in partial wave l reads:

$$\begin{aligned} V_l^{\pm, S=0}(q_1, q_2) &= \frac{1}{2} \frac{1}{(4\pi)^2} \int d\Omega_{\mathbf{q}_1 \mathbf{q}_2} P_l(\cos \theta_{\mathbf{q}_1 \mathbf{q}_2}) f \left[\frac{\mathbf{q}_1 \pm \mathbf{q}_2}{2}, \frac{\mathbf{q}_1 \pm \mathbf{q}_2}{2} \right] \\ &= \frac{1}{16} \int_{-1}^1 dx P_l(x) \sum_{S', l', J'} (2J' + 1) \left\langle \frac{q'_\pm}{2} \left| V_{l'S'}^{J'} \right| \frac{q'_\pm}{2} \right\rangle \end{aligned} \quad (\text{A.15})$$

with

$$q'_\pm = |\mathbf{q}_1 \pm \mathbf{q}_2| = \sqrt{q_1^2 + q_2^2 \pm 2q_1 q_2 x}.$$

A.3. Flow Equations in Vacuum

The low-momentum Lippmann-Schwinger equation in a certain partial wave reads

$$\langle k' | T(\omega) | k \rangle = \langle k' | V^\Lambda | k \rangle + \frac{2}{\pi} \mathcal{P} \int q^2 dq \langle k' | V^\Lambda | q \rangle \frac{f(q, \Lambda)}{\omega - q^2} \langle q | T(\omega) | k \rangle. \quad (\text{A.16})$$

Here, $f(q, \Lambda)$ is a cutoff function that cuts out the high lying momentum states. Simple examples would be $f(q, \Lambda) = \Theta(\Lambda - k)$ as a sharp cutoff or $f(q, \Lambda) = \frac{1}{e^{(q-\Lambda)/c} + 1}$ for a smooth cutoff function with width c .

The transition operator T and the interaction V^Λ are as usual [72] connected via the relation $\hat{T}(k^2) |k\rangle = \hat{V}^\Lambda |\chi_k^\Lambda\rangle$ with $\hat{H}^\Lambda |\chi_k^\Lambda\rangle = k^2 |\chi_k^\Lambda\rangle$ [72], where \hat{H} is the full effective Hamilton operator, $|k\rangle$ the free plane wave states and $|\chi_k^\Lambda\rangle$ are the

outgoing scattering states:

$$|\chi_k^\Lambda\rangle = |k\rangle + \frac{2}{\pi} \int q^2 dq \frac{f(q, \Lambda) \langle q| T(k^2) |k\rangle}{k^2 - q^2 + i\eta} |k\rangle, \quad \frac{2}{\pi} \mathcal{P} \int dq q^2 |\chi_q^\Lambda\rangle \langle \chi_q^\Lambda| = 1 \quad (\text{A.17})$$

If the energy ω is off-shell, i.e. independent of any momentum, the requirement $\frac{d}{d\Lambda} \langle k'| T(\omega) |k\rangle = 0$ leads to

$$\frac{d}{d\Lambda} \langle k'| V^\Lambda |k\rangle = -\frac{2}{\pi} \int q^2 dq \left(\frac{df(q, \Lambda)}{d\Lambda} \right) \langle k'| V^\Lambda |q\rangle \frac{1}{\omega - q^2} \langle q| V^\Lambda |k\rangle \quad (\text{A.18})$$

This prescription provides an energy dependent low-momentum effective interaction V^Λ .

However, not actually all elements but only the diagonal on-shell elements $\langle k| T(k^2) |k\rangle$ are constrained by experiment. The invariance of these elements can be achieved by imposing the invariance conditions to the half-on-shell matrix elements:

$$(1) : \frac{d}{d\Lambda} \langle k'| T(k^2) |k\rangle = 0, \quad (2) : \frac{d}{d\Lambda} \langle k'| T(k'^2) |k\rangle = 0 \quad (\text{A.19})$$

Both resulting effective interactions preserve the full on-shell scattering data but are in general not hermitian. Hermiticity can be achieved by adding the two resulting flow equations each weighted by a factor of $1/2$.

In order to see how this works in detail let us impose condition (1). This leads to

$$\begin{aligned} \mathcal{P} \int q^2 dq \left(\frac{d}{d\Lambda} \langle k'| V^\Lambda |q\rangle \right) \langle q| \chi_k^\Lambda \rangle &= \\ &= - \int dq \frac{q^2}{k^2 - q^2} \left(\frac{d}{d\Lambda} f(q, \Lambda) \right) \langle k'| V^\Lambda |q\rangle \langle q| V^\Lambda | \chi_k^\Lambda \rangle \end{aligned} \quad (\text{A.20})$$

Multiplying both sides with $\langle \chi_k | k'' \rangle$ and integrating over k we obtain:

$$\frac{d}{d\Lambda} \langle k'| V^\Lambda |k\rangle = -\frac{4}{\pi^2} \mathcal{P} \int dq q^2 \int dq' q'^2 \langle k'| V^\Lambda |q\rangle \langle q| V^\Lambda | \chi_{q'}^\Lambda \rangle \frac{\frac{df(q, \Lambda)}{d\Lambda}}{q'^2 - q^2} \langle \chi_{q'}^\Lambda | k \rangle, \quad (\text{A.21})$$

where we have renamed some momenta. Note that due to the momentum dependence of the propagator denominator on the momentum q' , the integral over q' gives not simply a unit matrix like in the off-shell case above, but rather the spectral representation of the full propagator:

$$\hat{G}^\Lambda(\omega) = \frac{1}{\omega - \hat{H}^\Lambda} = \frac{2}{\pi} \int q'^2 dq' |\chi_{q'}^\Lambda\rangle \frac{1}{\omega - q'^2} \langle \chi_{q'}^\Lambda|. \quad (\text{A.22})$$

Finally using $\hat{V}^\Lambda \hat{G}^\Lambda(\omega) = \hat{T}(\omega) \frac{1}{\omega - \hat{H}_0}$, we obtain

$$\frac{d}{d\Lambda} \langle k' | V^\Lambda | k \rangle = -\frac{2}{\pi} \int dq \frac{q^2}{k^2 - q^2} \left(\frac{d}{d\Lambda} f(q, \Lambda) \right) \langle k' | V^\Lambda | q \rangle \langle q | T(q^2) | k \rangle \quad (\text{A.23})$$

for the flow equation. Note that on the right hand side a left half-on-shell T-Matrix appears, which is in general *not* invariant under this flow equation and has to be recomputed in every RG step.

Clearly, the initial and final momenta k and k' are not treated on an equal footing in (A.23). Consequently, the effective interaction V^Λ is in general non-hermitian. The hermiticity can be restored as mentioned above by combining eq. (A.23) with the analogous flow equation for left half-on-shell T-Matrix elements. This equation can be derived in complete analogy, with the result:

$$\frac{d}{d\Lambda} \langle k' | V^\Lambda | k \rangle = -\frac{2}{\pi} \int dq \frac{q^2}{k'^2 - q^2} \left(\frac{d}{d\Lambda} f(q, \Lambda) \right) \langle k' | T(q^2) | q \rangle \langle q | V^\Lambda | k \rangle. \quad (\text{A.24})$$

Clearly both equations (A.23) and (A.24) leave the full on-shell elements invariant and consequently (2.14) provides a hermitian low momentum effective interaction, that is phase shift equivalent to the original interaction.

Bibliography

- [1] H. K. Onnes, Comm. Phys. Lab. Univ. Leiden **122**, (1911).
- [2] A. Bohr and B. Mottelson, *Nuclear Structure Volume I: Single-Particle Motion* (Benjamin Inc., New York, 1969).
- [3] D. D. Osheroff, R. C. Richardson, and D. M. Lee, Phys. Rev. Lett. **28**, 885 (1972).
- [4] J. Bardeen, L. N. Cooper, and J. R. Schrieffer, Phys. Rev. **106**, 162 (1957).
- [5] M. Salmhofer, C. Honerkamp, W. Metzner, and O. Lauscher, Prog. Theo. Phys. **112**, 943 (2004).
- [6] L. Gorkov and T. Melik-Barkhudarov, Sov. Phys. JETP **13**, 1018 (1961).
- [7] N. F. Berk and J. R. Schrieffer, Phys. Rev. Lett. **17**, 433 (1966).
- [8] P. W. Anderson and W. F. Brinkman, Phys. Rev. Lett. **30**, 1108 (1973).
- [9] A. J. Leggett, Rev. Mod. Phys. **47**, 331 (1975).
- [10] A. Larkin and A. Migdal, JETP **44**, 1703 (1963).
- [11] W. Keesom and J. van den Ende, Comm. Phys. Lab. Univ. Leiden **2196**, (1932).
- [12] W. Meissner and R. Ochsenfeld, Natwiss. **21**, 787 (1933).
- [13] F. London and H. London, Proc. Roy. Soc. (London) **A149**, 71 (1935).
- [14] C. Gorter and H. Casimir, Phys. Z. **35**, 963 (1934).
- [15] A. Fetter and J. Walecka, *Quantum Theory of Many-particle Systems* (McGraw-Hill, New York, 1971).
- [16] A. Pippard, Proc. Roy. Soc. (London) **A216**, 547 (1953).
- [17] V. Ginsburg and L. Landau, Sov. Phys. JETP **20**, 1064 (1950).
- [18] H. Fröhlich, Phys. Rev. **79**, 845 (1950).

-
- [19] C. A. Reynolds, B. Serin, W. H. Wright, and L. B. Nesbitt, *Phys. Rev.* **78**, 487 (1950).
- [20] E. Maxwell, *Phys. Rev.* **78**, 477 (1950).
- [21] E. Maxwell, *Phys. Rev.* **79**, 173 (1950).
- [22] J. Bardeen, *Rev. Mod. Phys.* **23**, 261 (1951).
- [23] M. Schafroth, *Helv. Phys. Acta* **24**, 645 (1951).
- [24] A. Migdal, *Sov. Phys. JETP* **1**, 996 (1958).
- [25] L. Cooper, *Phys. Rev.* **104**, 1189 (1956).
- [26] A. Abrikosov, L. Gorkov, and I. Dzyaloshinski, *Methods of quantum field theory in statistical physics* (Dover Publications, New York, 1963).
- [27] L. Landau, *Sov. Phys. JETP* **30**, 1058 (1956).
- [28] L. Landau, *Sov. Phys. JETP* **32**, 59 (1957).
- [29] L. Landau, *Sov. Phys. JETP* **35**, 97 (1958).
- [30] A. J. Leggett, *Phys. Rev.* **140**, A1869 (1965).
- [31] A. J. Leggett, *Phys. Rev.* **147**, 119 (1966).
- [32] A. Einstein, *Ber. Berl. Akad.* **261**, (1924).
- [33] A. Einstein, *Ber. Berl. Akad.* **3**, (1925).
- [34] J. Schrieffer, *Theory of Superconductivity* (Addison-Wesley, Redwood City, CA, USA, 1999).
- [35] J. Bardeen, L. N. Cooper, and J. R. Schrieffer, *Phys. Rev.* **108**, 1175 (1957).
- [36] N. Bogoliubov, *Nuovo Cimento* **7**, 6 (1958).
- [37] J. Valatin, *Nuovo Cimento* **7**, 843 (1958).
- [38] P. Kapitza, *Nature* **141**, 74 (1938).
- [39] J. Allen and A. Misener, *Nature* **141**, 75 (1938).
- [40] F. London, *Phys. Rev.* **54**, 947 (1938).
- [41] L. Tisza, *Nature* **141**, 913 (1938).
- [42] J. Allen and H. Jones, *Nature* **141**, 243 (1938).

-
- [43] L. D. Landau, *J. Phys. (USSR)* **5**, 71 (1941).
- [44] N. Bogoliubov, *J. Phys. (USSR)* **9**, 23 (1947).
- [45] R. P. Feynman and M. Cohen, *Phys. Rev.* **102**, 1189 (1956).
- [46] D. Henshaw and A. Woods, *Phys. Rev.* **121**, 1266 (1961).
- [47] A. J. Leggett, *Rev. Mod. Phys.* **71**, 318 (1999).
- [48] L. Landau and E. Lifschitz, *Vol 9 Statistical Physics, Part 2* (Pergamon Press, Oxford, 1981).
- [49] D. D. Osheroff, W. J. Gully, R. C. Richardson, and D. M. Lee, *Phys. Rev. Lett.* **29**, 920 (1972).
- [50] M. Baldo *et al.*, *Phys. Rev.* **C58**, 1921 (1998).
- [51] A. Bohr, B. R. Mottelson, and D. Pines, *Phys. Rev.* **110**, 936 (1958).
- [52] A. Migdal, *Nucl. Phys.* **13**, 655 (1959).
- [53] A. Migdal, *Sov. Phys. JETP* **10**, 176 (1960).
- [54] L. N. Cooper, R. L. Mills, and A. M. Sessler, *Phys. Rev.* **114**, 1377 (1959).
- [55] V. J. Emery and A. M. Sessler, *Phys. Rev.* **119**, 248 (1960).
- [56] D. Pines, R. Tamagaki, and S. Tsuruta, *The Structure and Evolution of Neutron Stars* (Addison Wesley, Redwood City, CA, USA, 1992).
- [57] J. Sauls, *Cesme Lectures on "Timing Neutron Stars"* (Kluwer Academic Press, Dordrecht, Holland, 1989).
- [58] M. Alpar and D. Pines, *Proceedings of the Los Alamos Workshop "Isolated Pulsars"* (Cambridge University Press, Cambridge, England, 1993).
- [59] S. Tsuruta, *Phys. Rep.* **292**, 1 (1998).
- [60] H. Heiselberg and M. Hjorth-Jensen, *Phys. Rep.* **328**, 237 (2000).
- [61] D. Yakovlev, A. Kaminker, O. Gnedin, and P. Haensel, *Phys. Rept.* **354**, 1 (2001).
- [62] D. G. Yakovlev and C. J. Pethick, *Ann. Rev. Astron. Astrophys.* **42**, 169 (2004).
- [63] T. Takatsuka and R. Tamagaki, *Prog. Theor. Phys. Suppl.* **112**, 27 (1993).
- [64] L. Amundsen and E. Ostgaard, *Nucl. Phys.* **A442**, 163 (1985).

-
- [65] O. Elgarøy and M. Hjorth-Jensen, Phys. Rev. **C57**, 1174 (1998).
- [66] M. Baldo, J.Cugnon, A. Lejeune, and U. Lombardo, Nucl. Phys. **A515**, 409 (1990).
- [67] V. Khodel, V. Khodel, and J. Clark, Nucl. Phys. **A598**, 390 (1996).
- [68] M. Baldo, J.Cugnon, A. Lejeune, and U. Lombardo, Nucl. Phys. **A536**, 349 (1992).
- [69] O. Elgarøy, L. Engvik, M. Hjort-Jensen, and E. Osnes, Nucl. Phys. **A607**, 425 (1996).
- [70] V. A. Khodel, V. V. Khodel, and J. W. Clark, Phys. Rev. Lett. **81**, 3828 (1998).
- [71] P. Nozières, *Theory of Interacting Fermi Systems* (Addison-Wesley, Redwood City, CA, USA, 1997).
- [72] C. Joachain, *Quantum Collision Theory* (North-Holland, Amsterdam, Holland, 1975).
- [73] G. Brown and A. Jackson, *The Nucleon-Nucleon Interaction* (North-Holland, Amsterdam, Holland, 1976).
- [74] J. Polonyi and K. Sailer, Phys. Rev. B **66**, 155113 (2002).
- [75] U. Tuber, B. Schmittmann, and R. Zia, J. Phys. **A34**, L583 .
- [76] C. R. Stephens and H. Waelbroeck, Phys. Rev. **E57**, 3251 (1998).
- [77] H. Gies and C. Wetterich, Phys. Rev. **D65**, 065001 (2002).
- [78] S. Weinberg, *The Quantum Theory of Fields, Volume 1: Foundations* (Cambridge University Press, Cambridge, England, 1995).
- [79] H. A. Bethe, Phys. Rev. **72**, 339 (1947).
- [80] J. B. French and V. F. Weisskopf, Phys. Rev. **75**, 1240 (1949).
- [81] J. Schwinger, Phys. Rev. **73**, 416 (1948).
- [82] F. J. Dyson, Phys. Rev. **75**, 1736 (1949).
- [83] H. Kragh, *Dirac: A scientific biography* (Cambridge University Press, Cambridge, England, 1990).
- [84] R. Feynman, *The Strange Theory of Light and Matter* (Penguin, Dordrecht, Holland, 1990).

-
- [85] L. Kadanoff, *Physics* **2**, 263 (1966).
- [86] K. G. Wilson, *Phys. Rev.* **B4**, 3174 (1971).
- [87] K. G. Wilson, *Phys. Rev.* **B4**, 3184 (1971).
- [88] K. G. Wilson, *Rev. Mod. Phys.* **47**, 773 (1975).
- [89] M. E. Fisher, *Rev. Mod. Phys.* **70**, 653 (1998).
- [90] N. Goldenfeld, *Lecture on Phase Transitions and the Renormalization Group* (Addison-Wesley, Redwood City, CA, USA, 1993).
- [91] G. P. Lepage, hep-ph/0506330 (1989).
- [92] B. Delamotte, *Am. J. Phys.* **72**, 170 (2004).
- [93] R. Shankar, *Rev. Mod. Phys.* **66**, 129 (1994).
- [94] N. Dupuis, *Eur. Jour. Phys.* **B3**, 315 (1998).
- [95] J. Polchinski, hep-th/9210046 (1992).
- [96] J. Hormuzdiar and S. Hsu, nucl-th/9811017 (1998).
- [97] C. Varma, Z. Nussinov, and W. van Saarloos, *Phys. Rept.* **361**, 267 (2002).
- [98] P. Kopietz and T. Busche, *Phys. Rev.* **B64**, 155101 (2001).
- [99] M. Salmhofer, *Comm. Math. Phys.* **194**, 249 (1998).
- [100] C. Halboth and W. Metzner, *Phys. Rev.* **B61**, 7364 (2000).
- [101] D. Zanchi and H. J. Schulz, *Phys. Rev.* **B54**, 9509 (1996).
- [102] J. González, *Phys. Rev.* **B63**, 045114 (2001).
- [103] M. Salmhofer and C. Honerkamp, *Prog. Theor. Phys.* **105**, 1 (2001).
- [104] N. Furukawa, T. M. Rice, and M. Salmhofer, *Phys. Rev. Lett.* **81**, 3195 (1998).
- [105] S. Andergassen *et al.*, *Phys. Rev.* **B70**, 075102 (2004).
- [106] C. Halboth and W. Metzner, *Phys. Rev. Lett.* **85**, 5162 (2000).
- [107] C. Honerkamp and M. Salmhofer, *Phys. Rev.* **B64**, 184516 (2001).
- [108] D. Zanchi and H. J. Schulz, *Phys. Rev.* **B61**, 13609 (2000).
- [109] B. Krippa, hep-ph/0610237 (2006).

-
- [110] D. Amit, *Field Theory, the Renormalization Group, and Critical Phenomena* (McGraw-Hill, London, 1978).
- [111] J. Zinn-Justin, Lecture notes, Cargèse Summer School (1973).
- [112] D. Entem and R. Machleidt, Phys. Rev. **C68**, 041001 (2003).
- [113] V. Stoks, R. Klomp, C. Terheggen, and J. de Swart, Phys. Rev. **C49**, 2950 (1994).
- [114] R. Wiringa, V. Stoks, and R. Schiavilla, Phys. Rev. **C51**, 38 (1995).
- [115] R. Machleidt, Phys. Rev. **C63**, 024001 (2001).
- [116] S. Bogner, R. Furnstahl, S. Ramanan, and A. Schwenk, nucl-th/0609003 (2006).
- [117] S. Lee and K. Suzuki, Phys. Lett. **B91**, 173 (1980).
- [118] K. Suzuki and S. Lee, Prog. Theo. Phys. **64**, 2091 (1980).
- [119] S. Okubo, Prog. Theo. Phys. **12**, 603 (1954).
- [120] S. Bogner, A. Schwenk, T. Kuo, and G. Brown, nucl-th/0111042 (2001).
- [121] K. Hebeler, A. Schwenk, and B. Friman, nucl-th/0611024 (submitted to Phys. Lett. **B**) (2006).
- [122] S. Bogner, T. Kuo, and A. Schwenk, Phys. Rep. **386**, 1 (2003).
- [123] S. Bogner *et al.*, Phys. Lett. **B576**, 265 (2003).
- [124] A. Schwenk, G. Brown, and B. Friman, Nucl. Phys. **A703**, 745 (2002).
- [125] S. Bogner, R. Furnstahl, S. Ramanan, and A. Schwenk, Nucl. Phys. **A773**, 203 (2006).
- [126] A. Bulgac, Phys. Rev. **C65**, 051305 (2002).
- [127] E. Epelbaum, W. Glockle, and U.-G. Meissner, Nucl. Phys. **A747**, 362 (2005).
- [128] C. Pethick and H. Smith, *Bose-Einstein Condensation in Dilute Gases* (Cambridge University Press, Cambridge, England, 2001).
- [129] U. Lombardo and H.-J. Schulze, Lect. Notes, Phys. **578**, 30 (2001).
- [130] N. Kaiser, T. Niksic, and D. Vretenar, Eur. J. Phys. **A25**, 257 (2005).

-
- [131] A. Sedrakian, T. T. S. Kuo, H. Müther, and P. Schuck, Phys. Lett. **B576**, 68 (2003).
- [132] A. Gardestig and D. Phillips, Phys. Rev. **C73**, 014002 (2006).
- [133] C. Wetterich, Phys. Lett. **B301**, 90 (1993).
- [134] T. Morris, Int. J. Mod. Phys. **A9**, 2411 (1994).
- [135] J. Polchinski, Nucl. Phys. **B231**, 269 (1984).
- [136] J. Hubbard, Phys. Rev. Lett. **3**, 77 (1959).
- [137] R. Stratonovich, Dokl. Akad., Nauk SSR **115**, 1097 .
- [138] U. Ellwanger and C. Wetterich, Nucl. Phys. **B423**, 137 (1994).
- [139] F. Schütz, L. Bartosch, and P. Kopietz, Phys. Rev. **B72**, 035107 (2005).
- [140] F. Schütz and P. Kopietz, Math. Gen. **39**, 8205 (2006).
- [141] C.-H. Yang and J. Clark, Nucl. Phys. **A174**, 49 (1971).
- [142] D. Pines, Proc. XIth Intern. Conf. on Low temperature physics, ed. E. Kandu (Tokyo, 1971).
- [143] J. W. Clark, C.-G. Källman, C.-H. Yang, and D. A. Chakkalal, Phys. Lett. **B61**, 331 (1976).
- [144] U. Lombardo, P. Schuck, and W. Zuo, Phys. Rev. **C64**, 021301 (2001).
- [145] P. Bozek, Nucl. Phys. **A657**, 187 (1999).
- [146] P. Bozek, Phys. Rev. **C62**, 054316 (2000).
- [147] P. Bozek and P. Czerski, Phys. Rev. **C66**, 027301 (2002).
- [148] U. Lombardo, H. Schulze, C. Shen, and W. Zuo, Int. J. Mod. Phys. **E14**, 513 (2005).
- [149] D. J. Dean and M. Hjorth-Jensen, Rev. Mod. Phys. **75**, 607 (2003).
- [150] A. Sedrakian and J. Clark, nucl-th/0607028 (2006).
- [151] H.-J. Schulze, A. Polls, and A. Ramos, Phys. Rev. **C63**, 044310 (2001).
- [152] J. Chen, J. Clark, R. Davé, and V. Khodel, Nucl. Phys. **A555**, 59 (1993).
- [153] T. Papenbrock and G. F. Bertsch, Phys. Rev. **C59**, 2052 (1999).

-
- [154] H. Heiselberg, C. J. Pethick, H. Smith, and L. Viverit, Phys. Rev. Lett. **85**, 2418 (2000).
- [155] S. Babu and G. E. Brown, Ann. Phys. (NY) **78**, 1 (1973).
- [156] S.-O. Bäckman, G. Brown, and J. Niskanen, Phys. Rept. **124**, 1 (1985).
- [157] O. Sjöberg, Ann. Phys. **78**, 39 (1973).
- [158] J. Wambach, T. L. Ainsworth, and D. Pines, Nucl. Phys. **A555**, 128 (1993).
- [159] T. L. Ainsworth, J. Wambach, and D. Pines, Phys. Lett. **B222**, 173 (1989).
- [160] H.-J. Schulze *et al.*, Phys. Lett. **B375**, 1 (1996).
- [161] C. Shen *et al.*, Phys Rev. **C67**, 061302 (2003).
- [162] C. Shen, U. Lombardo, and P. Schuck, Phys. Rev. **C71**, 054301 (2005).
- [163] A. Fabrocini, S. Fantoni, A. Illarionov, and K. Schmidt, Phys. Rev. Lett. **95**, 192501 (2005).
- [164] E. Krotscheck, R. A. Smith, and A. D. Jackson, Phys. Rev. B **24**, 6404 (1981).
- [165] A. Jackson, E. Krotschek, D. Meltzer, and A. Smith, Nucl. Phys. **A386**, 125 (1982).
- [166] J. Chen, J. Clark, E. Krotscheck, and R. A. Smith, Nucl. Phys. **A451**, 509 (1986).
- [167] A. Lande and R. Smith, Phys. Rev. **A45**, 913 (1992).
- [168] M. Hjorth-Jensen, Advances in Many-Body-Physics, edited by N. Walet and R.F. Bishop (World Scientific) **2**, (2002).
- [169] N. E. Bickers and S. R. White, Phys. Rev. **B43**, 8044 (1991).
- [170] A. Schwenk, B. Friman and G.E. Brown, Nucl. Phys. **A713**, 191 (2003).
- [171] A. Schwenk, Int. J. Mod. Phys. **B20**, 2724 (2006).
- [172] A. Schwenk, nucl-th/0611046 (2006).
- [173] G. Benfatto and G. Gallavotti, Phys. Rev. **B42**, 9967 (1990).
- [174] G. Benfatto and G. Gallavotti, J. Stat. Phys. **59**, 541 (1990).
- [175] G. Baym, Phys. Rev. **127**, 1391 (1962).

-
- [176] G. Baym and L. P. Kadanoff, Phys. Rev. **124**, 287 (1961).
- [177] J. M. Luttinger and J. C. Ward, Phys. Rev. **118**, 1417 (1960).
- [178] J. Cornwall, R. Jackiw, and E. Tomboulis, Phys. Rev. **D10**, 2428 (1974).
- [179] T. Morris, Nucl. Phys. **B458**, 477 (1996).
- [180] N. Dupuis, Eur. Jour. Phys. **B48**, 319 (2005).
- [181] P. W. Anderson and P. Morel, Phys. Rev. **123**, 1911 (1961).
- [182] S.-O. Bäckmann, O. Sjöberg, and A. Jackson, Nucl. Phys. **A321**, 10 (1979).

Danksagung

An erster Stelle möchte ich mich bei meinem Doktorvater Bengt Friman für die engagierte Betreuung während der letzten drei Jahre bedanken. Er war zu jeder Zeit ein sehr angenehmer und hilfreicher Ansprechpartner. Unsere zahlreichen Diskussionen trugen sehr häufig zu einem besseren Verständnis der Probleme bei und führten zur Entwicklung eines sehr freundschaftlichen persönlichen Verhältnisses.

Desweiteren danke ich Jochen Wambach für die Möglichkeit, in der Theoriegruppe der GSI die vorliegende Arbeit anzufertigen. Die sehr angenehme Atmosphäre innerhalb der Arbeitsgruppe führte zur Entwicklung einiger echter Freundschaften.

Insbesondere danke ich Felix Riek und Julian Hofmann für die "tiefschürfenden" Diskussionen bei unserem obligatorischen nach-mittäglichen Glas Aquamatenwasser. Bei auftretenden Problemen verschiedenster Art standen mir jederzeit kompetente Ansprechpartner zur Verfügung. Mein besonderer Dank gilt hierbei unseren Linux-Experten Jörn Knoll, Thomas Neff und Alexander Semke, dem Mann mit dem "goldenen Händchen". Computerprobleme konnten so in der Regel innerhalb kürzester Zeit gelöst werden. Weiter danke ich Borislav Stokic und Robert Cussons für ihre wertvolle Hilfe beim Korrekturlesen des Manuskripts, sowie Achim Schwenk für unsere fruchtbare Zusammenarbeit, die sich während des letzten Jahres entwickelt hat.

Nicht zuletzt danke ich meinen Eltern Georg und Hella für den starken familiären Rückhalt über all die Jahre, ohne den all dies nicht möglich gewesen wäre!

Lebenslauf

Name:	Kai Hebeler
Geburtsdatum:	5. Februar 1979
Geburtsort:	Bad Hersfeld
Eltern:	Georg und Hella Hebeler geb. Heß
Familienstand:	ledig
Nationalität:	deutsch
06/1985 - 06/1989	Besuch der Grundschule in Ludwigsau-Friedlos
06/1989 - 06/1995	Besuch der Gesamtschule Geistal in Bad Hersfeld
06/1995 - 06/1998	Besuch der Modellschule Obersberg mit Abiturabschluß
07/1998 - 04/1999	Wehrdienst in Limburg an der Lahn und Schwalmstadt
04/1999 - 08/2003	Physikstudium an der Technischen Universität Darmstadt
04/2002 - 07/2003	Anfertigung der Diplomarbeit bei der Gesellschaft für Schwerionenforschung mit dem Thema " <i>Relativistische Fermi-Liquid Theorie für Materie bei hohen Dichten</i> "
08/2003	Abschluß des Studiums (Gesamtnote: 1.0)
09/2003 - 01/2007	Wissenschaftlicher Mitarbeiter bei der Gesellschaft für Schwerionenforschung und Anfertigung der Dissertation